

Herausgeber:
Professor Dr.-Ing. H.-G. Kempfert

**Lateral spreading
in basal reinforced embankments
supported by pile-like elements**

Gourge Samir Fahmi Farag

Heft 20

März 2008

Diese Arbeit entstand am Fachgebiet Geotechnik als eine vom Fachbereich Bauingenieurwesen der Universität Kassel genehmigte Dissertation.

Erster Gutachter: Prof. Dr.-Ing. Hans-Georg Kempfert

Zweiter Gutachter: Prof. Dr.-Ing. Herbert Klapperich

Dritter Gutachter: Dr.-Ing. Berhane Gebreselassie

Tag der mündlichen Prüfung: 31. März 2008

Institut für Geotechnik und Geohydraulik

Universität Kassel – Fachgebiet Geotechnik

Mönchebergstraße 7 – 34125 Kassel

Telefon: (0561) 804 2630

Telefax: (0561) 804 2651

2008, kassel university press GmbH

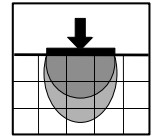
www.upress.uni-kassel.de

ISBN 978-3-89958-414-1

urn:nbn:de:0002-4148

Bibliographische Information der Deutschen Nationalbibliothek:

Die Deutsche Nationalbibliothek verzeichnet diese Publikation in der Deutschen Nationalbibliographie; detaillierte bibliographische Daten sind im Internet über <http://dnb.ddb.de> abrufbar.



Herausgeber:
Professor Dr.-Ing. H.-G. Kempfert

**Lateral spreading
in basal reinforced embankments
supported by pile-like elements**

Gourge Samir Fahmi Farag

Heft 20

März 2008

Preface

It is a common practice nowadays to place high stiffness geosynthetic reinforcement (usually geogrids) at the base of embankments on low-bearing underground. The reinforcement can be directly placed on the top of the soft underground or above pile-like elements, which transfer the embankment load into a bearing layer.

The main function of the horizontal geosynthetic reinforcement at an embankment base is to carry the vertical embankment load and the spreading forces that are directed outward. This particularly is of great importance for reinforced embankments on pile-like elements, since otherwise the piles may be subjected to bending, which they cannot withstand due to their small diameter and usually are unreinforced. At present, adequate scientific explanation is not yet available on the size and distribution of the spreading force at the label directly above and below the geosynthetic reinforcement, which are required to estimate the tension force and thus to consider the spreading forces in the design of the reinforcement.

Dr.-Ing. Gourage Fahmi had first compiled together the state of the art of the spreading force in embankments with and without geosynthetic reinforcements as well as with and without pile-like elements. An essential part of the investigation includes the large scale model tests, which were intended among others to validate numerical computations. After minor parameter calibrations a very good agreement could be achieved between the model tests and the numerical computations according to the finite element method, with the exception that the computed strains or tensile forces in the geosynthetic above pile-like elements were low. Thus a hypothesis was formulated based on own investigations and comparable results from literature, in which the computation results should be adjusted by means of a factor. With this the numerical computation model had been verified to a large extent for further parameter studies.

Based on these findings a series of parameter studies are performed using numerical and analytical methods to investigate the spreading problem on the prototype embankments. For this purpose a reasonable boundary conditions and parameter variations were selected that are applicable to the spreading problematic. The numerical investigations provided a deep knowledge of the mechanics and the behaviour of the whole system (embankment-reinforcement-pile-underground). The comparative analytical analysis was primarily used to validate the simplified analytical approaches for practical computations.

Summarising the results, it was found that the tensile forces in the geogrids due to spreading forces increase almost linear with the embankment height as expected. Furthermore, the stiffness of the underground soil plays an important role on the size of the spreading forces. It is worth mentioning here that the stiffness of the underground is not considered in the current available analytical approaches. The softest the underground, the more will be the spreading forces and the

difference between tensile forces in geogrids due to spreading and membrane effects. Similarly, a steeper embankment slope can result a higher spreading effect. In the case of multi-layer geogrids, the lower layer is mainly subjected to the membrane effect whereas the upper layer to spreading effect. Based on these results preliminary design approach has been recommended for practical applications, which however requires further optimisation.

Furthermore, the study includes the investigation of the performance of the pile-like elements when subjected to deformation and bending. It becomes evident that the pile elements can be subjected to a substantial deformation and bending, if a relative soft underground is present. This shows the necessity for adequate design and analysis approaches.

Hans-Georg Kempfert

Berhane Gebreselassie

Vorwort des Herausgebers

Bei Dämmen auf wenig tragfähigem Untergrund ist es zwischenzeitlich Stand der Technik, an der Dammbasis eine Bewehrung aus hochzugfesten Geokunststoffen (Gewebe oder Geogitter) einzulegen. Dabei können die Bewehrungslagen direkt auf den weichen Boden oder über Pfahlelementen angeordnet werden, die die Dammlasten in tiefere, tragfähigere Schichten abtragen.

Die horizontale Bewehrung an der Dammbasis hat die Aufgabe, die vertikalen Dammlasten und die nach außen wirkenden Spreizkräfte aufzunehmen. Dies ist besonders für bewehrte Tragschichten über Pfählen von großer Bedeutung, da sonst die Pfähle/Säulen eine Biegebeanspruchung erhalten, die sie aufgrund des geringen Durchmessers (oftmals unbewehrt) nicht aufnehmen können. Abgesicherte wissenschaftliche Erkenntnisse über Größe und Verteilung der Spreizspannung in Höhe ober- und unterhalb der Bewehrungslagen liegen derzeit noch nicht vor, aus denen dann auch die Beanspruchung abzuleiten ist, die aus der Spreizwirkung bei der Geokunststoffbemessung zu berücksichtigen ist.

Herr Dr.-Ing. Gourage Fahmi hat dafür zunächst den Kenntnisstand zur Spreizbeanspruchung ohne und mit Bewehrung sowie ohne und mit Pfahlelementen zusammengefasst. Ein wesentlicher Teil einer wissenschaftlichen Untersuchungen stellt die Modellversuche in einem relativ großen Maßstab dar, die u. a. auch zur Validierung von numerischen Berechnungen zur Fragestellung vorgesehen waren. Dabei konnte nach gewissen Parameteranpassungen überwiegend eine gute Übereinstimmung zwischen Modellversuchen und FEM-Berechnungen erreicht werden. Lediglich bei den Dehnungen bzw. Zugkräften in den Geogittern über Pfahlelementen ergab die FEM bei dem verwendeten Programmsystem viel zu niedrige Werte. Es wurde dazu in der Arbeit anhand eigener Untersuchungen und Vergleichsergebnissen aus der Literatur eine Hypothese formuliert und zunächst die Berechnungsergebnisse mit einem Faktor angepasst. Mit den durchgeführten Verifikationen stand damit dann ein weitestgehend abgesichertes numerisches Berechnungsmodell zur Verfügung.

Aufbauend auf diesen Vorarbeiten konnten Parameterstudien mit numerischen und analytischen Methoden zur Spreizproblematik durchgeführt werden. Dabei wurden die Randbedingungen und Parametervariationen sinnvoll und für die Fragestellung zutreffend gewählt. Die numerischen Verfahren ergaben vertiefte Erkenntnisse zur Mechanik und zum Verhalten der Konstruktion. Die analytischen Vergleichsberechnungen validierten primär die Güte dieser vereinfachten Ansätze für praktische Berechnungen.

Zusammenfassend wurde festgestellt, dass erwartungsgemäß die Spreizkräfte im Geogitter nahezu linear mit der Dammhöhe anwachsen. Von besonderer Bedeutung für die Größe der Spreizkräfte ist die Steifigkeit der Weichschichten. Dieser Parameter wird bei den bisher bekannten analytischen Berechnungsverfahren nicht berücksichtigt. Je weicher der Untergrund, je größer wird das

Verhältnis zwischen Spreiz- und Membranbeanspruchung. Eine steilere Dammböschung hat erwartungsgemäß ebenfalls eine höhere Spreizwirkung zur Folge. Des Weiteren ergeben sich bei mehrlagigen Geogittern die höheren Beanspruchungen in der unteren Lage aus dem Membranefekt und in der oberen Lage aus dem Spreizeffekt. Zu diesen Erkenntnissen wurden in der Arbeit erste Vorschläge für die praktischen Bemessungen gemacht, die aber noch weiter zu optimieren sind.

Schließlich erfolgt von Herrn Fahmi eine Betrachtung der Pfahlelementbeanspruchung aus Pfahlkopferschiebung und Biegemomenten. Dabei wurde ersichtlich, dass die Pfahlelemente bei hohen Dämmen erhebliche Beanspruchungen erhalten können, wenn relativ weicher Untergrund vorhanden ist, und es zeigt die Notwendigkeit entsprechend abgesicherter Bemessungsverfahren auf.

Hans-Georg Kempfert

Berhane Gebreselassie

Acknowledgements

This research work is developed in the years 2004 to 2007 during my participation as a researcher in the university of Kassel, Germany. The objective of this research was the analysis of stress-deformation behaviour under spreading effect and the investigations were performed on a structural system of basal reinforced embankment resting on soft underground supported by pile-like elements.

The most heartfelt thanks for Prof. Dr.-Ing. Hans-Georg Kempfert, my supervisor, for his richly Favours to me. I'm very thankful to him for his trust and scientific support. Also his encouragement, patience, advices and kindness helped me always in my life in Germany and will help me in my future life.

For his Interest, help, patience, advices, encouragement, kindness and friendship, I find no words but say thanks a lot for my second supervisor Dr.-Ing. Berhane Gebreselassie. He was not only my supervisor, but also as my brother who take care me.

My thanks are also given for Prof. Dr.-Ing. Herbert Klapperich for his interest as well as his acceptance of the co-supervision in this work. Also my thanks for his helpful discussions and comments which helped me so much.

Thanks are also due to Prof. Dr.-Ing. F. Hartmann and Prof. Dr.-Ing. S. Theobald for the participation in the examination committee.

The experimental part of this work was performed in support and help of the labour staff that I thank them all: Mr. Dirk Griesel, Mr. Günter Luleich, and Mr. Thomas Thielemann.

My thanks are given to the staff of the department of geotechnical engineering, who helped me so much and supported my work with the best advices and discussions. My special thanks to my former colleagues Dr.-Ing. B. Somaya, Dr.-Ing. M. Rudolf and Dr.-Ing. C. Heitz who helped me so much with his experience and his scientific discussions and advices.

My thanks are also given to my colleagues in the department who encouraged, helped and supported me Mrs. Christiana Heiss, Ms. Isabelle Joher, Mr. Florian Hörtkorn, Mr. Sebastian Thomas, Mr. Jan Lücking and my room-partner Mr. Patrick Becker who was a very helpful one in my work.

My great thanks are given to the Catholic Academic Exchange Service (KAAD) to the financial support of this work; my special thanks to Dr. C.-M. Walbiner, and Mr. H.-W. Landsberg from KAAD for their support, advice and help.

Finally, I would like to give all sincere thanks to my Family, my Mother, my sister Mary and my brother John for their love, support and their help. My research work is also presented to the spirit of my Father Samir Fahmy, who I'm indebted to him by all my life and all my success.

I would like to express my appreciations and love to my small family; my wife Sarah, for the excessive love and support and patience she gave me during this work. Also the unlimited love and thanks are given to my daughter Christina and my son Samir.

George S. Fahmi Farag

Table of contents

| | |
|--|-----------|
| 1 Introduction | 1 |
| 1.1 Statement of the problem | 1 |
| 1.2 Objectives and methodology | 2 |
| 2 State of the art | 5 |
| 2.1 General..... | 5 |
| 2.2 Lateral forces in embankments | 5 |
| 2.3 Spreading stresses at the embankment base..... | 7 |
| 2.3.1 Magnitude and distribution of shear stresses due to spreading..... | 7 |
| 2.3.2 Horizontal deformations due to shear stresses at the embankment base | 8 |
| 2.4 Spreading stresses in the reinforcement..... | 10 |
| 2.4.1 Embankment with pile-like elements | 10 |
| 2.4.2 Embankment without pile-like elements | 19 |
| 2.5 Pile elements | 21 |
| 2.5.1 General..... | 21 |
| 2.5.2 Stresses and displacements of piles | 21 |
| 2.6 summary..... | 23 |
| 3 Conception and results of model tests | 25 |
| 3.1 General..... | 25 |
| 3.2 Model theory and basics of the own model tests | 25 |
| 3.3 Test materials | 26 |
| 3.3.1 Bearing elements..... | 26 |
| 3.3.2 Model sand..... | 27 |
| 3.3.3 Geosynthetics reinforcement | 28 |
| 3.3.4 Soft layer..... | 31 |
| 3.4 Measuring procedures | 31 |
| 3.4.1 General..... | 31 |
| 3.4.2 Horizontal force measurement..... | 31 |
| 3.4.3 Strain in geosynthetics (Strain gauges, DMS) | 32 |
| 3.4.4 Stress measurement..... | 33 |
| 3.4.5 Displacement measurement | 34 |
| 3.5 Model test variations and extent | 34 |
| 3.6 Model preparation and dimensions | 36 |
| 3.6.1 Model building and external loading | 36 |
| 3.6.2 Model dimensions..... | 38 |
| 3.7 Representation and illustration of the test results | 39 |

| | |
|--|-----------|
| 3.7.1 Evaluation of shear stresses due to own weight at the base of homogeneous sand embankment under slope variations..... | 39 |
| 3.7.2 Stress and deformations in the reference test MT1, homogeneous sand embankment | 42 |
| 3.7.3 Effect of soft underground without geogrid reinforcement | 44 |
| 3.7.4 Comparing the test results of the unreinforced Embankment..... | 47 |
| 3.7.5 Effect of soft underground with geogrid reinforcement | 47 |
| 3.8 Summary | 54 |
| 4 Verification of the model test-results..... | 57 |
| 4.1 General..... | 57 |
| 4.2 Material parameters and constitutive relations | 57 |
| 4.2.1 Constitutive relations of the embankment sand layer | 57 |
| 4.2.2 Constitutive relations for the soft underground | 60 |
| 4.2.3 Numerical formulation of soil/reinforcement interface | 60 |
| 4.2.4 Constitutive relation for the pile-like elements..... | 60 |
| 4.3 FE-Model geometry and boundary conditions | 61 |
| 4.4 Verification of the reference test results with homogeneous sand MT1 | 62 |
| 4.5 Verification of the model test results MT2, unreinforced embankment on soft underground | 65 |
| 4.6 Verification of the model test results MT3, reinforced embankment on soft underground | 66 |
| 4.6.1 Investigation of some in-situ strain results | 67 |
| 4.7 Verification of the model test results MT4, unreinforced embankment on soft underground supported by pile-like elements..... | 68 |
| 4.8 Verification of the model test results MT5, reinforced embankment on soft underground supported by pile-like elements..... | 69 |
| 4.9 Evaluation of the results | 71 |
| 5 Parameter study | 73 |
| 5.1 Objectives and fundamentals of the parameter study | 73 |
| 5.2 Pre-calculation steps | 74 |
| 5.2.1 Studying the interface soil/reinforcement..... | 74 |
| 5.3 Material properties | 75 |
| 5.3.1 General..... | 75 |
| 5.3.2 Geogrid reinforcement..... | 75 |
| 5.3.3 Embankment fill | 76 |
| 5.3.4 Underground layer | 76 |
| 5.3.5 Pile-like supporting elements..... | 77 |
| 5.4 External load | 78 |

| | | |
|----------|---|------------|
| 5.5 | Pre-calculation steps for the numerical analysis..... | 78 |
| 5.5.1 | General..... | 78 |
| 5.5.2 | Steps to build a membrane model by FEM..... | 79 |
| 5.5.3 | Steps to determine the force due to spreading effect by FEM..... | 80 |
| 5.6 | Model dimension and variation matrix..... | 81 |
| 5.7 | Results of the numerical parameter study..... | 84 |
| 5.7.1 | General..... | 84 |
| 5.7.2 | Results of tensile forces under variation of the embankment height..... | 85 |
| 5.7.3 | Results of tensile forces under variation of the underground stiffness..... | 90 |
| 5.7.4 | Results of tensile forces under variation of the embankment slope..... | 94 |
| 5.7.5 | Results of tensile forces under variation of the geogrid reinforcement layers | 97 |
| 5.8 | Summary and evaluation of the numerical parameter study..... | 102 |
| 5.9 | Comparing the FEM-results with some available analytical methods..... | 103 |
| 5.9.1 | Objectives | 103 |
| 5.9.2 | Determination of the membrane forces in reinforcement due to arching effect. | 104 |
| 5.9.3 | Analytical methods to determine the total forces applied in reinforcement | 105 |
| 5.10 | Summary of the analytical calculation | 110 |
| 6 | Development of a modified analytical method | 111 |
| 6.1 | General..... | 111 |
| 6.2 | Empirical modification of the sliding soil wedge and the spreading force..... | 112 |
| 6.2.1 | Horizontal active earth pressure force due to own weight, E_{agh} | 113 |
| 6.2.2 | Horizontal active earth pressure force due to external load E_{aph} | 114 |
| 6.2.3 | Determination of the tensile force in reinforcement and estimation of a reference parameter-model | 115 |
| 6.3 | Determination of the earth pressure forces in the case of piled embankment..... | 116 |
| 6.3.1 | Determination of the angle θ according to the results of the parameter study ... | 116 |
| 6.3.2 | Derivation of the factors f_{Es} and f_{β} | 118 |
| 6.4 | Comparison of the modified analytical spreading forces with FEM-results and <i>EBGEO</i> (2007)..... | 121 |
| 6.4.1 | Spreading forces under variation of the underground stiffness | 122 |
| 6.4.2 | Spreading forces under variation of the embankment slope..... | 124 |
| 6.5 | Comparison of the modified analytical total forces with FEM-results and <i>EBGEO</i> (2007)..... | 126 |
| 6.5.1 | Determination of the membrane force | 126 |
| 6.5.2 | Total tensile force in reinforcement under variation of the underground stiffness | 127 |
| 6.5.3 | Total tensile force in reinforcement under variation of the embankment slope . | 130 |
| 6.5.4 | Spreading effect on the pile elements | 132 |

| | |
|--|------------|
| 6.6 Summary to the modified method | 133 |
| 7 Summary | 135 |
| Zusammenfassung..... | 140 |
| 8 References | 147 |

Appendices

Appendix A: Earth pressure forces

Appendix B: Model test results

Appendix C: Verification of the model test-results

Appendix D: Parameter study

Appendix E: List of frequently used symbols and expressions

1 Introduction

1.1 Statement of the problem

The construction of road/railroad embankments on weak or very soft soils such as peat is normally treated using a soil replacement method or by introducing pile-like-elements into the soft layer to partially support the embankment. In the slope zone of the embankment the underground is subjected to additional lateral stresses due to the spreading effect of the slope. In practice, the spreading stresses are assumed equal to the active earth pressure at a section through the shoulder of the embankment. The lateral spreading stresses influence the stability of the bearing system and possibly may result a horizontal displacement of the pile-like-elements or a horizontal displacement of the toe of the embankment slope. In most cases the pile-like-elements are not reinforced and hence a small horizontal displacement may cause damage on them. *Kempfert et al. (1997)* and *Zaeske/Kempfert (2002)* pointed out that the horizontal forces must be transferred to reinforced elements, such as horizontally lied geosynthetic reinforcement. The reinforcement must hold all the horizontal forces and avoid the displacements of the pile head through the bond effect with the soil. These horizontal forces are primary calculated using the effective earth pressure on the slope zone. Figure 1.1 shows the structural system and the load transfer mechanism of the lateral spreading.

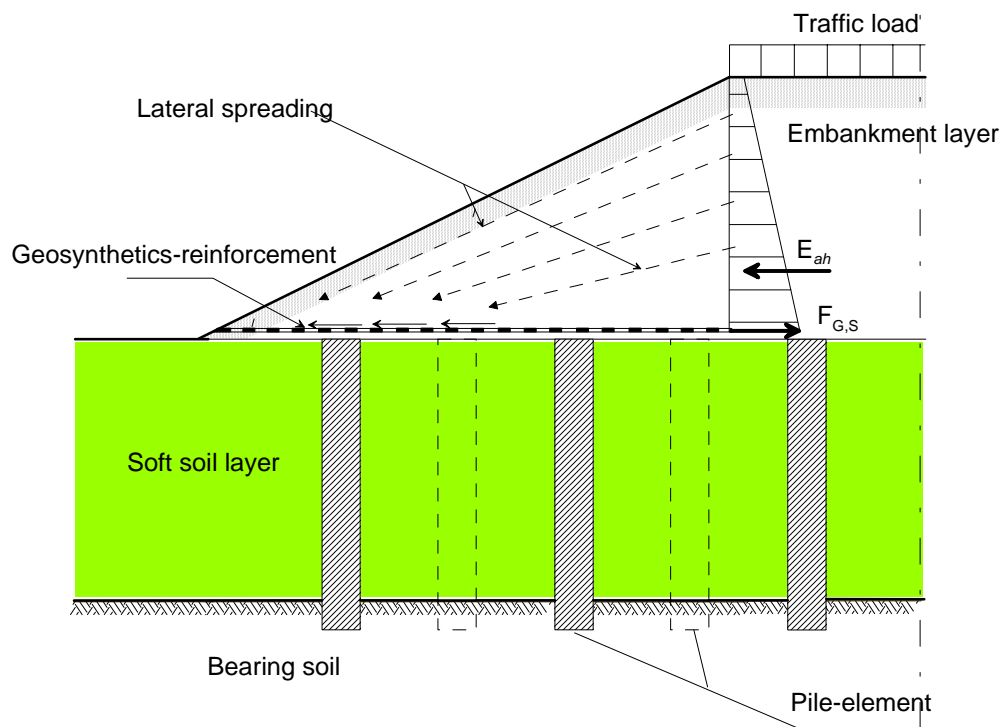


Figure 1.1: Lateral spreading of a reinforced embankment

With increasing embankment heights, the spreading forces, and as a result, the tensile forces on the reinforcement will be dramatically increased and lead to higher deformations in the system. Both the membrane effect (arching effect) and the spreading effect influence the behaviour of the bearing system (such as pile elements) and the tensile forces on the reinforcement. Therefore, there is a high need to analyse and evaluate these effects for higher embankments. Moreover, the behaviour of the bonded body (material behaviour of soil-reinforcement interaction) must be accurately described in order to attain the real stress-strain relations in such zones.

The determination and calculation of spreading stresses is illustrated in the *EBGEO (2007)* and the *British standard BS 8006 (1995)*. The calculation is based on the active earth pressure in the slope zone of the embankment. The basis for the above recommendations is the classical analytical or graphical methods of *Engesser (1880)*, *Rendulic (1938)*, *Culmann/Schmidt (1966)* and *Brauns (1980)*. Furthermore, the lateral spreading in embankments can be analysed using finite element methods.

Many authors had investigated the spreading effect on the reinforced embankments using analytical and numerical methods. However, there are significant discrepancies between the tensile stresses calculated using analytical and numerical methods. Hence, it is worthwhile to find out the cause of these discrepancies and to investigate the factors and parameters which control the spreading stresses and the tensile force of the embankment. The relation between the membrane forces and the spreading forces in reinforcement, especially for higher embankments has not also been clearly defined for the case of higher embankments. The increasing in spreading forces are very large compared to that of membrane forces, which in turn affect the horizontal force exerted on the head of pile elements. The unreinforced piles here are subjected to some horizontal displacements and tensile stresses. Therefore, the piles must sustain these stresses or the stresses must be transferred to other elements such as geosynthetics reinforcement. The accurate proportion of the stresses that can be sustained by reinforcement and that remains by the pile elements requires a further investigation, that include the variation of embankment height, tensile stiffness of the reinforcement, the underground conditions, etc.

1.2 Objective and methodology

In this research the influences of the spreading stresses in the slope zone of a reinforced embankment and partly supported by pile-like elements has been investigated to complement the

lack of knowledge in the determination of accurate stresses due to spreading forces by means of measuring actual earth pressure in the slope zone and hence, the shear stresses at embankment base. The determination of the shear stresses and the horizontal deformations at the embankment base, as well as the tensile forces in the geosynthetics reinforcement has been achieved through a series of large-scale model tests under variation of underground conditions. Similarly, the horizontal force on head of pile element due to spreading effect has also been measured and analysed.

The model tests are extension of the work of *Heitz (2006)*. A series of model tests has been carried out for different cases of base reinforcement and different underground conditions.

The effect of the embankment slope and the shear stresses at the slope base has been investigated first by a model test with homogeneous soil. An embankment on soft underground without pile-like elements has also been modelled and investigated in order to give a clear view of the FEM-calibration process and to investigate the role of pile-like elements in supporting the system. The model test with pile-like elements has also been carried out as the main structural system in the study.

The large-scale model test-results have been verified using a finite element method. The goal of the validation processes is to calibrate the soil parameters obtained from laboratory tests and derive suitable parameters for the constitutive soil model used in the FE-computation. It will also help to determine the parameters that could not be directly measured from the model tests and to extend the model test results to the prototype.

Some of the factors related to the reinforced embankment on soft soil might not be considered in analytical methods. Therefore, to identify all the factors influence the performance of reinforced embankment on soft soil, an extensive parameter study has been carried out by means of keeping one or more parameters constant and varying the others. The variation includes the effect of different underground conditions such as the tensile stiffness of the reinforcement, slope of the embankment and embankment height. The parameter study has given a clear overview of all the factors and the relations between each other as well as the role each parameter it plays in determining the tensile forces of the reinforcement.

Furthermore, a comparison has been carried out between the results of FE-computations and some analytical methods such as *Love et al. (2003)*, *Geduhn/Vollmert (2005)* and *EBGEO (2007)* in regard to the tensile forces in the reinforcement. The comparative analysis has also extended to include the study of the membrane and spreading effect separately, in order to find out which factors and parameters will control the results in each system.

A modified analytical method has been introduced and estimated to determine the analytical spreading force sustained by the reinforcement. The modified method could be applied to get a qualitative determination of the spreading and total force in reinforcement in the case of high and very high embankments. The different parameter variations such as the underground stiffness and the embankment slopes could also be considered in this study.

The following are further objectives of the research:

- Investigation of the most accurate values of the earth pressure used in the analytical methods.
- Analysis of the vertical distribution of the traffic loading at the level of the arching height, to investigate the membrane effect on the reinforcement and its relation with the spreading effect analytically.
- Study the relation of the membrane and the spreading forces in reinforcement under variation of system parameters.
- Analysis of the stability of the embankment system using multi-layer geosynthetics reinforcement.
- Investigation of the stress-strain behaviour of the unreinforced pile elements under various boundary conditions such as different underground conditions, embankment height and reinforcement stiffness. This will include the determination of the bending moments and horizontal displacements of pile elements due to the spreading effect and the role of the geosynthetics reinforcement to reduce these deformations in pile elements.

2 State of the art

2.1 General

Although the study focuses mainly on the investigation of spreading effect of an embankment on piled underground, this chapter presents the state of the art of the spreading effect in general. It includes the mechanisms of the lateral forces in the embankment, the determination of the horizontal earth pressure, the stress-deformation behaviour of the embankment, the performance of the pile elements, etc. There are plenty of studies in the literature regarding the spreading effect, however, only few of them have been presented and analysed in this study. Furthermore, a comparison has been made between reinforced and unreinforced embankments as well as piled and unpiled underground.

2.2 Lateral forces in embankment

The roadway or railway embankments over soft soils are subjected not only to the vertical loadings due to traffic and own weight, but also to horizontal forces due to the spreading effect of the soil slope (Figure 2.1). The spreading effect is caused by the spreading of the traffic loads and the horizontal components of the earth pressure and leads to some horizontal deformations in the embankment toe, and as a result, vertical deformations (settlement) may occur in the central zone of the embankment.

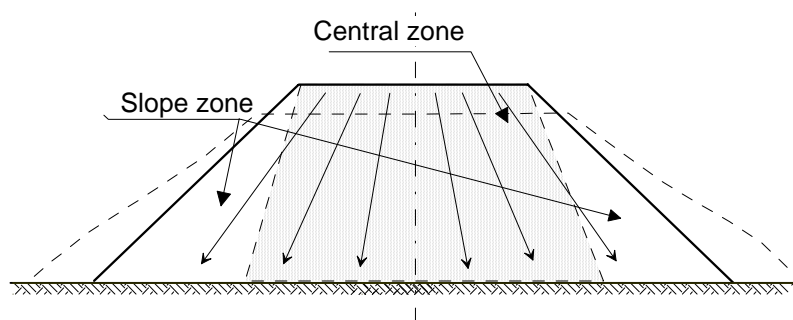


Figure 2.1:
Spreading effect in embankment

The spreading stresses concentrate at the toe of the slope and lead to a horizontal displacement. *Kempfert et al. (1997)* concluded that these lateral forces must be transferred to geosynthetic reinforcement at the base of the embankment which can prevent the embankment from sliding. Figure 2.2 illustrates the mechanism of load transfer of the lateral forces to the reinforcement. The lateral earth pressure forces develop outward shear stresses at the base. Without reinforcement the stresses can cause lateral displacement in the slope zone.

The reinforcement must sustain the shear stresses through the bond between the soil and reinforcement and through its tensile strength of reinforcement.

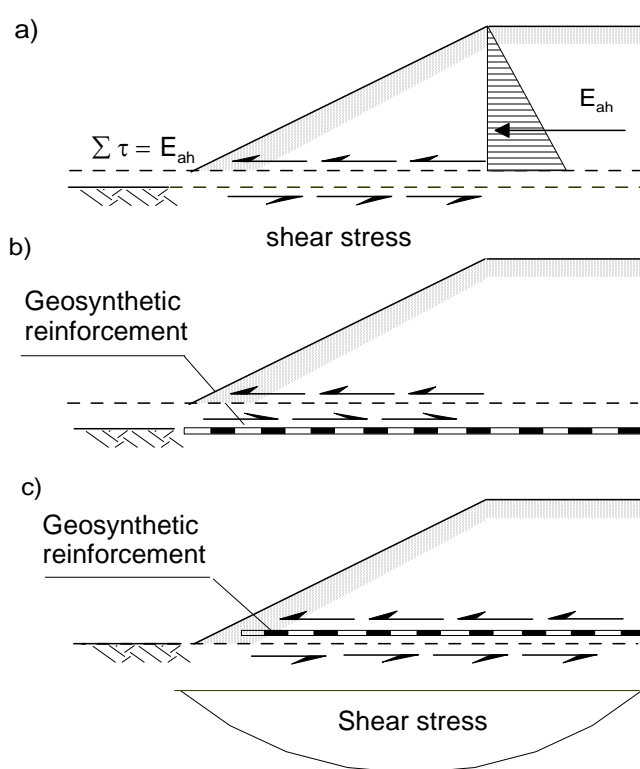


Figure 2.2:

Reinforcement in an embankment on soft underground:

- Spreading forces and shear stress at embankment base;
- Reinforcement sustains the stresses;
- Effect of stress on underground

The design stresses in the reinforcement include the stresses arising from lateral sliding and from rotational slip movements and extrusion. *Ochiai et al. (1996)* stated that the minimum factor of safety for sliding stability should be $FS \geq 2.0$ and for rotational stability $FS \geq 1.2 \sim 1.3$.

The draft of German recommendation *EBGEO (2007)* defined the spreading effect as the lateral forces resulting from the horizontal active earth pressure that acts from the embankment crest to the basal reinforcement. This active earth pressure is a function of the height of the embankment and the active earth pressure coefficient K_{ah} . The magnitude and distribution of the active earth pressure in the slope zone depend on plenty of parameters such as the type of fill soil, the slope angle and the height of the embankment. The British Standard *BS 8006 (1995)* specified the lateral sliding as an ultimate limit state and stated that the bond between the reinforcement and the soil must be adequate to generate the limit state tensile stress in the reinforcement. The proof of stability against lateral spreading would be established through many methods depending on the type of the soil. The methods developed by *Rendulic (1938)* and *Brauns (1980)* are applicable to cohesionless soils, where as the graphi-

cal method of *Engesser (1880)* is applicable to the cohesive soils. *Schwarz (1963)* had also modified the method of *Rendulic* to determine the stability in an inclined foundation basis.

2.3 Spreading stresses at the embankment base

2.3.1 Magnitude and distribution of shear stresses due to spreading

At the base of the embankment the lateral forces cause outward shear stresses on the reinforcement. To determine the shear stresses, an infinite vertical slice in the slope zone under *Rankine* case is analysed for equilibrium condition as shown in Figure 2.3.

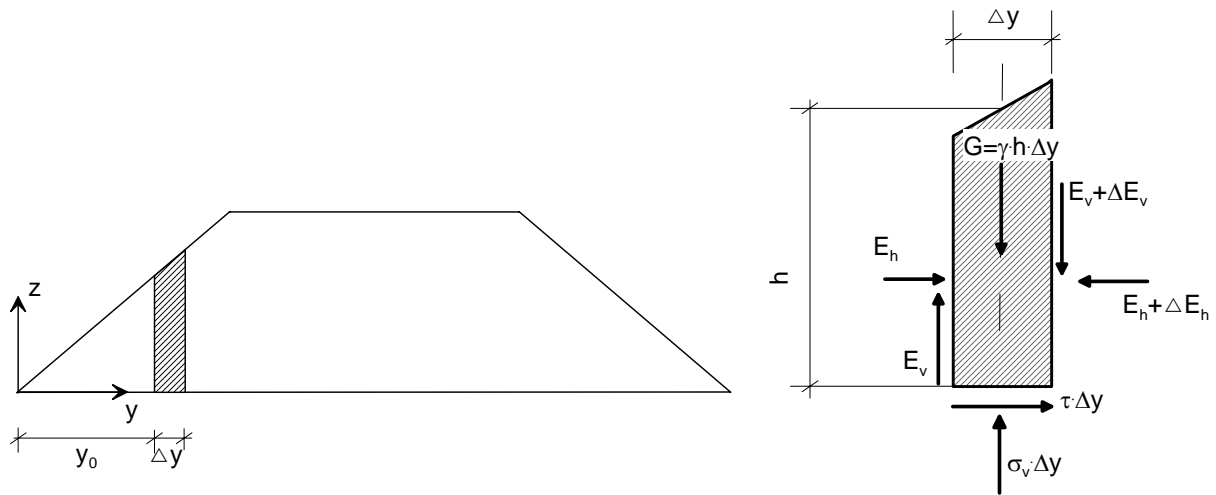


Figure 2.3: Equilibrium of forces on an infinite vertical slice in slope zone

Equilibrium of all forces on the vertical slice with a thickness Δy implies

$$\sum H = 0: \quad \tau \cdot \Delta y - \Delta E_h = 0 \quad \Rightarrow \quad \tau \cdot \Delta y = \Delta E_h \quad (2.1)$$

$$\sum V = 0: \quad \sigma_v \cdot \Delta y - \gamma \cdot h \cdot \Delta y - \Delta E_v = 0 \quad \Rightarrow \quad \sigma_v \cdot \Delta y = \Delta E_v + \gamma \cdot h \cdot \Delta y \quad (2.2)$$

Hence, the shear stresses due to lateral spreading can be written as a function of the earth pressure force as follows:

$$\tau = \frac{\partial E_h}{\partial y} \quad (2.3)$$

$$\sigma_v = \gamma \cdot h + \frac{\partial E_v}{\partial y} \quad (2.4)$$

The horizontal earth pressure force in the slope zone can be estimated using the method of *Rendulic (1938)* in the case of an embankment with a horizontal base, or the method of *Schwarz (1963)* in the case of an inclined base. The classical earth pressure theory is used to determine the horizontal active earth pressure force, (See Appendix A.1).

The determination of magnitude and direction of the earth pressure on each section in the slope zone would be graphically estimated by *Engesser's* graphical method. In this method the earth pressure vector, which is determined for each section, can be divided into horizontal and vertical components from the force equilibrium of each section, (see Appendix A.2).

From the resultant earth pressure force on every section, the curve and the equation which represent earth pressure force can be deduced. Hence, The distribution of the normal and the shear stresses can then be determined from the first derivative of the earth pressure forces as shown in Figure 2.4 and Figure 2.5.

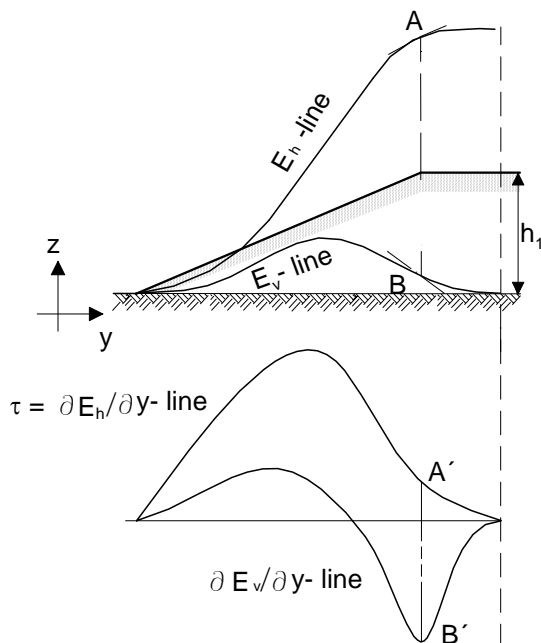


Figure 2.4:

Distribution of horizontal and vertical stresses and their derivatives

Figure 2.5:

Distribution of the shear and normal vertical stresses in the slope zone

2.3.2 Horizontal deformations due to shear stresses at the embankment base

The known approaches to compute the horizontal deformations in the embankment base apply only for the case of unreinforced embankments. The horizontal deformation at the embankment base due to spreading pressure results from the shear stresses at this level according to *Engesser (1880)*. The distribution of shear stresses is illustrated in Figure 2.5. The horizontal deformation due to spreading was also investigated by *Tölke (1990)* (cited in *GDA (1997)*). *Geduhn/Vollmert (2005)* derived an empirical linear relation for determination of the maxi-

imum horizontal displacement at the slope toe in the case of reinforced embankment. The deformation is a function of the maximum strain in the geosynthetics at the slope crest. Table 2.1 represents the two methods to determine the horizontal deformation due to spreading effect in the case of reinforced and unreinforced embankment.

Table 2.1: Determination of horizontal displacement in the slope zone due to spreading effect in the case of unreinforced and reinforced embankment

| <i>Tölke (1990)</i> | | | | | | | | | | | | | | | | |
|-------------------------|---|------|-----|------|---|---|----------------|------|------|-----|-----|----------------|------|-----|-----|------|
| | | | | | | | | | | | | | | | | |
| Horizontal displacement | <p>For the elastic-isotropic half space and according to the influence line of shear stresses the horizontal deformation is given by:</p> $v_y = f(\tau)$ $v_y(\tau_0) = \frac{-\tau_0}{4 \cdot \pi \cdot G} \sum_{i=1}^4 (-1)^i \left[(y + y_i) \cdot \operatorname{arctanh} \frac{x_i}{R_i} + 2x_i \cdot \operatorname{arctanh} \frac{y + y_i}{R_i} \right]$ $+ (1 - 2\nu) \cdot (y + y_i) \cdot \operatorname{arctanh} \frac{x_i}{R_i}$ <p>with $R_i^2 = (y + y_i)^2 + x_i^2$</p> <table border="1" style="margin-left: auto; margin-right: auto;"> <tr> <td style="text-align: center;">i =</td> <td style="text-align: center;">1</td> <td style="text-align: center;">2</td> <td style="text-align: center;">3</td> <td style="text-align: center;">4</td> </tr> <tr> <td style="text-align: center;">y_i</td> <td style="text-align: center;">-a/2</td> <td style="text-align: center;">-a/2</td> <td style="text-align: center;">a/2</td> <td style="text-align: center;">a/2</td> </tr> <tr> <td style="text-align: center;">x_i</td> <td style="text-align: center;">-b/2</td> <td style="text-align: center;">b/2</td> <td style="text-align: center;">b/2</td> <td style="text-align: center;">-b/2</td> </tr> </table> | i = | 1 | 2 | 3 | 4 | y _i | -a/2 | -a/2 | a/2 | a/2 | x _i | -b/2 | b/2 | b/2 | -b/2 |
| i = | 1 | 2 | 3 | 4 | | | | | | | | | | | | |
| y _i | -a/2 | -a/2 | a/2 | a/2 | | | | | | | | | | | | |
| x _i | -b/2 | b/2 | b/2 | -b/2 | | | | | | | | | | | | |
| Horizontal strain | $\varepsilon_h = dv_y / dy$ | | | | | | | | | | | | | | | |
| Notes | Determination of the horizontal displacement in the slope zone of unreinforced embankment as a function of influence line of shear stresses τ | | | | | | | | | | | | | | | |

Table 2:1 (continued)

| Geduhn/Vollmert (2005) | |
|-------------------------|---|
| | |
| Horizontal displacement | $v_{y,\max} = \frac{\varepsilon_{\max}}{2} \cdot L = \frac{\varepsilon_{\max}}{2} \cdot h \cdot n$ <p>The influence line of horizontal displacement:</p> $v_y = \frac{E_{sp}}{J} \cdot \frac{L-y}{L} \cdot y$ |
| Strain in reinforcement | $\varepsilon_{\max} = \frac{F_{G,S}}{J}$ |
| Notes | Determination of the horizontal displacement in the slope zone of reinforced embankment as a function of the strain in reinforcement. The strain in reinforcement depends on the maximum spreading forces according to <i>Geduhn/Vollmert (2005)</i> in Section 2.4.2.2 |

τ_0 the mean segmental shear stress at any point along the influence line of shear stress;

G the shear modulus $G = E/2 \cdot (1-\nu)$, and ν is Poisson ratio.

2.4 Spreading stresses in the reinforcement

2.4.1 Embankment with pile-like elements

2.4.1.1 General

To increase the stability of the soft foundation soil and to control the post-construction settlement of such soil, pile-like elements may be introduced into the soft soil layer. Herein, the base reinforcement is used to transfer the embankment and traffic load onto the piles.

On the other hand, the pile elements may not be able to sustain the horizontal forces, which resulted from the spreading effect of the slope zone as shown in Figure 2.6 where they are usually unreinforced. Therefore, according to *Kempfert et al. (1997)* the geosynthetic reinforcement must resist all the horizontal forces and the horizontal deformations due to shear stresses at the base of the embankment.

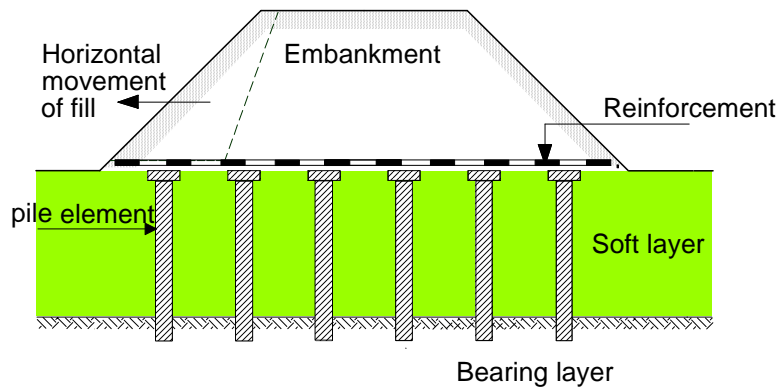


Figure 2.6:
Spreading effect on basal reinforced embankments with pile-like elements

The British standard *BS 8006 (1995)* also recommends that the reinforcement should resist the horizontal force due to lateral sliding and it should be strain compatible with allowable lateral pile movements thereby eliminating the need for raking piles. The tensile load in the reinforcement can be estimated using the horizontal active earth pressure. The tensile force in the reinforcement in the case of pile elements has two main components. These are the tensile forces due to spreading effect and due to membrane effect or arching effect between pile elements. Different authors use different approaches to analyse these effects. Some of the analysis methods will be discussed and analysed hereunder.

2.4.1.2 Analytical methods and approaches to investigate the spreading effect

The tensile force in reinforcement due to spreading effect and the relation between that force and the force due to membrane effect in reinforcement and arching effect in soil between pile elements has been investigated by different approaches and methods. *BS 8006 (1995)* as well as *EBGEO (2007)* is considered of the main approaches to analyse the stress-strain behaviour of reinforcement and structural elements in the case of piled embankments. Other analytical methods presented by *Zaeske (2001)*, *Maihold et al. (2003)*, *Love et al. (2003)* and *Geduhn/Vollmert (2005)* are based on the two approaches and analysed the relationship between spreading and membrane forces. Table 2.2 represents some of these analytical methods, where the tensile force in reinforcement is represented by symbol F_G deviated from “E” in *EBGEO*.

Table 2.2: The Analytical methods to investigate the spreading effect in the case of reinforced embankment on soft underground supported by pile-like elements

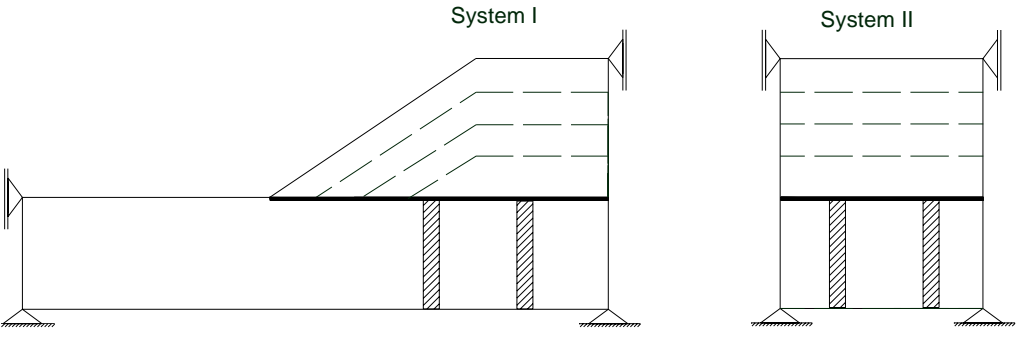
| <i>Zaeske (2001)</i> | |
|--|--|
|  | |
| Tensile force in reinforcement | <p>System I $\rightarrow F_G = F_{G,S} + F_{G,M}$</p> <p>System II $\rightarrow F_G = F_{G,M}$</p> <p>The tensile forces in the reinforcement both in the central zone and the slope zone of the embankment had been investigated by <i>Zaeske (2001)</i> using the finite element method (FEM). He investigated two systems to determine the tensile forces in the reinforcement in each system. The resulting tensile forces in the reinforcement can be explained in the following notes.</p> |
| Notes | <ul style="list-style-type: none"> The tensile forces in the system I represent the stresses due to both membrane effect in the reinforcement over the pile elements and the spreading effect in the slope zone, while system II provides tensile forces due to the membrane effect only. The difference between the two curves of system I and system II represents the tensile force in the reinforcement due to spreading effect in the slope zone. <p>With increasing pile stiffness E_P as compared to the stiffness of the soft underground E_u the two curves increase further and remain parallel, which shows that the spreading effect remains constant.</p> |

Table 2.2 (continued)

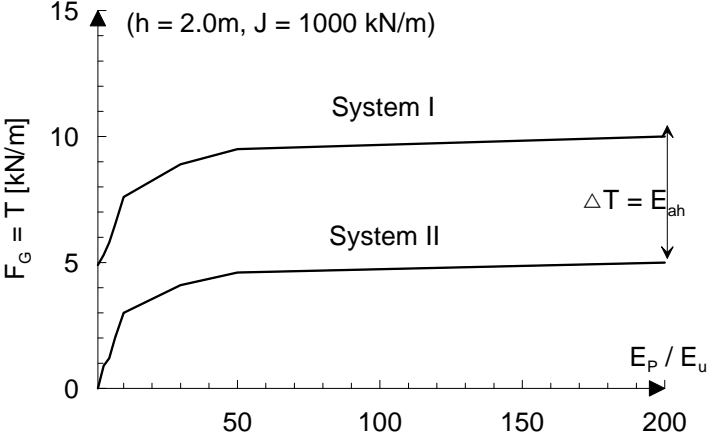
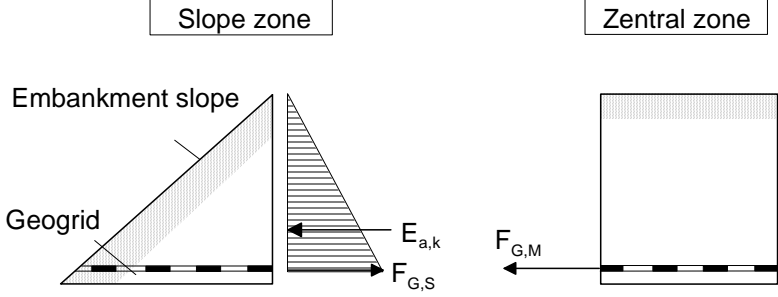
| | |
|-------------------------------------|---|
| <p>Notes</p> | <p>The separation of the systems to filter out the membrane effect (system II) cannot supply the correct membrane effect, especially for the part of geogrid that lies in the slope zone. In other words, the membrane effect in this zone had not been considered and computed in this system. The spreading stresses increase substantially with increasing embankment height, so that the relationship between the tensile forces in the two systems I and II must be reanalysed in this case.</p>  |
| <p><i>Maihold et al. (2003)</i></p> | |
| |  |
| <p>Notes</p> | <p><i>Maihold et al. (2003)</i> investigated the relation between the membrane forces in the central zone of the embankment $F_{G,M}$ due to the vertical stresses and the spreading force in the slope zone $F_{G,S}$ due to the spreading effect from the horizontal earth pressure force $E_{a,k}$.</p> |

Table 2.2 (continued)

| | |
|-------|---|
| Notes | <p>Three possibilities controlling the relation between the membrane force and the active earth pressure has been identified comparing with the earth pressure at rest $E_{0,k}$.</p> <p>a) $E_{a,k} < F_{M,k} < E_{0,k}$</p> <p>Here the tensile force due to membrane effect is greater than that due to active earth pressure but smaller than that due to earth pressure at rest. Enough anchoring length of the reinforcement in the slope zone can balance the tensile forces. In this case, the effective pressure in the embankment axis will be the passive earth pressure.</p> <p>b) $F_{M,k} < E_{a,k}$</p> <p>Here the reinforcement can be pulled out of the slope zone, as the active earth pressure is greater than the tensile strength from the membrane effect. In this case the reinforcement must be designed for earth pressure at rest.</p> <p>c) $E_{0,k} < F_{M,k}$</p> <p>Here the membrane is very stiff and the reinforcement can be pulled in direction of the embankment axis, the tensile force must be developed through the friction between the reinforcement and the soil. The anchoring length must also be large enough to supply anchorage against the membrane effect. The passive earth pressure will be effective in this case.</p> |
|-------|---|

Table 2.2 (continued)

| <i>Love et al. (2003)</i> | |
|--------------------------------|--|
| | |
| Tensile force in reinforcement | <p><u>Total force in reinforcement:</u> $F_G = \max \begin{cases} F_{G,M} \\ F_{G,S} \end{cases}$</p> |
| Notes | <p>According to <i>Love et al. (2003)</i>, the tensile force in the reinforcement is the larger of the tensile forces due to the membrane and the spreading effect under assumption of a free section system with frictionless base.</p> <p>Similarly, they assumed a value of the earth pressure coefficient K, where $K_a < K < K_p$ and it is dependant on the state of the membrane effect.</p> <p><i>Klobe (2007)</i> adopted the same concept by considering only the larger tensile force due to membrane- or spreading effect.</p> |
| <i>Geduhn/Vollmert (2005)</i> | |
| | |

Table 2.2 (continued)

| | |
|--------------------------------|--|
| Tensile force in reinforcement | $E_{ah} = \frac{1}{2} \cdot \gamma_1 \cdot h_1^2 \cdot k_{ah} + p \cdot k_{ah} \cdot h_1$ $R_u = \frac{1}{2} \cdot h_1^2 \cdot n \cdot \gamma_1 \cdot \mu \cdot \tan \varphi_2$ <p>Spreading force: $F_{G,S} = E_{ah} - R_u$</p> <p>Total force in reinforcement: $F_G = F_{G,S} + F_{G,M}$</p> <p>where</p> <p>μ friction coefficient of the reinforcement with the underground and</p> <p>φ_2 internal friction angle of the underground.</p> |
| Notes | <p><i>Brendlin (1962)</i> analysed the safety of the system in the slope zone considering the base friction. He stated that the safety factor of the system at the slope toe under the own weight of the embankment is $\eta = 1.0$. In the direction of the slope crest, the safety factor increases with the increasing of the base friction R_u. Applying the base friction according to <i>Brendlin (1962)</i> in the case of an embankment over vertical supporting elements, the system will not be safe with a factor of safety $\eta = 1.0$. In this method the horizontal displacements in the embankment body can be transferred to the embankment base creating unallowable horizontal forces on the head of the vertical supporting elements. <i>Geduhn (2005)</i> and <i>Geduhn/Vollmert (2005)</i> developed this method by increasing the safety factor to $\eta = 1.3$ instead of $\eta = 1.0$. The required base friction angle can be obtained from:</p> $\delta_{req} = \arctan(1.30 \cdot K_{ah} \cdot \tan \beta)$ <p>where β is the embankment slope angle</p> <p>They concluded that the spreading effect in the slope zone is developed through the friction at the embankment base R_u. This means that the geosynthetic reinforcement must develop the deformations at the embankment base. Hence, the required tensile force $F_{G,S}$ in reinforcement due to spreading effect can be estimated from the horizontal active earth pressure. The total tensile force in reinforcement F_G is resulted from both the membrane force $F_{G,M}$ and spreading force $F_{G,S}$.</p> |

Table 2.2 (continued)

| <i>EBGEO (2007)</i> | |
|---|---|
| | |
| <p>Left: Forces in reinforcement after <i>Heitz (2006)</i>, right: Spreading effect after <i>EBGEO (2007)</i></p> | |
| <p>Tensile force in reinforcement</p> | $\Delta E_{G,k} = E_{ah,G,k} = \left(\frac{1}{2} \cdot cal\gamma_{1,k} \cdot (h_1 - z) + p_{G,k} \right) \cdot (h_1 - z) \cdot K_{agh} \text{ (Details in App. A.1)}$ $\Delta E_{G+Q,k} = E_{ah,G+Q,k} = \left(\frac{1}{2} \cdot cal\gamma_{1,k} \cdot (h_1 - z) + p_{G+Q,k} \right) \cdot (h_1 - z) \cdot K_{agh}$ <p><u>Tensile force due to spreading effect:</u></p> <p><u>Method's option 1:</u> Spreading force is computed from the horizontal active earth pressure and added to the membrane force.</p> $F_{G,S,k} = \Delta E_{G,k} \text{ where } \Delta E_{G,k} = E_{ah,G,k}$ $F_{G+Q,S,k} = \Delta E_{G+Q,k} \text{ where } \Delta E_{G+Q,k} = E_{ah,G+Q,k}$ <p>The index <i>G</i> and <i>Q</i> represents the dead load and live load respectively</p> <p><u>Method's option 2:</u> The force in reinforcement is computed as the maximum of membrane or spreading force (in Method's option 1).</p> $F_{G,k} = \max \left\{ \begin{matrix} E_{ah,G,k} \\ F_{M,G,k} \end{matrix} \right. \text{ as well as } F_{G+Q,k} = \max \left\{ \begin{matrix} E_{ah,G+Q,k} \\ F_{M,G+Q,k} \end{matrix} \right.$ |
| <p>Notes</p> | <p>According to <i>EBGEO (2007)</i> the total tensile force in a geosynthetic-reinforcement is defined as the force at the limit state that includes both the tensile force due to membrane effect and spreading effect. In the method's option 2, there must be additionally a proof against deformations of the vertical bearing elements, for example by numerical methods.</p> |

The spreading force after *EBGEO (2007)* is determined using the active earth pressure force at a section through the slope crest down to the reinforcement level. The recommendation emphasise however that the exact effective earth pressure needs more investigations in the case of higher embankments.

The design spreading force acting on the reinforcement according to the concept of partial safety factors in *DIN 1054* is given by:

$$F_d = E_{k,G} \cdot \gamma_G + (E_{k,G+Q} - E_{k,G}) \cdot \gamma_Q \quad (2.5)$$

The verification of geosynthetics reinforcement for the ultimate limit state ULS requires to satisfy the inequality:

$$R_{B,d} \geq \Delta F_d + F_{M,d} \quad (2.6a)$$

where

ΔF_d design load value due to spreading effect;

$F_{M,d}$ design loading value due to the membrane effect in the reinforcement;

$R_{B,d}$ design strength of the geosynthetics reinforcement.

The design strength of the geosynthetics reinforcement can be estimated from

$$R_{B,d} = \frac{R_{B,k0,5\%}}{A_1 \cdot A_2 \cdot A_3 \cdot A_4 \cdot A_5} \cdot \frac{\eta_M}{\gamma_M} \quad (2.6b)$$

where

$R_{B,k0,5\%}$ the characteristic short time strength of the reinforcement at (5 % quantile),

γ_M the partial material factor and

$\eta_M = 1.1$ is a model factor for modifying the safety level in the ultimate limit state.

A_1 reduction factor for considering the creep effect

A_2 reduction factor considering possible damage during structure operations

A_3 reduction factor considering manufacturing processes (bonding, ...)

A_4 reduction factor considering environment's effect (weathering, chemicals,..)

A_5 reduction factor considering the effect of dynamical influences

In practice, the proof of safety of the horizontal bearing capacity of the pile elements is enough to not consider the Equation 2.6a. The proof of the bearing capacity of the pile elements in ULS is given by:

$$R_d \geq F_{s,d} \quad (2.6c)$$

where

R_d design bearing capacity of the pile elements;

$F_{s,d}$ design effective stress according to equation 2.5.

2.4.2 Embankment without pile elements

2.4.2.1 General

The use of reinforcement in the case of embankments on a weak soil layer without pile-like elements has the function to transfer the load to the underground soil as uniformly as possible and thus to reduce differential settlement and improve the stability and bearing capacity of the embankment fill.

Many authors analysed the stress-strain behaviour of the structural system of the basal reinforced embankment rested soft underground. The forces in reinforcement due to the own weight of embankment and the external loads have been analysed and investigated by *Houlsby et al. (1989)*, *Van Impe/Silence (1989)*, *Espinoza/Bray (1995)*, *Rowe/Li (2002)*, *Rowe/Li (2005)* and others.

The spreading effect on reinforcement in the slope zone of an embankment on soft underground without pile elements has been analysed and presented in different approaches such as *Ochiai et al. (1986)*, *BS 8006 (1995)* and *EBGEO (2007)*.

In Table 2.3, one example of the method of analysis of the tensile force in reinforcement in the slope zone due to spreading effect is presented.

Table 2.3: Spreading effect in the slope zone of an embankment on soft underground

| <i>Ochiai et al. (1986)</i> | |
|--|---|
| | |
| <p>Factor of safety and Tensile force in reinforcement</p> | <p><u>Factor of safety against lateral sliding</u></p> $FS = R_u / E_{ah}$ <p>where</p> $R_u = 0.5 \cdot \gamma_1 \cdot n \cdot h_1^2 \cdot \tan \varphi_{sg}$ $E_{ah} = 0.5 \cdot K_{ah} \cdot \gamma_1 \cdot h_1^2$ <p>where</p> <p>φ_{sg} friction angle between reinforcement and soil and</p> <p>n slope.</p> <p><u>Spreading force in reinforcement</u></p> $F_{G,S} = E_{ah} - R_u$ |
| <p>Notes</p> | <p>According to <i>Ochiai et al. (1986)</i>, the contribution of the geosynthetics reinforcement to the stability of an embankment against rotational slope failure arises from its tensile strength; where as its contribution to stability against sliding failure arises from the frictional resistance between the soil and the reinforcement. According to them the minimum factors of safety against slip failure and lateral sliding should be $FS \geq 1.2 \sim 1.3$ and $FS \geq 2.0$ respectively.</p> <p>The tensile force in reinforcement due to lateral spreading is calculated as the horizontal earth pressure force considering a base friction between the reinforcement and the adjacent soil.</p> |

2.5 Pile elements

2.5.1 General

The main function of the pile elements in soft soil is to provide stability and to withstand any bending stresses which might be induced due to the lateral forces transferred from the embankment. The approaches and recommendations for the pile group dimensions and extent under embankment can be reviewed for example in *BS 8006 (1995)* and *EBGEO (2007)*.

2.5.2 Stresses and horizontal displacements of piles

The lateral thrust on embankment slope induces lateral deflections and horizontal stresses on the pile. The stresses in pile depend mainly on the relative stiffness of the pile and the soft soil. Other factors include the embedment depth of the pile in the lower bearing layer and the depth of the soft layer. The preliminary empirical estimation of the bending moment of a pile was developed by *Goh et al. (1997)*, who numerically solved the system for one pile element near the toe of the embankment. The bearing parameters of the underground were assumed to consider the undrained shear parameter for a soft underground and the effective shear parameters for sand underground as in Figure 2.7.

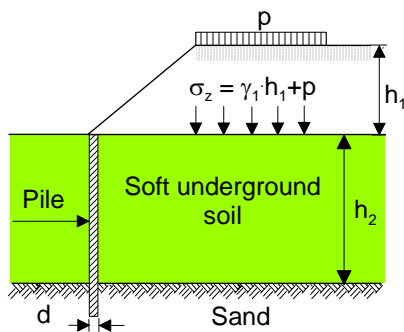


Figure 2.7:
System configuration

Goh et al. (1997) developed a dimensionless parameter M^* which is used to calculate the maximum bending moment of a pile in a soft underground as follows.

$$M^* = \frac{M_{\max}}{c_u \cdot d \cdot h_2^2} \quad \text{or} \quad M^* = \lambda \cdot \exp\left[\beta \cdot \left(\frac{\sigma_z}{c_u}\right)\right] \quad (2.7)$$

where M_{\max} is the maximum computed bending moment of a pile, d is the width of the pile, c_u is the undrained shear strength of the soft soil, σ_z is the total load from the embankment, and λ

and β are constants depending on the relative pile-soil stiffness ratio K_R (Poulos 1973; Stewart 1992) as shown in Equation 2.8 and Figure 2.8.

$$\lambda = 1.88 \cdot (K_R)^{0.5} \quad \beta = 0.18 \cdot (K_R)^{-0.1} \quad (2.8a)$$

where

$$K_R = \frac{E_p \cdot I_p}{E_{50,u} \cdot h_2^4} \quad (2.8b)$$

E_p, I_p the stiffness modulus and moment of inertia of the pile material respectively;

$E_{50,u}$ the undrained secant modulus of the soft underground at 50 % of ultimate load;

h_2 the depth of the soft underground.

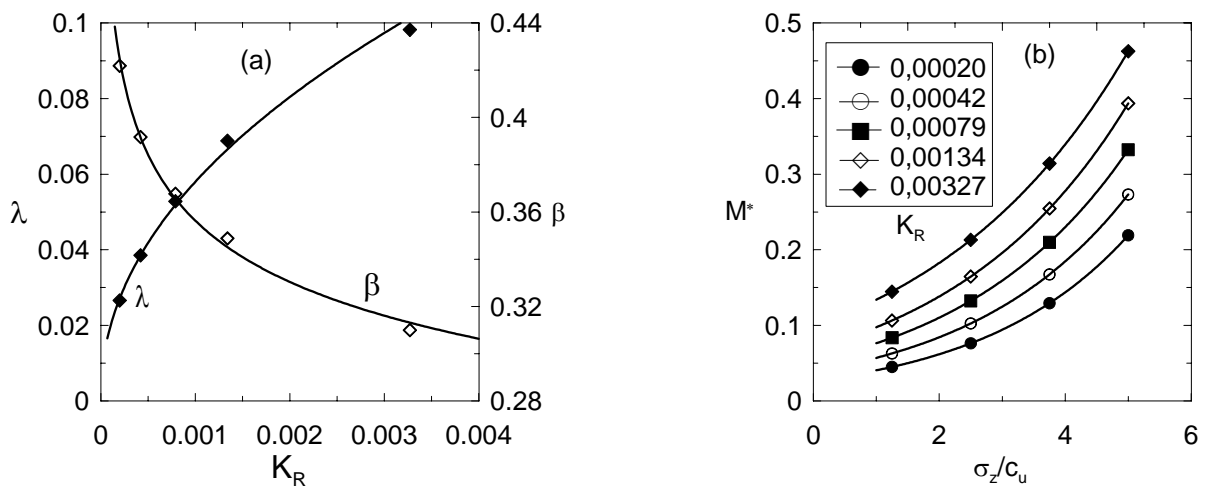


Figure 2.8: a) Values of λ and β , b) Dimensionless plot of M^* versus (σ_z/c_u)

Aubeny *et al.* (2002) simulated the behaviour of a reinforced embankment on pile element using a finite element program. They perform a series of 3-D analyses and compute the bending moments and axial forces in piles, lateral movements, and settlement of piles. They concluded that the current method to estimate lateral movement is limited to unreinforced embankments and no method is available so far for calculating the lateral movements and settlement of reinforced piled embankment. They also reported that the distribution of the load from the embankment own weight and traffic load on geosynthetics along the base of the embankment is not constant. Higher load concentration is located at the top of the piles. The same results have been reported by Kempfert *et al.* (1999).

2.6 Summary

An overview on the methods to analyse the spreading effect on a basal reinforced embankment.

Table 2.4: Methods to analyse the spreading effect in the case of underground supported by pile-like elements

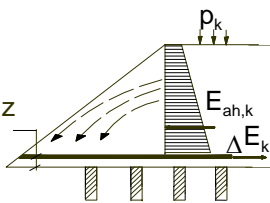
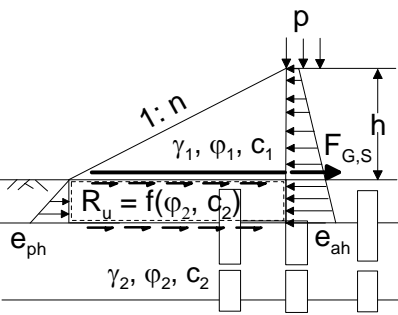
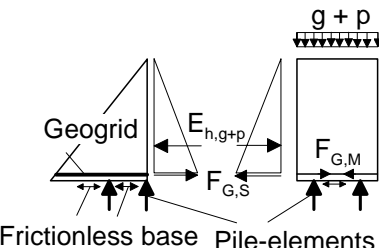
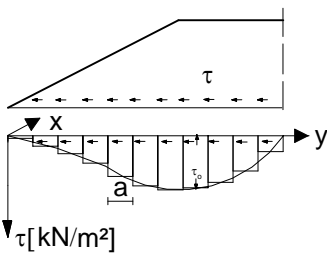
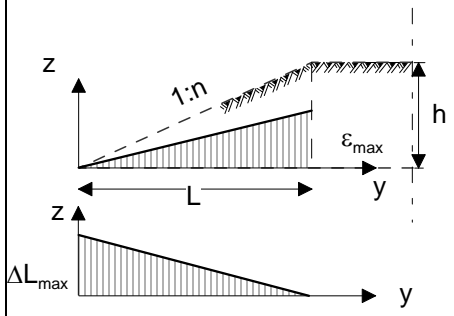
| | <i>EBGEO (2007)</i> | <i>Geduhn/Vollmert (2005)</i> | <i>Love et al. (2003)</i> |
|-------------|--|--|--|
| |  |  |  |
| Force in GG | $F_{G,total} = F_{G,M} + F_{G,S}$ with $F_{G,S} = E_{ah}$ | $F_{G,total} = F_{G,M} + F_{G,S}$ $F_{G,S} = E_{ah} - R_u$ $R_u = \frac{1}{2} \cdot h^2 \cdot n \cdot \gamma_1 \cdot \mu \cdot \tan \varphi_2$ | $F_{G,total} = \max \left\{ \begin{matrix} F_{G,M} \\ F_{G,S} \end{matrix} \right\}$ |
| Notes | The horizontal active earth pressure at the slope crest acts as a tensile force in GG added to the membrane force. | Reduced horizontal earth pressure by a base resistance between the underground and GG acts as a tensile force in GG added to the membrane force. | Assuming a frictionless base, the active earth pressure force acts as a tensile force in GG and compared with the membrane force to take the maximum as a tensile force. |

Table 2.5: Determination of horizontal displacement in slope zone due to spreading effect of an unreinforced and a reinforced embankment

| | <i>Tölke (1990)</i> | <i>Geduhn/Vollmert (2005)</i> |
|-------------------------|--|---|
| |  |  |
| Horizontal displacement | $v_y = f(\tau)$ | $\Delta L_{\max} = \frac{\varepsilon_{\max}}{2} \cdot L = \frac{\varepsilon_{\max}}{2} \cdot h \cdot n$ $\Delta L_y = \frac{E_{sp}}{J} \cdot \frac{L-y}{2} \cdot y$ |
| Notes | Determination of the horizontal displacement in the slope zone of unreinforced embankment as a function of shear stresses τ . | Determination of the horizontal displacement in the slope zone of reinforced embankment as a function of the strain in reinforcement. |

3 Conception and results of model tests

3.1 General

In this chapter, a series of large-scale model tests has been carried out to investigate the spreading effect in the slope zone of an embankment. The main system of the model tests consists of a basally reinforced sand embankment with geosynthetic reinforcement resting on soft underground supported by pile-like elements. Although the study focuses on the spreading effect on piled embankment system, some model tests have been carried out on unpiled embankment system. The goal of these model tests is to identify the tensile forces in the base-reinforcement and to verify these results by numerical computations. Also, it served to evaluate the stress-displacement behaviour of the system with and without pile-like elements.

3.2 Model theory and basics of the own model tests

The study focuses on the estimation and investigation of the spreading effect on reinforced embankment. Therefore, large-scale model tests have been carried out to fulfil this objective.

The fundamentals of practice and limits of the model tests in soil mechanics were widely presented as in *Walz (1982)*, *Jessberger/Güttler (1988)*, *Pregel (1998)*, *Jaup (1999)* and others. Principally, the model tests were classified into three types depending on the objectives of these tests. The types of model tests include (see *Jaup 1999*):

- a) Model tests to transform the results to the nature (prototype);
- b) Model tests for the determination of relative differences;
- c) Model test for investigation of the failure mechanism.

Regarding this study, the accomplished model tests to investigate the spreading problem can be classified in the categories a) and b). The scale of the model tests must be chosen as large as possible, with which the test results can be numerically verified by the FE-method (Chapter 4). This represents in this contribution the main goal of the model tests. The verification process serves to estimate the unmeasured parameters numerically.

Furthermore, the verification process presents a qualitative structural model, which provides a basis for a developed parameter study to investigate the system parameters. (Chapter 5).

The dimensionless parameters considered in the model tests are arranged in Table 3.1 after the dimension-analysis according to *Görtler (1975)*. Further, it served to fix and define which parameters to be kept in the model tests and which not due to the boundary conditions.

| | Dimensionless parameter* |
|--------------|--|
| Geometry | $\lambda_L = L_P / L_M$ |
| Stress | $\lambda_\sigma = \sigma_P / \sigma_M$ |
| Displacement | $\lambda_s = s_P / s_M$ |

Table 3.1:
Dimensionless parameters

* P = Prototype and M = Model

The used dimensions of the model tests imply a scale factor λ in the range of $\lambda=1$ to $\lambda=3$. Because of the availability of the experimental possibilities and complex boundary conditions of the various parameters, which govern the behaviour of the structural system under the spreading effect (such as the height of the embankment and the tensile stiffness of the reinforcement) beside the reinforcing system itself, the large-scale model tests have been chosen with $\lambda = 3$. With this scale, a suitable number of tests can be implemented to investigate the shear stresses due to spreading pressure under variations of parameters as illustrated before.

3.3 Test-materials

3.3.1 Bearing elements

The chosen bearing elements in the model tests were illustrated by *Zaeske (2001)*. In the case of the study, the used pile elements are unreinforced concrete (plain concrete) pile-elements with concrete C 12/15. Table 3.2 represents the important parameters for pile-elements including the tensile strength f_{ctm} .

Table 3.2: Properties of unreinforced pile-elements according to *DIN 1045-1:2001-07*

| Element | Material | f_{ck} | $f_{ck, cube}$ | f_{cm} | f_{ctm} | E_T | ε_T |
|---------------|---------------------|----------------------|----------------------|----------------------|----------------------|----------------------|-----------------|
| Pile-elements | Concrete C 12/15 | [MN/m ²] | [MN/m ²] | [MN/m ²] | [MN/m ²] | [MN/m ²] | [%] |
| | | 12 | 15 | 20 | 1.57 | 25800 | 0.9 |

3.3.2 Model sand

The embankment fill material consists of washed and fire-dried industry-special sand taken from a gravel-work in Bobenheim (Germany). The sand material in the model tests is a uniformly distributed sand with a grain size distribution 0.063 – 4.00 mm, uniformly graded sand, SE, the sand material was classified and characterised according to the German approach, *DIN 18196* as mS, fs, gs. The grain size distribution of the model sand is represented in Figure 3.1.

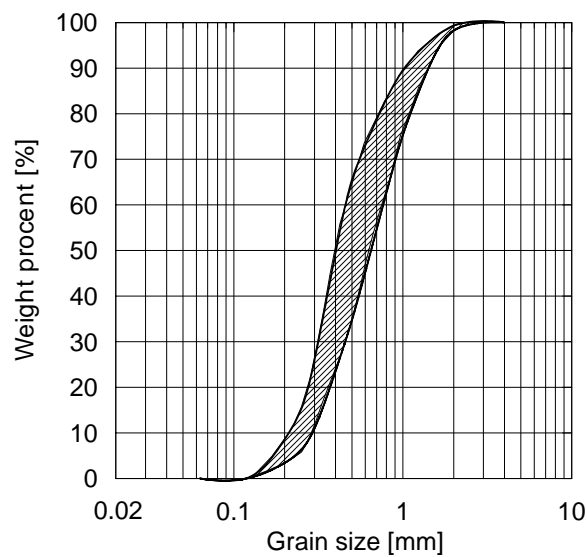


Figure 3.1:

The grain size distribution of the model sand

The soil-mechanical characteristics of the model sand have been estimated using the results of many triaxial tests. Under different stress levels the soil characteristics should be accomplished through the relations between various parameters under variation of the compactness of the model sand. The triaxial test results showed a non-linear elastic behaviour under small stress levels. This behaviour has been qualitatively developed as a hardening soil model (HSM) behaviour, which means that the soil under primary deviatoric loading shows a decreasing stiffness and simultaneously irreversible plastic strain develop. The influence of the stress path will not be considered in this model.

The shear strength parameters of the sand have been developed between the range of the maximum and minimum density of the sand with a friction angle φ' between $\varphi' = 32^\circ$ to $\varphi' = 40^\circ$. The relation between the normal stresses and the friction angle φ' had been mathematically estimated after *Kempfert (1987)* with a potential function as follows:

$$\varphi' = \varphi_0 \cdot \left(\frac{\sigma_n}{\sigma_{ref}} \right)^n \quad (3.1)$$

The reference stress σ_{ref} was considered as 100 kN/m² and the parameters φ_0 and n could be derived from the regression analysis of the triaxial test results. The estimated relation between friction angle φ' and the applied normal stress was also investigated by *Rainer/Fellin (2006)* and *Fannin et al. (2005)* who concluded that the friction angle is stress-dependant and exhibits a linear relation with logarithm of effective stress (inverse proportion). The relation between φ' and the stress level under variations of the compactness of the model sand have been estimated from the triaxial-test results from *Witzel (2004)* with a compactness of the sand $D = 0.71$ and *Heitz (2006)* with $D = 0.89$, which represents the maximum available compactness used in the model tests. The stress-dependant characteristic curves of the sand (φ' and E_{50}) under different compactness D are illustrated in Appendix B.1. The constitutive relations of the sand at different compactness have been widely investigated in Chapter 4.

Table 3.3: Soil-mechanical characteristics of the model sand

| | | |
|--|---|-------------------|
| Maximum density | $\rho_d = 1.725 \text{ g/cm}^3$ | $n_{min} = 0.348$ |
| Minimum density | $\rho_d = 1.44 \text{ g/cm}^3$ | $n_{max} = 0.456$ |
| Specific gravity | $\rho_s = 2.646 \text{ g/cm}^3$ | |
| Uniformity coefficient and curvature coefficient | $U / C = 2.9 / 1.0$ | |
| The largest particle size in the smallest 50% of particles | $d_{50} = 0.4 - 0.65$ | |
| Angle of internal friction | $\varphi' \approx 39^\circ$ for $D = 0.89$ | |
| Effective cohesion | $c' = 0.0$ | |
| Secant modulus (at $\sigma'_3 = 100 \text{ kN/m}^2$) | $E_{50} = 47.7 \text{ MN/m}^2$ for $D = 0.89$ | |

In the model tests, the maximum dry density of sand ($\rho_{d(max)} = 1.694 \text{ g/cm}^3$) is given at fall height of the standard sieve 60 cm and $D = 0.89$ (see Appendix B.2). Table 3.3 represents the soil parameters of the built model.

3.3.3 Geosynthetics reinforcement

Several model tests have been carried out under different boundary conditions with and without geosynthetics reinforcement, in order to investigate the effect of reinforcement on the stability of the system and on the stress-strain behaviour of the other components of the system. Furthermore, the investigations have the goal to determine if the reinforcement can develop the shear stresses at the embankment base without additional effects on the pile elements or

soft layer. In the large-scale model tests, the used geosynthetics reinforcement is a polyester-biaxial geogrid material consists of woven plastic threads. In practice it is called GW 60 PET or FORTRAC 60/60-20. Table 3.4 explained some of the technical properties used for the geogrid in model tests.

Table 3.4: Technical data of FORTRAC 60/60-20

| Technical data | Unit | FORTRAC 60/60-20 |
|--|-----------------------------------|------------------|
| Type | [-] | PET (Polyester) |
| Nominal stiffness | [kN/m] | Long/width 60/60 |
| Tensile stiffness with respect to range of serviceability limit load | [kN/m] | 750 by 9.7 % |
| Maximum measured tensile force ($F_{k,0}$) | [kN/m] | Long/width 71/75 |
| Failure strain at $F_{k,0}$, (ϵ_{max}) | [-] | 10.6/8.8 |
| Average friction factor Geosynthetics/model sand (R) | [-] | 0.97 |
| Aperture size | [mm] | 20 x 20 |
| Bar area of the geogrids at 1m ² | [m ² /m ²] | 0.42/0.42 |

The stress-strain relation of that geogrid is given by the producer as a relationship between the tensile force and the strain both alongside the width and the length; it is used as a characteristic relation of the geogrid. *Zaeske (2001)* carried out some tests to evaluate the curves given by producer. He concluded that both curves from tests and from producer were approximately the same. In this result the characteristic curves of the geogrid have been used to represent the stress-strain relationship (see Figure 3.2).

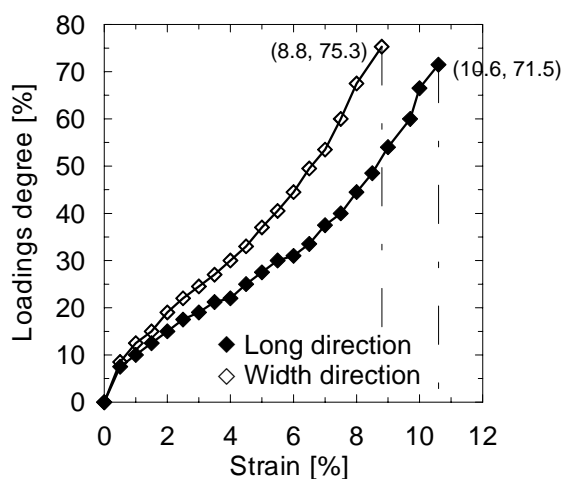


Figure 3.2:
Tensile force-strain curve of:
FORTRAC 60/60-20

The longitudinal direction of the geogrid has been used in the model tests as the main direction of strain gauges. Therefore, the curve of stress-strain at long direction represents the characteristic curve of geogrid in the model tests with a minimum point (0,0) and a maximum point at failure (10.6, 71.5). The shear angle in the contact area sand/reinforcement is related to the friction angle of the sand by the bond (friction) coefficient R , where:

$$R = \frac{\tan \varphi_{\text{geogrid / sand}}}{\tan \varphi_{\text{sand}}} \quad (3.2)$$

In general, the bond coefficient between the dry sandy soils and the geosynthetics reinforcement (geogrids) ranges from 0.85 to 1.00, and the higher soil-geosynthetics friction angles are measured when the surface has significantly sized apertures (geogrids), or allows the penetration of soil particles into the geosynthetics. The main factors affecting the development of shear in the interface are the roughness of contact face, grain size of reinforced soil and loading (see *Chenggang, 2005*). For more related literatures, see also *Eigenbrod/Locker (1987)*, *Eigenbrod et al. (1990)*, *Lopes et al. (2001)*, *Rüegger (2002)*, *Meyer et al. (2003)*, etc. Table 3.5 represents the friction coefficient for different types of geotextiles and geogrids.

| Geotextile construction | Friction (bond) coefficient R |
|--------------------------|---------------------------------|
| Conventional geotextiles | |
| WOVENS | |
| Monofilaments | 0.6-0.8 |
| Multifilament | 0.75-0.9 |
| NONWOVENS | |
| Melt-bonded | 0.7-0.8 |
| Needle-punched | 0.7-0.8 |
| Reisin-bonded | 0.6-0.7 |
| STITCH-BONDED | 0.75-0.9 |
| Special geotextiles | |
| GEOGRIDS | |
| Cross-laid strips | 0.85-1.00 |
| Punched sheets | 0.85-1.00 |

Table 3.5:
Friction coefficients for various geotextiles types, *Terram designing (2000)*

The bond coefficient between the used geogrid and the sandy soil in the model tests had been estimated by *Zaeske (2001)* through the shear box tests where $R = 0.99$, this means that the

friction between the sand and the reinforcement (FORTRAC 60/60) is about the same as friction soil/soil, and the reinforcement mobilizes about 99 % of the sand friction.

3.3.4 Soft layer

The soft underground (peat) is simplified and simulated by a foam material as an extension of the model tests carried out by *Heitz (2006)*.

3.4 Measuring procedures

3.4.1 General

The spreading effect phenomena in the embankment slope zone has been observed and investigated in the large-scale model tests through the tensile stresses in the reinforcement and the shear stresses at the base of the embankment. Besides, the horizontal deformations at the slope toe and the horizontal forces in the pile-like elements would give a good indication and measuring help to determine the effect of the spreading pressures in the slope zone. The measuring sensors must give much information in the same time with little disturbances. The shear stresses in the soil have been measured through measuring the resulting spread horizontal forces, which causes the shear stresses under a certain area.

The boundary disturbances, such as the friction between the model walls and the soil, must be avoided. This has been achieved by using a Plexiglas wall, which possesses approximately no friction with other material. The unequal compactness of the built sand model has also been avoided. The building of sand in the corners of the model walls has been carried out by using a smaller sieve considering the same compactness of the layered sand. The measurements were concentrated in the slope zone of the embankment, where the horizontal force in the pile-like elements, the shear stresses in the soil, and the tensile forces in the reinforcement under variations of outer loading have been measured.

3.4.2 Horizontal force measurement

The horizontal forces in the pile elements due to the spreading pressure in the slope zone of the embankment have been measured by means of force cell connected to the top of the pile

elements, which were chosen as mostly affected elements in the front of the slope zone. Figure 3.3 represents the place and the chosen pile elements and the fixation of the force cell to be capable of measuring the horizontal force in the pile elements.

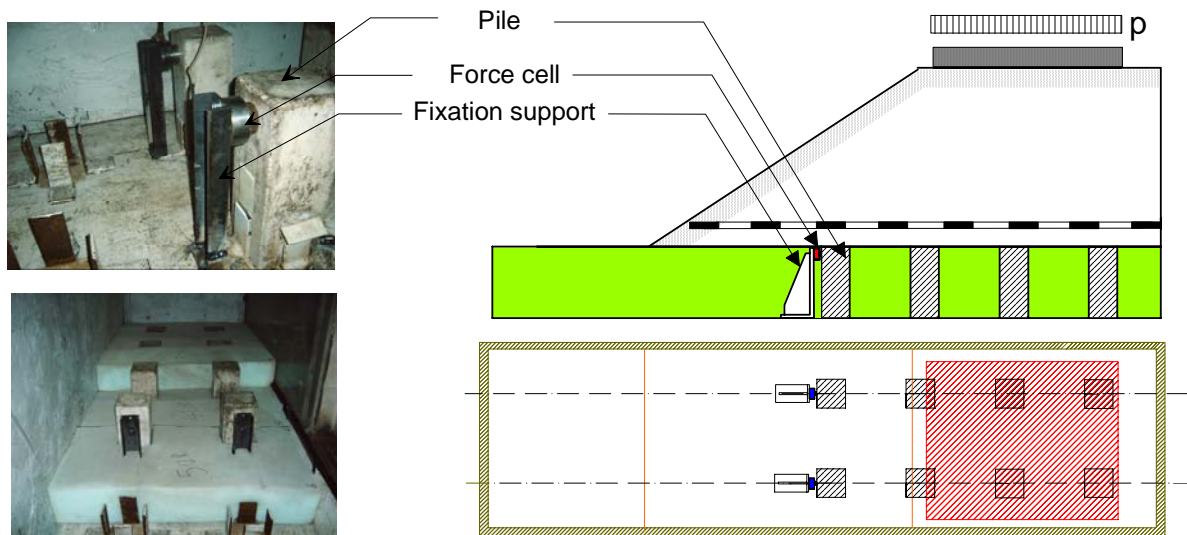


Figure 3.3: The position of the force-cells to measure the horizontal force in the pile element.

3.4.3 Strain in geosynthetics (Strain gauges, DMS)

The tensile forces in the reinforcement resulting from the spreading effect of the embankment height have been measured in the reinforcement by using strain gauges. In the model tests, the used strain gauges are LY61-6/120A, which were small dimensional strain gauges, (6 mm), suitable for the model tests. The strain gauges were applied in one direction of the reinforcement, at which the reinforcement strains and sags due to spreading effect. The distribution of the strain gauges at the surface of geosynthetics reinforcement is represented in Figure 3.4.

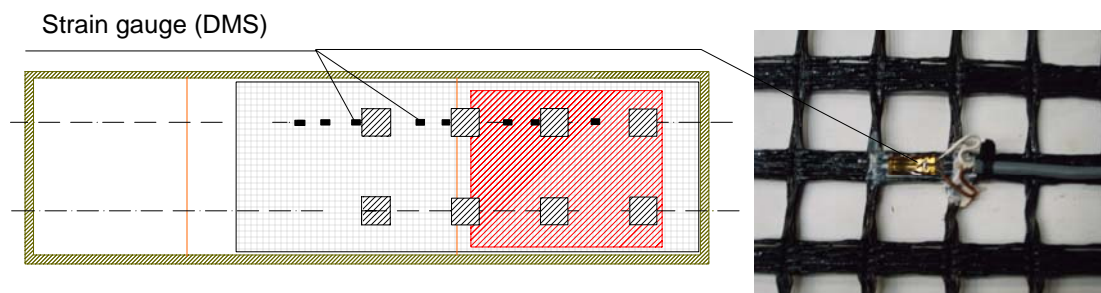


Figure 3.4: The positions of the strain gauges on the reinforcement

According to the manufacturer data, the DMS in a strain range from 0 to 3% follows a linear-elastic behaviour. The effect of the temperature change (day/night) was not considered as the model tests were carried out in labour. Conversion of the electrical measuring signals [mV/V] into an equivalent strain ε [%] was applied with the help of the strain formula for a quarterly-bridge electric connection as in Equation 3.3, where K -factor of the DMS is about 2.07.

$$\varepsilon = \frac{[mV/V] \cdot 4}{K \cdot 1000} \cdot 100 \quad [\%] \quad (3.3)$$

Other alternative was the calibration of DMS before every model test by loading the GG with a defined load and observing the electrical measuring signals [mV/V]. A mathematical relation can then be estimated for every DMS. In the model test, the [mV/V] can be transformed into load and aligned on the characteristic curve of GG to determine the equivalent strain values. This method needs more time and not exact, where it depends on a linear relationship between the strain and the load.

3.4.4 Stress measurement

The important stress to be measured is the horizontal stresses, with which the horizontal earth pressure can be measured and represented. Hence, the shear stresses at the embankment base can be derived using the relationship in Equation 3.4. The horizontal earth pressure in the slope zone of embankment extremely changed in the first half of the slope zone after embankment crest, so that the earth pressure cells were concentrated in this zone as shown in Figure 3.5, where the cells were organized in a vertical distance of 30 cm in the first column of the pressure cells. The first row of pressure cells was laid 3 cm over the base of the embankment.

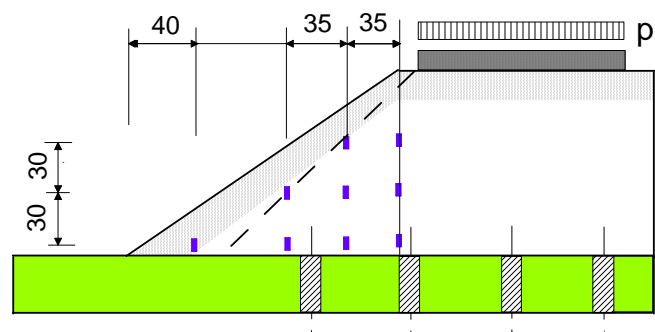


Figure 3.5: Positions of the horizontal earth pressure cell

3.4.5 Displacement measurement

The main objective in the measuring procedure is measuring the deformation in the slope zone due to spreading effect, which was represented by a horizontal displacement in the slope body of the embankment, especially at the toe of the slope.

These displacements have been optically observed using a surveying device, Tachymeter TCR 702, with which the measuring process based on the displacement of each point corresponding to constant coordinate-points, then graphically estimated and analysed to represent the horizontal displacement.

The device observes certain points over the side of the slope zone after every loading phase and the displacement of these points from a certain axes have been analysed. Figure 3.6 illustrates the certain points to be optically observed.

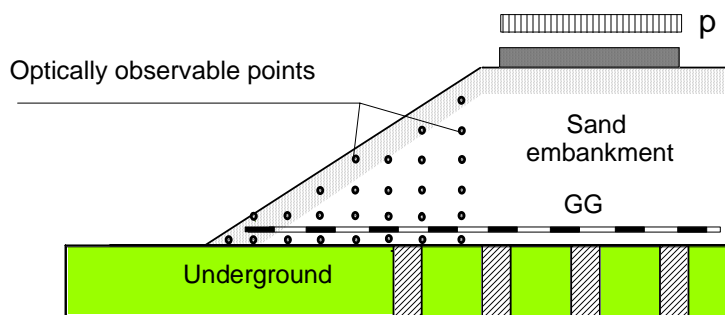


Figure 3.6:
Positioning of the points to measure the displacement

3.5 Model test variations and extent

The objective of the model tests is mainly concerned with the determination of the relationships between the loading, displacement, load distribution, tensile forces in the reinforcement, and the shear stresses at the embankment base. One can also observe and determine the role of the reinforcement to develop the shear stresses and deformations due to the spreading effect in the slope zone. The model tests have been estimated and chosen to check and observe the serviceability limit state of the bearing system, where the stresses and deformations in the soil due to spreading were measured together with the tensile forces in the reinforcement. The tests were graduated in developed steps started from the total homogeneous embankment model and passing then through different underground conditions and base reinforcement variations.

In Table 3.6 the different boundary conditions of each model test and the variations in the bearing systems of every system have been presented.

Table 3.6: Accomplished large-scale model tests

| Name | Bearing system | Geogrid reinforcement | Measured | | | |
|------|---|-----------------------|-------------------------|-------------------|---------------|---------------------------|
| | | | horizontal displacement | horizontal stress | tensile force | horizontal force in piles |
| MT0 | Homogeneous sand embankment with slope variations and without external load | without | – | ✓ | – | – |
| MT1 | Homogeneous sand embankment with slope 1:1.5 with external load | without | ✓ | ✓ | – | – |
| MT2 | Sand embankment on soft underground | without | ✓ | ✓ | – | – |
| MT3 | Sand embankment on soft underground | Fortrac 60/60 | ✓ | ✓ | ✓ | – |
| MT4 | Sand embankment on soft underground supported by pile-like elements | without | ✓ | ✓ | – | ✓ |
| MT5 | Sand embankment on soft underground supported by pile-like elements | Fortrac 60/60 | ✓ | ✓ | ✓ | ✓ |

The first model test MT0 has been carried out as a reference model test, in order to investigate the influence of the shear stress at the base of the embankment due to spreading under the own weight of sand and variations of the slope degrees.

The slope variations start from slope 1:3 and slope 1:2 and end with slope 1:1.5. In this model test the influence of the shear stress at the embankment base and the grain-to-grain shear behaviour have been clearly investigated, where the underside of the embankment is sandy soil with the same properties and boundary conditions. The horizontal displacement and the horizontal earth pressure in the slope zone have been measured.

The shear stresses at the embankment base can be calculated directly from the horizontal earth pressure as in Equation 3.4.

$$\tau \approx \frac{\partial E_h}{\partial y} \approx \frac{\Delta E_h}{\Delta y} \quad (3.4)$$

In the second model test MT1 a homogeneous sand embankment with slope 1:1.5 was subjected to an externally increasing static load. The model included only a homogeneous sand embankment and sand underground layer, where shear stresses in the slope zone resulting from the spreading effect can be calculated. The objective is to investigate the effect of the external static load on the shear stresses at the embankment base.

The third model test MT2 included a soft underground to determine the change in the shear stresses at the embankment base and horizontal deformation in the slope zone according to the behaviour of the total bearing system. The shear stresses in both the first and the second model tests have been compared and verified according to the bearing system and variation in the boundary conditions.

As in the case of the model test MT2, the model test MT3 has been carried out but using geosynthetics reinforcement, which, theoretically resists the shear stresses and the deformations in the slope zone. Therefore, the measured shear stresses and horizontal deformations in both tests MT2 and MT3 were compared and the effect of the reinforcement to resist the stresses due to spreading was determined.

Unreinforced sand embankment on soft underground supported by pile-like elements has been represented in the model test MT4, where the resulting horizontal force in the piles due to spreading pressure in the slope zone was additionally measured, with the same measuring procedures.

The complete bearing system has been represented in the last model test MT5, where the system consists of a reinforced sand embankment on soft underground supported by pile-like elements. The horizontal force in the pile elements has been again measured to establish the role of the reinforcement to minimize the stresses and deformations due to spreading in the pile elements and in the embankment toe.

3.6 Model preparation and dimensions

3.6.1 Model building and external loading

The model test serves mainly to investigate the effect of external loads and own-weights on the stress-strain behaviour of the system, in order to record and compute the actual values of stresses (shear) and displacements. Therefore, the other occasional stresses like the friction between the bearing soil (sand) and the model walls must be avoided or minimised. This was

done by laying a lubricant material (Vaseline) on the walls and covering by a thin plastic film. The sand layers have been built by using the sieve at 60 cm height to create the compactness $D = 0.89$ as illustrated in Section 3.3.2. The layers of sand have been divided into 10 cm and levelled in the corners by using a small hand sieve with the same properties of compactness. Three cylinders of sand specimen have been taken parallel with layers building to control the compactness of the built sand. In the first model test, where the slope of the embankment was changed, the change of this slope has been developed using a vacuum dust-cleaner machine. In the case of soft underground, the foam material which simulated the peat underground has been installed in the model cast into two layers each of 20 cm high.

The static traffic load on the model has been simulated using a pressure cushion filled with water, which functions as a flexible foundation under traffic load. A laboratory test has been carried out to determine the actual distribution of vertical stresses under the pressure cushion. 5 pressure-cells were axially distributed 10 cm under the pressure cushion to record the vertical stresses and stress distribution under variation of load surcharge. Figure 3.7 represents the magnitude and distribution of vertical stresses under the pressure cushion. It is significant that the pressure cushion functions as a flexible fundament under loads.

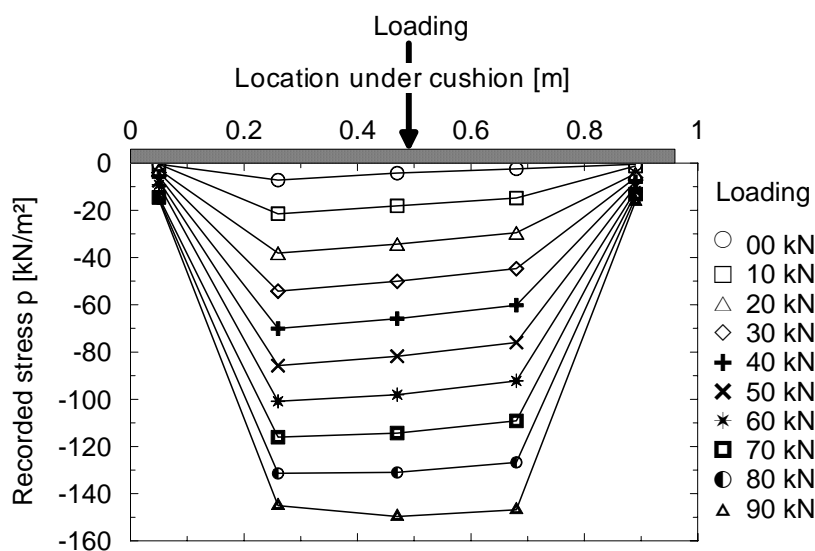


Figure 3.7:
Stress distribution under the pressure cushion

On the other hand, a steel plate has been used on the cushion to transport the mechanical pressure to it. The external load on the model has been developed as statically traffic railway load of $p_{static} = 60 \text{ kN/m}^2$ on the upper structure. In the model tests, the upper structure was not considered or represented, specially the lower structure or the embankment. Therefore, according to the load propagation at 45° , the external static load was added as 50 kN/m^2 on the embankment top. However, the loading steps in the model tests have been taken as 6 kN step of the machine till maximum 60 to 80 kN. The stand time under a loading step depended on

the primary settlement of the foam material, and as the material behaves elastically, then the stand time of every loading step can be taken as 30 minutes. Figure 3.8 illustrates the loading scheme.

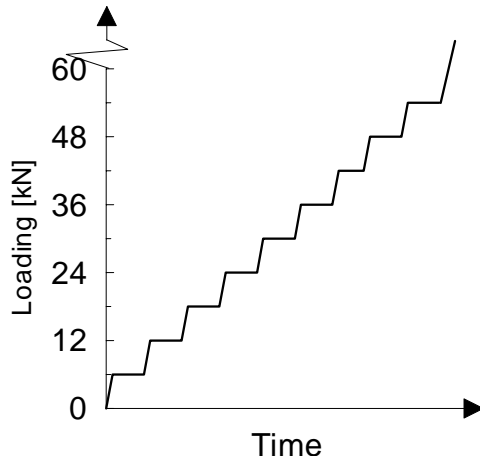


Figure 3.8:
Loading scheme of model test

3.6.2 Model dimensions

As illustrated in Section 3.2, the scale of the model test has been taken approximately 1:3, where the height of the embankment in the model was 1 m. The pile-like-elements have been fixed in the system base by using steel angles or steel casting welded with the steel base of the model to serve as total fixation of the pile-toe with the base. The front side of the model was a Plexiglas's plates to attain the optically observation of the loading procedure and the displacement. Figure 3.9 & 3.10 represent the model dimensions and the structural system of the model and the pressure cushion filled with water.

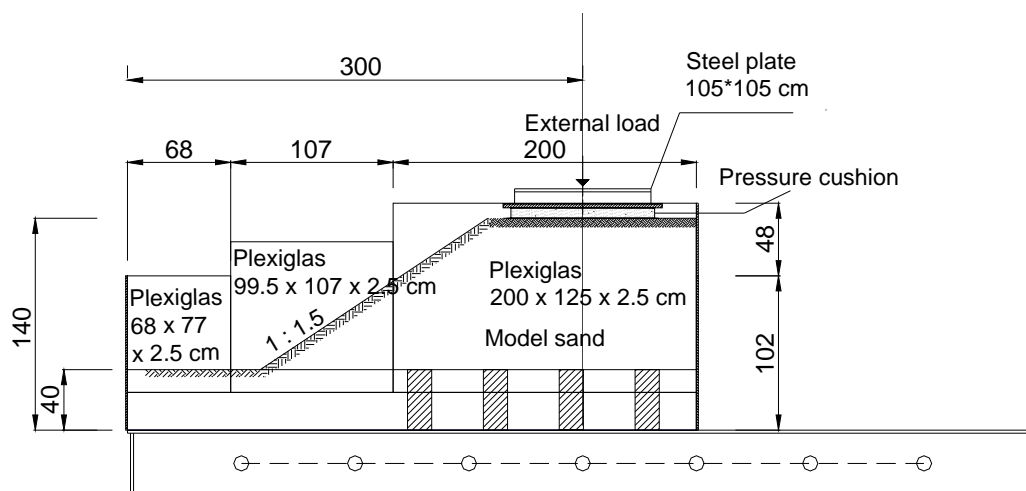


Figure 3.9: Model dimensions

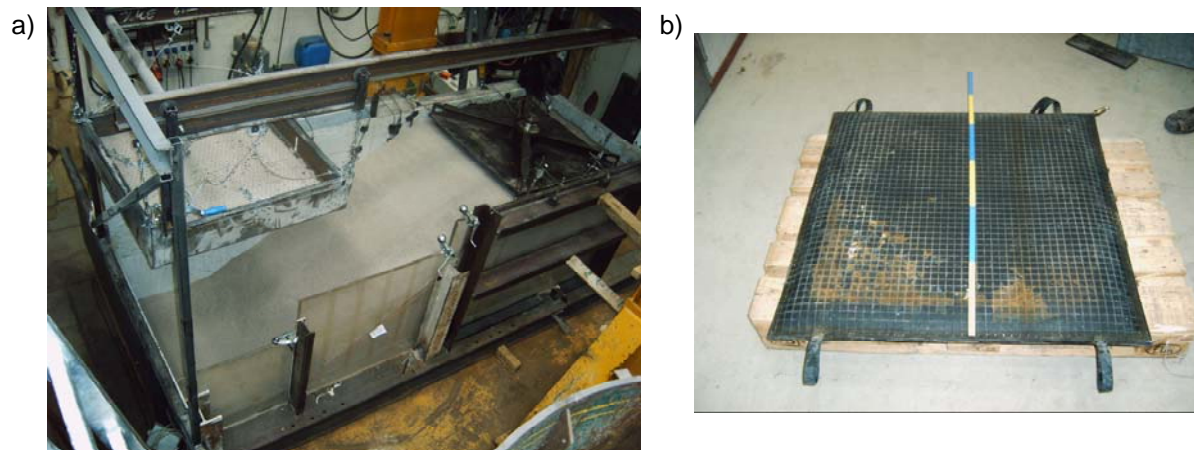


Figure 3.10: a) Model stand and b) Pressure cushion

3.7 Representation and illustration of the test results

3.7.1 Evaluation of shear stresses due to own weight at the base of homogeneous sand embankment under slope variations

In the model stand it was available to change the slope degree of the embankment from 1:3 to 1:2 and 1:1.5. The removing of sand from one slope to another has been made by using a dust cleaner machine in order to remove the sand without changing the rest state of the soil structure. Figure 3.11 represents the model stand and the slope degrees. In every slope degree, the readings of the earth pressure cells were saved as horizontal stresses in every vertical section.

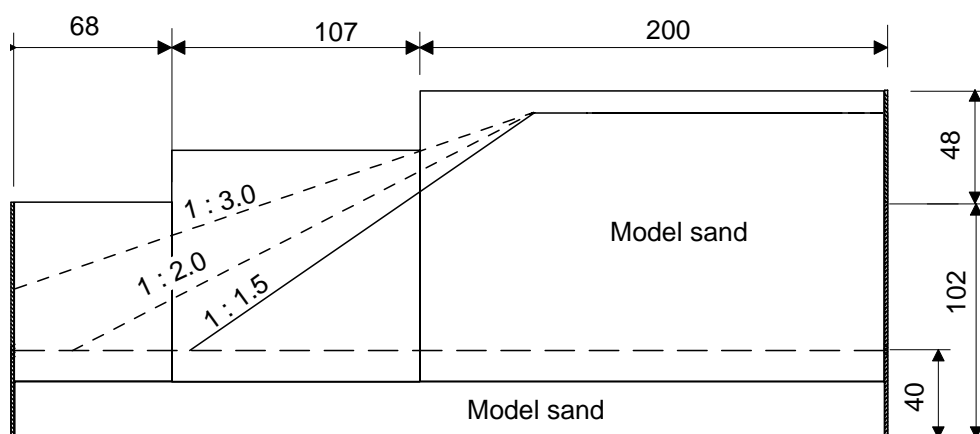


Figure 3.11: Model stand of the homogeneous sand embankment under variation of slope degrees

The calculation of the earth pressure from the read horizontal stresses was adopted by determining the resultant in every vertical section, which represented a point in the curve of the horizontal earth pressure force at the base of the embankment.

Figure 3.12 represents the calculation of the horizontal earth pressure force at every vertical section in the slope zone of the embankment, as an example here of the slope degree 1:1.5.

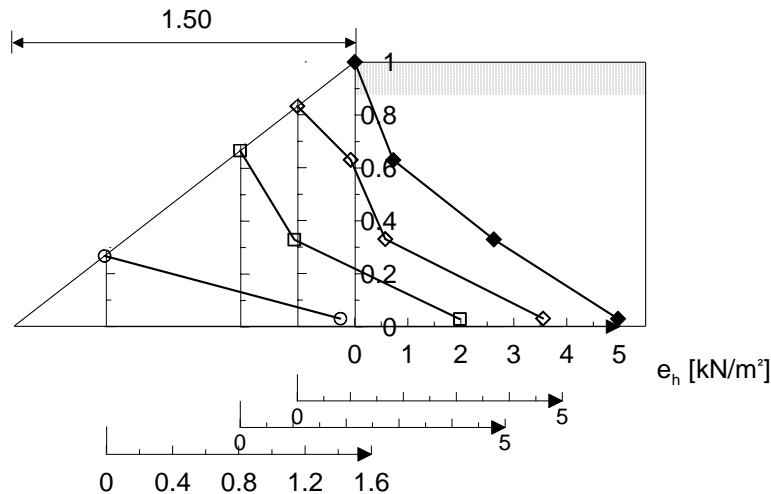


Figure 3.12:
Horizontal earth pressures at the vertical cross-sections in the slope zone

The resulting graphical representation can be approximated by a mathematical equation to represent the relationship between the earth pressure force E_h and the location at the embankment base y . As in Equation 3.4, the values of the shear stresses can also be calculated as the differential equation of the earth pressure force equation. Figure 3.13 shows the estimation of shear stress from the horizontal earth pressure force for the specific case of slope 1:1.5 (the slope degree of the model tests).

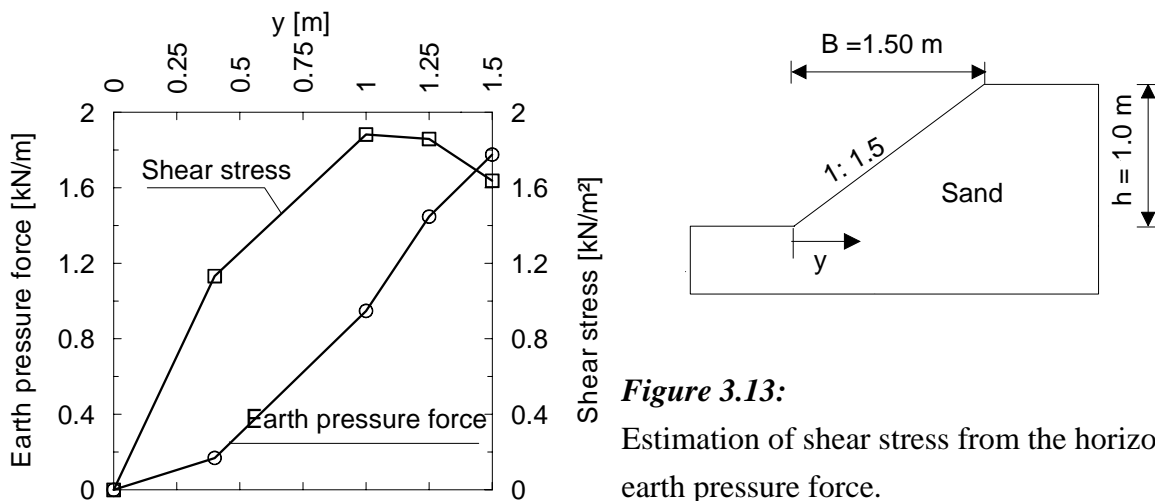


Figure 3.13:
Estimation of shear stress from the horizontal earth pressure force.

The same procedures have been carried out with all slope degrees to get finally the shear stresses at the base of the embankment in the slope zone under the own weight only. Figure 3.14 represents the non-dimensional comparison of the shear stress under slope variations. Where B is the base length according to the slope degree $B = n \cdot h$, $n = 1.5, 2.0$, and 3.0 and $h = 1.0$ m.

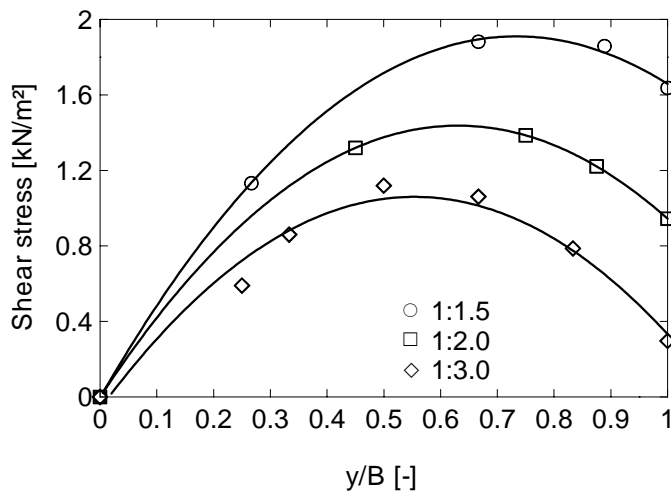


Figure 3.14:
Shear stresses under slope variations

From the Figure 3.14, the location of maximum shear stress occurs in the range of $1/2$ to $2/3$ the slope zone in direction of the embankment axis. When the slope is steep, the maximum shear will be near the slope crest (at $2/3$ slope base), and when the slope is flatter, the location of maximum shear moves in the direction of slope toe. The shear stress at the embankment base increases directly with the slope angle where the maximum shear stress occurs with the slope 1:1.5 and decreased with flattening the slope. Figure 3.15 represents the maximum values of shear stress under every slope.

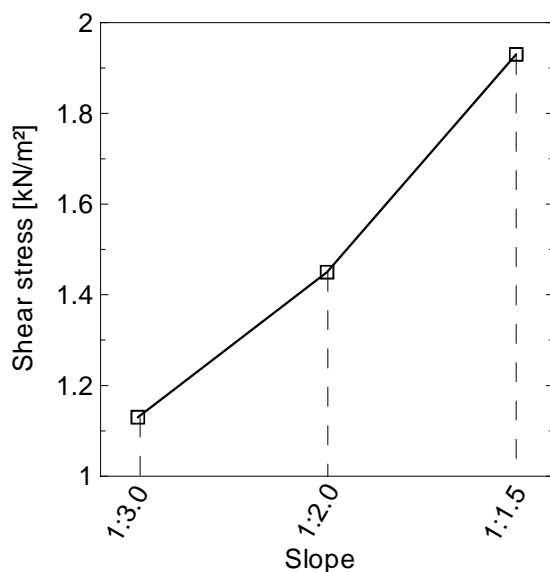


Figure 3.15:
Maximum shear stress under own weight and slope variations

3.7.2 Stress and deformations in the reference test (MT1), homogeneous sand embankment

3.7.2.1 General

In the case of homogeneous sand embankment, which is considered as a reference test, the underground layer in the model was considered as stiff sand (the same embankment sand). The grain-to-grain behaviour controls the stress-strain behaviour in this test. In the reference test the stresses and deformations (mainly the horizontal displacement in the slope zone) have been measured and determined as reference data for all other model tests. The graphical representations of earth pressure forces and shear stresses have been adopted for three external load steps as an example for loading steps. These loads were 42 kN/m², 50 kN/m² (which the results will be explained and discussed in detail) and 72 kN/m² respectively. The area of pressure cushion exposed directly to sand surface, which consequently transfers a certain stress on the embankment surface, changes with the change of the external load, this means that the applied stress has not the same contact area with the applied load. Table 3.7 shows the change of contact area with the applied load.

Table 3.7: Contact area under different applied loads

| | External load (kN) | Contact area (m. x m.) | Computed stress (kN/m ²) |
|---|--------------------|------------------------|--------------------------------------|
| 1 | 0 → 30 | 0.84 x 0.85 | 0 → 42 |
| 2 | > 30 → 60 | 0.91 x 0.92 | 42 → 72 |
| 3 | > 60 | 0.94 x 0.94 | > 72 |

3.7.2.2 Test results

As explained before, the earth pressure force has been computed from the horizontal stresses at every measuring point. The geometrical resultant of the horizontal stresses at every vertical section corresponds to the total horizontal earth pressure force at the section and acts on a point at the embankment base, at which the vertical section located. Figure 3.16 represents both the model stand and the total horizontal earth pressure forces at 3 cm over the embankment base in the slope zone under variations of externally applied loads.

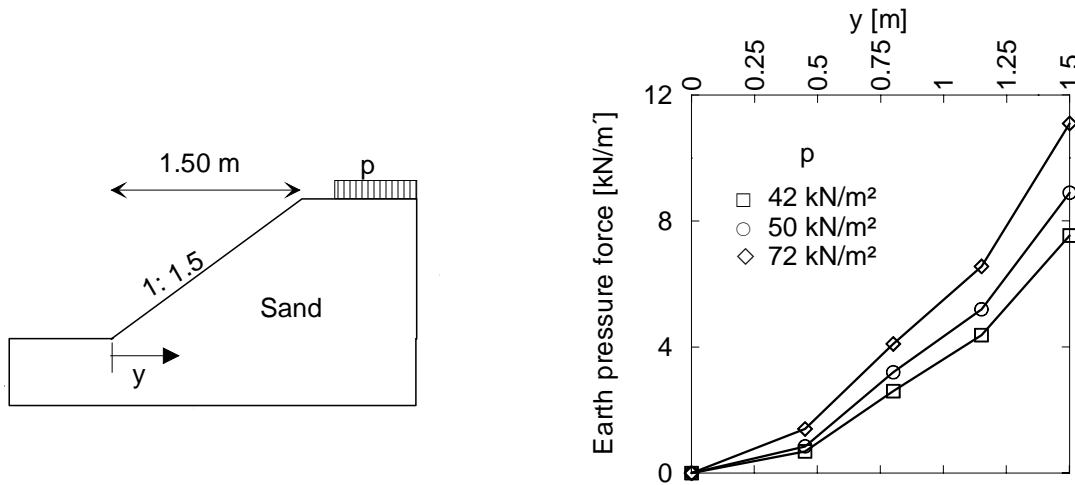


Figure 3.16: a) Model stand

b) Total horizontal earth pressure forces at the embankment base in the slope zone

The graphical representation of the earth pressure force and the geometrical equation of the curve can be used to compute the geometrical and the point values of the resultant shear stresses at every location of the vertical sections at the embankment base by using the differential equation of the earth pressure curves under boundary condition that at the slope toe ($y = 0.0$) both the horizontal earth pressure and the shear stresses are zero. Figure 3.17 represents the shear stresses at 3 cm over the embankment base in the slope zone under variations of externally applied loads.

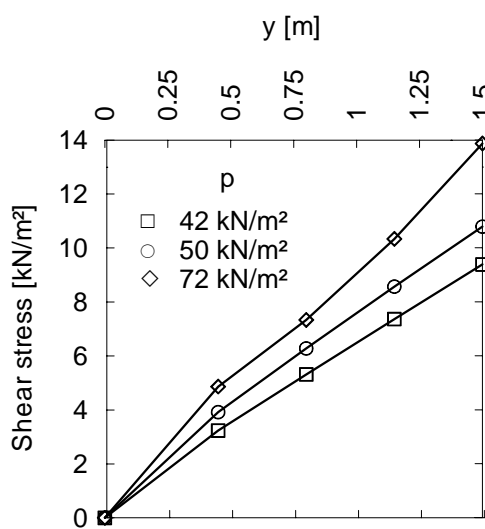


Figure 3.17:

Shear stresses at the embankment base in the slope zone

The deformations in the slope zone have been optically observed using a serving device that observes the points before and after every loading-phase coordinated to certain constant

points or axes. Figure 3.18a & b explain both the horizontal and the vertical displacements in the slope zone of the embankment under external applied load of 50 kN/m^2 .

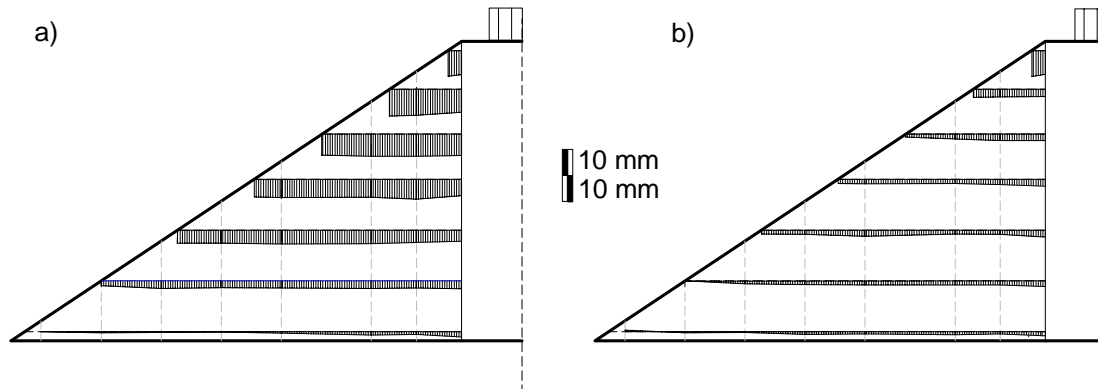


Figure 3.18: a) Horizontal displacement, b) Vertical displacement

The maximum horizontal displacement at the embankment base in the slope zone was 1.8 mm. The deformed shape, scaled 10 times greater, and the moving direction of the slope zone in arrows were explained in Figure 3.19a & b respectively. The Figures show that the main and maximum deformations are horizontal displacements.

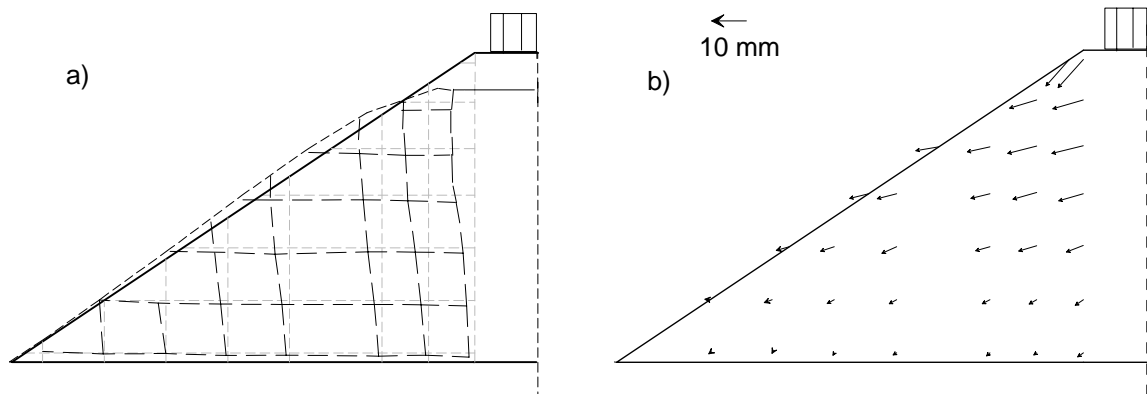


Figure 3.19: a) Deformed shape b) Displacement arrows of the slope zone

3.7.3 Effect of soft underground without geogrid reinforcement

The soft underground as peat material has been simplified and simulated in the large-scale model test as foam material with considerable small stiffness modulus and a pure elastic material behaviour. In the model tests the soft underground conditions include tests with and without pile-like elements.

3.7.3.1 Soft underground without pile-like elements

The model test in this case is considered as the optimum condition of very soft underground, where the underground has been simulated as soft underground only without supporting or reinforcement. The peat-simulated foam material has been constructed with a depth of 0.40 m directly under the sand embankment.

It was observed that, after 72 kN/m² external load, the sand embankment, the pressure cushion and steel plate moved together horizontally in the direction of the slope. This means that the horizontal movement and shear stresses influence the soft underground to be extruded outward. Figure 3.20a & b show both the horizontal earth pressure force and the shear stresses at 42, 50, and 72 kN/m² as examples for the external loads respectively.

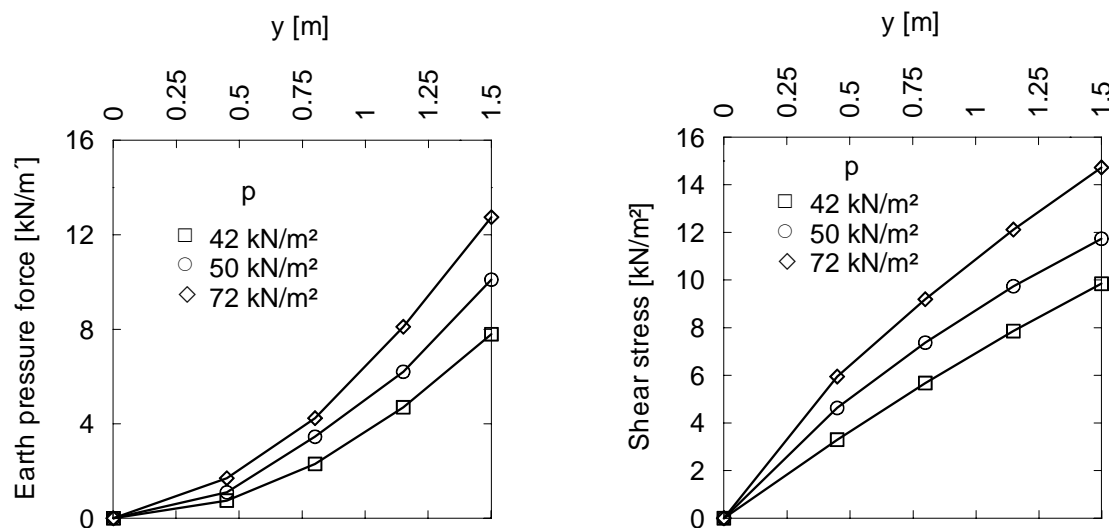


Figure 3.20: a) Horizontal earth pressure force, b) Shear stresses

The displacement of the slope zone under the external loads (as in the example) is graphically represented in Appendix B.3 (It is 5 times greater). It is observed that the deformation of the slope zone has both horizontal (displacement) and vertical components (settlement). The assumption that the spreading stress influences the horizontal displacement of the slope toe is clearly approved through the measuring of the deformations in the slope zone.

3.7.3.2 Soft underground supported by pile-like elements

The pile-like elements of concrete have been constructed with a square mesh of 50 cm. Axeto-axe distance. In this model test, the horizontal forces on the top of the last pile-element in the direction of slope have been measured using a force-cell.

Figure 3.21a & b show both the total horizontal earth pressure force and shear stresses at 42, 50, and 72 kN/m² as examples for the external loads respectively and Figure 3.22 represents the measured horizontal force on the top of the last pile-element.

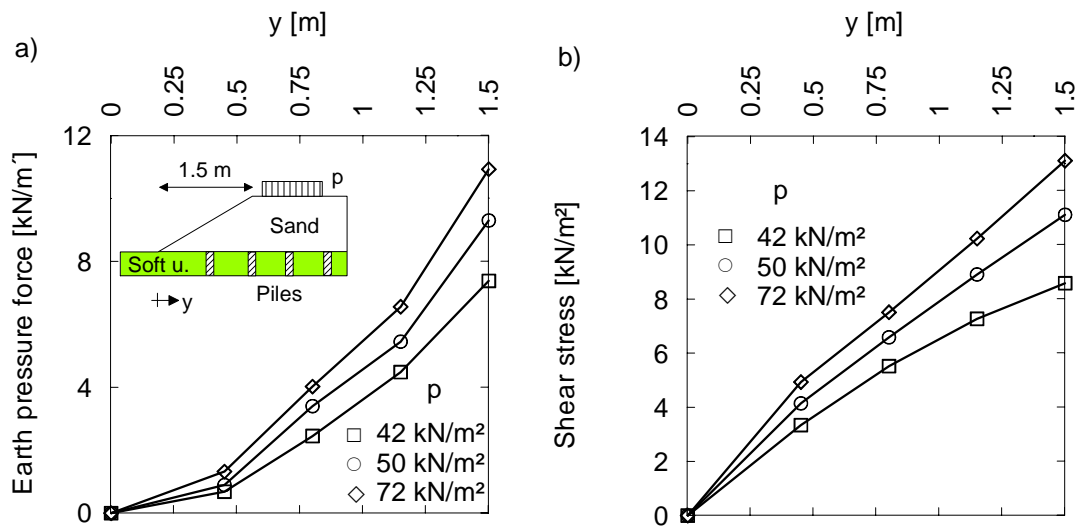


Figure 3.21: a) Horizontal earth pressure force, b) Shear stress

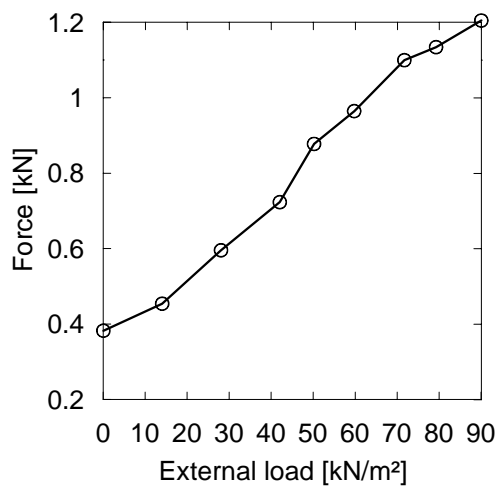


Figure 3.22:
Horizontal force on pile-top of the last pile-element in direction of Embankment slope

The test results show a substantially increased horizontal force in the last pile head in the slope zone. The horizontal force on the head of unreinforced concrete pile elements must be reduced and transferred to a horizontal reinforcement such as geosynthetics reinforcement.

The displacements in the slope zone have been influenced by the position of the pile elements, which somewhat prevented part of the horizontal displacement as shown in Appendix B.4.

3.7.4 Comparing the test results of the unreinforced embankment

The test results of the unreinforced embankment which include the reference test, the soft underground test and the soft underground supported by pile-elements test, have been compared for the external load 50 kN/m^2 to clarify the difference in the magnitude and influence of the shear stresses at the embankment base in the slope zone. The horizontal earth pressure force and the shear stresses of the three tests are shown in Figure 3.23a & b respectively.

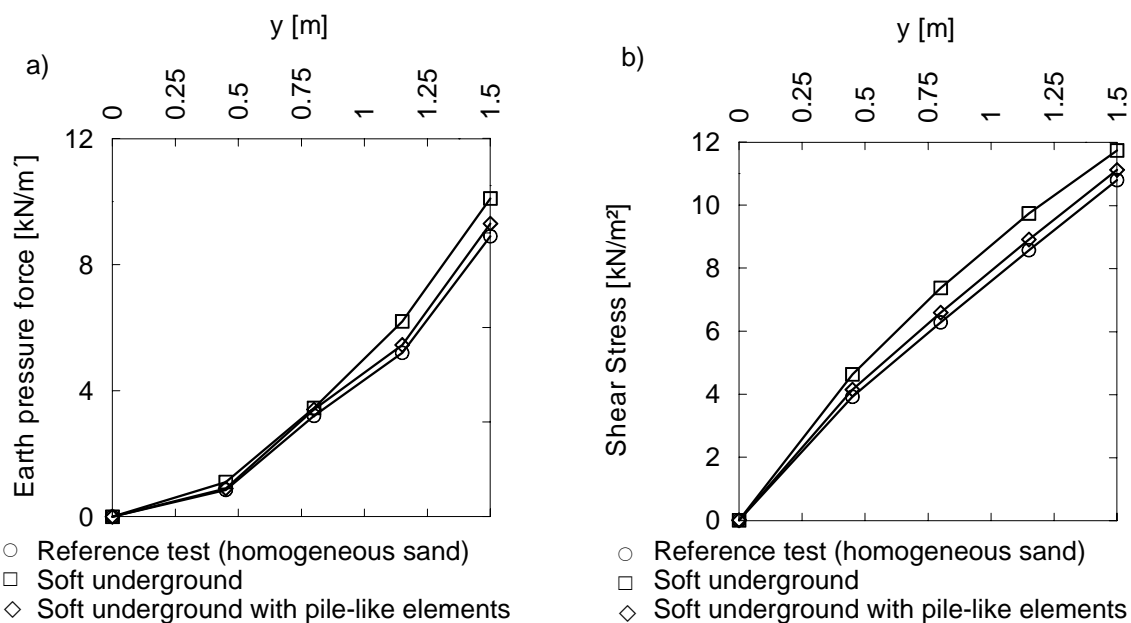


Figure 3.23: a) Comparing total horizontal earth pressure, $p = 50 \text{ kN/m}^2$

b) Comparing the shear stresses, $p = 50 \text{ kN/m}^2$

From Figure 3.23b the maximum shear stress in the case of soft underground is greater than that in the case of homogeneous (reference test) one. The reason is that the deformations are smaller in the homogeneous embankment as illustrated. The distribution of shear stresses in the reference test shows a regular homogeneous distribution along the slope zone whereas that is not clear in the soft underground tests.

3.7.5 Effect of soft underground with geogrid reinforcement

3.7.5.1 Introduction

The geogrid reinforcement at the embankment base plays an important role in the development of stresses and minimizing the deformations of the soft underground. In the case of soft

underground without pile-elements, the reinforcement is responsible for both the global stability (rotational failure) and local stability (spreading effect). Also in the case of soft underground with pile-elements, the reinforcement develops two effects, the spreading effect from the slope zone and the membrane effect from arching effect between the pile elements. The stresses on the reinforcement have been measured through strain gauges in the main direction of strain on the reinforcement.

The horizontal force on the top of the last pile element has also been measured to compare the values with and without reinforcement, in order to evaluate the stresses which can be hold through the reinforcement.

3.7.5.2 Reinforced embankment on soft underground without pile-like elements

In this model test, the tensile strains in the reinforcement have been measured and represented according to Section 3.3.3. The resulting horizontal earth pressure forces and the shear stress at the embankment base are represented in Figure 3.24a & b respectively.

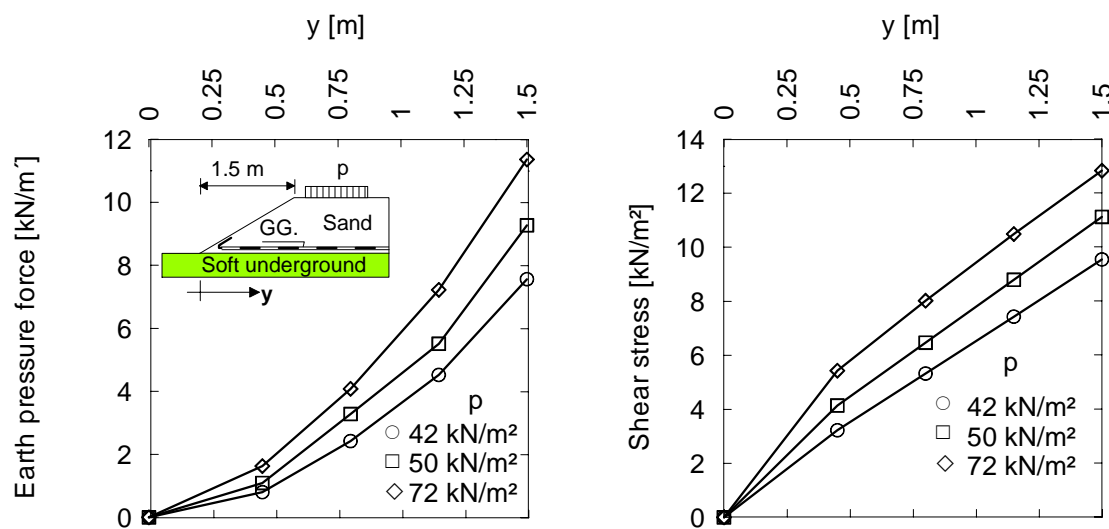


Figure 3.24: a) Horizontal earth pressure forces

b) Shear stresses

The tensile strains of the geogrid reinforcement are represented in Figure 3.25, which shows that the maximum tensile strains of the reinforcement are concentrated under the pressure cushion and the strains go to zero in the last third of the slope in direction of the slope toe (approximately at 0.50 m. from the slope toe). This means that the spreading forces apply tensile forces and strains in the reinforcement in the slope zone.

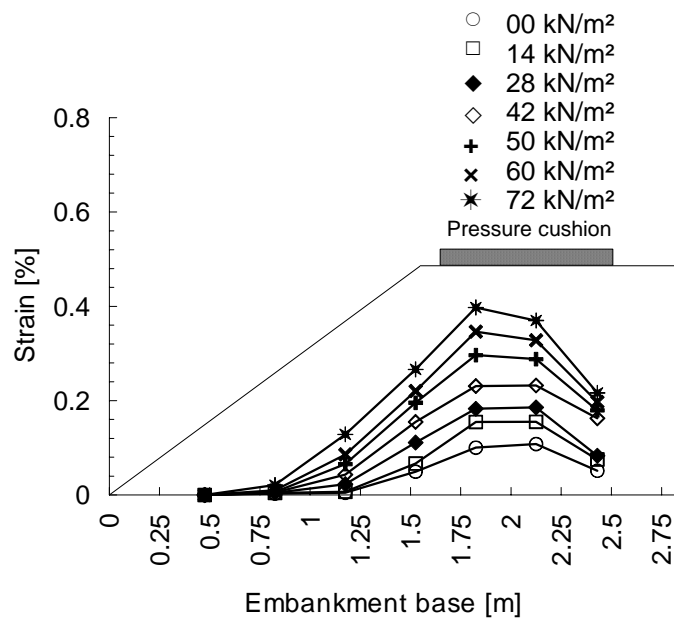


Figure 3.25:
Tensile strains of the reinforcement

The displacement of the slope zone under external loads (for examples 42, 50 and 72 kN/m²) is represented in Figure 3.26. For the external load of 50 kN/m², the maximum horizontal displacement at the embankment base in the slope zone was 7.7 mm. Figure 3.26 also proves that the reinforcement has sustained great portion of the vertical deformations, and great portion of the horizontal deformations, the stresses on the reinforcement were hold through the pull-out (tensile) strength and the friction or the bond effect between the reinforcement and the embankment soil.

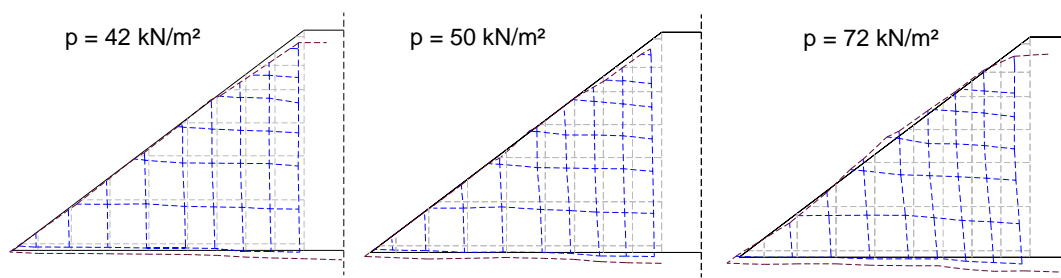


Figure 3.26: Displacement of the slope zone under external loads

3.7.5.3 Comparing the tests on soft underground with and without reinforcement

In order to evaluate the stresses and strains hold through the reinforcement, and to determine if the reinforcement resists the spreading effects without transferring any deformation to the soft underground. Figure 3.27a & b represent the compared horizontal earth pressure forces and shear stresses for the external load 50 kN/m² respectively.

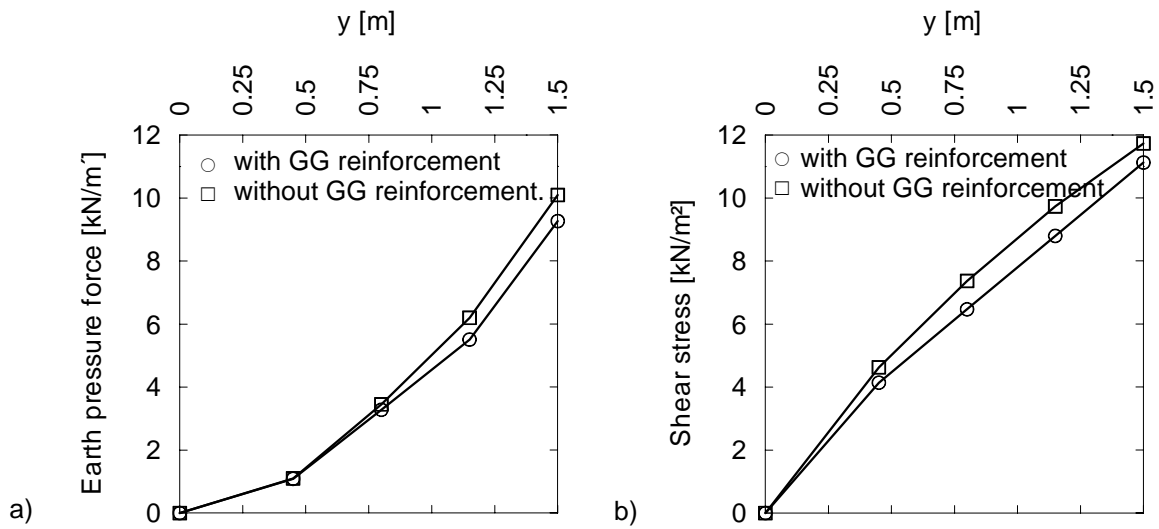


Figure 3.27: a) Compared earth pressure forces,
 $p = 50 \text{ kN/m}^2$

b) Compared shear stresses,
 $p = 50 \text{ kN/m}^2$

It is clear from the shear stress diagram, that the maximum shear stress on the embankment base is obviously reduced by using the base reinforcement. One can also see from Figure 3.28 (comparison between the slope displacement with and without reinforcement) that the maximum horizontal displacement of the slope toe without reinforcement is 13.3 mm, while with the reinforcement is 7.7 mm, this means that the reinforcement sustained and reduced about 50 % of the deformations in the slope zone due to spreading effects.

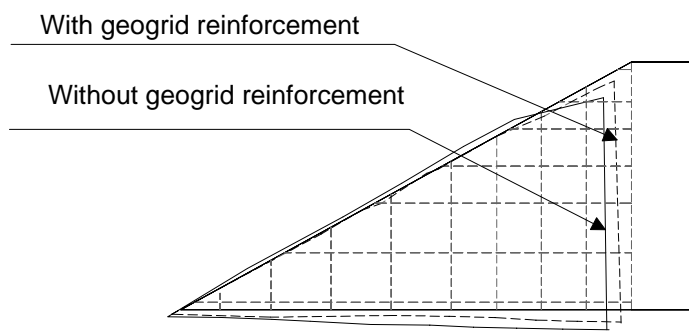


Figure 3.28:
Comparing the displacement of
the slope zone under load

It is also to see from Figure 3.28 it is clear that the reinforcement improves the stress-strain behaviour of structure around it to somewhat continuum material at the interface soil/reinforcement, which in result decreased the deformations. The shear strength and bearing capacity of the reinforced soil are increased significantly. As a result, the stability of structure is increased while total settlements are reduced.

3.7.5.4 Reinforced embankment on soft underground with pile-like elements

In this test, the horizontal force in the top of the last pile element in direction of slope toe, has also been measured to evaluate the effect of reinforcement to develop the horizontal spreading forces from the pile elements, where in most cases the pile elements are not reinforced (plain concrete elements). The horizontal forces then cause some deformations on the pile elements. Figure 3.29a & b represent the horizontal earth pressure forces and the shear stresses respectively.

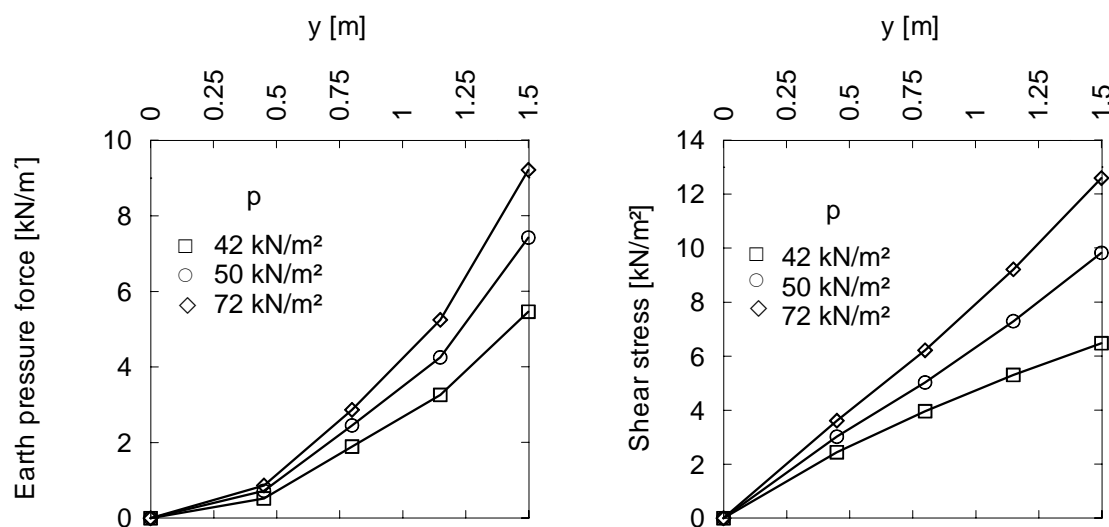


Figure 3.29: a) Horizontal earth pressure force, b) Shear stresses

The horizontal forces on the head of the last pile and the tensile strain in the reinforcement due to the external loads are both represented in Figures 3.30 and 3.31 respectively.

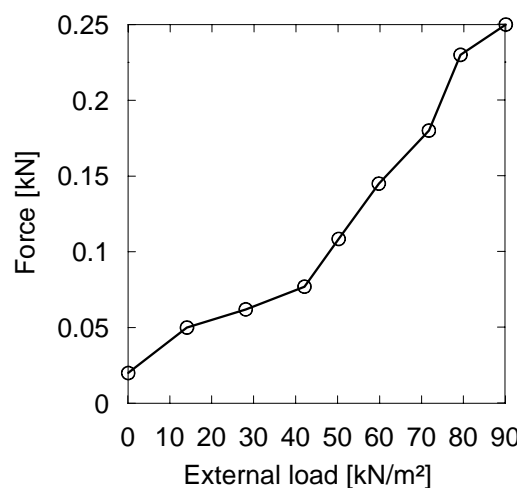


Figure 3.30: Horizontal force on pile-top for the last pile-element in direction of Embankment slope

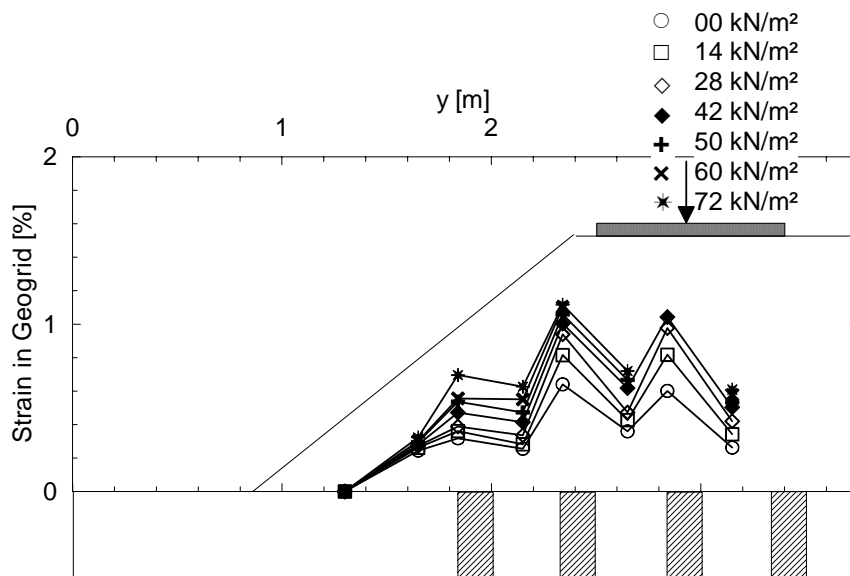


Figure 3.31:
Tensile strain of the geogrid reinforcement due to external loads

The displacement of the slope zone due to the external loads is represented in appendix B.5, for the selected external loads 42, 50, and 72 kN/m². It is observed that the vertical displacement is tremendously decreased. The reinforcement resists the stresses through the bond effect between the embankment soil and the geogrid reinforcement.

3.7.5.5 Comparison of the tests on soft underground supported by pile-like elements with and without geogrid reinforcement

The compared results include the earth pressure forces and the shear stresses at the embankment base with and without reinforcement for the external load 50 kN/m² as represented in Figure 3.32a & b respectively. The objective is to observe and clarify the effect of the geosynthetic reinforcement to sustain the additional stresses due to spreading effect in the slope zone. The horizontal force on the top of the last pile element has also been compared and evaluated in order to investigate the effect of using the horizontal reinforcement in reducing the stresses in pile head (Figure 3.33).

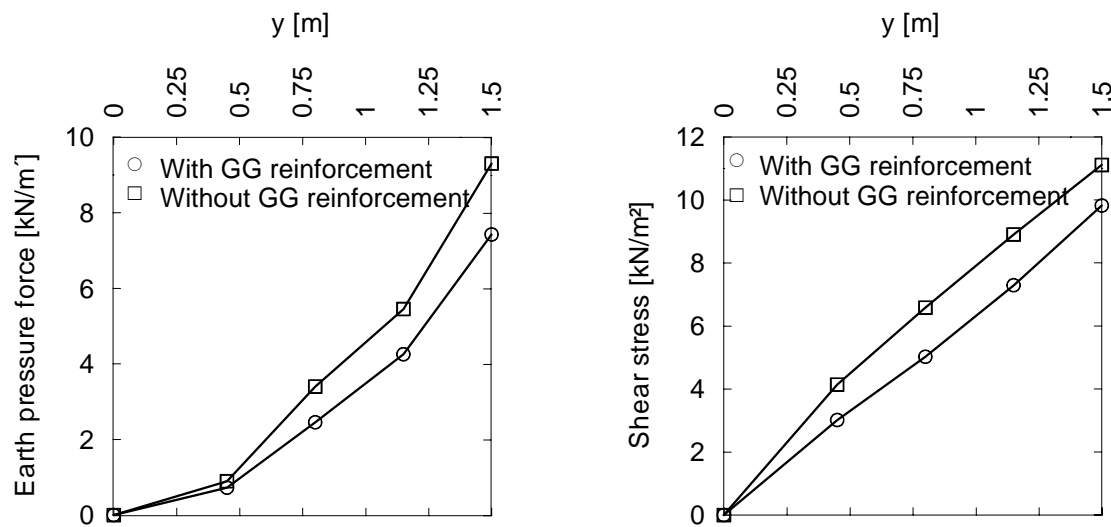


Figure 3.32: Comparison of the earth pressure forces and shear stresses of an embankment on pile-like elements with and without reinforcement, $p = 50 \text{ kN/m}^2$

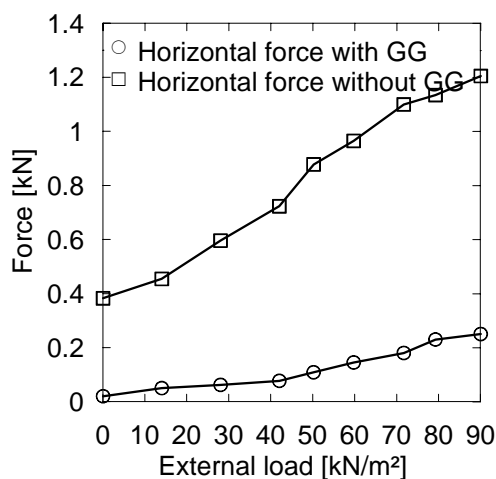


Figure 3.33: Horizontal force on the last pile-element in the tests with and without base-reinforcement

From Figure 3.32, the shear stress at the embankment base in the case of using base reinforcement is reduced than that without base reinforcement. It is also noted from Figure 3.33 that the horizontal force on the head of the last pile-element, in the case of base-reinforcement, is reduced (at $p = 50 \text{ kN/m}^2$) by about 70 % from the force without base-reinforcement. This reduction is developed by the base-reinforcement as tensile forces. This result ensures that the reinforcement develops the horizontal forces on the pile-elements due to spreading effect, as in *Kempfert et al. (1997)* and *Han/Gabr (2002)*.

The displacement in the slope zone due to the external load, with and without base-reinforcement is represented in Figure 3.34.

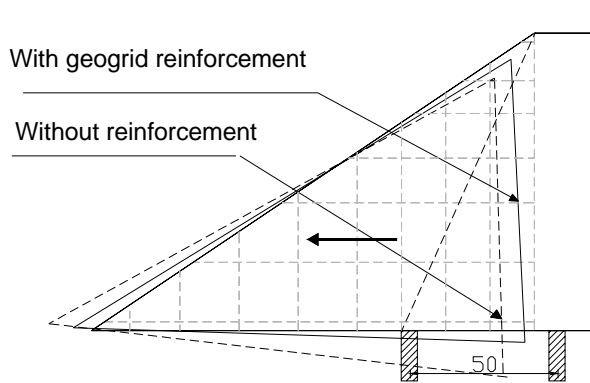


Figure 3.34:

Comparing the displacement of the slope zone with and without geogrid base-reinforcement

From Figure 3.34 the reinforcement hold most of the vertical displacement, and the deformation of the slope body as a horizontal displacement. This means that the reinforcement separates the upper part of the embankment from the lower one and the upper part of the embankment was prevented from sliding by the bond effect between the embankment fill material and the reinforcement, which transfer the additional stresses to the reinforcement.

3.8 Summary

The results of the model tests and conclusions are summarized as follows.

- The spreading effect of the embankment slope leads to some horizontal deformations in the slope toe and shear stresses at the embankment base. In the case of own weight, the maximum shear stresses at the embankment base are concentrated in the slope zone.
- By varying of the embankment slope from flatter slope to steeper slope, it is concluded that the steeper the embankment slope, the greater the shear stresses.
- In the case of external loading, the maximum shear stresses at the embankment base lie on the embankment shoulder under the embankment crest.
- In the case of embankments on soft underground without pile elements, the soft underground has been extruded under high external loads.
- The supporting with pile elements decreases the shear stresses at the embankment base, which confirm that the pile elements can sustain the horizontal stresses due to spreading effect.

-
- The reinforcement improves the stress-strain behaviour of structure around it to somewhat continuum material at the interface soil/reinforcement, which in result decreased the deformations. The shear strength and bearing capacity of the reinforced soil are increased significantly. As a result, the stability of structure is increased while total settlements are reduced.
 - The geosynthetics reinforcement reduced the horizontal force in the pile head, this agrees with the assumption that the reinforcement can sustain the stresses due to the spreading effect and can reduce the deformations on the pile elements.
 - The geosynthetics reinforcement develops the vertical deformation in the slope zone of the embankment with some existence of horizontal displacements; this may lead to some settlement in the internal section of the embankment.
 - The upper part of the embankment is separated from the lower one through the geogrid reinforcement. However, the upper part of the embankment was prevented from sliding by the bond effect between the embankment fill material and the reinforcement, which transfer the additional stresses to the reinforcement.
 - The tensile strains in the reinforcement are smaller in the case of soft underground without pile elements than that with pile elements. This is attributed to the arching effect between the pile elements which cause more strains and forces in the reinforcement.
 - In the case of soft underground without pile elements, all the structural system tends to extrude in direction out of the embankment. This leads to more horizontal displacement than the system contains supporting pile element, where the system supplies more resistance against the horizontal displacement. The increase in horizontal displacement in the system without pile elements leads to decreasing the strain of the reinforcement of this system without pile elements compared to that with pile elements.

4 Verification of the model tests

4.1 General

The constitutive relations of model test materials can only be validated by comparing the model test results with a simulated mathematical or numerical model results, *Schwer (2001)*, *Babuska/Oden (2003)*. It will also help to determine the parameters that could not be directly measured from the model tests and to extend the model test results to the prototype.

The FE-program systems PLAXIS-2D (model without pile-like elements) and PLAXIS-3D Tunnel (model with pile-like elements) have been used in the computation processes. The first step of the computation is verification of the reference model results, whereas the model system consists only of a homogeneous sand-soil. The objective of this verification step is to derive suitable parameters for the constitutive soil model of the embankment-sand that will be used in the other verification steps with sand embankments on soft underground. The second step will be the verification of the unreinforced embankment on soft underground without pile-like elements to calibrate the soil parameters of the soft underground. In this step, the input soil parameters of the embankment sand are the calibrated parameters resulting from the first step.

4.2 Material parameters and constitutive relations

4.2.1 Constitutive relations of the embankment sand layer

The soil parameters of the embankment sand have been derived from plenty of triaxial tests, which were evaluated and analysed to get the main parameters of the sand material according to the real constitutive relations which control the stress-strain behaviour of the material. Triaxial test-results showed that by small stresses the soil provides a non-linear elastic material behaviour. For the FE-system PLAXIS widely known as hardening soil model (HSM), which used the theory of plasticity rather than the theory of elasticity. The main parameters and relations are constructed from the stress-strain relation of the model as shown in Figure 4.1.

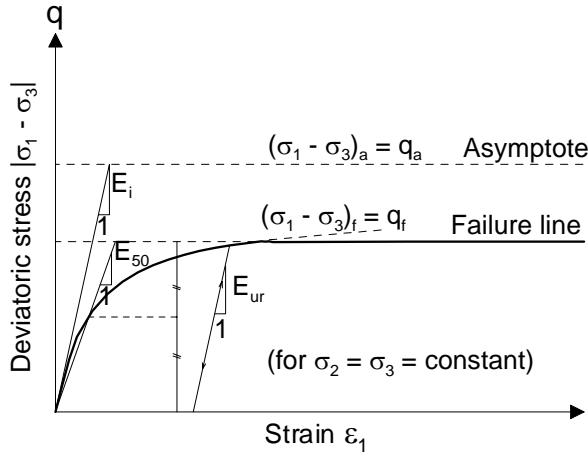


Figure 4.1:
Hyperbolic stress-strain relation for
a standard drained triaxial test in HSM

The formulation of the HSM depends basically on the hyperbolic relationship between vertical strain ε_l and the deviatoric stress q in triaxial test. The triaxial tests tend to yield curves that can be described by:

$$-\varepsilon_1 = \frac{1}{2 \cdot E_{50}} \cdot \frac{q}{1 - (q/q_a)} \quad (4.1)$$

where

q_a Asymptotic value of the shear strength.

The corresponding plastic strains can be derived from a yield function of the form:

$$f = \bar{f} - \gamma^p \quad (4.2)$$

where

$$\bar{f} = \frac{1}{E_{50}} \cdot \frac{q}{1 - (q/q_a)} - \frac{2q}{E_{ur}} \quad \text{and} \quad \gamma^p = -(2\varepsilon_1^p - \varepsilon_v^p) \approx -2\varepsilon_1^p \quad (4.3)$$

The function \bar{f} refers to a function of stress and the function γ^p refers to a function of plastic strain. In the hard soil, the volumetric plastic strain ε_v^p is very small and can be neglected.

The main relations in HSM can then be presented for a standard stress level p^{ref} as follows:

$$E_{50} = E_{50}^{ref} \left(\frac{c \cdot \cot \varphi - \sigma'_3}{c \cdot \cot \varphi + p^{ref}} \right)^m \quad (4.4)$$

$$E_{oed} = E_{oed}^{ref} \left(\frac{c \cdot \cot \varphi - \sigma'_1}{c \cdot \cot \varphi + p^{ref}} \right)^m \quad (4.5)$$

$$E_{ur} = E_{ur}^{ref} \left(\frac{c \cdot \cot \varphi - \sigma'_3}{c \cdot \cot \varphi + p^{ref}} \right)^m \quad (4.6)$$

$$q_f = (c \cot \varphi - \sigma'_3) \frac{2 \sin \varphi}{1 + \sin \varphi} \quad \text{and:} \quad q_a = q_f / R_f \quad (4.7)$$

where

E_{50} confining stress dependent stiffness modulus for primary load at 50 % deviatoric stress;

E_{oed} tangent stiffness modulus;

E_{ur} unloading/reloading stiffness modulus;

p^{ref} reference stress for stiffness (as a standard $p^{ref} = 100 \text{ kN/m}^2$);

m power for stress-level dependency of stiffness ($m = 1$ for soft soils);

R_f failure ratio (should be smaller than 1) and

E_{50}^{ref} , E_{oed}^{ref} , E_{ur}^{ref} are the same predefined stiffness parameters but under a reference stress $p^{ref} = 100 \text{ kN/m}^2$.

As mentioned in Section 3.2.2, the compactness of the model sand used was $D = 0.89$ and the relationship between the stresses and the soil parameters under small stresses is illustrated in Appendix B.1. The secant modulus of the embankment sand (E_{50}) in the case of compactness $D = 0.89$ can be formulated as follows:

$$E_{50} = 47660 \cdot \left(\frac{\sigma'_3}{P^{ref}} \right)^{0.58} \quad (4.8)$$

and the internal friction angle φ' at $D = 0.89$ can also be formulated as follows:

$$\varphi' = 38.8 \cdot \left(\frac{\sigma'_3}{P^{ref}} \right)^{-0.04} \quad (4.9)$$

The standard calculated parameters will be used as input data for the verification of the model test results (see Table 4.1), and then will be changed and calibrated till the results of the FE-computation agrees and compatible with that of the model test, especially with the deformation results (see Figure 4.9). Hence, the calibrated HSM parameters of embankment sand will be used later as an input data for the other computation processes with the other model tests with soft underground.

4.2.2 Constitutive relations for the soft underground

The soft underground used in the model test was foam material, which behaves elastically. Therefore, the constitutive relation for that underground is related to Hook's law. Here the used data is the modulus of elasticity of the material, which will be input and compared with the model test, which contains an unreinforced sand embankment on foam underground without pile elements (MT2). The stiffness modulus of the foam material will be calibrated with the input data, where the model-results are verified using FEM.

4.2.3 Numerical formulation of soil/reinforcement interface

The study focuses on the estimation and evaluation of the spreading effect on reinforced embankment on soft underground. Therefore, the model tests must achieve this objective through determining the parameters relating to the system. The spreading effect on reinforced embankment applies shear stresses at the base of the embankment, tensile stresses in the reinforcement, and horizontal deformations in the system. In the case of study the most critical zone to investigate the stresses is the interface between soil and reinforcement, where a composite material is represented, in such case, the soil structure is modelled as a homogeneous orthotropic material with enhanced stiffness and strength properties. *Romstad et al.* (cited in *Bull, 1994*) used the concept of the 'unit cell', they assumed that the strains in the composite are the same as in the soil and no relative slip occurs between the soil and reinforcement. They concluded also that the deformation due to shear stresses in the soil/reinforcement interface is the same as from the simple elastic theory and in principle is dependent only on the soil characteristics. The interface soil/reinforcement plays no role in the determination of shear deformations. In PLAXIS-program the geogrid reinforcement is assumed to be totally bonded with the soil. Hence, both the soil and the geogrid have the same deformation pattern.

4.2.4 Constitutive relation for the pile-like elements

The pile-like elements have been simulated as a linear elastic material, where the strains in the pile elements can accurately be estimated. The elasticity parameters of the piles were presented in Table 3.2.

4.3 FE-Model geometry and boundary conditions

The system in FEM must be the same as in the model test with the same dimensions and the same boundary conditions in the model test. Figure 4.2 represents the FE-model dimensions and fixation system, which is typical to the model test boundary conditions. Figure 4.3 represents the FE-model and the mesh generation of the system.

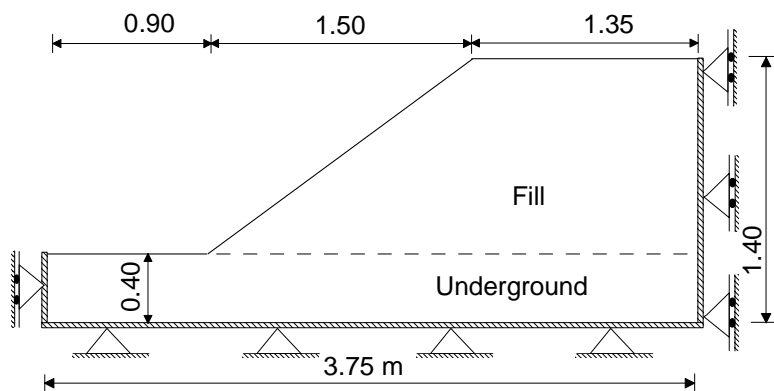


Figure 4.2: FE-Model; dimensions and structural system

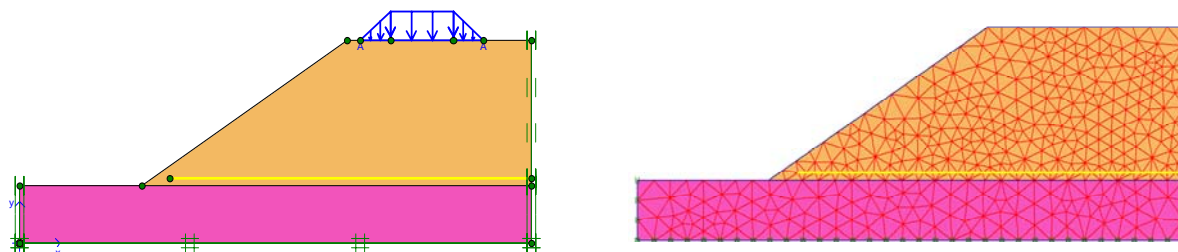


Figure 4.3: Left: 2D- FE-Model; loading system, right: Mesh-generation

In terms of the results, there will be two sections in the system to clarify the results and to compare with test results. Section **A-A** as a vertical section at the shoulder of the embankment slope from the crest of the slope vertically down to the base. This section will serve to obtain the horizontal and vertical deformations at the embankment shoulder. Also section **B-B** is a horizontal section at the embankment base in the slope zone. This will serve as a section to investigate the horizontal earth pressure force and the shear stress distribution along the embankment base (Figure 4.4).

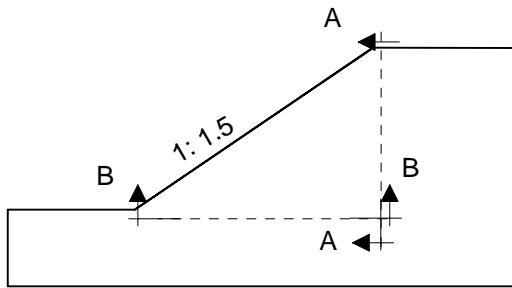


Figure 4.4:
Sections in the model test

In addition, the simulation of the loading process using the pressure cushion has also been carried out by comparing the stress distribution under the pressure cushion (illustrated in Figure 3.7) with a trapezoidal loading system in the FE-model. Figure 4.5 represents the verification of the loading system in model tests using FEM results for a specific external load 50 kN/m^2 , with which all the numerically computed results will also be represented in the next steps.

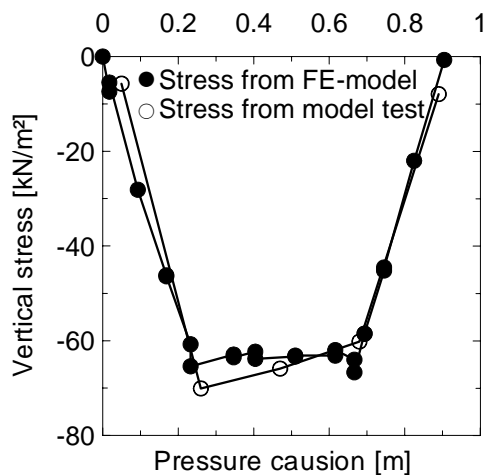


Figure 4.5:
Verification of vertical stress distribution
under the pressure cushion using FEM ($p = 50 \text{ kN/m}^2$)

4.4 Verification of the reference test results with homogeneous sand MT1

In the case of homogeneous sand soil, the first verification process has dealt with getting the calibrated sand parameters, which will be later used as input data in the other computation processes. In this way, the resulting deformation and stress from the model test are compared with a FE-model which has input parameters of the sandy soil from the triaxial test as shown in Table 4.1. Then, the input parameter will be changed and calibrated to give an acceptable verification of the model test results. Figure 4.6 shows the verification of the test results using the numerical computation of the deformations in section A-A.

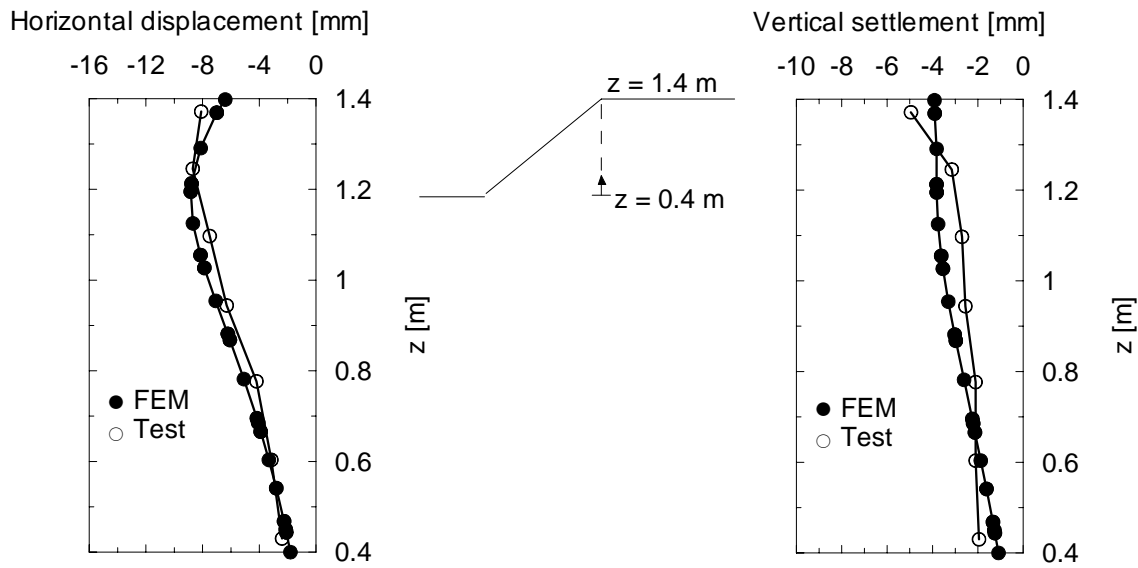


Figure 4.6: Comparing the horizontal and vertical deformations at section A-A ($p = 50 \text{ kN/m}^2$)

In the first numerical computation step, the resulting earth pressure force will be compared with that from the test results as shown in Figure 4.7a. Also the explanation of the deriving of the shear stress from the horizontal earth pressure force equation is represented in Figure 4.7b. The shear stress from section B-B is represented compared with the shear stress resulting from the first derivative of the equation of earth pressure force.

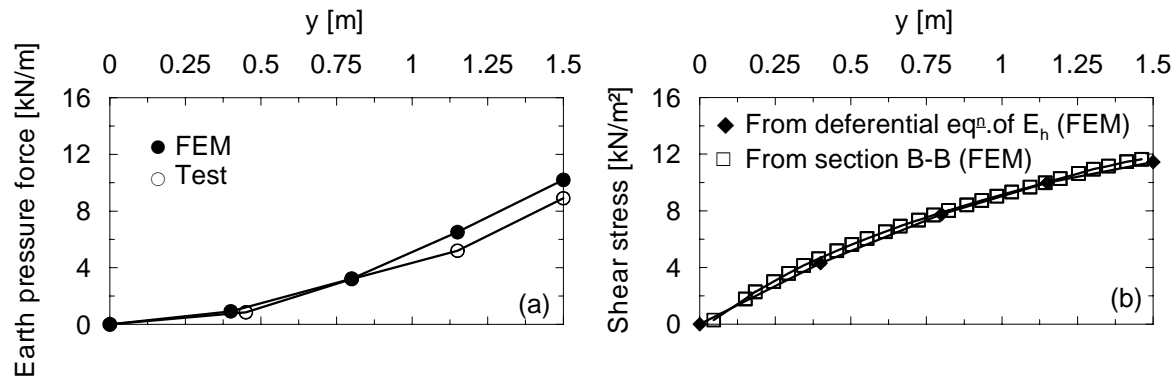


Figure 4.7: a) Comparing the earth pressure forces, b) Comparing the derived shear stress with FEM ($p = 50 \text{ kN/m}^2$)

From Figure 4.7b it is obvious that the derivation of the shear stress from the equation of the horizontal earth pressure force can successfully supply the actual shear stress at the embankment base. Figure 4.8 represents the validated shear stress at the embankment base.

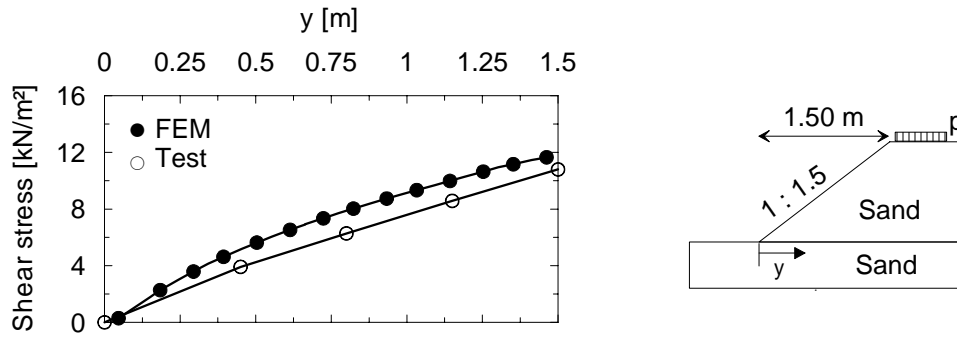


Figure 4.8: Comparing the shear stress distribution at section B-B ($p = 50 \text{ kN/m}^2$)

The standard input parameters for HSM for sand in the model tests before the calibration process is represented in Table 4.1.

Table 4.1: The input model sand parameters for HSM

| c' | φ' | ψ' | p^{ref} | E_{50}^{ref} | E_{oed}^{ref} | E_{ur}^{ref} | m | R_f | γ |
|----------------------|------------|---------|----------------------|----------------------|----------------------|----------------------|-------|-------|----------------------|
| [kN/m ²] | [°] | [°] | [kN/m ²] | [MN/m ²] | [MN/m ²] | [MN/m ²] | [-] | [-] | [kN/m ³] |
| 0 | 38.8 | 11 | 100 | 47.7 | 47.7 | 143.0 | 0.575 | 0.89 | 17.0 |

The calibrated parameters of the sand from this process are indicated in Table 4.2. As mentioned before, these parameters will be used as input parameters of the sand in the next verification processes.

Table 4.2: The calibrated embankment sand parameters for HSM

| c' | φ' | ψ' | p^{ref} | E_{50}^{ref} | E_{oed}^{ref} | E_{ur}^{ref} | m | R_f | γ |
|----------------------|------------|---------|----------------------|----------------------|----------------------|----------------------|-------|-------|----------------------|
| [kN/m ²] | [°] | [°] | [kN/m ²] | [MN/m ²] | [MN/m ²] | [MN/m ²] | [-] | [-] | [kN/m ³] |
| 0 | 40.5 | 11 | 100 | 21.1 | 21.1 | 63.5 | 0.575 | 0.9 | 17.0 |

The increase in the friction angle by 2° can be explained by applying equation 4.9 with consideration of the small stress available in the model test. The reduction in the stiffness of the sand by more than 50 % can perhaps be attributed to the compaction of the sand. During the placement of the sand, it was expected to reach a compactness of $D = 0.89$. In reality, it seems however that this had not been reached. If it is assumed that the density was lower than the planned, the stiffness of the sand becomes also lower. Figures B3 and B4 in Appendix B can be referred for the dependency of the stiffness of the model sand on the compactness D .

An example of the results before and after calibration process is represented in Figure 4.9.

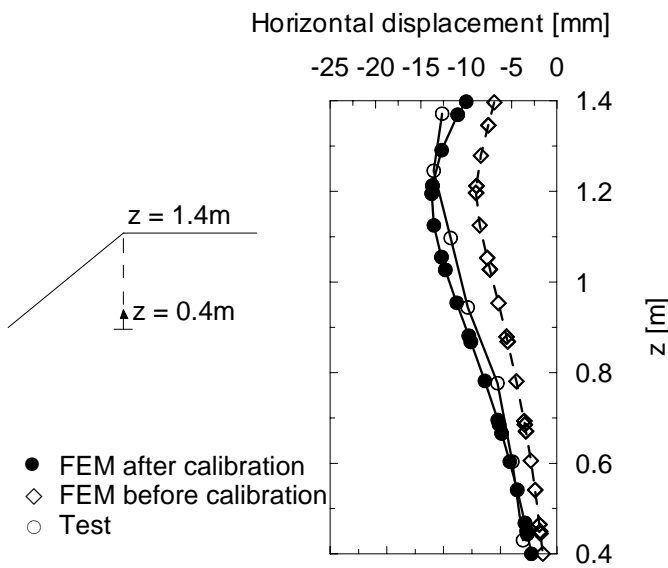


Figure 4.9:
The horizontal displacement
in section A-A ($p = 50 \text{ kN/m}^2$)

4.5 Verification of the model test results MT2, unreinforced embankment on soft underground

In this verification process, the stiffness modulus of the foam material will be computed using the well ready calibrated sand parameters. The calibrated stiffness modulus will be used as input parameter in the next verification processes. Figures 4.10 & 4.11 show the verification of test results. From the computation process, the calibrated stiffness modulus of the foam material was 635 kN/m^2 , which will be used as input data for the next computation steps.

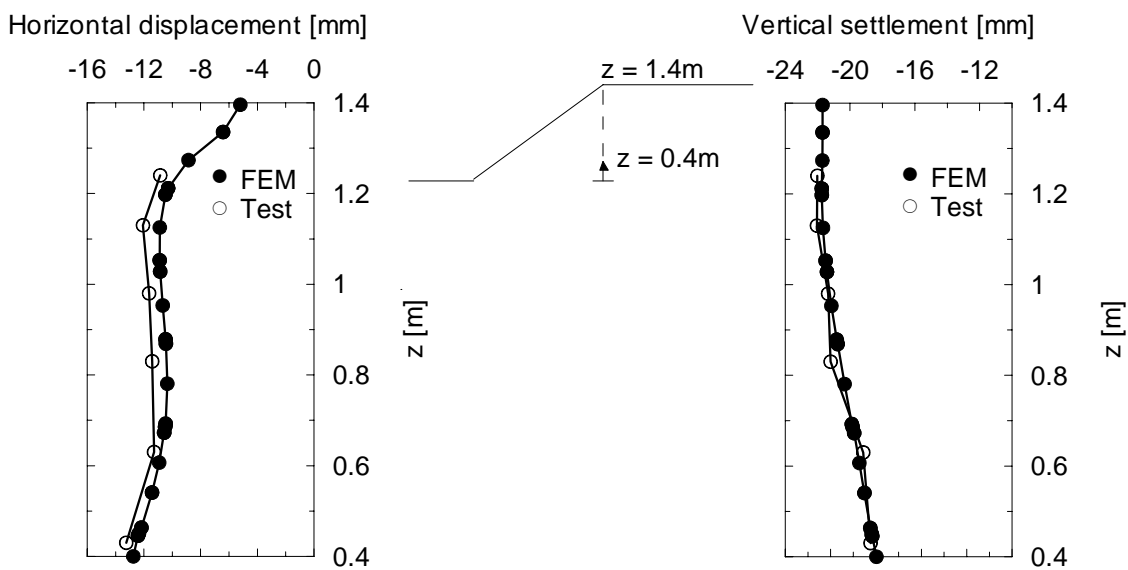


Figure 4.10: Comparing the horizontal and vertical deformations at section A-A, ($p = 50$)

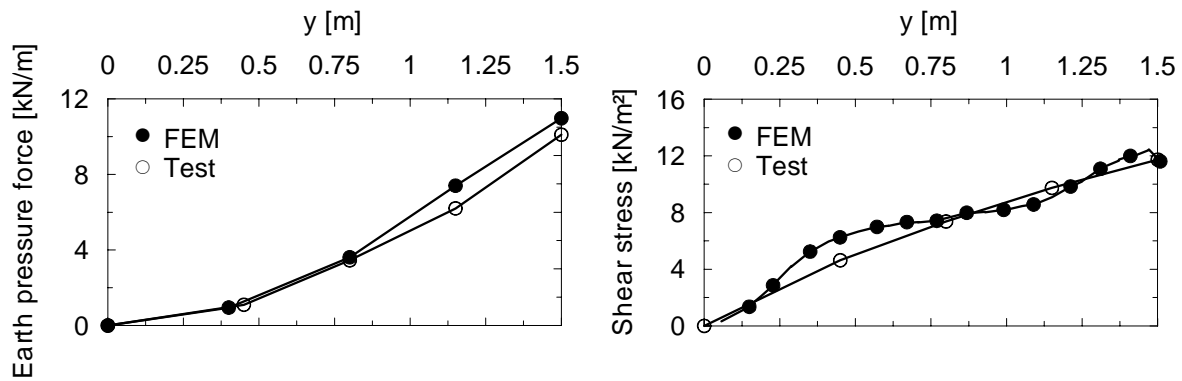


Figure 4.11: Comparing the horizontal earth pressure force and shear stress distribution at section B-B ($p = 50 \text{ kN/m}^2$)

4.6 Verification of the model test results MT3, reinforced embankment on soft underground

In this verification process, the calibrated parameters of both the embankment sand material and soft underground material will be used as input data to validate the model test results (MT3). The resulting deformations in section A-A and the shear stress in section B-B are represented in Appendix C.1. Besides, in this model test the tensile strain of the geogrid reinforcement has also been observed and measured. This resulting tensile strain in model test has been compared with that from FEM computation. Figure 4.12 shows the tensile strain results in reinforcement in the test and FEM.

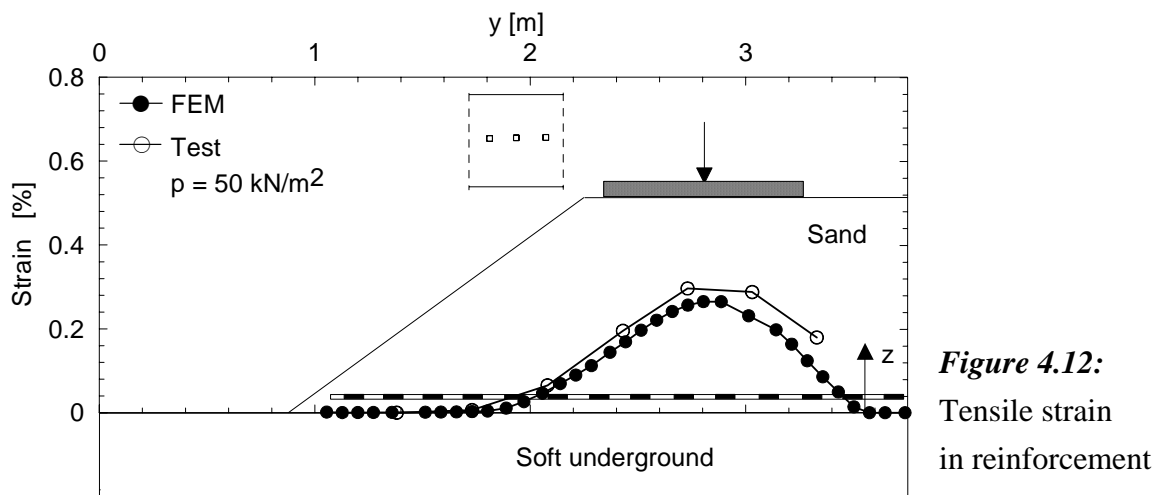


Figure 4.12: Tensile strain in reinforcement

The comparison process shows a very small difference between the test results and 2D-FEM results, this means that computation of the tensile forces in 2D-FEM results in significantly compatible values with the test results. The test results on a 2D-Model system by *Zaeske (2001)* concluded the same concept when compared with the 2D-FEM results.

In the contrary, the existing analytical methods to calculate the spreading force in reinforcement for unpiled embankment result in analytical forces with large deviations from the FEM and model tests. Therefore, the FE methods can be adopted to develop and simulate the case of unpiled embankment and this part of embankment systems would not be considered in the parameter study. To qualify this result, a case history has been represented to investigate in-situ measured strains in reinforcement compared with simulated FEM-results.

4.6.1 Investigation of some in-situ strain results

A case history has been represented in this section to investigate the in-situ measured data with the FEM-model results. The “Großenmeer” by-pass in Germany has been chosen as an example of a reinforced embankment system on soft underground. The measured stress-deformation behaviour of the system elements were plotted and represented in *Blume (1995)*. The analysed embankment sections are represented in Figure 4.13 including the construction stages.

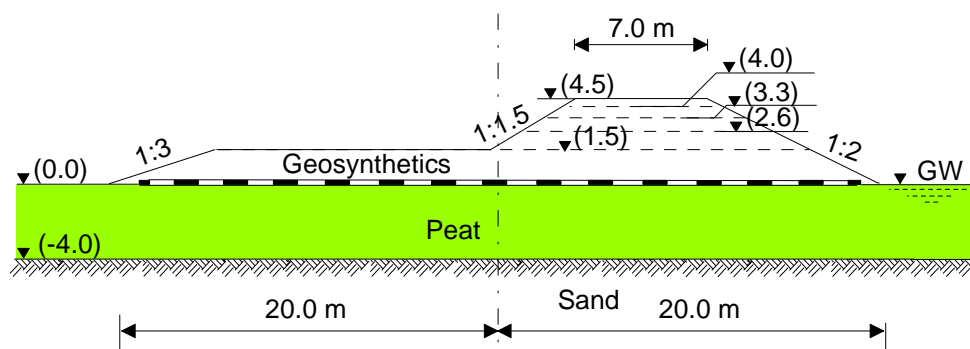


Figure 4.13:
Test section
MQ 2A

Figure 4.13 represents the test cross-section of the roadway and the 5 stages of the construction with heights 1.5 m, 2.6 m, 3.3 m, 4.0 m and 4.5 m respectively. Appendix C.2 represents the construction and the consolidation stages of the test cross-section and Appendix C.3 represents the available soil data of the embankment fill and the soft underground.

The test cross-section MQ 2A has been numerically modelled using PLAXIS 2D-programm to investigate the stress-strain behaviours of the system under consolidation stages and compare the results with the in-situ measured data. A long-term strain results have also been investigated and compared with the measured strain results.

Figure 4.14 represents the measured strain results in reinforcement compared with the FEM-results of the computed strain in GG during the construction phase of the embankment as well as the long-term strain results.

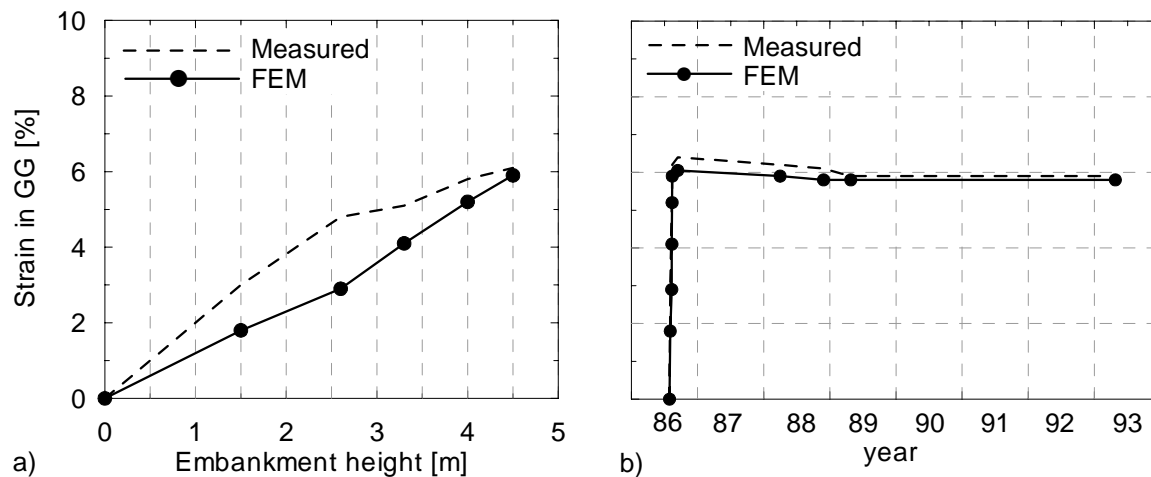


Figure 4.14: The results of the test cross-section MQ 2A:

- Strain in reinforcement; measured strain compared with FEM and with analytical methods due to spreading effect
- Long-term strain measurements compared with FEM

The analytical methods to calculate the horizontal force in reinforcement due to spreading and extrusion effect exhibit a small strains compared with the measured strains. The computation of the long-term strain using FEM can considerably represent the measured strains.

4.7 Verification of the model test results MT4, unreinforced embankment on soft underground supported by pile-like elements

The numerical computation of this model test has been carried out using 3D-FEM in order to simulate the 3D boundaries of the pile elements and their dimensions and positions. The building of FE-Model is represented in Figure 4.15.

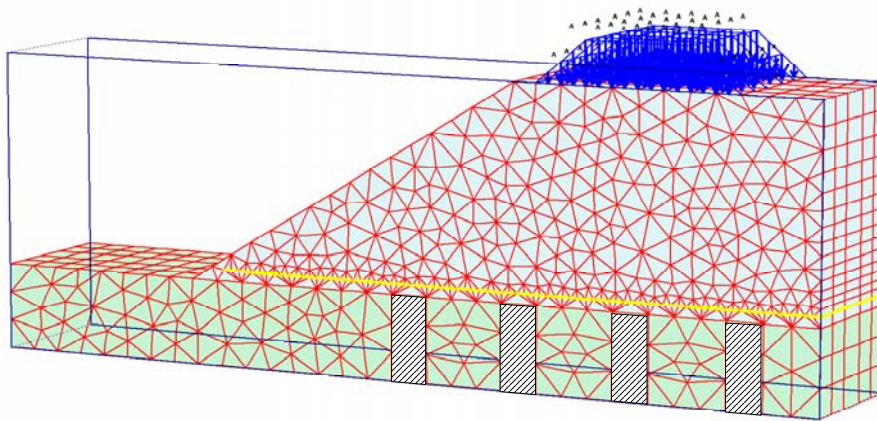


Figure 4.15: 3D-FE-model with pile elements; Loading system and mesh generation

The validated deformation results in section A-A and the shear stress in section B-B are represented in Appendix C.4. The results support the good compatibility of the deformations and the stresses between the model test and the FE-Model.

4.8 Verification of the model test results MT5, reinforced embankment on soft underground supported by pile-like elements.

The structural system of this model test represents the complete bearing system, which contains a reinforced sand embankment and supported pile elements in soft underground. The numerical computation process has also been carried out using the 3D-FEM.

The resulting deformations in section A-A and the shear stress in section B-B are represented in Appendix C.5. Besides, in this model test the tensile strain of the geogrid reinforcement has been observed and measured. This resulting tensile strain in model test has also been compared with that from FEM computation (See Figure 4.17).

Comparing the 3D-FE-results with the model tests produces underestimated FE-values. This was reported by this verification process, in addition to many other 3D-model verification results after *Zaeske (2001)*, *Bussert et al. (2004)*, *Jenck et al. (2005)*, *Heitz (2006)*, and others. A factor related the model test and 3D-FE- results can be mathematically obtained using the 3D-model of *Zaeske (2001)*, *Heitz (2006)*, *Heitz et al. (2006)*, and MT5 in this study.

Figure 4.16 represents the different obtained factors from the available test results.

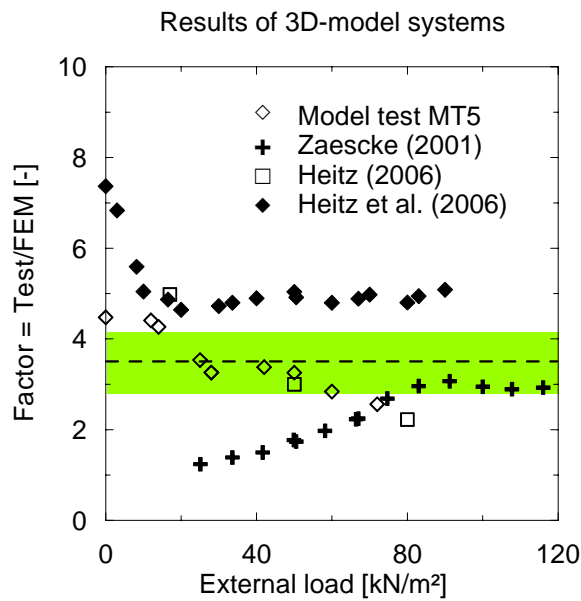


Figure 4.16: Factor related the test results and FEM-results of 3D model tests for strain in GG

From Figure 4.16 it is clear that the factor deviates considerably from test to test and depends on the boundary conditions of every test. However, in the case of loaded system a mathematically mean value as 3.5 can be used to express the relation between the test results and FEM results in the 3D- model tests. This factor would be used in the parameter study in Chapter 6 to study the analytical methods in compare with the FEM results on the prototype.

Figure 4.17 represents the resulting tensile strain in the model compared with that from FEM computation. Further, the factored FE-results can also be represented after multiplying with the estimated factor 3.5.

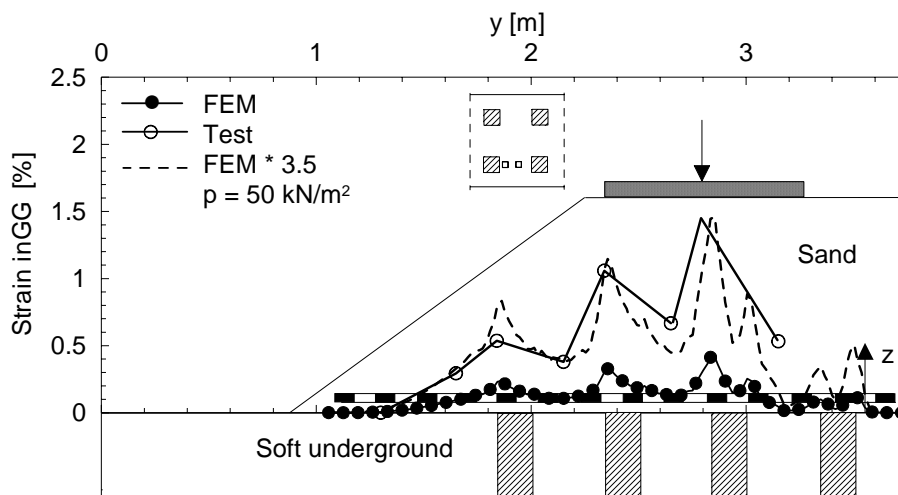


Figure 4.17: Tensile strain in reinforcement in the case of piled underground

Figure 4.17 illustrated that the computed strain in the reinforcement using 3D-FEM was smaller than the measured one. On the other hand, by applying the factor 3.5 to the FE-results,

the strain in reinforcement using FEM can provide a qualified representation of the model test results.

4.9 Evaluation of the results

- The model results have been verified using the 2D- and 3D-FEM in PLAXIS program.
- The FE-Models have qualitatively simulated the model test dimensions and boundary conditions. The loading system on the pressure cushion in the model tests has also been perfectly simulated.
- The constitutive models of the embankment materials have been estimated and calibrated from the verification of the model test results.
- The tensile strain of the geogrid reinforcement in the case of underground without pile elements can be approximately typically simulated using 2D-FEM.
- The tensile strain of the geogrid reinforcement was 3.5 times smaller in the FE-calculations than model test results, when the system is simulated using 3D-FEM.
- The tensile strain in the 3D-FEM is smaller than the strain in 2D-FEM. This might be attributed to the distribution of the tensile force of the geogrid in two directions of the pile grid. Figure 4.18 represents the deformed mesh of the geogrid in both 2D- and 3D-FEM.

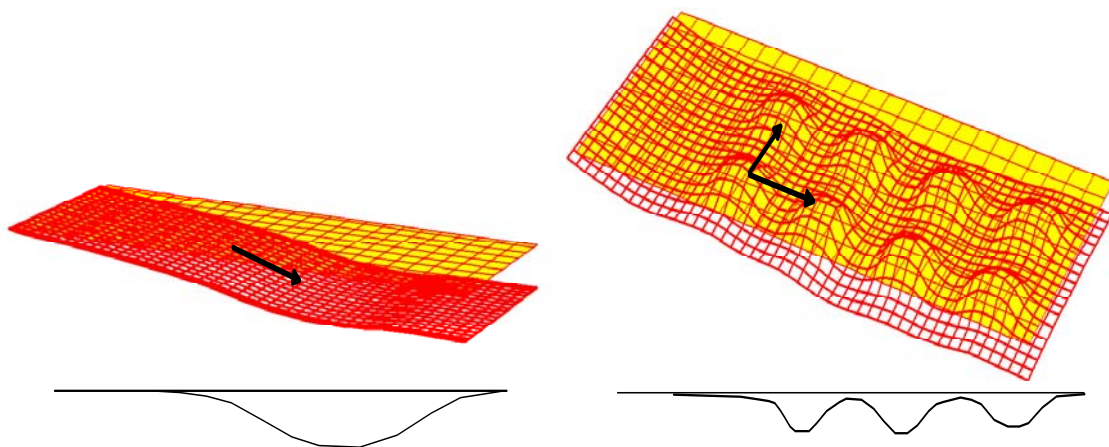


Figure 4.18: a) Deformed geogrid in 2D-FEM, b) Deformed geogrid in 3D-FEM

From Figure 4.18 it is observed from the FEM-computation that the tensile force in the 3D-system is distributed in the two directions of the pile-grid.

However, in the 2D-system without piles the deformation is concentrated in one direction and the geogrid functions as a wire element as in prototype.

Analysing the same embankment system but taking a slice of only one row of piles can also qualify this observation. Figure 4.19 represents the difference between the strain results in both systems. The strain in the two piles-row is divided in the two directions, while in the one pile-row was not divided.

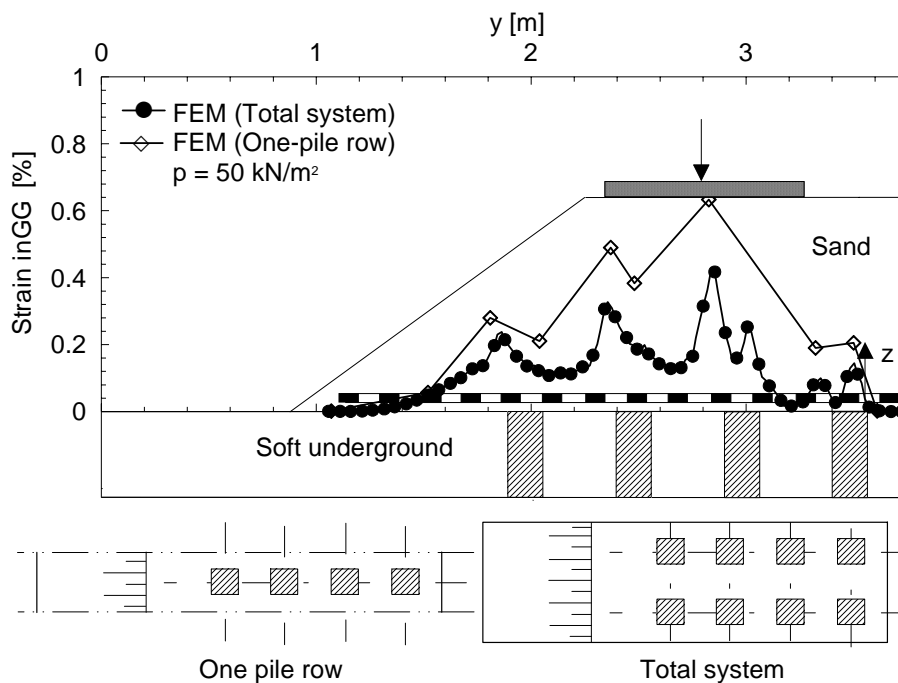


Figure 4.19:
Strain in reinforcement using 3D-FEM in one-pile row and in total system

The analysis of the system contains one row of piles demonstrates in a strain of reinforcement greater than that when analysing the total system contains a pile grid in two directions.

- The extension of the model system with the help of FEM to the prototype is possible. The deformations and stresses are applicable in the numerical computation, but on the other hand, the tensile forces in the geogrid fail smaller in the FEM.

5 Parameter study

5.1 Objectives and fundamentals of the parameter study

From the verification of the model tests in Chapter 4, it was concluded that the recomputation of the structural system “basal reinforced embankment over underground with and without pile-like elements” could successfully be carried out on the prototype model. The prototype model is investigated using some variations that analyse the behaviour of each element under different parameter-conditions. This is known as the parameter study. The objective of the parameter study is to control the analytical methods through the variation of different parameters in the system. Hence, comparing the analytical and numerical methods can be correctly accomplished. Furthermore, a possible modification can be derived to find out which parameters influence the stress-strain behaviours of the structural system. The finite element method (FEM) is provided as the best method for this. The parameter study is carried out by varying one parameter and keeping the others constant and then corresponding and comparing this behaviour with some analytical methods.

This study will include all the effective parameters and boundary conditions that investigated in the model tests. The study is focused on the case of a reinforced sand embankment on an underground supported by pile-like elements. A modified analytical method to determine and investigate the spreading effect has been developed in basis of the results of the parameter study in Chapter 6.

The parameter study in Chapter 5 will deal with the various parameters which will control the load/deformation relations of each element in the system especially the tensile forces, the strain in reinforcement and the horizontal displacement of the pile heads. The embankment heights chosen in this case are restricted with the practical objectives of the embankments. Hence, small to very high embankments (2 m, 5 m and 10 m) were chosen in this parameter study.

The program PLAXIS 3D Tunnel was used in the case with pile-like elements. 15-nodes triangular elements were applied. The hardening soil model (HSM) was applied to simulate the embankment soil material and the soft soil model (SSM) to simulate the soft soil material, depending on the material characteristics. The structural elements (the piles-like elements and GG-reinforcement) were assumed to behave elastically according to Hook’s law. The main results to be determined in this study focuses on the tensile force in the reinforcement, the deformation of the system and the stress-strain behaviour of the pile-like elements.

5.2 Pre-calculation steps

The pre-calculation steps served to evaluate the used items and material behaviours in the system, as well as the effect of external parameters such as traffic surcharge. The steps would include the behaviour of the interface soil/reinforcement.

5.2.1 Studying the interface soil/reinforcement

The effect of the friction coefficient of the reinforcement with embankment soil on the tensile force in the reinforcement was numerically discussed under variation of the interface soil/reinforcement, R . Practically, the friction coefficient of the geogrid reinforcement ranges from 0.85 to 1.00 (see Table 3.5 in Section 3.2.3). The shear box tests carried out by *Zaeske (2001)* on the geogrid determined the friction coefficient between the geogrid (FORTRAC 60/60-20) and the embankment sand and it was found that $R = 0.99$.

In the case of underground with pile elements the interface soil/geogrid has a significantly effect on the tensile forces where the smaller values of interface provided smaller values of load contribution to the geogrid and more stresses on the pile elements. Figure 5.1 represents the tensile forces on the reinforcement under variation of the interface soil/geogrid.

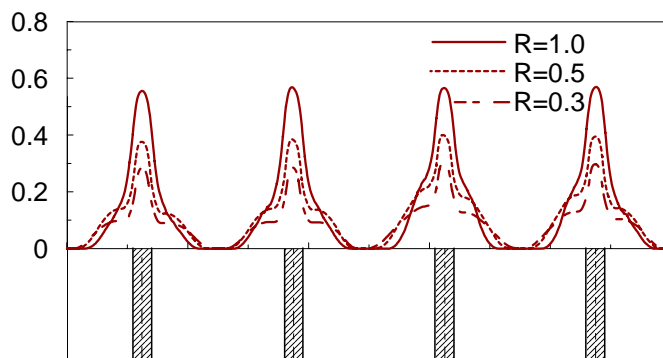


Figure 5.1:
Tensile force in Geogrid under variation of interface soil/reinforcement on piled underground

The tensile forces in the geogrid provided the maximum values under the case that the interface $R = 1$ which has been chosen to the parameter study in the case of underground supported with pile elements.

5.3 Material properties

5.3.1 General

The prototype model to be analysed and studied is chosen under variation of the most effective parameters, which control the stress-strain behaviour of the basal reinforced embankment on an underground without pile-like elements. The height of the embankment is one of the most effective parameters, which control this behaviour. The tensile force in reinforcement increases considerably with the increase of embankment height (theoretically). Also the stiffness of the underground has an important role to control the tensile force in reinforcement due to the spreading effect and vertical stresses. The spreading effect is dependent on the slope angle of the embankment, where the shear stress at embankment base increases with the steeper slopes. The direction of the study will concern mainly with the comparison of the results under constant tensile stiffness of the geogrid reinforcement. Furthermore, multi layer geosynthetics reinforcement can also be considered.

5.3.2 Geogrid reinforcement

The geogrid was used as a geosynthetics reinforcement in the parameter study under elastic behaviour according to Hook's law with a constant tensile stiffness $J = 2000$ kN/m for all computations. Furthermore, stiffer GG reinforcement with higher stiffness has been provided in order to investigate the effect of less strain-GG on the stability of the system and the stress-deformation behaviour of the structural elements. Multi-layer GG has also been applied to the system to investigate the development of the deformations of the system and to determine the relation between spreading and membrane effect in such case, (see Table 5.1).

Table 5.1: Stiffness and layers of GG-reinforcement in the parameter study

| | |
|------------------|------------------------------|
| | Tensile stiffness J [kN/m] |
| Reference system | 2000 |
| | No. of GG-layers |
| Reference system | 1 |
| Variations | 2 |
| | 3 |

5.3.3 Embankment fill

One of the most effective parameters controlling the spreading and the membrane forces in reinforcement is the embankment height. The spreading forces due to horizontal earth pressure in the slope zone depend mainly on the embankment height as shown in Equation A.1 in Appendix A.1. So the tensile force in reinforcement increases substantially with the increasing of the embankment height. The variation of embankment height involves examples of a low embankment ($h_l = 2.0$ m), a middle height embankment ($h_l = 5.0$ m) and a very high embankment ($h_l = 10.0$ m). The embankment slope will be considered as a variation parameter in the study. The shear stress and consequently the horizontal deformation in the slope zone increases with steeper embankment slopes. The variation of the embankment slope will involve a slope of 1:1.5 (inclination angle $\beta = 33.7^\circ$) as an example of steep slope and a slope of 1:2.5 (inclination angle $\beta = 21.8^\circ$) as an example of flatter slope. Basically, the hardening soil model (HSM) was used to simulate the soil behaviour and constitutive relations of sand material in the embankment fill (see Table 5.2).

Table 5.2: Material parameters for the embankment sand

| Soil parameters (HSM) | | | | | | | | | | |
|-----------------------|------------|----------------------|---------|----------------------|----------------------|----------------------|----------------------|----------------------|---------|-----|
| | φ' | c' | ψ' | γ_{unsat} | γ_{sat} | E_{50}^{ref} | E_{oed}^{ref} | E_{ur}^{ref} | ν_m | m |
| | [°] | [kN/m ²] | [°] | [kN/m ³] | [kN/m ³] | [MN/m ²] | [MN/m ²] | [MN/m ²] | [-] | [-] |
| Embankment fill | 35 | 2 | 7 | 18.0 | 21.0 | 32 | 32 | 192 | 0.15 | 0.5 |

5.3.4 Underground layer

The variation of the soft underground layer will include graduate stiffness from a very soft soil such as high moor peat, then normally consolidated clay, to a slightly over consolidated clay as an example of a high stiffness soil. The thickness of the soft layer will be constant in all computations as 5 m depth. The soft soil model (SSM) will simulate the constitutive relations of both the high moor peat and the normally consolidated clay, while the hardening soil model (HSM) will simulate the constitutive relations of slightly over consolidated clay.

Table 5.3a and 5.3b represent the soil parameters of the soft underground variations according to each constitutive relation.

Table 5.3: a) Soil parameters of the soft underground materials (SSM)

| | φ' | c' | ψ | γ_{unsat} | γ_{sat} | λ^* | κ^* | $E_s^{[1]}$ |
|--------------------------------|------------|----------------------|--------|----------------------|----------------------|-------------|------------|----------------------|
| | [°] | [kN/m ²] | [°] | [kN/m ³] | [kN/m ³] | [-] | [-] | [kN/m ²] |
| Peat (P) | 15.0 | 5 | 0 | 12.0 | 12.0 | 0.12 | 0.04 | 800 |
| Normal consolidated clay (ncc) | 25.0 | 1 | 0 | 19.5 | 19.5 | 0.03 | 0.01 | 3333 |

[1] für $p^{ref} = 100 \text{ kN/m}^2$

b) Soil parameters of the underground materials (HSM)

| Soil parameters (HSM) | | | | | | | | | | |
|------------------------------|------------|----------------------|--------|----------------------|----------------------|----------------------|----------------------|----------------------|---------|-----|
| Over consolidated clay (occ) | φ' | c' | ψ | γ_{unsat} | γ_{sat} | E_{50}^{ref} | E_{oed}^{ref} | E_{ur}^{ref} | ν_m | m |
| | [°] | [kN/m ²] | [°] | [kN/m ³] | [kN/m ³] | [MN/m ²] | [MN/m ²] | [MN/m ²] | [-] | [-] |
| | 20 | 20 | 0 | 18.5 | 18.5 | 11.25 | 11.25 | 120.0 | 0.2 | 0.6 |

5.3.5 Pile-like supporting elements

The pile-like elements in the system will be simulated as unreinforced pile elements in a square grid raster 2.0 m axe-to-axe span. The cross section of the pile element is squared 0.6 m width. The pile elements rested on a firm sand layer with a penetration depth of 1 m. The plain concrete material of the piles (C12/15) is classified under the German standard *DIN 1045-1: 2005-1*. The Hook's law of elastic material controls the stress-strain behaviour of the piles. Table 5.4 represents the material properties of the pile elements, where f_{ctm} represents the characteristic tensile stress of the plain concrete.

Table 5.4: Material properties of the pile elements

| γ_{unsat} | γ_{sat} | ν | ε | E_s | f_{ctm} |
|----------------------|----------------------|-------|---------------|----------------------|----------------------|
| [kN/m ³] | [kN/m ³] | [-] | [%] | [MN/m ²] | [MN/m ²] |
| 24 | 24 | 0.2 | 0.9 | 25800 | 1.6 |

The 3D FE-model implies two rows of piles as an example of the pile-grid. This means that the 3D system will extend to 4 m in the direction of the embankment length.

5.4 External load

The parameter study has been carried out for an external static load (e.g. a traffic load) variation. The external load SLW-60 (for $p = 30 \text{ kN/m}^2$) has been presented as the main external load on the system, in order to illustrate the influence of load process on the stress-strain behaviour of reinforcement.

5.5 Pre-calculation steps for the numerical analysis

5.5.1 General

In the case of reinforced embankment on soft underground supported by pile-like elements the parameter study has been dealt with the behaviour of the reinforcement under loading conditions. In addition to the spreading forces the reinforcement developed also membrane forces due to the arching effect of the soil between piles. The loads in this system transferred from the base reinforcement to the pile elements. Therefore, the arching effect on the reinforcement compared with the spreading effect has been widely investigated and evaluated under the parameter variations. Figure 5.2 represents the arching and membrane effect in reinforcement.

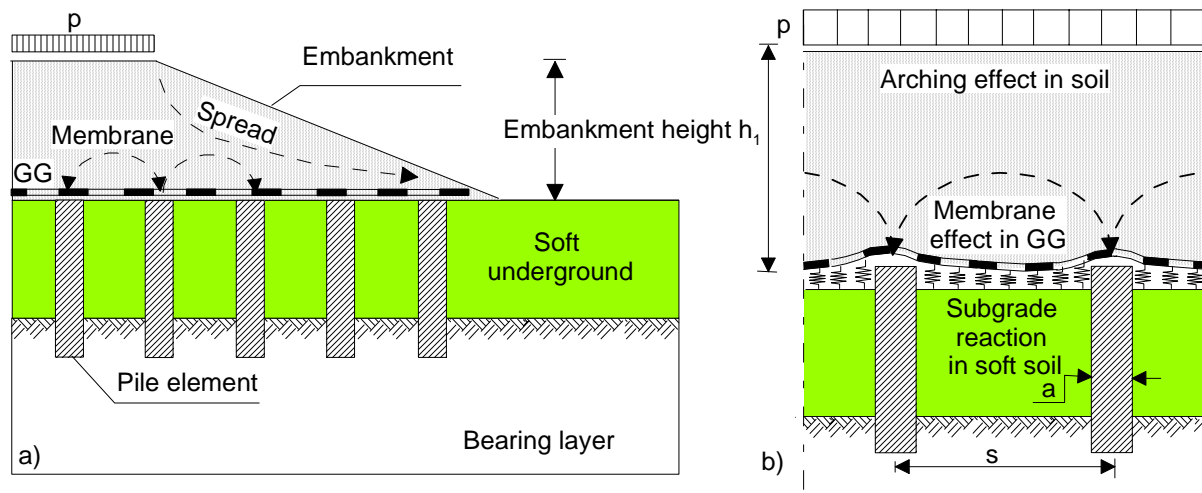


Figure 5.2: a) Spread and membrane forces in reinforcement, b) Arching effect in soil

Moreover, the stress-deformation of the pile elements has also been investigated under the effect of applying basal reinforcement. The program PLAXIS 3D-Tunnel would be used for the computation processes. The FE-model in the study includes two geometrical models. The first FE-model is the complete embankment model with slope zones, with which the total stress-

deformation behaviour of the system and reinforcement would be investigated and analysed. In this FE-model, both the spreading effect and arching effect influence the behaviour of the system. The second FE-model includes only a membrane model without slope zones to investigate the arching effect in the reinforcement separately. The results of each FE-model would be analysed and investigated to determine the relation between spreading forces and membrane forces in the reinforcement. The study has been dealt with the analysis of the system under a defined external load in order to optimise the analysis of the system behaviour.

5.5.2 Steps to build a membrane model by FEM

The numerical system to compute the tensile forces in reinforcement due to membrane effect must consider both the distribution of external load in the slope zone and the membrane effect in reinforcement lies in the slope zone. The system used in this study has been carried out in some calculation steps by considering a box model which includes the slope zone:

1. The membrane effect of the own weight of each slice ($F_{M,1gi}$) can be computed in a soil weight according to the height of each slice (the soil weight of strip 1 is equivalent to the soil weight of vertical slice (1)) and compute the tensile force for each weight slice as shown in Figure 5.3a for the example of an embankment height $h_I = 2$ m.

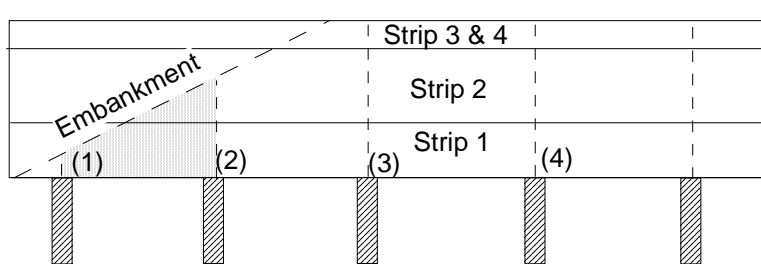


Figure 5.3a:
Tensile force in reinforcement due to the own weight of the vertical slices $F_{M,1gi}$

2. Under the total own weight, the tensile force in reinforcement is determined for each slice $F_{M,2gi}$ (force in the reinforcement lies in between the two piles limit this slice). Figure 5.3b represents the determination of tensile force according to the total own weight of the embankment.

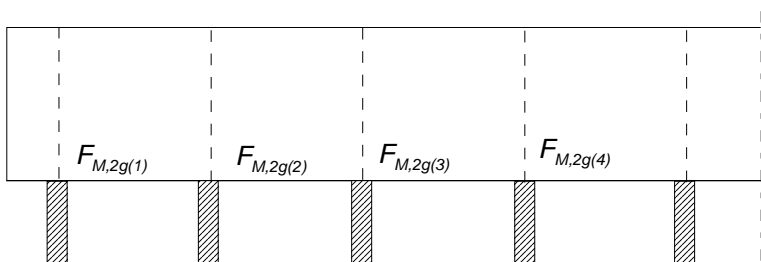


Figure 5.3b:
Tensile force in reinforcement due to the total own weight of the embankment $F_{M,2gi}$

3. Applying the external load p over the total system and then the determined tensile force in each slice in the reinforcement $F_{M,(g+p)i}$ describes the tensile force due to a total embankment weight and an external applied load p (Figure 5.3c).

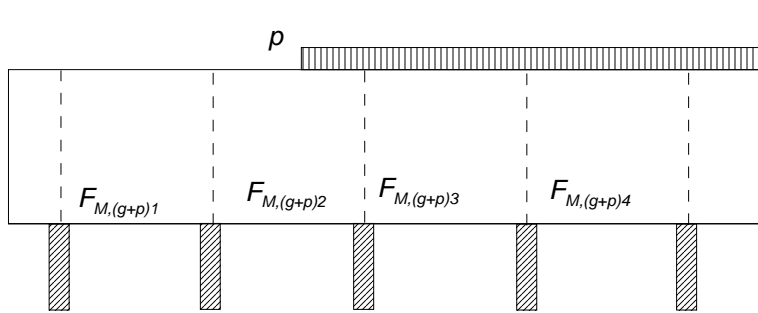


Figure 5.3c:

Tensile force in reinforcement due to the total own weight of the embankment and the external load $F_{M,(g+p)i}$

4. The tensile force in the reinforcement in each slice due to the external load only can now be determined by subtracting the force due to the own weight from that due to the external surcharge and own weight as shown in Equation 5.1.

$$F_{M,pi} = F_{M,(g+p)i} - F_{M,2gi} \quad (5.1)$$

5. Now by adding the tensile force due to the own weight for each slice to the tensile force due to the distribution of external surcharge at each slice, the total tensile force in each slice $F_{M,i}$ can be determined as shown in Equation 5.2.

$$F_{M,i} = F_{M,pi} + F_{M,1gi} \quad (5.2)$$

The tensile force in the reinforcement according to the membrane effect can be graphically represented by a unique value for each slice in the embankment.

5.5.3 Steps to determine the force due to spreading effect by FEM

The embankment system involving the slope zone is to be numerically computed. The resulting tensile force in the reinforcement will be the force due to both the membrane effect and the spreading effect. Hence, the tensile forces due to the membrane effect only is to be subtracted mathematically from the total tensile forces to get the tensile forces due to spreading effect only. Figure 5.4 shows an example of the tensile forces in the three components.

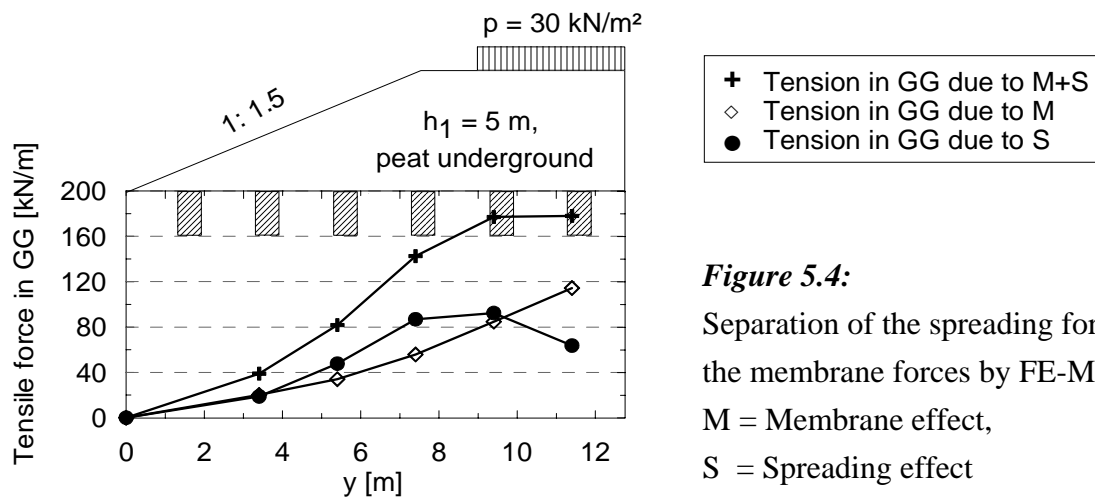


Figure 5.4:

Separation of the spreading forces from the membrane forces by FE-Model;
 M = Membrane effect,
 S = Spreading effect

5.6 Model dimension and variation matrix

The model geometry depends on the applied slope, which varies from flat slope (1:2.5) to steep slope (1:1.5) and on the embankment height, which varies from low embankment (2 m height), middle embankment (5 m height) to very high embankment (10 m height). The highway type RQ 10.5, see *RAS-Q 96 (1996)*, represents the embankment surface.

A square grid 2.0 m x 2.0 m of unreinforced concrete pile elements with cross-section 0.60 m will be simulated in the FE-model by a continuum.

Figure 5.5 represents the symmetry model geometry of the embankment and Table 5.5 represents the main data and the number of piles for each model. The results in the case of piled embankment have been mainly evaluated and represented with the applied external load SLW-60 (for $p = 30 \text{ kN/m}^2$). Furthermore, the stress-deformation behaviour of the pile elements under the different parameter variations has also been investigated and evaluated under the same external load.

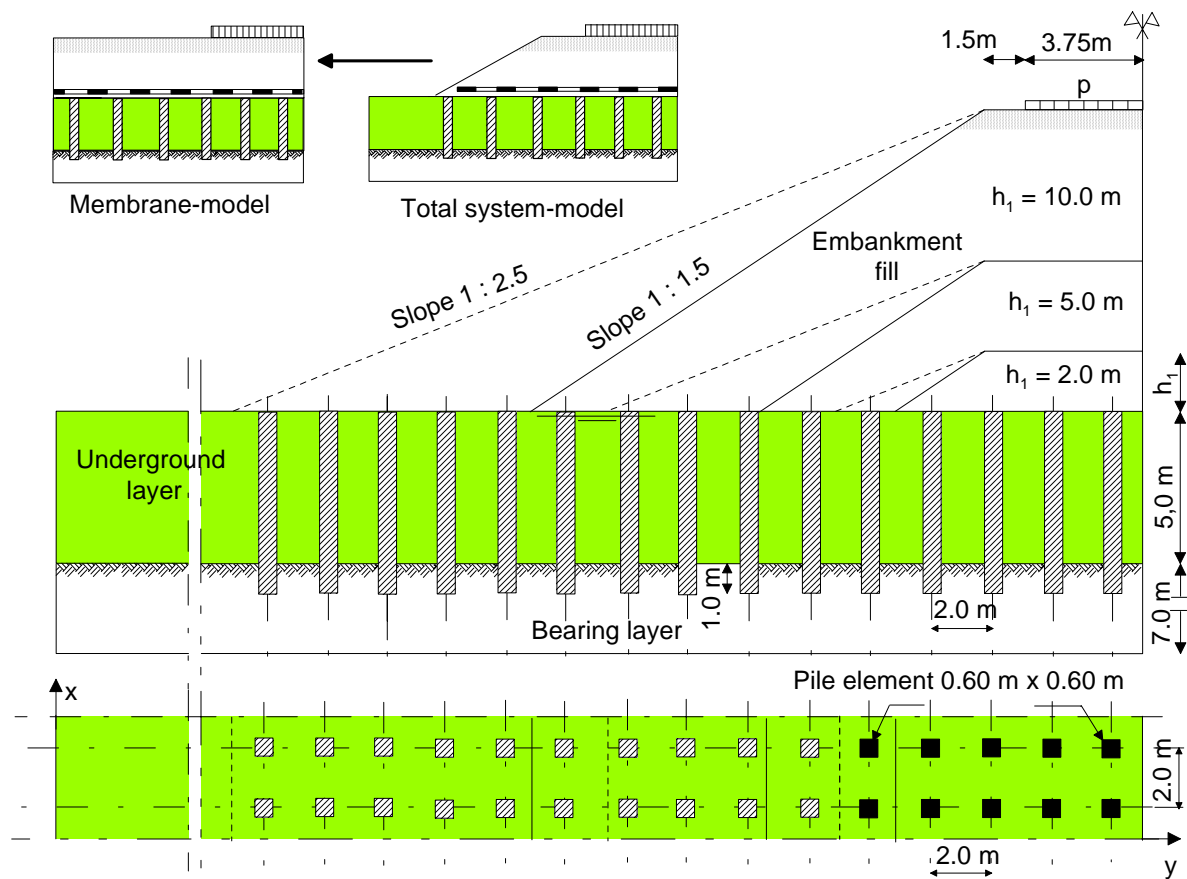


Figure 5.5: Geometry and dimensions of the piled embankment FE-model

Table 5.5: The main data for each FE-model

| | | | | | | | |
|-----------------------------|-----|-------------|-------|-------------|-------|--------------|-------|
| Embankment height | [m] | $h_1 = 2.0$ | | $h_1 = 5.0$ | | $h_1 = 10.0$ | |
| Slope | [-] | 1:1.5 | 1:2.5 | 1:1.5 | 1:2.5 | 1:1.5 | 1:2.5 |
| Underground-layer thickness | [m] | 5.0 | | | | | |
| Pile distance $s_x = s_y$ | [m] | 2.0 | | | | | |
| Pile dimensions $b_x = b_y$ | [m] | 0.6 | | | | | |
| No. of piles for each model | [-] | 4 | 5 | 6 | 9 | 10 | 15 |

The computation matrix can then be built according to the basis of keeping one parameter constant and variation of the others. Table 5.6 represents the variation matrix.

Table 5.6: Variation matrix for parameter study

| Height [m] | Geogrid | Slope | Underground | Name of the Model |
|--------------------------|---------------|-------|--------------------------|-------------------|
| $h_l = 2.0$ | 0 GG | 1:1.5 | Peat | F_h2_01G_15_p |
| | | | Normal consolidated clay | F_h2_0,1G_15_ncc |
| | | | Over consolidated clay | F_h2_0,1G_15_occ |
| | | 1:2.5 | Peat | F_h2_0,1G_25_p |
| | | | Normal consolidated clay | F_h2_0,1G_25_ncc |
| | | | Over consolidated clay | F_h2_0,1G_25_occ |
| | 1 GG (PET) | 1:1.5 | Peat | F_h2_0,1G_15_p |
| | | | Normal consolidated clay | F_h2_0,1G_15_ncc |
| | | | Over consolidated clay | F_h2_0,1G_15_occ |
| | | 1:2.5 | Peat | F_h2_0,1G_25_p |
| | | | Normal consolidated clay | F_h2_0,1G_25_ncc |
| | | | Over consolidated clay | F_h2_0,1G_25_occ |
| | 2 GG | 1:2.5 | Peat | F_h2_2G_25_p |
| | 3 GG | 1:2.5 | Peat | F_h2_3G_25_p |
| | $h_l = 5.0$ | 0 GG | 1:1.5 | Peat |
| Normal consolidated clay | | | | F_h5_0,1G_15_ncc |
| Over consolidated clay | | | | F_h5_0,1G_15_occ |
| 1:2.5 | | | Peat | F_h5_0,1G_25_p |
| | | | Normal consolidated clay | F_h5_0,1G_25_ncc |
| | | | Over consolidated clay | F_h5_0,1G_25_occ |
| 1 GG | | 1:1.5 | Peat | F_h5_0,1G_15_p |
| | | | Normal consolidated clay | F_h5_0,1G_15_ncc |
| | | | Over consolidated clay | F_h5_0,1G_15_occ |
| | | 1:2.5 | Peat | F_h5_0,1G_25_p |
| | | | Normal consolidated clay | F_h5_0,1G_25_ncc |
| | | | Over consolidated clay | F_h5_0,1G_25_occ |

continued

Table 5.6 (continued)

| Height [m] | Geogrid | Slope [-] | Underground | Name of the Model |
|--------------|---------|-----------|--------------------------|-------------------|
| $h_l = 10.0$ | 0 GG | 1:1.5 | Peat | F_h10_0,1G_15_p |
| | | | Normal consolidated clay | F_h10_0,1G_15_ncc |
| | | | Over consolidated clay | F_h10_0,1G_15_occ |
| | | 1:2.5 | Peat | F_h10_0,1G_25_p |
| | | | Normal consolidated clay | F_h10_0,1G_25_ncc |
| | | | Over consolidated clay | F_h10_0,1G_25_occ |
| | 1 GG | 1:1.5 | Peat | F_h10_0,1G_15_p |
| | | | Normal consolidated clay | F_h10_0,1G_15_ncc |
| | | | Over consolidated clay | F_h10_0,1G_15_occ |
| | | 1:2.5 | Peat | F_h10_0,1G_25_p |
| | | | Normal consolidated clay | F_h10_0,1G_25_ncc |
| | | | Over consolidated clay | F_h10_0,1G_25_occ |

The programs in the computation matrix would also be again computed for the membrane system only as mentioned in Section 5.5.2. The names of the membrane systems are the same adding (M).

5.7 Results of the numerical parameter study

5.7.1 General

The parameter study in the case of underground supported by pile elements has been focused on the separation between the tensile forces in the reinforcement due to membrane effect between piles and due to spreading effect in the slope zone. The relation between the membrane and spreading forces under the parameter variations has also been discussed and detailed with respect to the main parameter in the study which deals with the embankment height. The FE-results have been multiplied by the factor 3.5 which estimated in Chapter 4. The results of the FE-computations in this case would be filtered to an external load $p = 30 \text{ kN/m}^2$ and with an embankment slope 1:1.5 in order to concentrate the large number of evaluation and results steps. The results in the case of peat underground have also been represented in detail in this

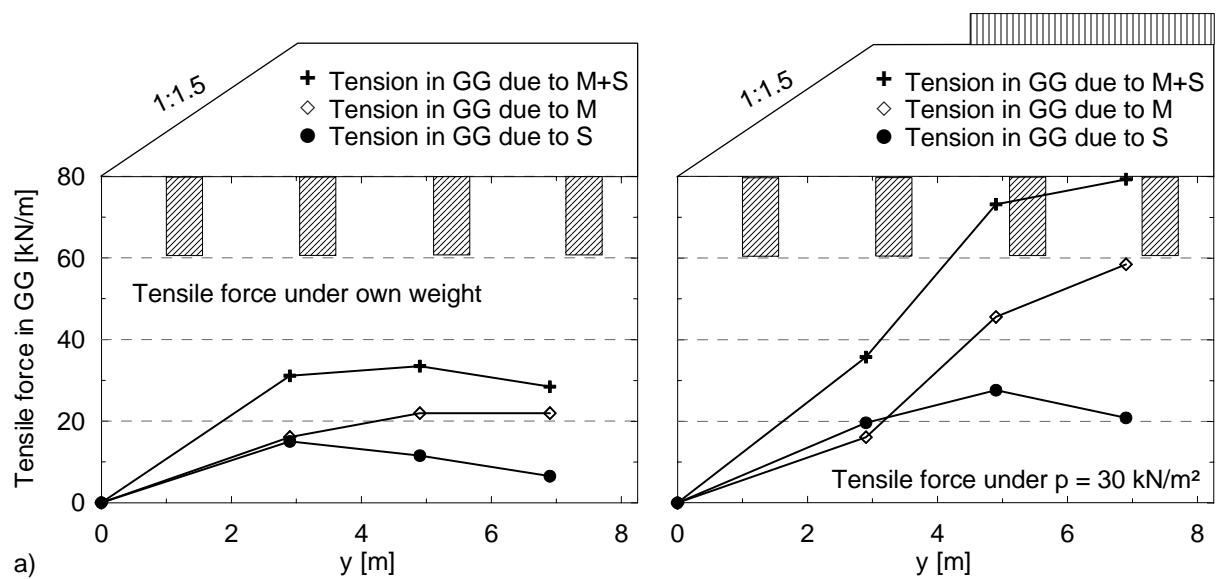
Chapter; however, the other results have been represented in (Appendix D). Table 5.7 represents the data of the reference system in this parameter study.

Table 5.7: Parameters of the reference system

| Embankment height h_1 | Embankment slope | Underground soil | Reinforcement layers | External load | |
|-------------------------|------------------|------------------|----------------------|----------------------|----------------------|
| | | | | Own weight | p |
| [m] | [-] | [-] | [-] | [kN/m ²] | [kN/m ²] |
| 2 | 1:1.5 | Peat | 1 GG-layer | 0 | 30 |

5.7.2 Results of tensile forces under variation of the embankment height

The effect of embankment height on the spreading forces in the reinforcement has been analysed by varying of the embankment heights and computing the total system, which includes the central and slope zones. Then, the membrane system is computed according to Section 5.5.2 and the spreading force is separated from the membrane force in each embankment height. The analysis of the tensile forces in the reinforcement along the length of the geogrid layer provided a detailed view of the influence of the stresses and their effects on the reinforcement behaviour and also the evaluation of the points of maximum tensile forces. The tensile force in reinforcement due to membrane and spreading effect under variation of the embankment heights is represented in Figure 5.6.



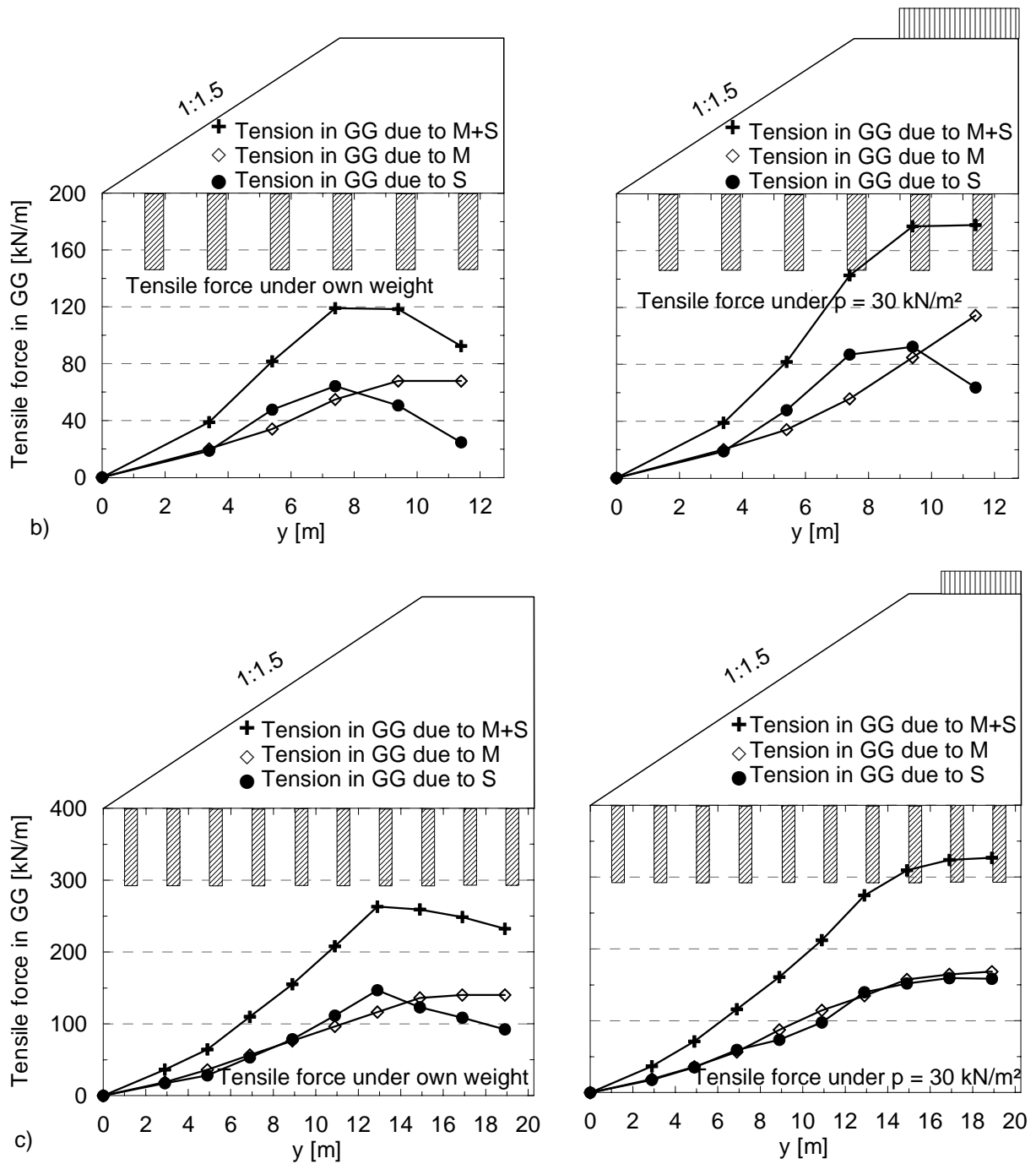


Figure 5.6: Spreading, membrane and total forces along the geosynthetics reinforcement; Embankment on peat underground, a) $h_1 = 2$ m, b) $h_1 = 5$ m and c) $h_1 = 10$ m

In the case of unloaded embankment the spreading effect in the slope zone applies more stresses on the reinforcement than that from the membrane effect. On the contrary, the spreading forces decreased in the central zone. This resulted in a maximum tensile force due to spreading at/near the slope crest. The behaviour of the reinforcement in the slope zone shows that with increasing the embankment height increased consequently the spreading tensile

force compared with membrane tensile force in the slope zone. In the case of loaded embankment the maximum spreading force located in the central zone of the embankment. The membrane effect in this case applies more stresses on the reinforcement in the central zone, with which the maximum membrane force is larger than that of the spreading force. By increasing the embankment height increased also the effect of spreading. Therefore, the spreading and membrane have approximately equal effect on the reinforcement behaviour in the case of a very high embankment (10 m). The detailed forces in the reinforcement in the case of normal and over consolidated clay underground are represented in Appendix D.1 and D.2.

The increase of the spreading force by loading the 10 m-height embankment is very small that is the soil in very high embankment behaves near rest state and then the loading process has small effective changes in soil behaviour, especially in the slope zone, where the own weight of the soil is the most effective load-parameter. Figure 5.7 represents the spreading and membrane forces in the reinforcement under variation of the loaded/unloaded embankment height.

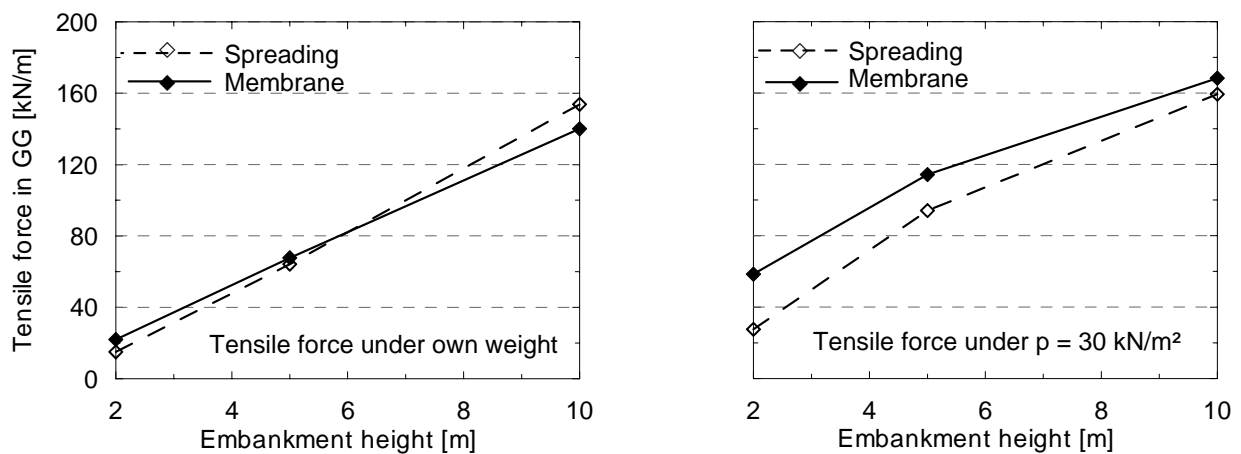


Figure 5.7: Spreading and membrane forces in the reinforcement of unloaded/loaded embankment

Figure 5.7 shows that in the case of unloaded embankment the system applied approximately an equal spreading and membrane effect while in the loaded embankment the membrane force tended to be larger than the spreading force.

The spreading force in the embankment depends mainly on the horizontal earth pressure force at the embankment base. In the case of very high embankments, the active earth pressure force due to the own weight of the embankment is very large as a function of the embankment height. The effect of the external load in the earth pressure force is small compared with the own weight in such case.

The stress-deformation behaviour of the pile elements has also been investigated to determine the horizontal stresses on the pile elements due to spreading effect in the slope zone. The horizontal stresses in the top of the pile elements apply shear stresses along the pile element and tension stresses in the sectional area of the pile and bending moments. The unreinforced concrete material of the pile element develops a small resistance to the tensile stresses which is according to the standard *DIN 1045-1:2005-1* for a normal concrete C12/15 the characteristic tensile stress f_{ctm} is 1.6 MN/m^2 . Tensile stresses and bending moments in piles were estimated in the study by taking cross section in the most deformed pile and computing the resultant of both the compression and tension forces and computing the bending moment in this section. The most deformed pile has been investigated by taking the pile head deformed with the maximum horizontal displacement. This has been observed as the first, the third and the fifth pile from slope toe in the embankment heights 2 m, 5 m and 10 m respectively. Figure 5.8 explains the place and the influence of the maximum horizontal displacement at pile head in variation of the embankment heights.

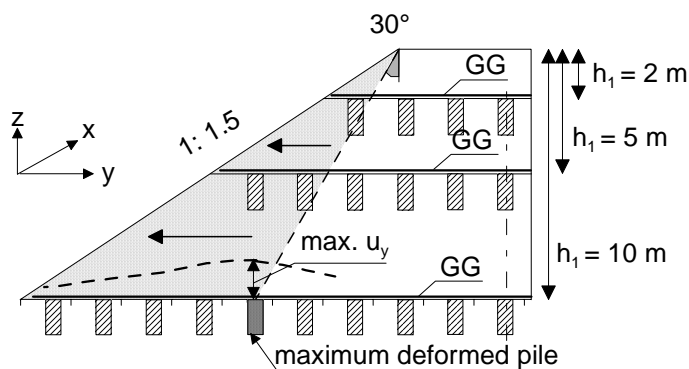


Figure 5.8:
Location of the piles with maximum horizontal displacement and the horizontally displaced soil-wedge

The diagram shows that a soil wedge inclined about 30° vertically from slope crest can represent the sliding body of the slope zone that slides over the base reinforcement. In such zone the horizontal deformations constitute approximately the deformation component of the soil in the slope zone. The same result has been concluded with the same embankment heights under the flatter slope 1:2.5, with which the soil wedge can be represented with an angle 45° to the vertical from the slope crest.

Many sections were computed along the pile to plot the influence of bending moment and tensile stresses along the pile element. Figure 5.9 represents the stress-deformation of the pile elements under variation of the embankment heights on peat underground and external load $p = 30 \text{ kN/m}^2$ with a slope 1:1.5. The tensile stress in the pile sections is plotted against the allowable characteristic tensile stress $f_{ctm} = 1.6 \text{ MN/m}^2$. The same results for the underground

normal consolidated clay and over consolidated clay are in Appendix D.3 and D.4 respectively.

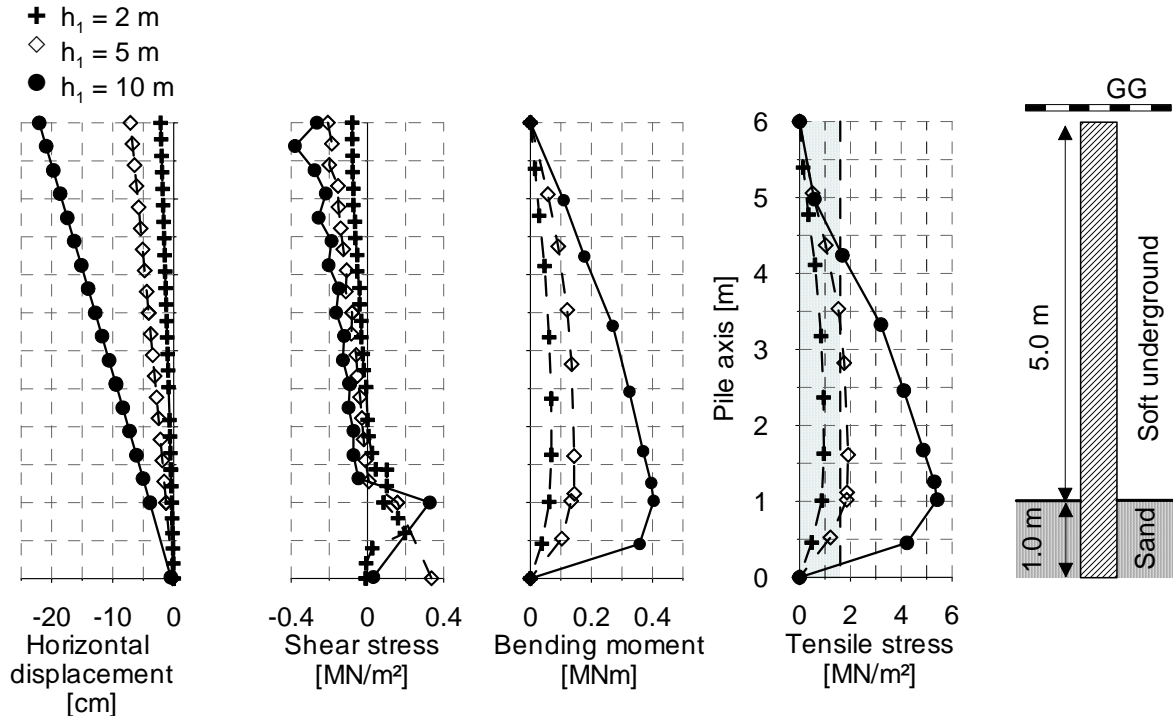


Figure 5.9: Stress-deformation results of pile element under variation of the embankment heights (peat underground, slope 1:1.5)

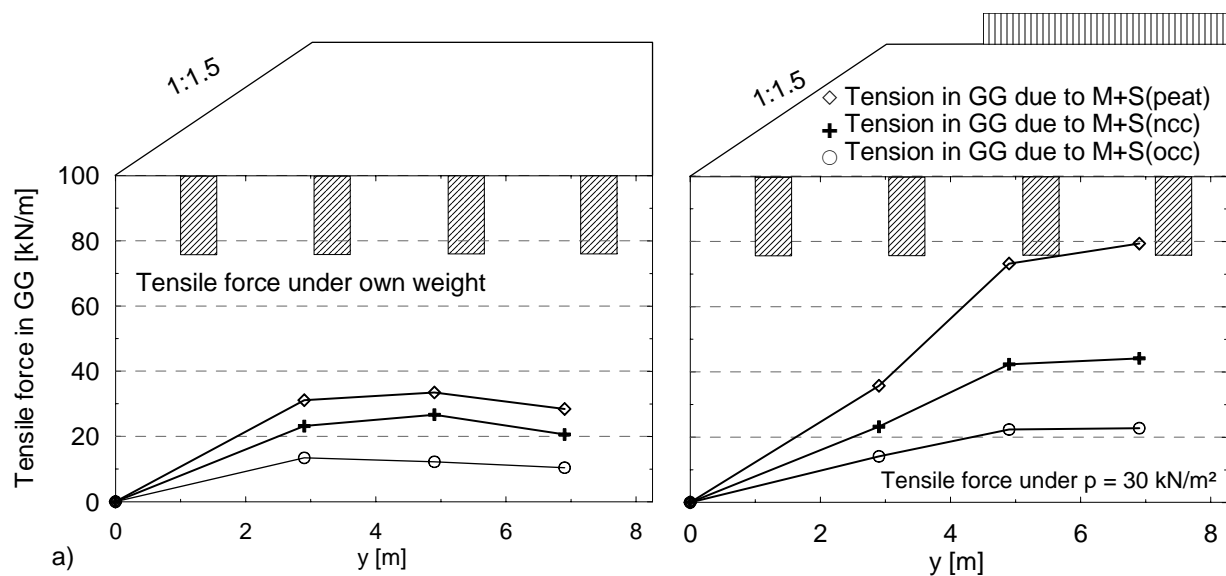
The diagrams show a considerable effect of embankment height on the pile element. Under higher embankment the spreading forces exerted on the pile top are also increased and the horizontal deformation and stresses consequently increased. The very soft peat underground has a small coefficient of lateral soil spring stiffness, which is defined by *Goh et al. (1997)*.

The lateral soil stiffness is dependent mainly on the stiffness of the soil around the pile element $E_{50,u}$ (see Section 2.5.2). In the case of peat underground the stiffness $E_{50,u}$ is too small, and hence, the lateral soil stiffness is also small. The very soft peat underground develops a small response to the horizontal stresses, and then the deformations due to the spreading stresses would only be sustained by the pile elements. Furthermore, the tension stress on the pile section was overestimated in the case of higher embankments 5 and 10 m.

5.7.3 Results of tensile forces under variation of the underground stiffness

The underground stiffness plays a main role to control the stress-deformation behaviour of the system and the reinforcement. According to *EBGEO (2007)* the membrane force in the reinforcement depends mainly on the parameters of the underground such as the stiffness and the depth of the soft underground. The horizontal outward thrust of the embankment fill is resisted by the reinforcement and the base friction between the underground and the reinforcement which depends mainly on the friction parameters of the underground (ϕ' , c) and the interaction soil/geogrid. The available underground in the study has been provided both small friction parameters in the peat underground and high friction parameters for the clay. Also in the case of very soft underground the passive earth pressure of the underground can be neglected under the effective stress conditions. Consequently, the resistance of the soft soil at the pile face can also be neglected.

The stiffness of the underground in the study has been derived through the compression index λ^* using SSM for both peat and normal consolidated clay underground. A full stress-dependent underground stiffness has also been derived for a stiff underground of over consolidated clay underground. The results of the tensile forces in reinforcement for the three underground soil types under a 2 m embankment-height are represented in Figure 5.10. The other results for 5 m and 10 m embankments are represented in Appendix D.5 and D.6 respectively.



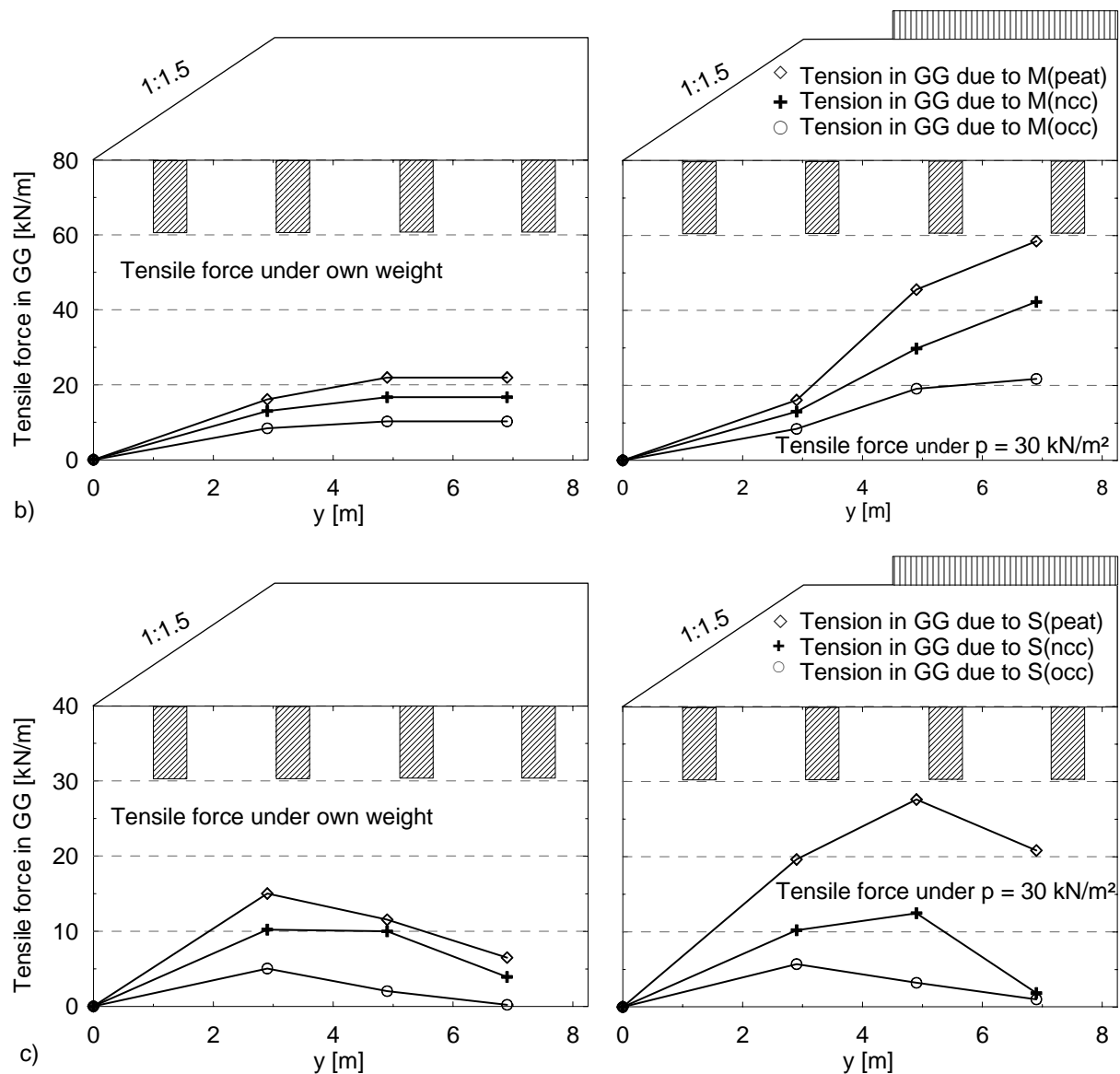


Figure 5.10: Tensile forces along the GG-reinforcement under variation of underground stiffness; (ncc = normal consolidated clay, occ = over consolidated clay); $h_l = 2$ m; a) total force, b) force due to membrane, c) due to spreading

The results showed that with a very soft underground (peat) the tensile force due to membrane and spreading was larger than the force with a very stiff underground (over consolidated clay). For unloaded embankment the maximum spreading force located near/at slope zone, while in the case of loaded embankment the maximum located in the central zone of the embankment. For a very stiff underground the maximum spreading force located near the slope zone also. It is attributed to the small membrane effect in this soil type, especially in the slope zone. This results in a larger spreading force in such zones. The relation between the spread-

ing and membrane forces in reinforcement under variation of the underground stiffness at different embankment heights is represented in Figure 5.11.

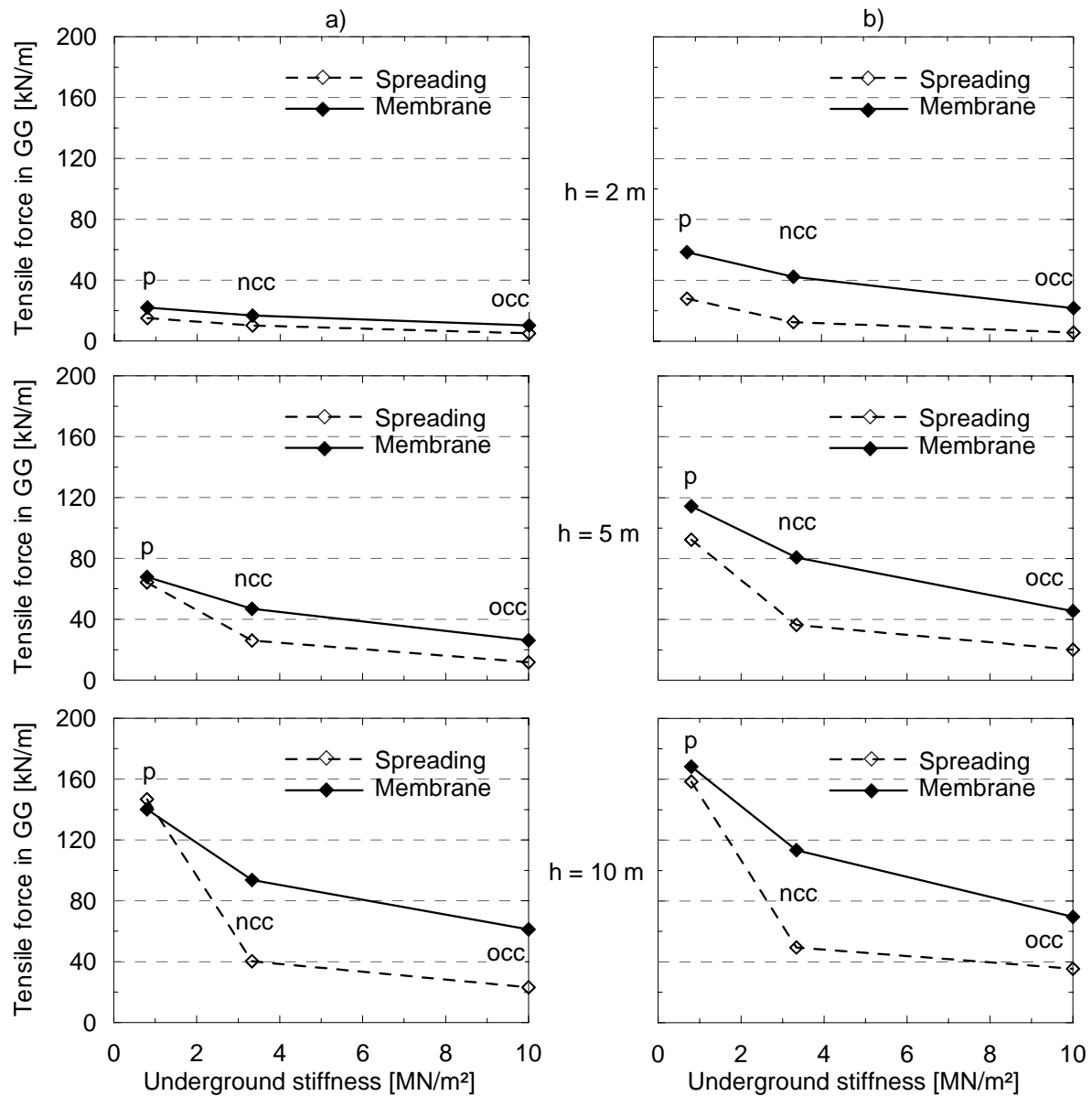


Figure 5.11: Spreading and Membrane tensile forces in reinforcement under variation of underground stiffness with different embankment heights; (p = peat, ncc = normal consolidated clay, occ = over consolidated clay); a) under own weight, b) under $p = 30 \text{ kN/m}^2$

From the diagrams the spreading forces in the case of very stiff underground were smaller compared with that of a soft underground. Furthermore, the high stiffness and shear parameters of the underground (clay underground) reduced the spreading force considerably due to the small shear deformations in the underground with a larger stiffness. The small shear de-

formations in the underground reduce the effect of spreading and then, the tensile forces developed by the reinforcement.

The difference between membrane and spreading forces in the case of peat underground was gradually smaller under higher embankments. This is attributed to the small shear deformations of the soil compared with the existed horizontal earth pressure force on the embankment fill. On the other side, this difference in the case of clay underground was gradually larger under higher embankment; this is attributed to the large shear parameters of the clayey soil compared with the existed horizontal earth pressure force on the embankment fill.

The stress-deformation behaviour of the pile element was also investigated under variation of the underground stiffness for a 2 m-pile element as in Figure 5.12. The same results of the embankment heights 5 m and 10 m are represented in Appendix D.7 and D.8 respectively.

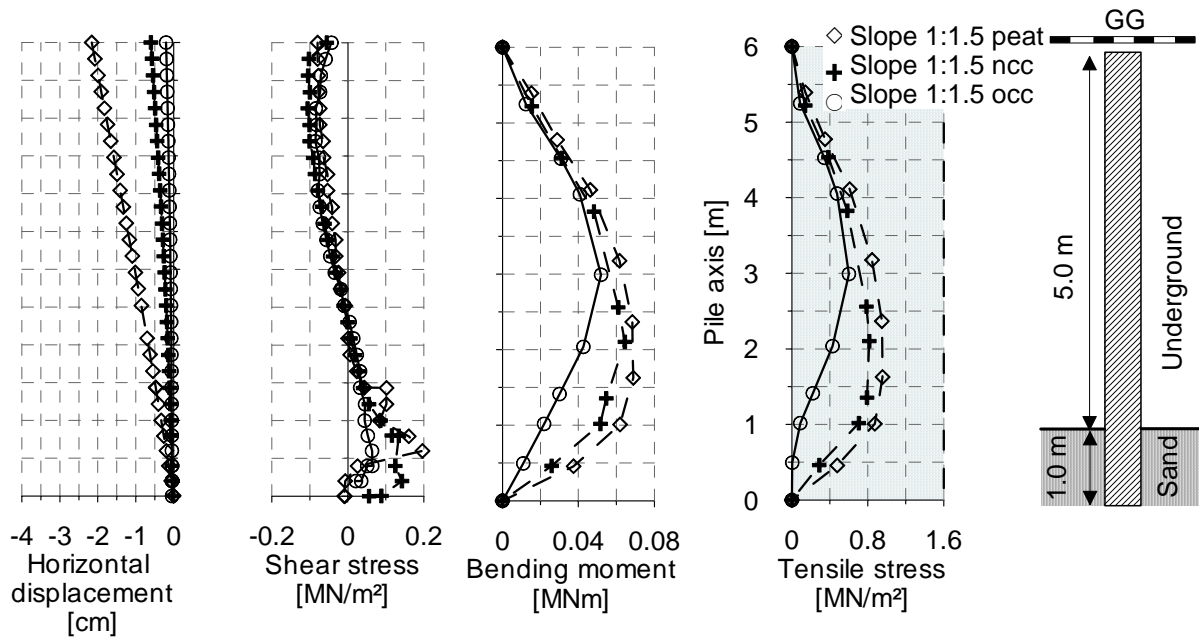


Figure 5.12: Stress-deformation results of pile element under variation of the underground stiffness ($h_1 = 2$ m)

The results show that the deformations, bending moments and tension stresses in the case of very stiff underground (over consolidated clay) were very small compared with that in the case of very soft underground (peat). The relation between the stiffness of the pile and stiffness of the underground soil controls the stress-deformation behaviour of the piles. The relative pile-soil stiffness ratio k_R , is defined by *Stewart (1992)* as a function of the underground stiffness $E_{50,u}$, with which a decrease in the underground stiffness results in an increase in k_R ratio, consequently, an increase in the stress and deformations in the pile element.

5.7.4 Results of tensile forces under variation of the embankment slope

The geometry of the embankment fill such as the embankment height and the slope of the embankment has also an influence on the existed stresses on the structural system and the reinforcement. In the case of flatter slopes the spreading stresses due to the horizontal earth pressure are distributed on a larger embankment base rather than the steeper slopes. Further, the shear stresses at the embankment base are also distributed at larger base. On the other side, the bond stress between the soil and the reinforcement can considerably be increased as a function of the embankment slope.

The model tests on a homogeneous soil resulted in the same concept (see Chapter 3). In the case of a reinforced embankment the shear stresses at embankment base are additionally resisted by the reinforcement. The flatter slopes provide a longer reinforcement and longer friction bond length against lateral sliding due to spreading stresses at the base. The bond length of reinforcement is a function of the horizontal earth pressure. The parameter study focused on a steep slope of 1:1.5 and a flat slope 1:2.5 in order to investigate the effect of the slope on the spreading and total tensile forces in the reinforcement. Figure 5.13 represents the results of the total and spreading forces in the reinforcement.

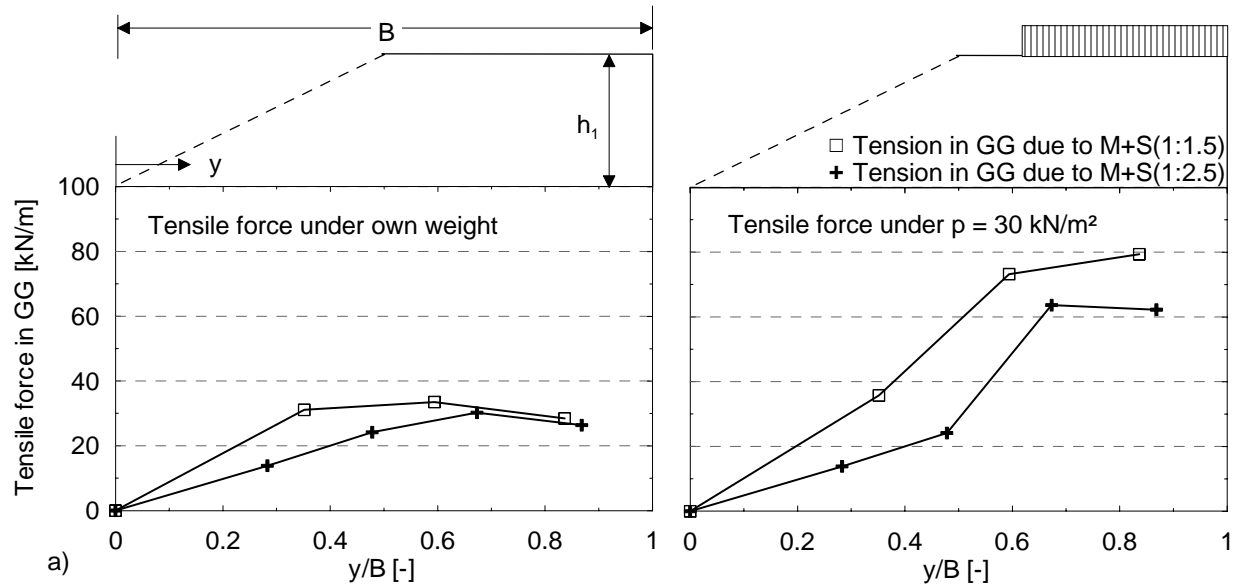


Figure 5.13a: Total forces along the reinforcement under slope variation at $h_1 = 2 \text{ m}$ (peat underground)

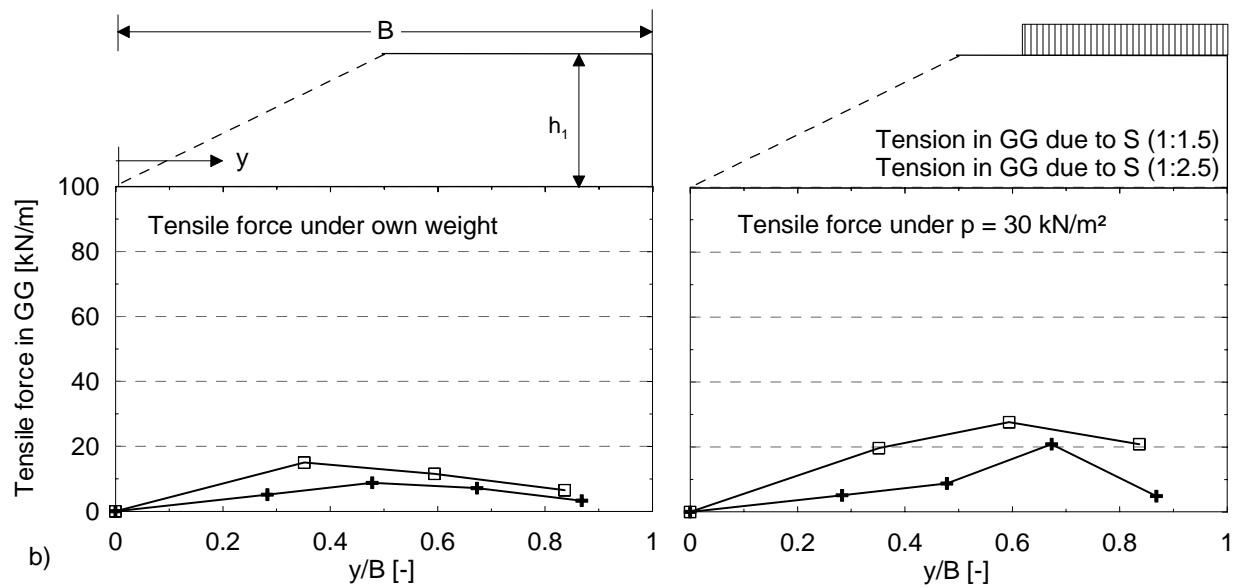


Figure 5.13b: Spreading forces along the reinforcement under slope variation at $h_1 = 2$ m (peat underground)

The results showed that in the case of a steep slope with unloaded embankment the tensile force in reinforcement was larger than that of a flat slope, and the difference was increased by loading the embankment. The same results have been concluded for the other embankment heights are represented in Appendices D.9 and D.10 respectively.

The relation between the spreading and membrane forces in the case of slope variation can also be indicated with the different embankment heights in order to give a precisely investigation of the slope variation. Figure 5.14 represents the values of spreading and membrane forces for different slopes and different embankment heights for the three underground soils investigated in the study.

The diagrams in Figure 5.14a, b and c show that the spreading forces ($F_{G,S}$) increased linearly with the membrane forces ($F_{G,M}$). In the steep slope 1:1.5 the relation has a steep inclination than that in the flatter slope 1:2.5. The relation $F_{G,S}/F_{G,M}$ in the slope 1:1.5 can be determined as 1.2 for peat underground and about 0.6 for clay underground. In the slope 1:2.5 the relation $F_{G,S}/F_{G,M}$ can be determined as 0.55 for peat underground and 0.34 for clay underground. The results adopt the concept that the flatter slopes provide smaller spreading stresses and larger base frictions.

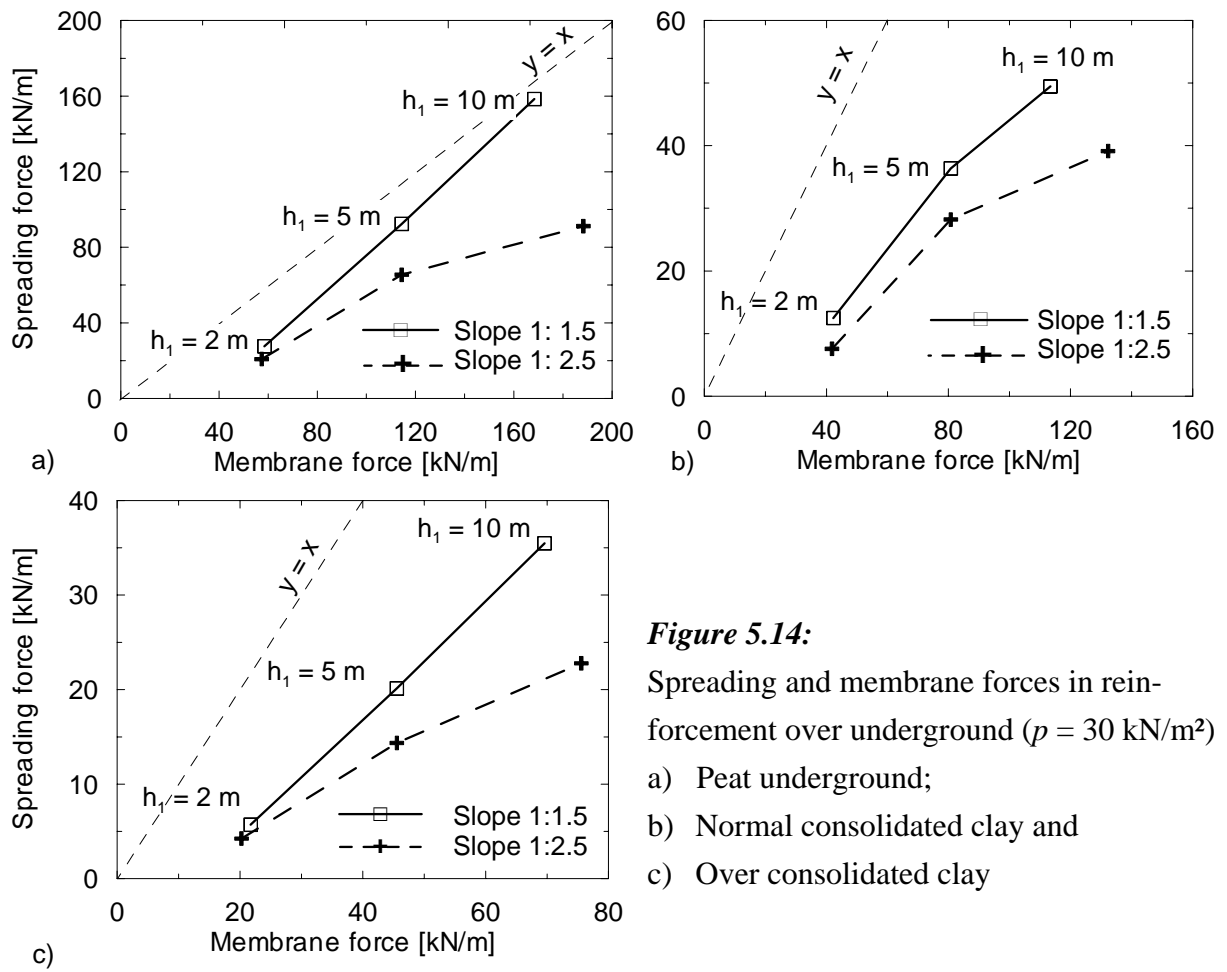


Figure 5.14: Spreading and membrane forces in reinforcement over underground ($p = 30\text{ kN/m}^2$)
 a) Peat underground;
 b) Normal consolidated clay and
 c) Over consolidated clay

The stress-deformation behaviour of pile elements was determined for the slope variation of 2 m embankment-height on peat underground. The results are represented in Figure 5.15.

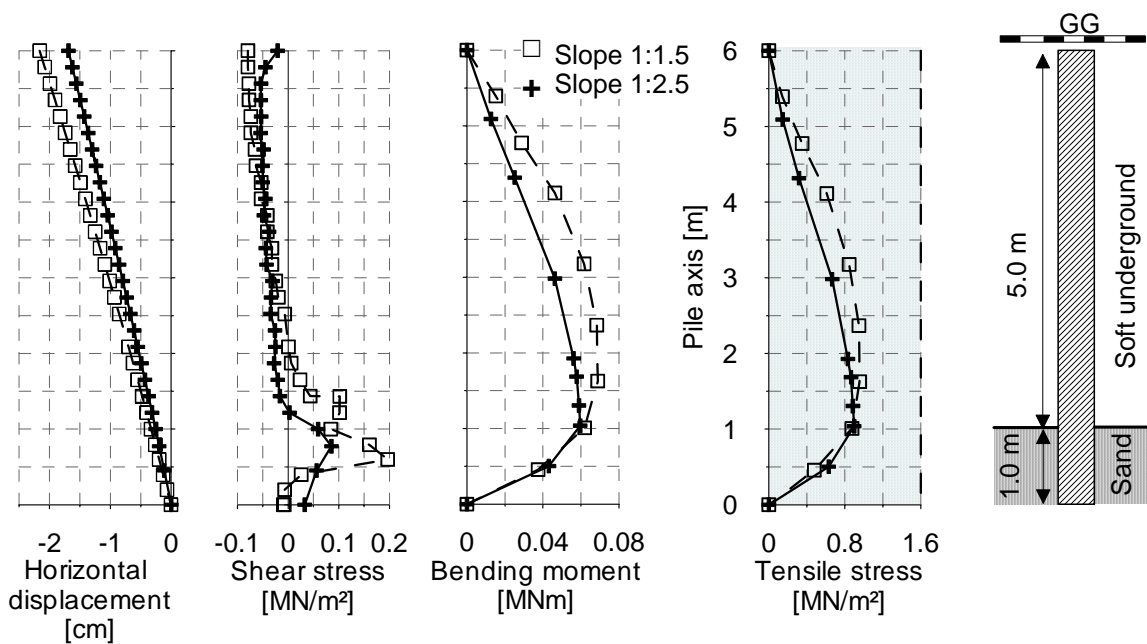


Figure 5.15: Stress-deformation results of pile element under slope variation ($h_1 = 2\text{ m}$)

The diagrams show that in a steeper slope 1:1.5 the horizontal displacement on the pile head increased by about 28 % than that of a flatter slope 1:2.5, this is attributed to the larger spreading horizontal force in the pile head in this case. The larger horizontal force applied also a larger bending moment and tension stresses on the pile section. The same results for 5 m and 10 m are represented in Appendices D.11 and D.12 respectively.

5.7.5 Results of tensile forces under variation of the geogrid reinforcement layers

Multi geogrid-layers at the base of the embankment function as a stiff foundation layer. This resulting stiff layer functions to increase the stability and reduces the deformations of the system.

The stress-strain behaviour of the multi-layer geogrid reinforcement under the arching and membrane effect has been investigated by many literatures such as *Wang et al. (1996)*, *Zaeske (2001)*, *Collin et al. (2004)*, and *Heitz (2006)* to determine the relation between the tensile forces for each layer. The distribution of tensile force for each layer developed more tensile forces in the lower layer than the upper one according to a load propagation of 45° on the pile head as represented in Figure 5.16.

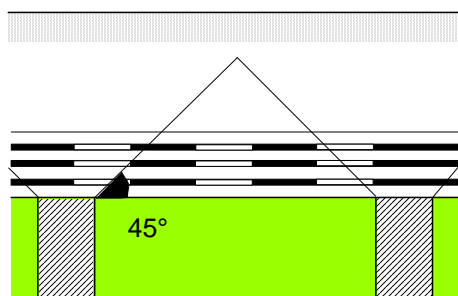


Figure 5.16:
Distribution of Membrane effect on GG-Layers,
Heitz (2006)

From the model test results of *Heitz (2006)* and the other mentioned literatures, the lower GG-Layer developed more stresses than the upper ones. The behaviour of the multi-layer reinforcement under both membrane and spreading effects has been investigated in the parameter study for two and three layers of reinforcement to determine the behaviour and distribution of the tensile forces on each layer in such cases. Firstly a two-layers reinforcement was applied to the system and the tensile forces in each reinforcement layer has been computed and evaluated. Figure 5.17 represents the results of tensile forces in each layer.

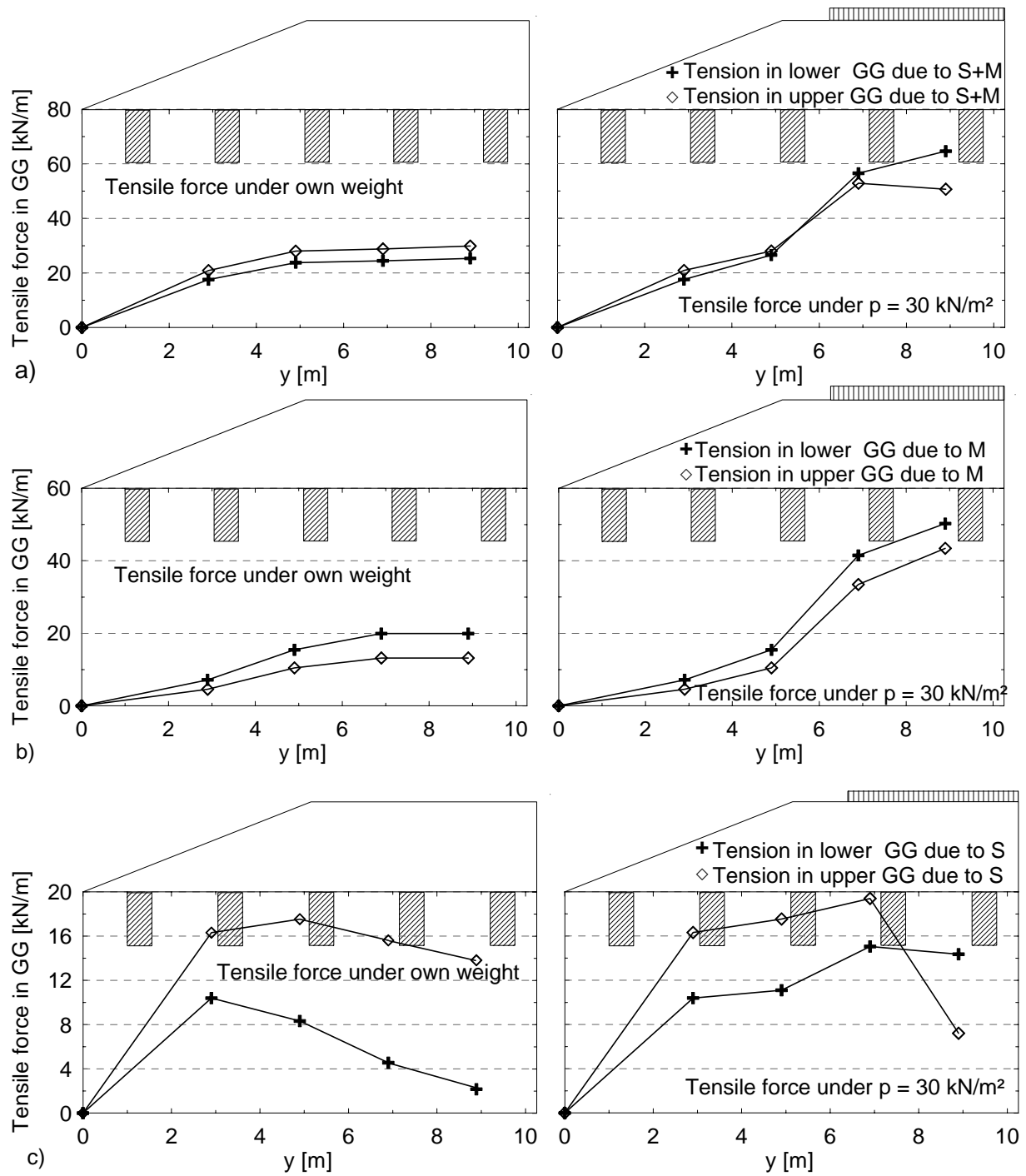


Figure 5.17: Tensile forces along the reinforcement under variation of two geogrid layers
 a) Total tensile force, b) Membrane force and c) Spreading force

The results showed that in the case of unloaded embankment the spreading forces increased with respect to the membrane forces such that the maximum tensile forces due to spreading located in the slope zone of the embankment either for the lower or the upper GG-layer. In the

case of loaded embankment the membrane effect due to external loads increased in the central zone such that the total maximum tensile forces located in the central zone. The maximum tensile force due to spreading in this case moved also to the central zone. The membrane effect on the upper and lower GG-layer ensured the concept that the lower GG-layer developed more tensile stresses. Under own weight of the embankment the upper GG-layer developed about 67 % of the tensile force in the lower GG-layer and about 85 % in the case of applied load $p = 30 \text{ kN/m}^2$. The spreading effect applied more tensile forces on the upper GG-layer than the lower one, that is the upper layer developed about 170 % of the lower GG-layer under own weight of the embankment and 140 % in the case of applied load $p = 30 \text{ kN/m}^2$. The more spreading effect in the upper GG-layer is attributed to the horizontal earth pressure in the slope zone which has been resisted in the upper GG-layer only by the bond effect between the GG-Layer and the fill soil. On the other hand, by the lower GG-layer the base friction between the underground layer and the GG-layer, which alter the strains and forces in this layer (see Figure 5.18).

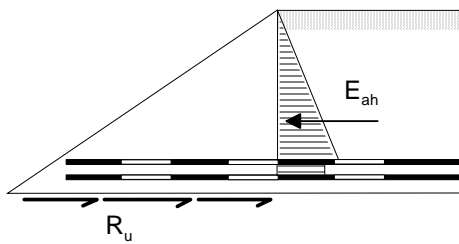
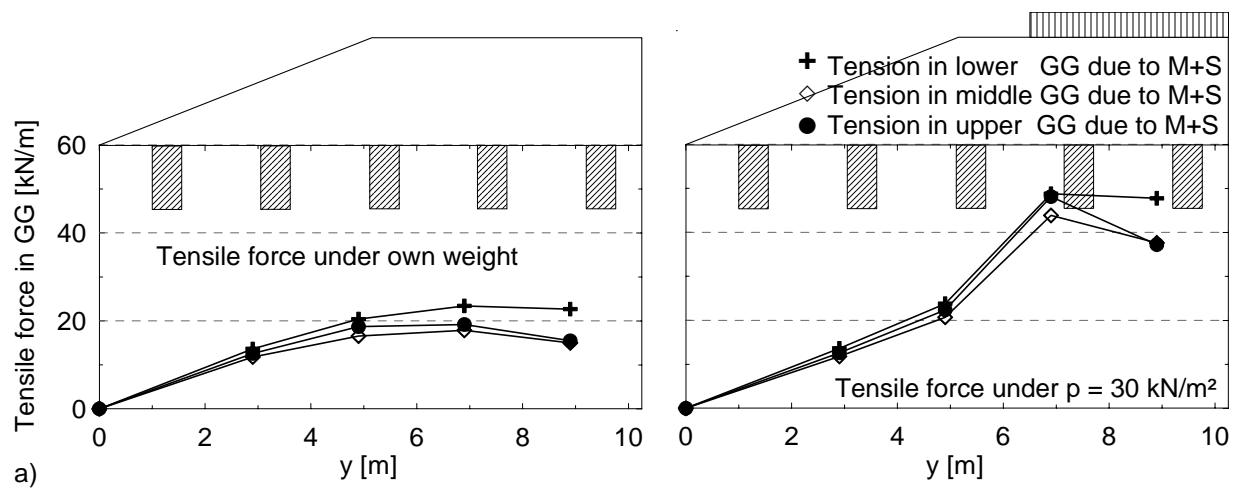


Figure 5.18:
Spreading forces in a multi-layer reinforced embankment

More investigations to the behaviour of multi-layer reinforcement has been analysed by using three-GG layer reinforcement. The tension in the upper, middle and lower layer can be analysed and evaluated to state the relation between the stresses on each layer. The results of the tensile forces in each layer are represented in Figure 5.19.



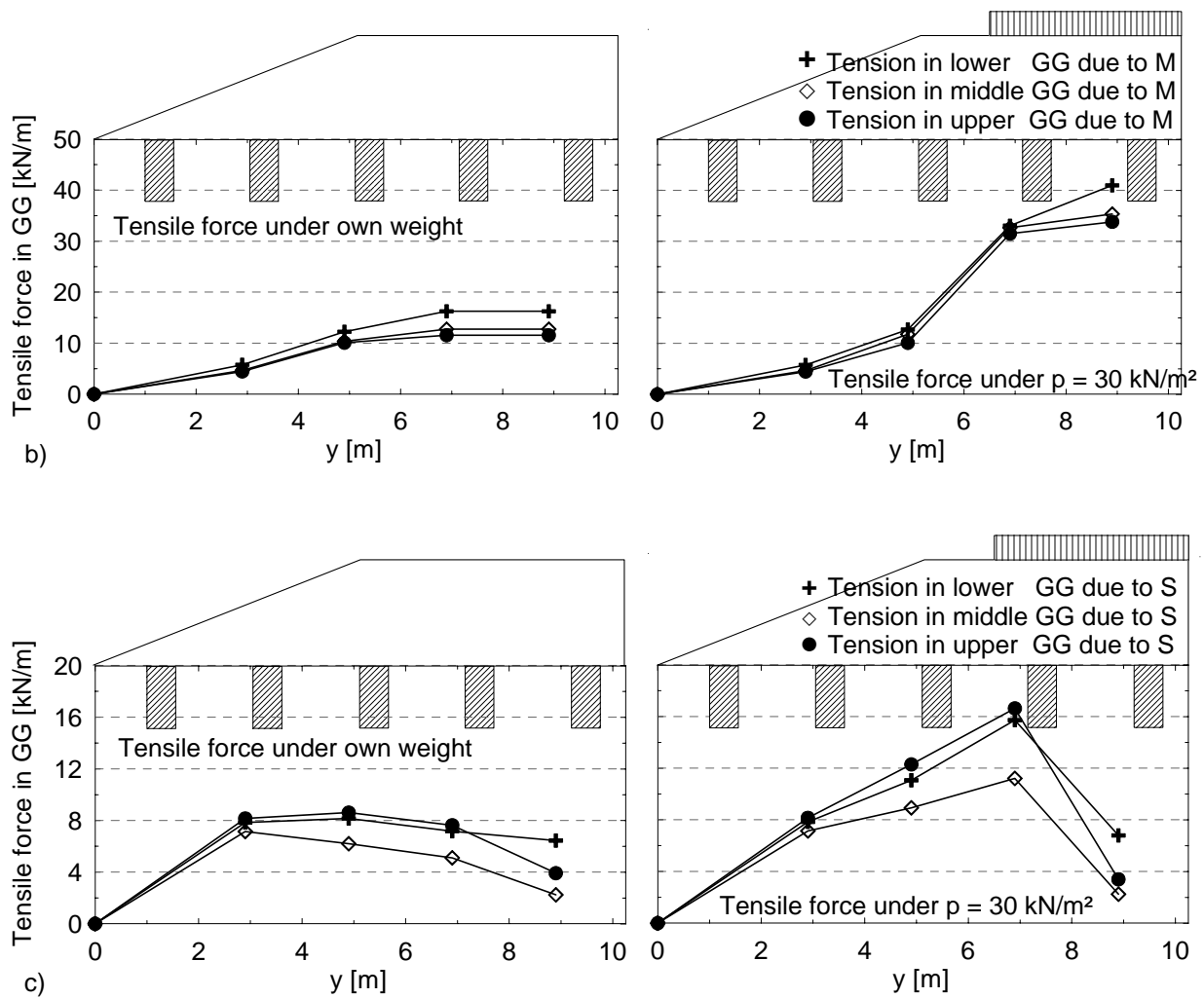


Figure 5.19: Tensile forces along the reinforcement under variation of two geogrid layers
a) Total tensile force, b) Membrane and c) Spreading force

The results of the three GG-layers were compatible with those of two GG-layers under the concept that the lower GG-layer develops more of the membrane effect than the middle and the upper GG-layer. Ratio of membrane forces under own weight of the embankment for every GG-layer $F_{M, lower} : F_{M, middle} : F_{M, upper}$ was about 1:0.80:0.70, while in the case of applied external load $p = 30 \text{ kN/m}^2$ was about 1:0.9:0.8. The increase of tension in the upper and middle GG-layers by loading the embankment is attributed to the increase in membrane effect due to loading of the system. The results of spreading forces showed small tensile forces in the middle layer than the upper and lower layer. The ratio of spreading force in the case of loaded and unloaded embankment for every GG-layer $F_{S, upper} : F_{S, middle} : F_{S, lower}$ was about 1:0.70:0.94. The results provide a maximum tensile spreading at the upper layer while the middle layer develops 70 % of the upper one. The smaller tensile force in the middle layer is attributed to the block action of the reinforcement that is the three layers develops the load as

a block layer, with which the middle layer experiences some strains as a reaction with the strain developed in the block system.

The stress-deformation in the pile elements in the case of multi-layer reinforced embankment has also been investigated to determine the effect of a stiff reinforcement layer on the response of the pile elements. The results in the case of multi-layer reinforcement compared with that in the case of one-layer reinforcement are represented in Figure 5.20.

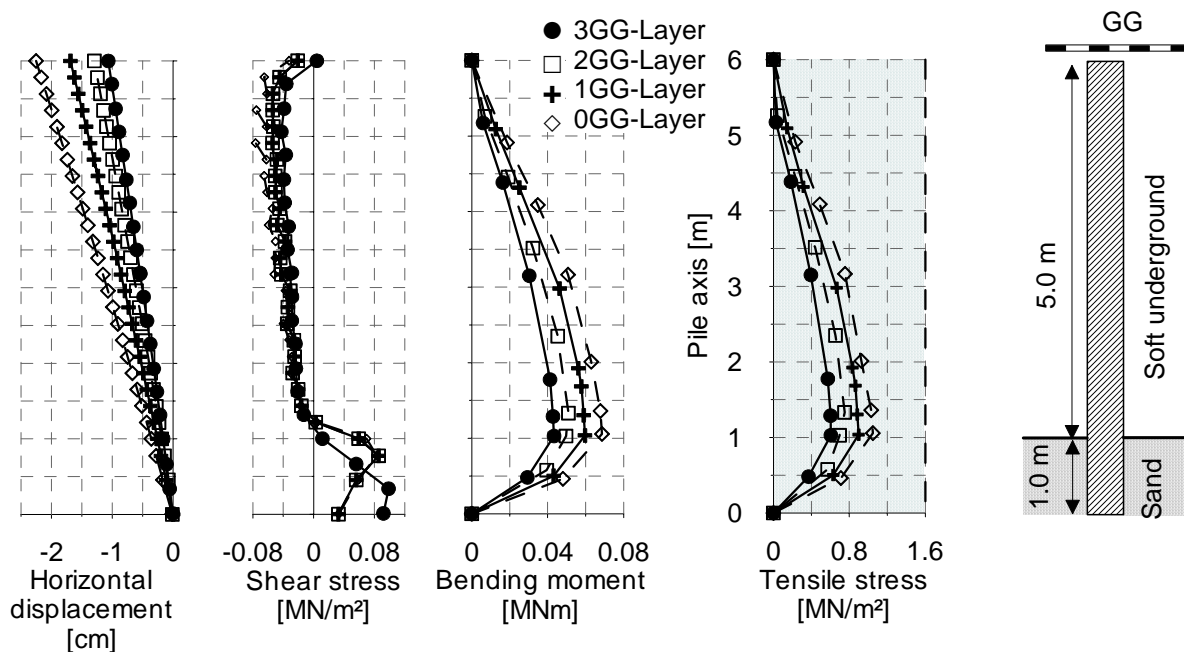


Figure 5.20: Stress-deformation results of pile element under variation of reinforcement GG-layers ($h_1 = 2$ m, slope 1:2.5)

The effect of applying more GG-layers can be considerably evaluated from the results of the horizontal deformation of the pile head. Applying one GG-reinforcement layer has reduced 25 % of the horizontal displacement of the pile head under unreinforced embankment. Similarly, applying 3 GG-layers have reduced about 53 % of the horizontal displacement of the pile head under unreinforced embankment and 37 % of the horizontal displacement of the pile head under one GG-layer. The ratio of the horizontal displacement on the pile head under different GG-layers $Displ_{0GG} : Displ_{1GG} : Displ_{2GG} : Displ_{3GG}$ was about 1:0.75:0.59:0.47. By applying 3 GG-layer the horizontal spreading force exerted on the pile head has been reduced, consequently, the tension stresses on the pile section has also been reduced resulting in a smaller bending moments on the pile-axis.

5.8 Summary and evaluation of the numerical parameter study

In this numerical parameter study dealt with the case of reinforced embankment on soft underground supported by pile-like elements the study investigated the strain-deformation behaviour of the system related with the spreading- and membrane effect on the basal reinforcement under different parameter variations. The stress-deformation behaviour of the pile elements due to the horizontal spreading effect has also been investigated and evaluated. The following results would be concluded in such case:

- Under variation of the embankment height the spreading forces increased linearly by increasing the embankment height. By increasing the embankment height the behaviour of the soil tends to act between the active earth pressure and earth pressure at rest. In the case of 10 m-embankment height the external load has small effect on the behaviour of the system compared with the effect of the own weight of the embankment fill.
- Under variation of the embankment height the sliding soil body in the slope zone can be represented by a soil wedge inclined 30° of the slope crest in order to meet the maximum horizontally deformed piles.
- Under variation of the underground soil stiffness the spreading forces increased by decreasing stiffness and friction parameters of the underground. The relation S/M increased in the case of peat underground and in the case of clay underground decreased this relation substantially. The horizontal soil response and the subgrade reaction of the clay underground provided a smaller horizontal deformations on the pile head compared with the peat underground material.
- In the case of steeper embankment slope the spreading effect increased compared with membrane effect. This is attributed to the increasing in shear stresses at the embankment base by steeping the slope. The relation S/M in the steeper slope 1:1.5 lies about double of that in the case of flatter slope 1:2.5 in the case of very high embankment. As a result of the increasing spread forces increased also the horizontal deformation and bending moment on the pile element.
- Applying multi-GG-layers the membrane effect provided more tensile forces in the lower layer than the upper layer. On the contrary, the spreading effect provided more tensile forces on the upper layer. This is attributed to the base friction of the underground which resisted the spreading effect in the lower layer.

- By applying multi GG-layer the middle GG-layer provided smaller spreading forces than the others. This is attributed to the block action of the reinforcement that is the three layers develops the load as a block layer, with which the middle layer experiences some strains as a reaction with the strain developed in the block system. The stress-deformation behaviour of the pile elements has considerably influenced by applying multi-layer reinforcement. The deformation in the case of 3 GG-layers provided 37 % reduction in the horizontal displacement of the pile head when applying one GG-layer.

5.9 Comparing the FEM-results with some available analytical methods

5.9.1 Objectives

In the case of reinforced embankment on soft underground supported by pile-like elements the forces in the reinforcement is compound of two components (see Figure 5.21) the force due to arching effect of soil between piles and the spreading effect. To investigate the spreading effect on the reinforcement the membrane forces in the reinforcement must separately be determined, hence the spreading effect can be determined and evaluated.

The membrane force in GG applies constant values in the central zone of the embankment under own weight. However, it is maximal at the center of embankment in the case of external loads according to the distribution of vertical stresses.

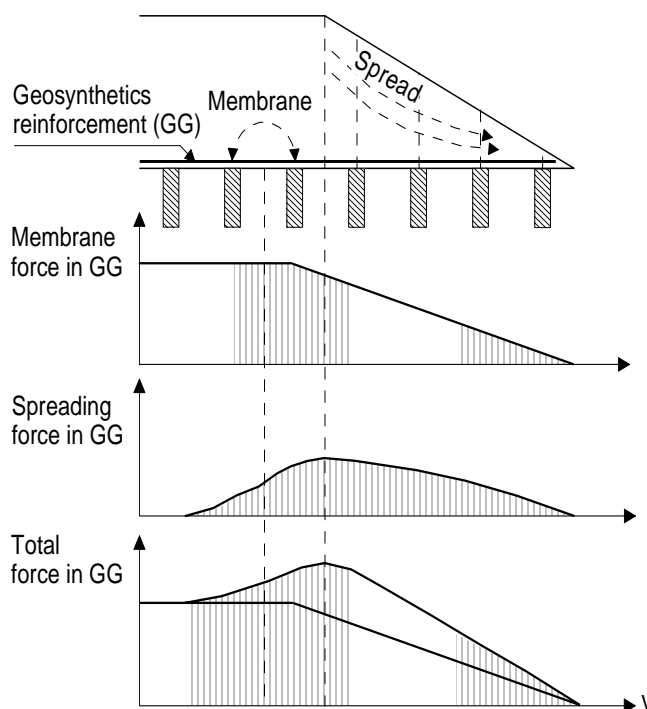


Figure 5.21:

Forces in GG reinforcement in the case of piled embankment

5.9.2 Determination of the membrane forces in reinforcement due to arching effect

The arching effect from the soil between piles applies membrane forces on reinforcement. By using the term efficacy E_L , the portion of the total embankment load which arches onto the pile head without geosynthetics can be calculated. A detailed definition and determination of the vertical soil pressure acting on the pile heads and reinforcement as well as the determination of the membrane forces in reinforcement can be reviewed in *Heitz (2006)*.

Many authors have investigated and determined the arching effect and membrane forces. The available methods to calculate the membrane forces after *Guido et al. (1987)*, *Carlson (1987)*, *BS 8006 (1995)*, *Russell et al. (1997)*, *Hewlett et al. (1997)*, *Rogbeck (1998)*, *Sentiff/Svano (2000)*, *Klobe (2007)* and *EBGEO (2007)* are applied in the study.

The membrane effect on the soil has been widely discussed and investigated. The analysis of the arching effect and the membrane forces has not been reinvestigated or discussed in this study, but only comparing the results of each available analytical calculation method with the FE-results of the parameter study as well.

As the first step of the analysis of the spreading effect on the piled embankment, an analytical membrane method must be applied according to the results of FEM. The FE results have been multiplied by factor 3.5 to be comparable with analytical methods as explained and concluded in Chapter 4. The applied analytical membrane model results have been explained as an example for the embankment of a slope 1:1.5 on a peat underground provided the different embankment heights. Figure 5.22 represents the results of the analytical methods compared with a factored FE results in the case of $p = 30 \text{ kN/m}^2$.

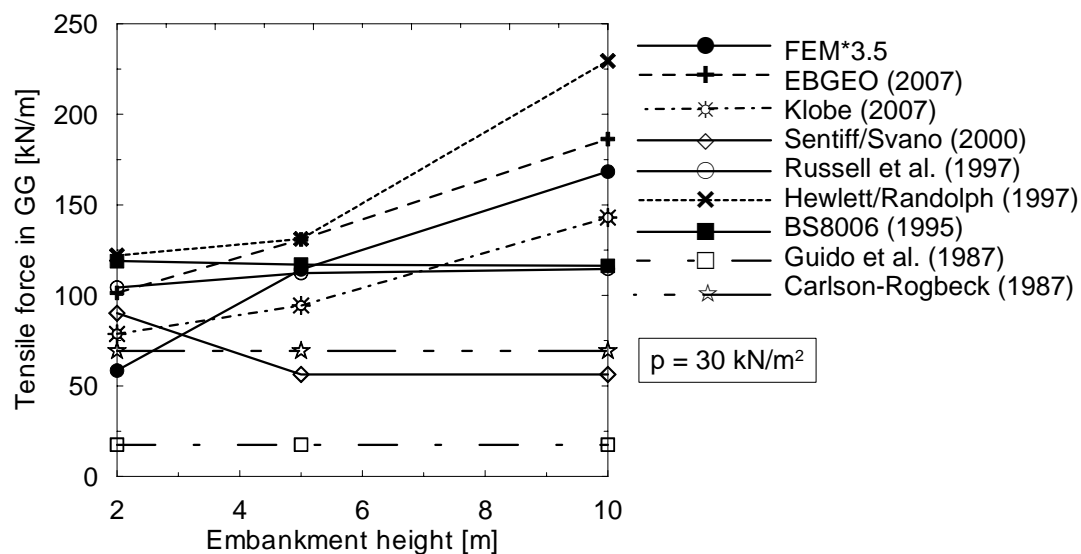


Figure 5.22: Applied analytical membrane models compared with FEM-results

The results showed that the analytical membrane model of *EBGEO (2007)* was approximately convenient with that of the factored FEM-results. However, the analytical results in the case of a small embankment height were overestimated in the analytical model system. The very small results of *Guido et al. (1987)* were attributed to the pyramid-like arching form which independent of the model height and the loads. The results of the membrane model after *Hewlett/Randolph (1997)* has also a good agreement with FEM-results but in the case of higher loaded embankment it was overestimated. In general, the results of the analytical membrane model according to *EBGEO (2007)* can be used as the membrane forces in the reinforcement.

5.9.3 Analytical methods to determine the total forces applied in reinforcement

The analysis of the total forces in reinforcement in the case of membrane and spreading forces applied in the system recognizes three available analytical methods. The first analytical method adopts the adding of the horizontal earth pressure force to the membrane force which is approached by *BS 8006 (1995)* and *EBGEO (2007)* for the method's option 1. In this method, the maximum horizontal force due to spreading is added totally to the membrane force in the slope zone to get the total tensile force in reinforcement as in Equation 5.3.

$$F_G = F_{G,M} + F_{G,S} \quad (5.3)$$

The spreading force in this case is represented by the horizontal active earth pressure force.

Another analytical method has been estimated by *Love et al. (2003)* as well as the option 2 in *EBGEO (2007)*. In these methods it is adopted that in the transverse direction of embankment the basal reinforcement can only have one tension, however, and the tension has to be in equilibrium with all the forces acting upon it. The transverse reinforcement in this case should be designed for whichever is the greater from membrane force or spreading force not their sum (the same concept is adopted by *Klobe (2007)* to calculate the tensile force in reinforcement):

$$F_G = \max \begin{cases} F_{G,M} \\ F_{G,S} \end{cases} \quad (5.4)$$

By applying the *EBGEO (2007)* option 2, it cannot be assumed any longer that the vertical bearing elements do not exhibit inadmissible deformations. Therefore, a proof of the deformations in the vertical bearing elements (for example by the numerical methods) is recommended. Under equilibrium conditions, when spreading forces are greater than membrane

forces, a small outward movement of the pile elements increases the arching effect and membrane forces. Likewise, when membrane forces are greater than spreading forces then the piles move together to increase the coefficient of earth pressure and increasing the spreading forces. The spreading force in such case is represented by the maximum horizontal earth pressure force at the slope crest according to the classical earth pressure calculation explained in Appendix A.1.

The third analytical method to calculate the total tensile forces in reinforcement is represented by *Geduhn/Vollmert (2005)* who reported that the base friction of the underground soil under the reinforcement layer can reduce the earth pressure force transformed to the embankment base, i.e. the total spreading force in the reinforcement is a resultant of the horizontal earth pressure force and the base friction. However, the total horizontal force in the reinforcement is calculated by adding the membrane force to the resulting spreading force which can be computed as follows:

$$F_{G,S} = E_{ah} - R_u \quad (5.5)$$

Where R_u can be calculated from Section 2.4.1.2. The base friction in higher embankment heights gives a considerable greater friction forces which can eliminate the resultant analytical spreading forces, especially with the higher and flatter slopes. The non-value of spreading force cannot be accepted practically. However, the FEM-results indicated spreading forces and horizontal deformation in such cases.

The results of the parameter study to analyse the variation of the embankment height dealt with the very extreme embankment height $h_l = 10$ m. However, this variation has been analysed to investigate the stress-deformation behaviour of the GG and the pile elements. The higher and very high embankments on peat underground result in extreme strains in GG (9 % at $h_l = 5$ m and 16 % at $h_l = 10$ m at $p = 30$ kN/m²). The very large strain values cannot be compared and reanalysed using the analytical approaches, which includes a limited allowable strain in GG from 4 % to 6 % maximum. Therefore, another FEM-calculations have been carried out in order to investigate the tensile stiffness of GG with which the resulting strain lies in the range of the allowable analytical limits. Figure 5.23 represents the effect of the tensile stiffness J on the resulting total strain in GG in the case of 5 m- and 10 m-embankment heights. However, the strain values in the case of $h_l = 2$ m lie in the range of the allowable analytical limits with a tensile stiffness of $J = 2000$ kN/m, which was applied in the parameter study.

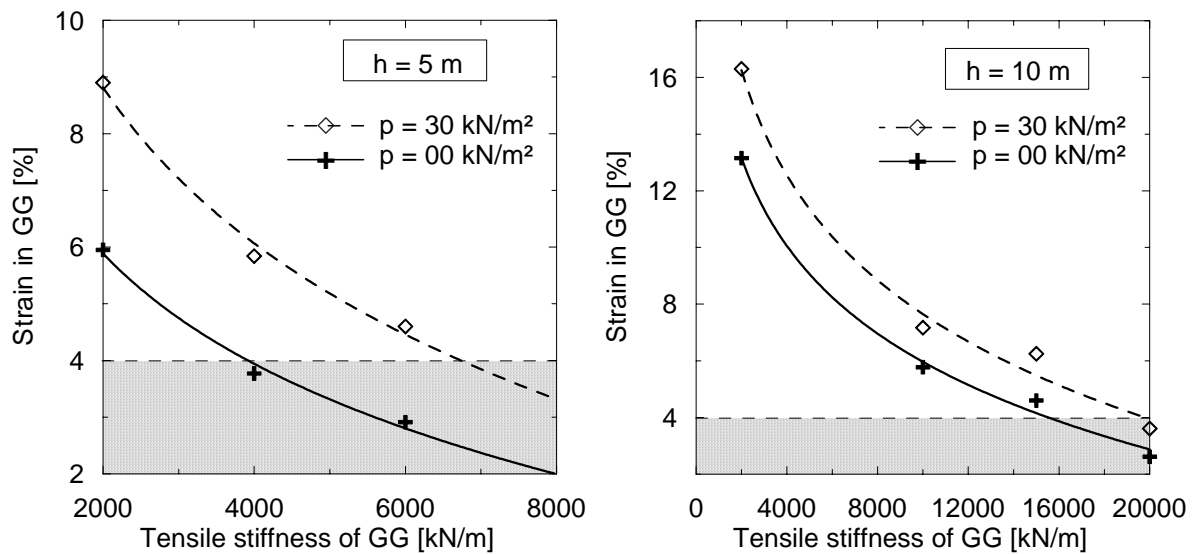


Figure 5.23: Effect of tensile stiffness J on the resulting strain in GG:

a) $h_l = 5$ m, b) $h_l = 10$ m

The diagrams show that by applying a tensile stiffness $J = 7000$ kN/m in the case of $h_l = 5$ m and applying a tensile stiffness $J = 20000$ kN/m in the case of $h_l = 10$ m, the resulting strain in GG can be stated in the allowable analytical limits. Although the tensile stiffness $J = 20000$ kN/m is unpractical value, but it would be used in the analytical methods to compare the results in the extreme embankment height $h_l = 10$ m.

Table 5.8 represents the applied tensile stiffness J of the reinforcement according to the embankment height.

Table 5.8: Applied reinforcement tensile stiffness J

| | Embankment height h_l | Applied tensile stiffness J |
|----------|-------------------------|-------------------------------|
| Branch 1 | 2 m – 4 m | 2000 kN/m |
| Branch 2 | 4 m – 7 m | 7000 kN/m |
| Branch 3 | 7 m – 10 m | 20000 kN/m |

The different analytical methods can be compared with the factored FEM-results of the total tensile force in reinforcement. The comparison is aimed to give a qualified investigation of the different concepts applied to calculate the tensile force. Figure 5.24 represents a comparison between the analytical methods and the numerical results for the three applied branches.

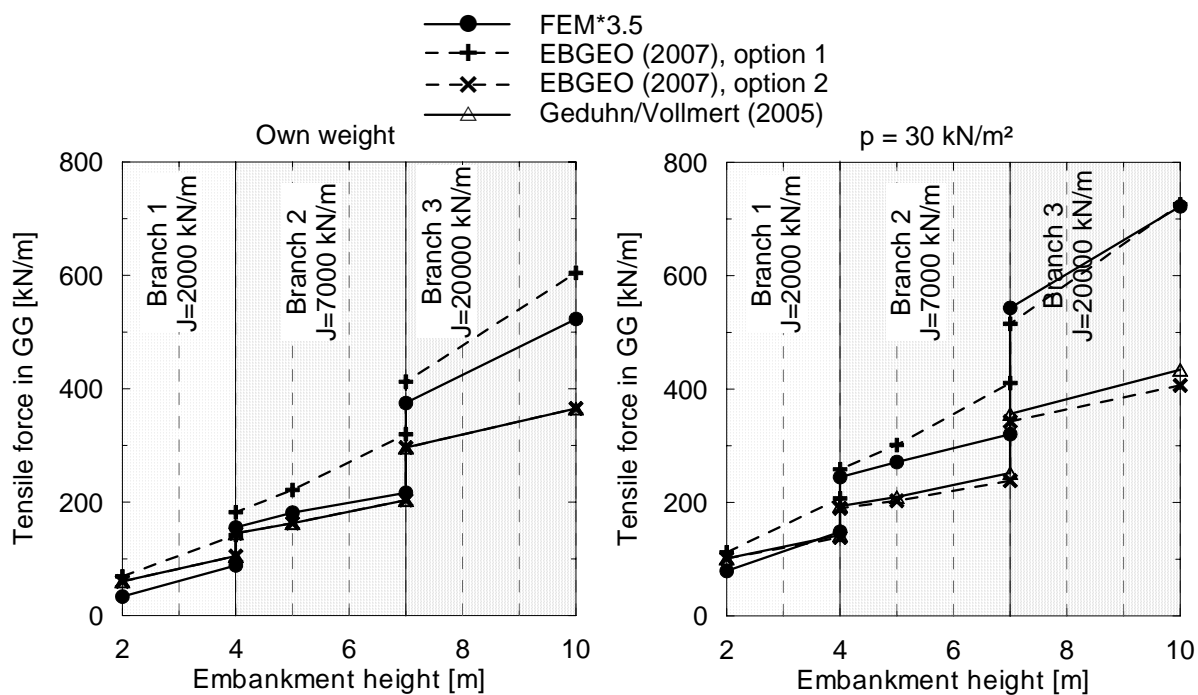


Figure 5.24: Comparing the analytical methods with the numerical results of the total tensile forces in reinforcement on piled embankment system.

Figure 5.24 shows the tensile forces in reinforcement under different embankment heights resulting from the numerical computations compared with different analytical methods. The results after *EBGEO (2007)* option 1 were overestimated compared with option 2.

The tensile force in option 1 results from both the spreading and membrane forces, while in option 2 it results from the maximum of the two forces. In the case of the high tensile stiffness, the membrane force represents the maximum tensile force. The FEM-results are compatible with the results of *EBGEO (2007)* option 1; this is attributed to the higher membrane force in GG due to the extreme tensile stiffness in the third branch. The overestimated results in the small embankment height are attributed to the overestimated analytical membrane forces in *EBGEO (2007)*.

The same comparison can also be derived for the other underground materials in the case of normal consolidated clay and over consolidated clay. Analytically, the membrane force in the reinforcement on normal- or over-consolidated clay underground provides smaller values than the forces on peat underground. However, the analytical spreading force due to active earth pressure is applied as the same force in all underground cases. In the case of normal consolidated clay underground the tensile stiffness of GG must be increased to 4000 kN/m in the second branch. In the third branch J must be increased to 10000 kN/m in order to result strain in GG in the allowable analytical limits. In the case of over consolidated clay underground,

the resulting strain in GG lies in the allowable limits under tensile stiffness of $J = 2000 \text{ kN/m}$. The analytical results versus FEM results of the total tensile force are shown in Figure 5.25.

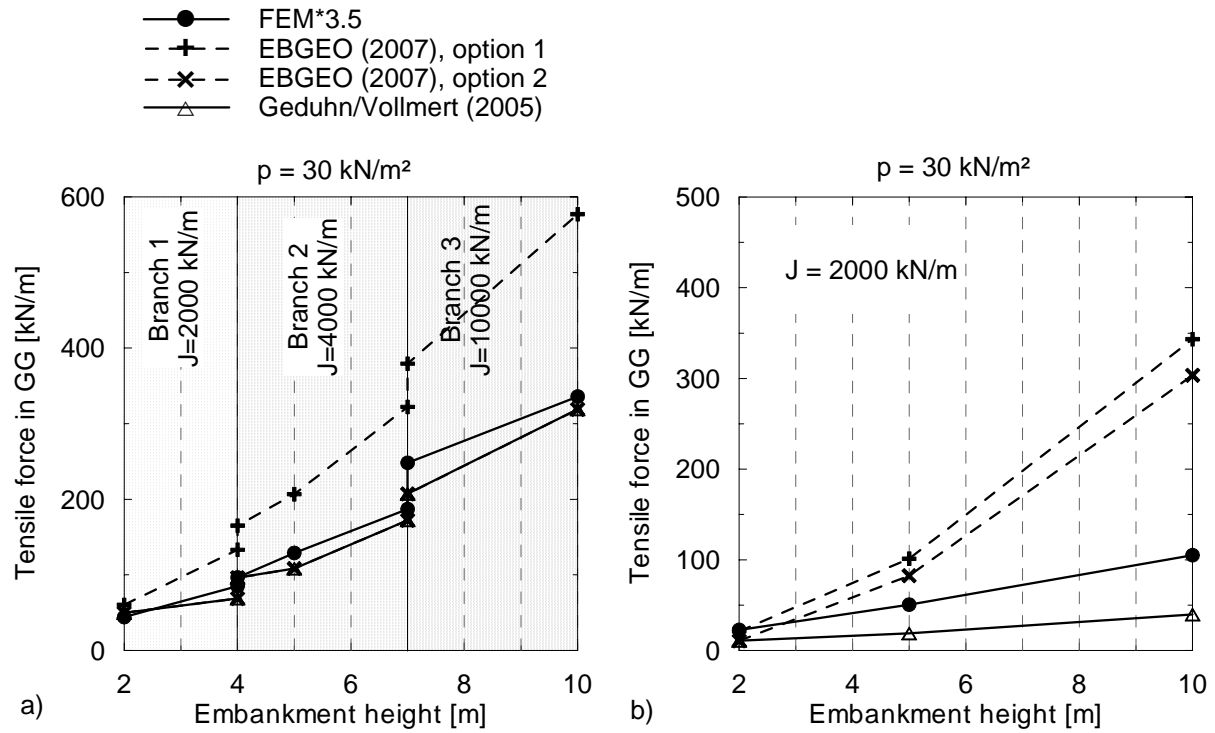


Figure 5.25: Comparing the analytical methods and the numerical results of the total tensile forces in reinforcement on piled embankment system on: a) normal- and b) over-consolidated clay underground.

In Figure 5.25a the analytical results according to *Geduhn/Vollmert (2005)* coincide with *EBGEO (2007)* option 2, where

- The analytical results according to *Geduhn/Vollmert (2005)* are presented by the membrane force only. This is attributed to the large applied base friction which eliminates the spreading effect totally.
- Because of the high tensile stiffness of the reinforcement, the membrane force has been evaluated larger than the spreading force. Therefore, the analytical results according to *EBGEO (2007)* option 2 is presented by the membrane force.

Figure 5.25b shows that the analytical results according to both *EBGEO (2007)* option 1 and option 2 would be large overestimated compared with the FEM-results. This is attributed to apply the spreading force as the horizontal active earth pressure, without considering the large

stiffness of the underground. Therefore, the existing analytical methods apply very large spreading forces, which were not agreed with the computed spreading force using FEM.

5.10 Summary of the analytical calculation

- In the case of reinforced embankment on soft underground supported by pile-like elements the membrane force in reinforcement due to the arching effect of soil between piles must be investigated in addition to the spreading effect in the slope zone.
- Plenty of methods can be used to determine the membrane force in reinforcement. The approach *EBGEO (2007)* can be considerably applied, where the analytical results were good agreed with the numerical ones. The approach *EBGEO (2007)* depends not only on the geometry of the embankment and the underground, but on the stiffness of the structural elements such as geogrid, embankment fill and the underground as well.
- Applying the analytical earth pressure theory to determine the spreading forces resulted in overestimated spreading forces, which were observed considerably in the case of very high embankments. The same result has been concluded in the case of stiffer underground, where the spreading forces were very large compared with the numerical results.
- Applying the method of *Geduhn/Vollmert (2005)* by adding the base friction along the slope base as a resistance force to spreading eliminates the resultant spreading force, especially in the case of flatter slopes and in the case of clay underground.
- The total analytical force in the reinforcement determined by adding the spreading force and membrane force according to *EBGEO (2007)* gives an overestimated resultant force in the high and very high embankments on clay undergrounds. This is attributed to the very high spreading forces, which depends on the embankment height.
- The maximum analytical tensile force in reinforcement according to *Love et al. (2003)* as well as *EBGEO (2007)* option 2 gives an overestimated force in the case of higher embankments and in the case of stiffer underground.
- The determination of the spreading force must be modified according to the sliding mechanism due to spreading stresses in the slope zone, which was explained in Section 5.4.2.

6 Development of a modified analytical method

6.1 General

The investigation of the spreading effect in the slope zone of an embankment has been carried out in the study by different means. The model tests to investigate the stress-displacement behaviour of the embankment system conclude that the spreading effect develops shear stresses in the embankment base. The stresses apply horizontal deformations in the slope toe and the upper part of embankment. The upper part of the embankment is separated from the lower one through the geogrid reinforcement forming a sliding soil wedge in the slope zone. The spreading forces in the slope zone are transferred to the reinforcement through the bond effect between the fill material and the reinforcement.

The parameter study, which investigates many parameters and boundary conditions in the case of piled embankments, has come to the following conclusions:

- The spreading effect in the slope zone develops tensile force in the reinforcement. In the case of piled embankment, this tensile force can be separated and determined.
- In the case of piled embankments, some of the spreading forces transfer to the pile heads causing horizontal deformations and bending moments in the piles.
- In the case of very high embankments on soft underground, the maximum horizontal deformation in the pile heads is determined at the piles placed in the slope zone. Figure 6.1 represents the horizontal displacements of the embankment base as well as the pile heads for an example of a 10 m-embankment on peat underground.

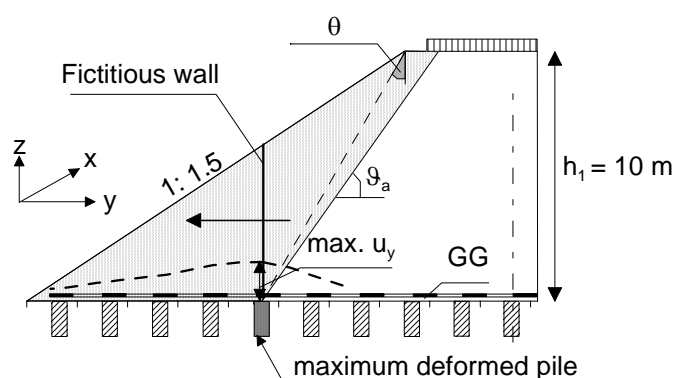


Figure 6.1:

The horizontal displacement of the pile heads and the sliding soil wedge of a 10 m-embankment on peat underground, at $p = 30 \text{ kN/m}^2$

- From Figure 6.1, a sliding soil wedge can be determined; where the spreading effect in the slope zone is effective. Herein, the maximum horizontal displacement in this soil

wedge located. In the example the position of the fictitious wall is dependent on an angle θ from the slope crest.

- The value and direction of the angle θ depends mainly on the embankment height and the existing external traffic load on the system.
- The horizontal active earth force on the fictitious wall can be determined according to the angle θ .
- In the case of stiff underground, the analytical methods such as *BS 8006 (1995)* and *EBGEO (2007)* determine a constant spreading force (as a function of E_{ah}) without considering the underground stiffness. Therefore, in a stiff and very stiff underground the analytical spreading force is found to be over estimated.
- In the case of flatter embankment slopes, the analytical methods such as *BS 8006 (1995)* and *EBGEO (2007)* determine a constant spreading force (as a function of E_{ah}) without considering the slope degree. The embankment slope plays an important role in the developing of the shear stresses at the embankment base and then the spreading forces (see Figure 3.14 and 3.15 in Chapter 3). Therefore, with a flatter embankment slope (1:2.5) the analytical spreading force is found to be over estimated.

6.2 Empirical modification of the sliding soil wedge and the spreading force

A model for the sliding soil wedge can be modified to calculate the analytical active earth pressure force due to spreading effect. The tensile force in the reinforcement due to spreading can be determined as shown in Equation 6.1.

$$F_{G,S} = E_{ah}(h = h_w) \quad (6.1)$$

The soil wedge represented in Figure 6.2 depends mainly on the angle θ . The situation of the imposed wall with height h_w is a function of θ .

The force E_{ah} in this case is calculated at the height h_w according to the earth pressure theory.

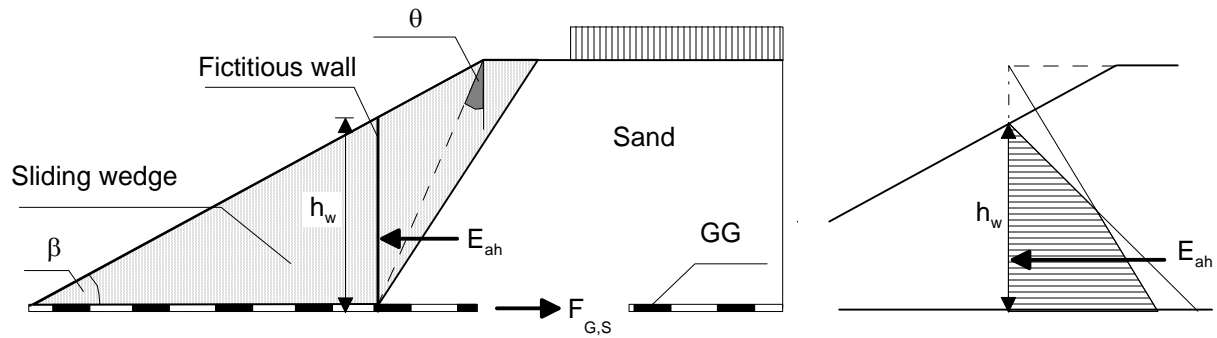


Figure 6.2: The analytical model of the sliding soil wedge and the active earth pressure

The angle θ can be either negative or positive to a vertical line from the slope crest. This depends on the geometry of the soil wedge. (Figure 6.3)

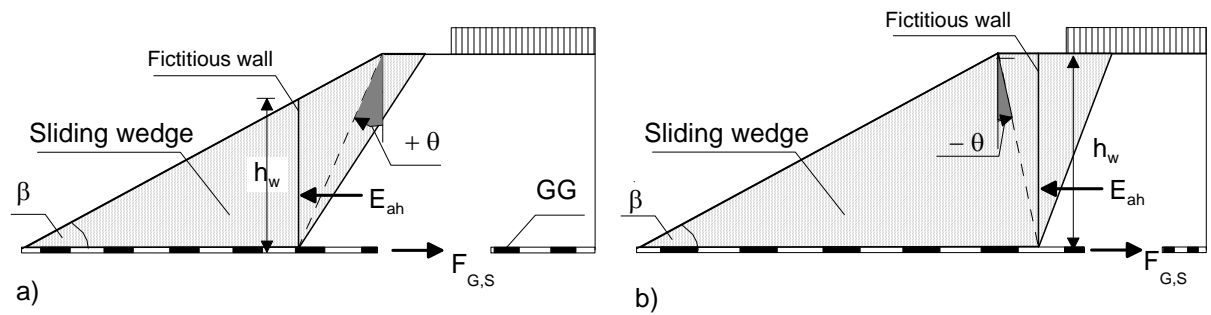


Figure 6.3: The angle θ : a) positive angle, b) negative angle

The angle θ in this model can be empirically determined from the results of the parameter study.

6.2.1 Horizontal active earth pressure force due to own weight, E_{agh}

The horizontal active earth pressure E_{agh} can be determined as a function of the angle θ . For $\theta \leq 0$, $h_w = h_1$, thus

$$E_{agh} = 0.5 \cdot \gamma_1 \cdot h_1^2 \cdot K_{agh} \quad \text{where} \quad K_{agh} = \tan^2 \left(45 - \frac{\varphi'}{2} \right) \quad (6.2)$$

For $\theta > 0$, then E_{agh} can be determined in the slope zone according to the earth pressure theory as represented in Figure 6.4.

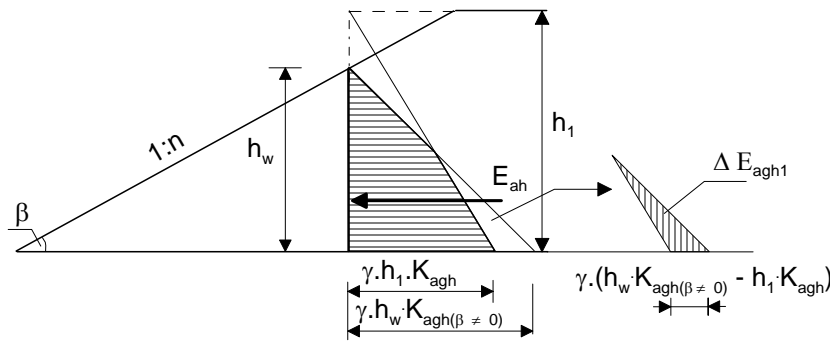


Figure 6.4:
 E_{agh} in the slope zone

E_{agh} in such case can be determined according to Equation 6.3:

$$E_{agh} = 0.5 \cdot \gamma_1 \cdot h_w^2 \cdot K_{agh(\beta \neq 0)} - \Delta E_{agh1} \quad (6.3)$$

where

$$h_w = \frac{\left(\frac{1}{\tan \beta} - \tan \theta \right) \cdot h_1}{1 / \tan \beta} = h_1 \cdot (1 - \tan \beta \cdot \tan \theta)$$

At h_w ; the coefficient $K_{agh(\beta \neq 0)}$ can be determined with $\alpha = 0$ and $\delta_a = \beta$:

$$K_{agh(\beta \neq 0)} = \left[\frac{\cos \varphi'}{1 + \frac{\sqrt{\sin(\varphi' + \beta) \cdot \sin(\varphi' - \beta)}}{\cos \beta}} \right]^2 \quad (6.4)$$

where

φ' the internal friction angle of the embankment fill;

β the slope angle of the embankment, $\beta = \tan^{-1}(1/n)$

$$\Delta E_{agh1} = 0.5 \cdot \gamma_1 \cdot \frac{(h_w \cdot K_{agh(\beta \neq 0)} - h_1 \cdot K_{agh})^2}{(K_{agh(\beta \neq 0)} - K_{agh})} \quad (6.5)$$

6.2.2 Horizontal active earth pressure force due to external load, E_{aph}

The earth pressure E_{aph} can be determined according to the standard *DIN 4085:2007-02*. Here, 3 different cases are investigated and determined as shown in Figure 6.5.

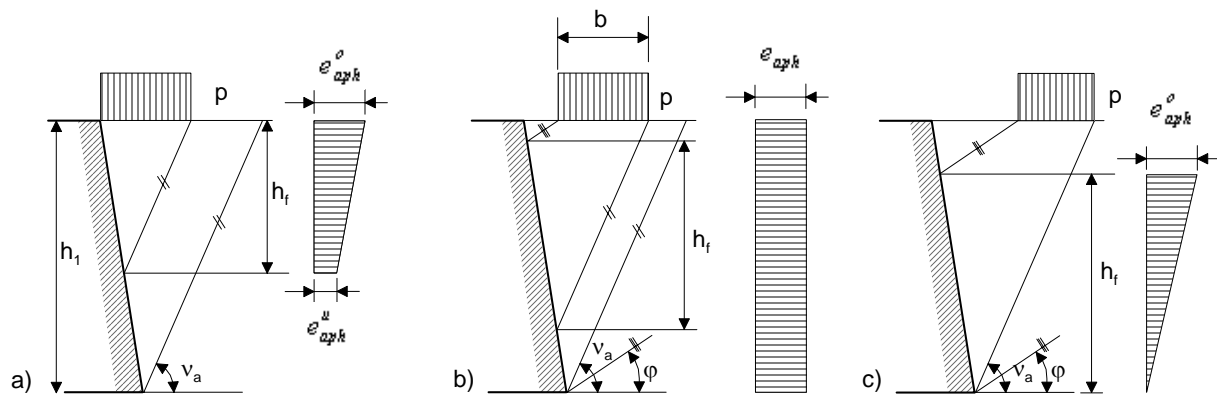


Figure 6.5: Determination of the horizontal earth pressure force due to external load

For simplified determination of E_{aph} the earth pressure is calculated according to Figure 6.5:

- $e_{aph}^u > 0$, then $E_{aph} = 0.5 \cdot (e_{aph}^o + e_{aph}^u) \cdot h_f$, where: $e_{aph}^o = e_{aph}$
- $e_{aph}^u > e_{aph}$, then $E_{aph} = e_{aph} \cdot h_1$, where: $h_f = E_{avh} / e_{aph}$
- $e_{aph}^u \leq 0$, then $E_{aph} = 0.5 \cdot e_{aph}^o \cdot h_f$, where: $e_{aph}^o = 2 \cdot E_{avh} / h_f$

where

$$e_{aph}^u = \frac{2 \cdot E_{avh}}{h_f} - e_{aph}$$

$$e_{aph} = p \cdot K_{aph} = p \cdot K_{agh}$$

E_{avh} Earth pressure force due to vertical loading, $E_{avh} = f(v_a, p, b)$, see *DIN 4085:2007-02*.

6.2.3 Determination of the tensile force in reinforcement and estimation of a reference parameter-model

A reference parameter-model with peat underground and embankment slope of 1:1.5 was taken for analysis to calculate the angle θ and the earth pressure E_{ah} . A factor f_{E_s} can be derived to relate E_{ah} in the case of different underground stiffness to E_{ah} of peat as a function of the stiffness of the underground (for peat $E_s = 0.8 \text{ MN/m}^2$), see Section 6.3.2.1. A factor f_β can be derived to relate E_{ah} in the case of different slopes to E_{ah} of slope 1:1.5 ($\beta = 33.7^\circ$) as a function of the embankment slope, see Section 6.3.2.2. The modified tensile force can now be determined as follows:

$$F_{G,S} = E_{ah}(h = h_w) \cdot f_{E_s} \cdot f_{\beta} \quad (6.6)$$

where $f_{E_s} = 1.0$ in the case of peat underground, and $f_{\beta} = 1.0$ in the case of slope 1:1.5.

6.3 Determination of the Earth pressure forces in the case of piled embankment

6.3.1 Determination of the angle θ according to the results of the parameter study

The determination of the angle θ in the reference parameter-model can be obtained by comparing the spreading force in the reinforcement from FEM with the modified analytical horizontal earth pressure force E_{ah} under variations of the angle θ for every embankment height under its own weight and loaded embankment. Firstly, a small embankment height $h_I = 2$ m is investigated to determine the angle θ of the sliding wedge in the case of peat underground at slope 1:1.5 as represented in Figure 6.6.

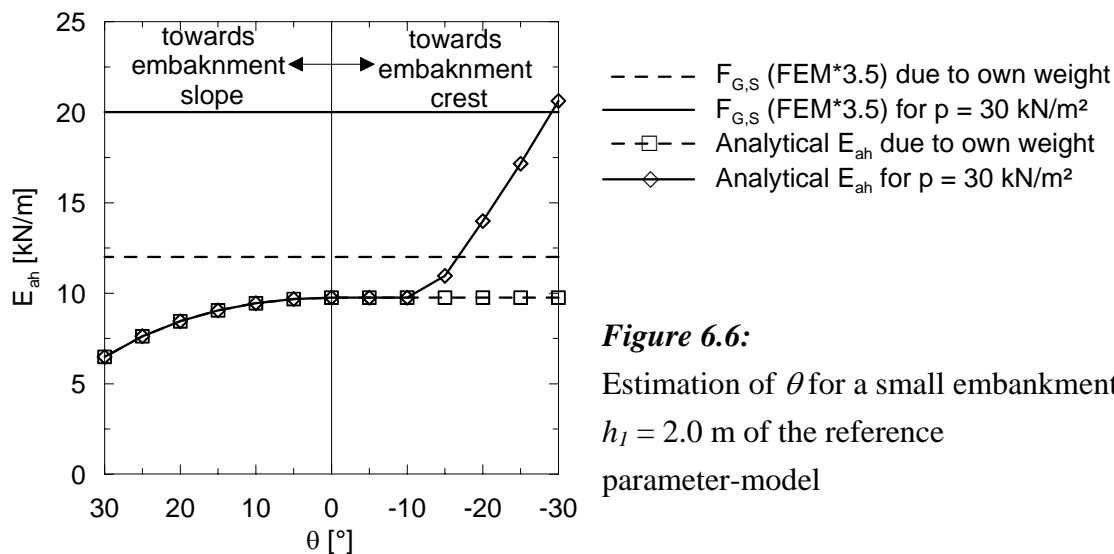


Figure 6.6:
Estimation of θ for a small embankment height $h_I = 2.0$ m of the reference parameter-model

In the case of a small embankment height, the external load can be observed to have a considerable effect to determine the spreading force compared with the own weight. By $\theta = 0$ at the slope crest, the external load has no effect on the determination of E_{ah} . At a negative angle $\theta = -30^\circ$ the analytical E_{ah} can be compared with FEM-result. To simplify the computation method, the angle θ can be taken as $\theta = 0^\circ$ i.e. $h_w = h_I$.

Figure 6.7 represents the estimation of the angle θ in the case of a middle embankment height $h_I = 5.0$ m of the reference parameter-model.

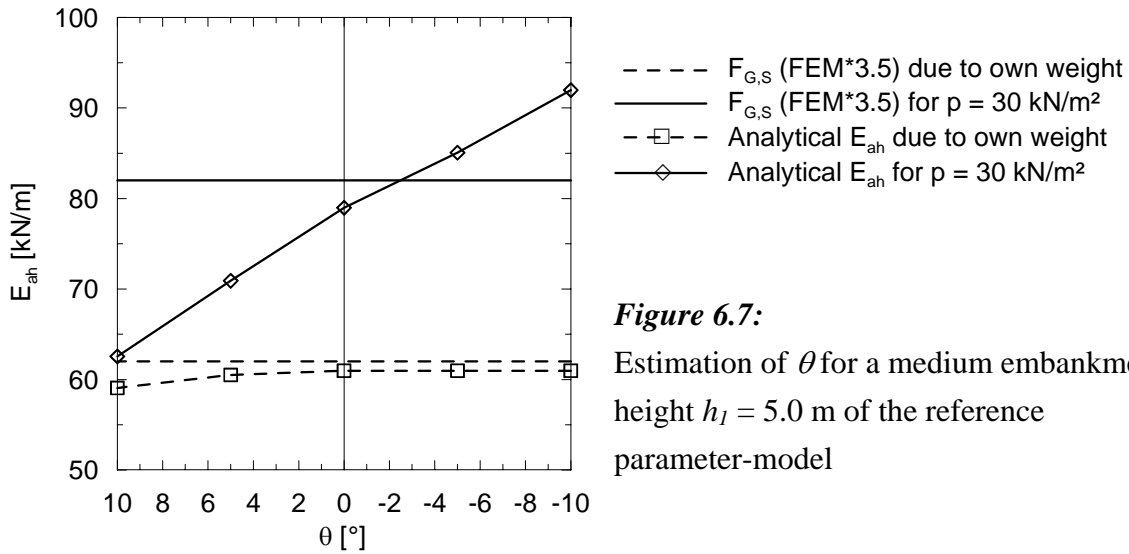


Figure 6.7:
 Estimation of θ for a medium embankment height $h_l = 5.0$ m of the reference parameter-model

In the case of $h_l = 5.0$ m, the angle θ can be taken as $\theta = 0^\circ$, with which the height $h_w = h_l$ for both loaded and unloaded embankment.

The estimation of the angle θ in the case of a large embankment height $h_l = 7.5$ m of the reference parameter-model is added to the study and represented in Figure 6.8.

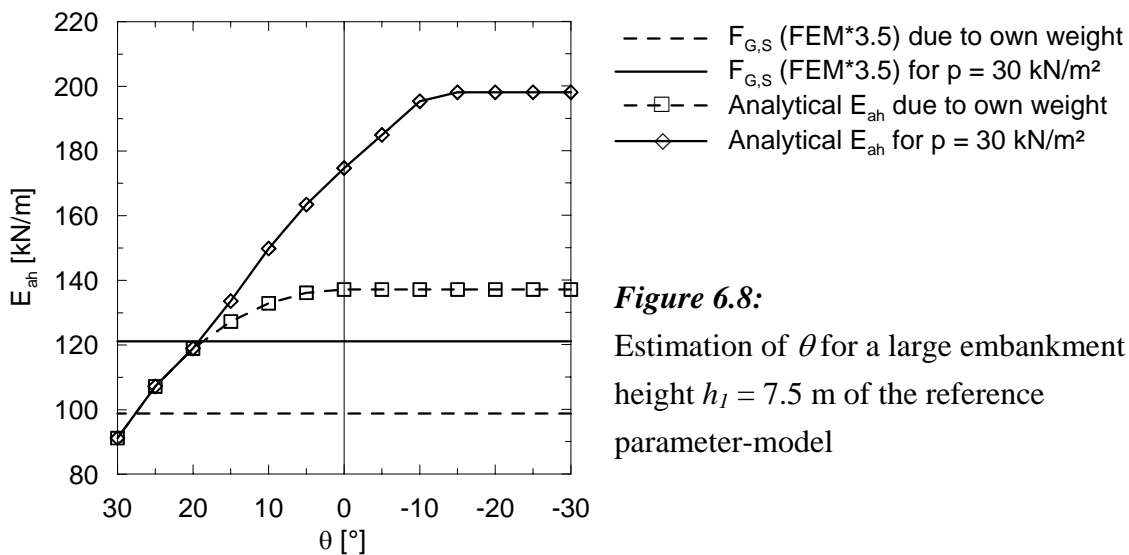


Figure 6.8:
 Estimation of θ for a large embankment height $h_l = 7.5$ m of the reference parameter-model

In the case of $h_l = 7.5$ m, it is observed that the sliding soil wedge due to spreading can be represented in the slope zone with an angle $18^\circ < \theta < 27^\circ$.

The estimation of the angle θ in the case of a very large embankment height $h_l = 10.0$ m of the reference parameter-model is represented in Figure 6.9.

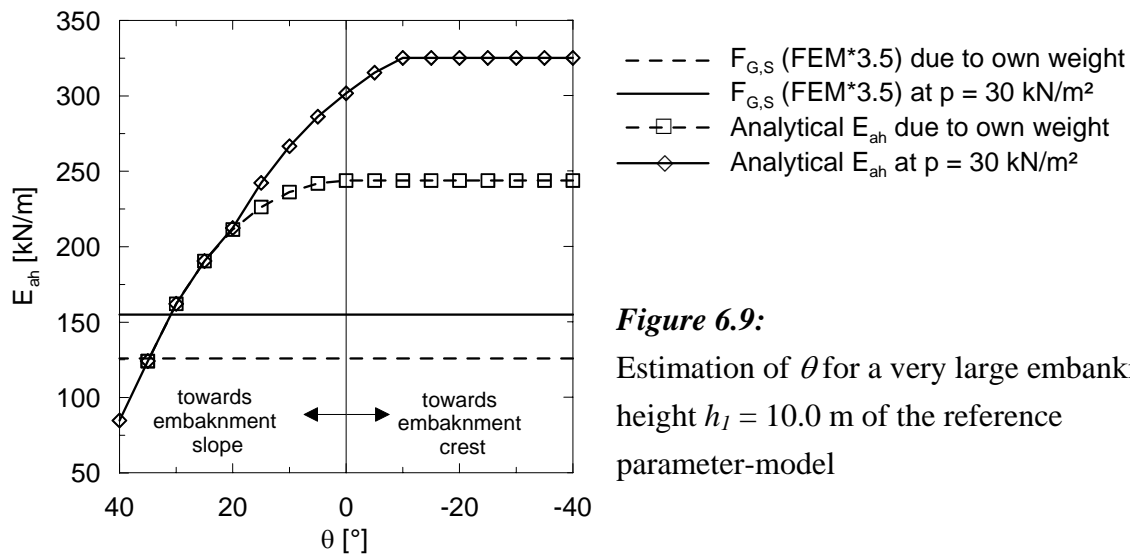


Figure 6.9:
Estimation of θ for a very large embankment height $h_l = 10.0$ m of the reference parameter-model

In the case of a very large embankment height, it is observed that the sliding soil wedge due to spreading can be represented in the slope zone with an angle $30^\circ < \theta < 35^\circ$. On the other hand, by applying the available analytical methods (at $\theta = 0^\circ$ and $h_w = h_l$), the analytical spreading force is over estimated compared with FEM-results.

6.3.2 Derivation of the factors f_{E_s} and f_β

The factors f_{E_s} and f_β can be empirically determined by comparing the tensile force in reinforcement due to spreading in the reference parameter-model with the tensile forces under the other parameters. The factors f_{E_s} and f_β can be defined as follows:

$$f_{E_s} = \frac{F_{G,S}(\text{stiffer underground with } E_s > 0.8 \text{ MN/m}^2)}{F_{G,S}(\text{peat underground with } E_s = 0.8 \text{ MN/m}^2)} \quad (6.7)$$

$$f_\beta = \frac{F_{G,S}(\text{slope flatter than } 1:1.5)}{F_{G,S}(\text{slope } = 1:1.5)} \quad (6.8)$$

6.3.2.1 Factor f_{E_s} to relate the underground stiffness

The FEM-parameter study includes normal consolidated clay-underground ($E_s \geq 3.0 \text{ MN/m}^2$) and over consolidated clay-underground ($E_s \geq 10.0 \text{ MN/m}^2$). The factor f_{E_s} can be graphically represented for various underground stiffness as in Figure 6.10.

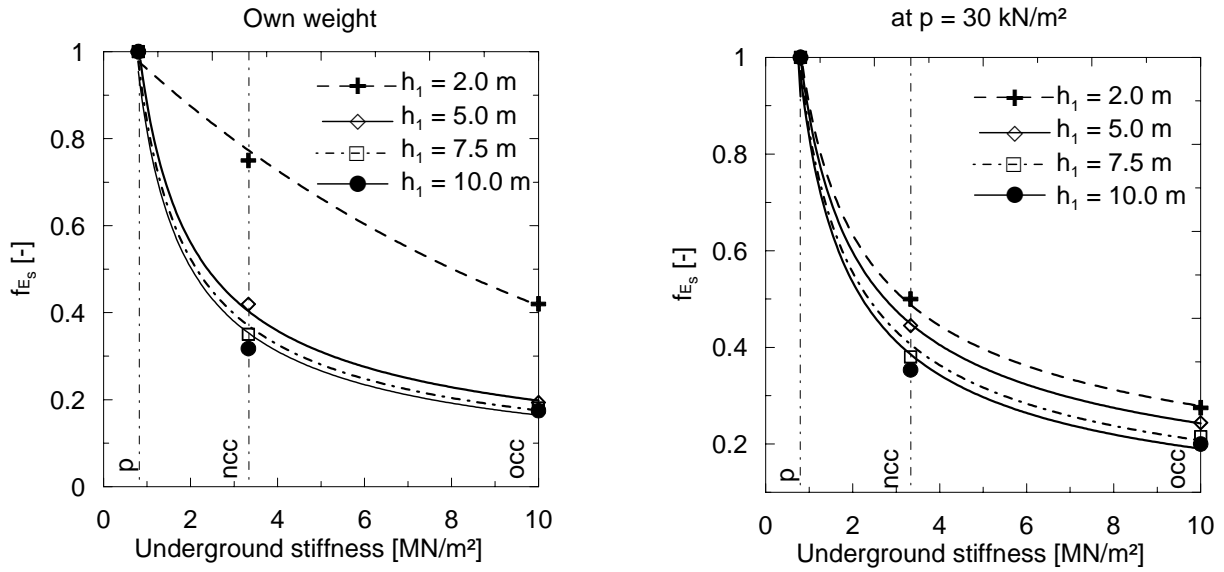


Figure 6.10: Determination of the factor f_{E_s} , p = peat, ncc = normal consolidated clay, occ = over consolidated clay

From Figure 6.10, the factor f_{E_s} can generally be expressed as a potential function in dependence of the underground stiffness E_s and the embankment height h_1 as follows:

$$f_{E_s} = \kappa_1 \cdot E_s^{(\kappa_2)} \quad (6.9)$$

where κ_1 and κ_2 are factors which can be represented as a function of the height h_1 .

In the case of unloaded embankment, the factors κ_1 and κ_2 can be represented by linear relations with the embankment height h_1 , where

$$\kappa_1 = 1.0066 - 0.02 \cdot h_1 \text{ and } \kappa_2 = -0.5979 - 0.01 \cdot h_1 \quad (6.9a)$$

Thus the general equation to represent the factor f_{E_s} in the case of unloaded embankment is:

$$f_{E_s} = (1.0066 - 0.02 \cdot h_1) \cdot E_s^{(-0.5979 - 0.01 \cdot h_1)} \quad (6.10)$$

The same formula can be applied to represent the factor f_{E_s} in the case of loaded embankment by deriving κ_1 and κ_2 as functions in h_1 :

$$\kappa_1 = 0.92 - 0.0085 \cdot h_1 \text{ and } \kappa_2 = -0.4768 - 0.0165 \cdot h_1 \quad (6.11)$$

Thus the general equation to represent the factor f_{E_s} in the case of loaded embankment is:

$$f_{E_s} = (0.92 - 0.0085 \cdot h_1) \cdot E_s^{(-0.4768 - 0.0165 \cdot h_1)} \quad (6.12)$$

6.3.2.2 Factor f_β to relate the embankment slopes

The FEM-parameter study includes a steep slope 1:1.5, which represents the reference slope in the modification process. Also a flatter slope of 1:2.5 has been analysed in the parameter study. A slope 1:2.0 has also been added to investigate the mathematical relation between the different slopes and the spreading force in reinforcement. Factor f_β who expresses this relation can be graphically represented for various embankment slopes in Figure 6.11.

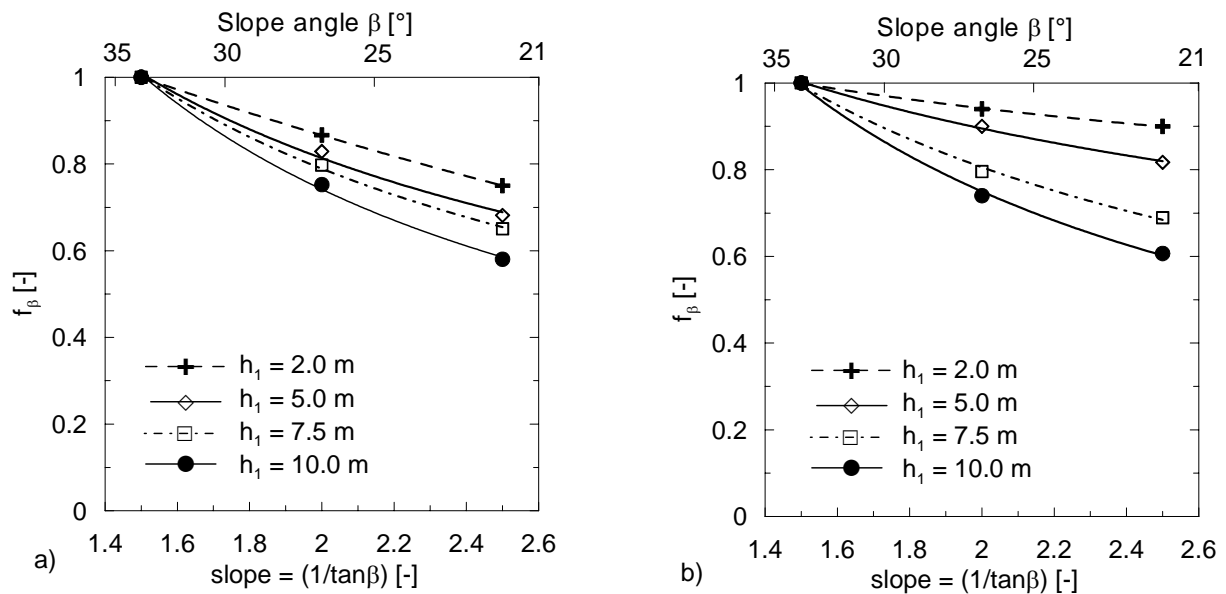


Figure 6.11: Determination of the factor f_β , a) under own weight, b) at $p = 30 \text{ kN/m}^2$

From Figure 6.11, the factor f_β can generally be expressed as a potential function in dependence of the embankment slope angle β and the embankment height h_1 as follows:

$$f_\beta = \kappa_3 \cdot \left(\frac{1}{\tan \beta} \right)^{\kappa_4} \quad (6.13)$$

In the case of unloaded embankment, the factors k_3 and k_4 can be represented by linear relations with the embankment height h_1 and the factor f_β is:

$$f_\beta = (1.1883 + 0.0358 \cdot h_1) \cdot \left(\frac{1}{\tan \beta} \right)^{(-0.4338 - 0.0627 \cdot h_1)} \quad (6.14)$$

In the case of loaded embankment

$$f_{\beta} = (0.962 + 0.0504 \cdot h_1) \cdot \left(\frac{1}{\tan \beta} \right)^{(0.0334 - 0.099 \cdot h_1)} \quad (6.15)$$

The equation of the modified spreading force can now be expressed in the general form in both cases of the embankment: under its own weight and loaded.

In the case of embankment under its own weight the general spreading force equation is:

$$F_{G,S} = E_{ah} \cdot (1.0066 - 0.02 \cdot h_1) \cdot E_s^{(-0.5979 - 0.01 \cdot h_1)} \cdot (1.1883 + 0.0358 \cdot h_1) \cdot \left(\frac{1}{\tan \beta} \right)^{(-0.4338 - 0.0627 \cdot h_1)} \quad (6.16)$$

In the case of a loaded embankment the general spreading force equation is:

$$F_{G,S} = E_{ah} \cdot (0.92 - 0.0085 \cdot h_1) \cdot E_s^{(-0.4768 - 0.0165 \cdot h_1)} \cdot (0.962 + 0.0504 \cdot h_1) \cdot \left(\frac{1}{\tan \beta} \right)^{(0.0334 - 0.099 \cdot h_1)} \quad (6.17)$$

6.4 Comparison of the modified analytical spreading forces with FEM-results and *EBGEO* (2007)

In this section the modified analytical spreading force in every embankment height can be represented according to Equations 6.2 and 6.3 for every embankment height. The following angle θ is considered for every embankment height:

- at $h_l = 2.0$ m, $\theta = 0^\circ$ under own weight and at $p = 30$ kN/m²
- at $h_l = 5.0$ m, $\theta = 0^\circ$ under own weight and at $p = 30$ kN/m²
- at $h_l = 10.0$ m, $\theta = 30^\circ$ under own weight and at $p = 30$ kN/m²

Figure 6.11 represents the modified spreading force compared with FEM-results of the spreading forces of the reference parameter-model under own weight and at $p = 30$ kN/m². The spreading forces at embankment heights from $h_l = 2$ to 5 m have been presented in a larger scale than the forces at $h_l = 10$ m in order to give a clear view of the difference in the estimated forces compared with FEM-results. That is the left axis refers to $h_l = 2$ to 5 m and the right axis to $h_l = 5$ to 10 m. This presentation will also apply for Figure 6.12 to Figure 6.17.

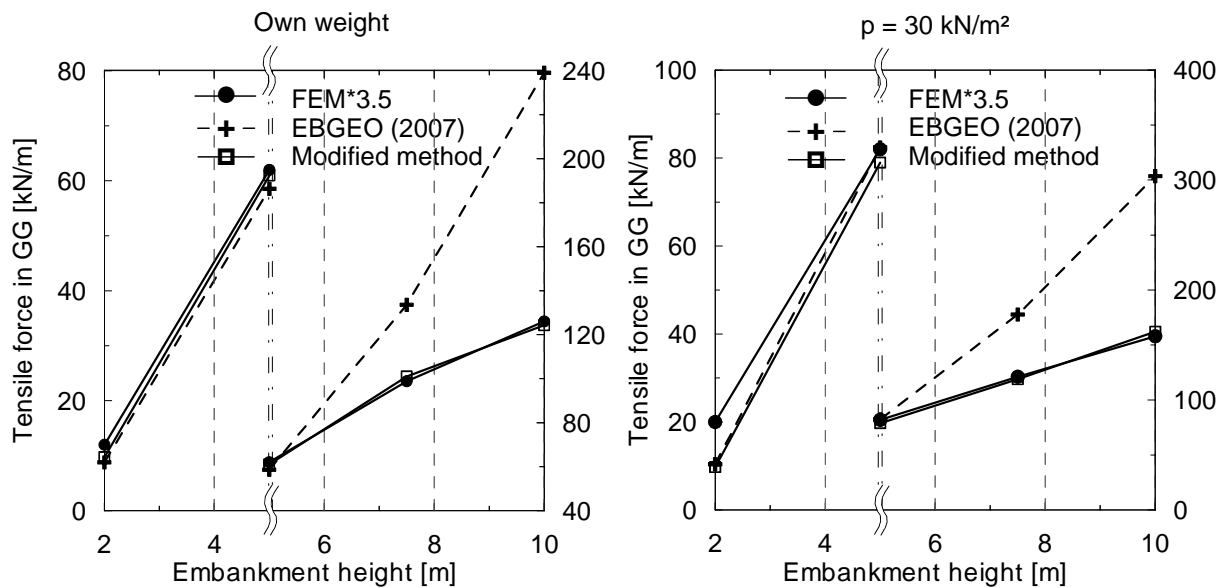


Figure 6.12: Comparing analytical modified analytical method with FEM-results and analytical spreading force according to *EBGEO (2007)*, slope 1:1.5 for peat underground, a) under own weight, b) at $p = 30 \text{ kN/m}^2$

From Figure 6.12, the determination of the spreading force under high embankment heights according to *EBGEO (2007)* is over estimated compared with FEM-results. The modified method results in good comparable forces.

6.4.1 Spreading forces under variation of the underground stiffness

In the case of stiffer underground, the spreading force according to the modified method can be calculated by applying Equation 6.6. However, the earth pressure force in dependence of θ would be multiplied by the factor f_{Es} (see Equation 6.10 under own weight and Equation 6.12 at $p = 30 \text{ kN/m}^2$). The factor f_{β} is 1.0 for a slope 1:1.5. The results of spreading forces in the case of normal consolidated clay underground are presented in Figure 6.13 and in the case over consolidated clay underground in Figure 6.14.

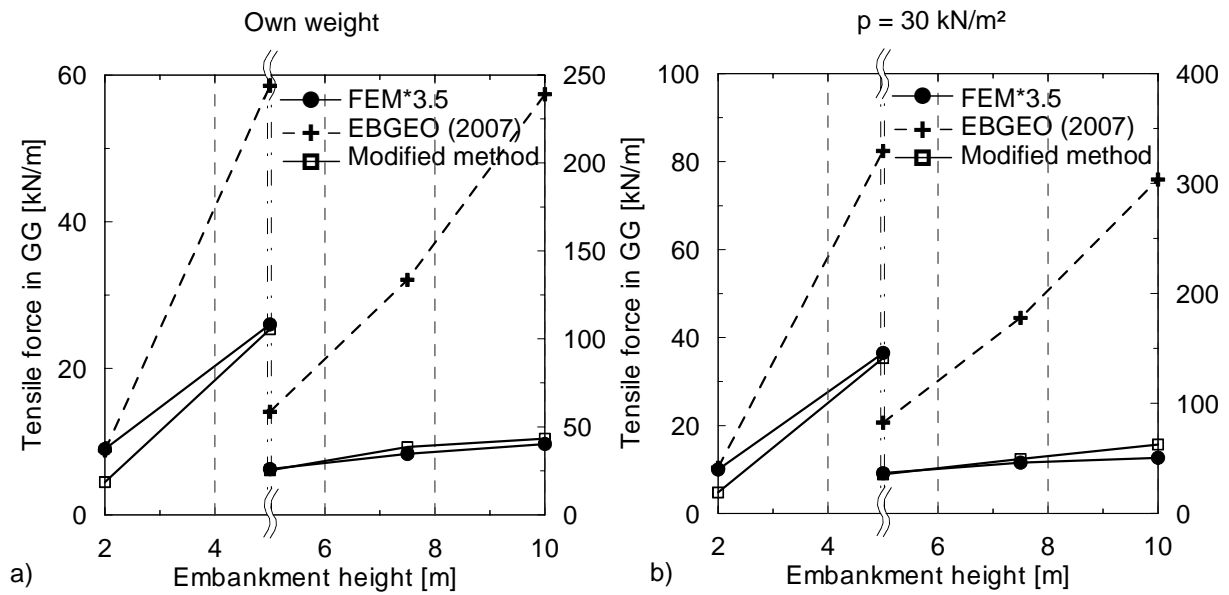


Figure 6.13: Comparing modified analytical method with FEM-results and analytical spreading force according to *EBGEO (2007)*, slope 1:1.5, normal consolidated clay underground, a) under own weight, b) at $p = 30 \text{ kN/m}^2$

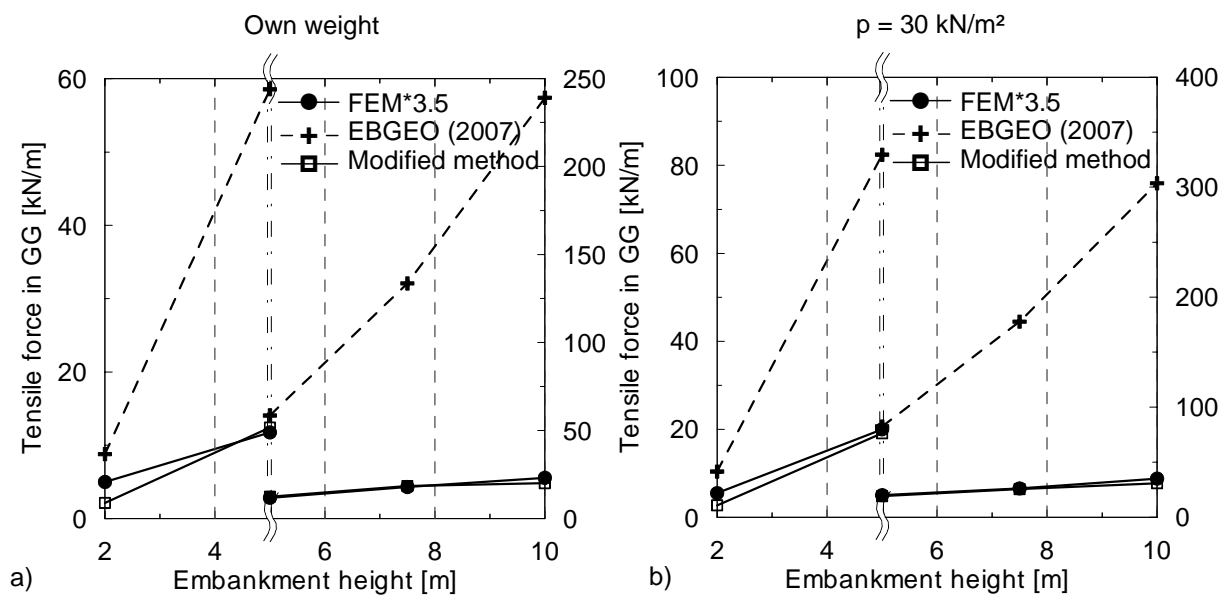


Figure 6.14: Comparing modified analytical method with FEM-results and analytical spreading force according to *EBGEO (2007)*, slope 1:1.5, over consolidated clay underground, a) under own weight, b) at $p = 30 \text{ kN/m}^2$

According to *EBGEO (2007)* the spreading force in reinforcement is calculated as the horizontal active earth pressure without consideration of the underground stiffness. Therefore, the spreading force in such method was found to be overestimated compared with FEM-results.

The modified analytical method gives a spreading force that is widely applicable with the FEM-results.

6.4.2 Spreading forces under variation of the embankment slope

In the case of flatter embankment slopes, the spreading force according to the modified method can be calculated by applying Equation 6.6. In the case of flatter slopes on peat underground, the earth pressure force in dependence of θ would be multiplied by the factor f_β (see Equations 6.14 under own weight and 6.15 at $p = 30 \text{ kN/m}^2$) and the factor $f_{Es} = 1.0$. In the case of a stiffer underground and flatter embankment slope, the earth pressure force in dependence of θ would be multiplied by the factor f_β and the factor f_{Es} (see Equation 6.10 under own weight and 6.12 at $p = 30 \text{ kN/m}^2$). Figure 6.15 represents the results in the case of slope 1:2.5 on peat underground.

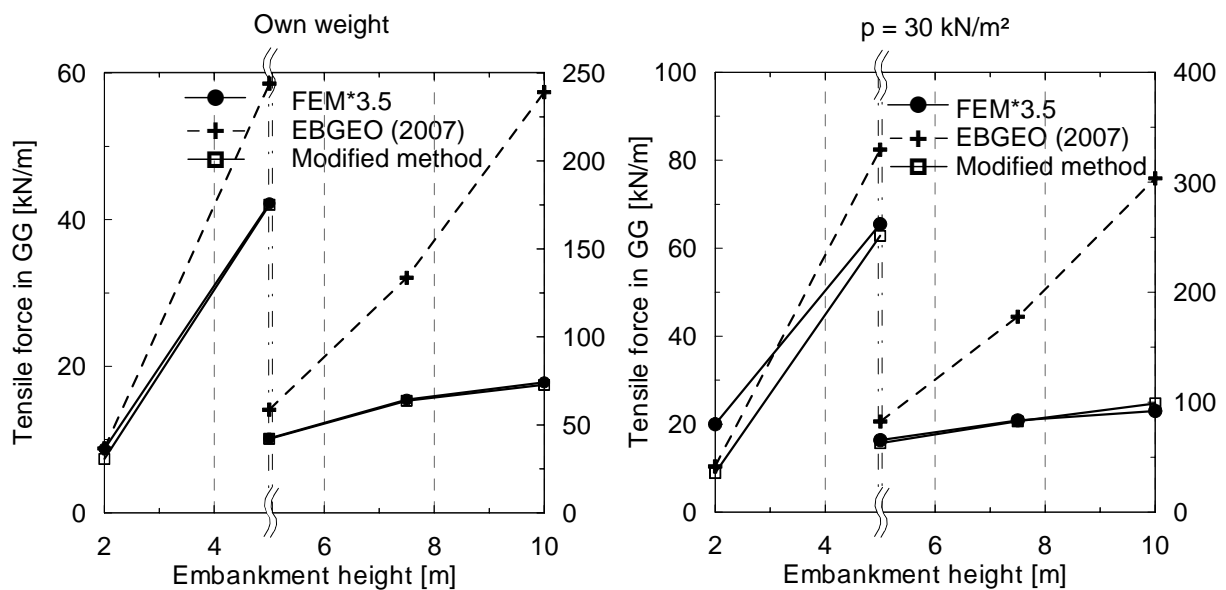


Figure 6.15: Comparing modified analytical method with FEM-results and analytical spreading force according to *EBGEO (2007)*, slope 1:2.5, peat underground, a) under own weight, b) at $p = 30 \text{ kN/m}^2$

According to the existing analytical methods, the embankment slope plays no role in the determination of the spreading force. However, the modified method considered the effect of the embankment slope and the resulting spreading forces has developed compatible values to the FEM-results. Figure 6.16 and Figure 6.17 represent the results in the case of slope 1:2.5 on both normal- and over consolidated clay underground. In this case, both the factors f_β and f_{Es} has been calculated according the equations (6.10) to (6.15) and applied to $F_{G,S}$.

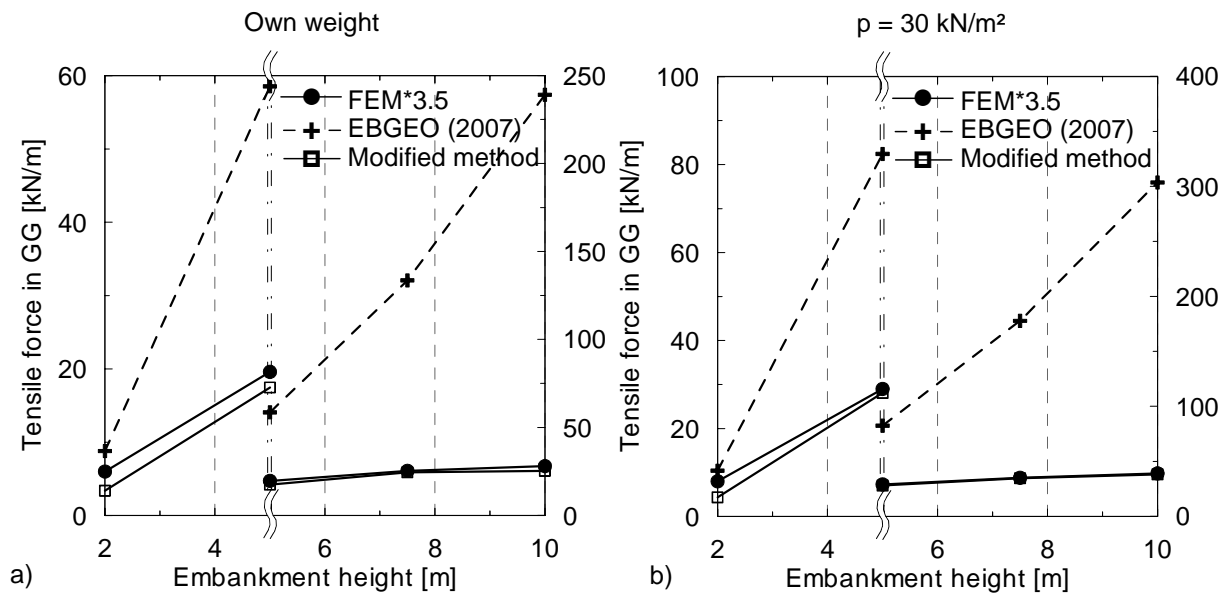


Figure 6.16: Comparing modified analytical method with FEM-results and analytical spreading force according to *EBGEO (2007)*, slope 1:2.5, normal consolidated clay underground, a) under own weight, b) at $p = 30 \text{ kN/m}^2$

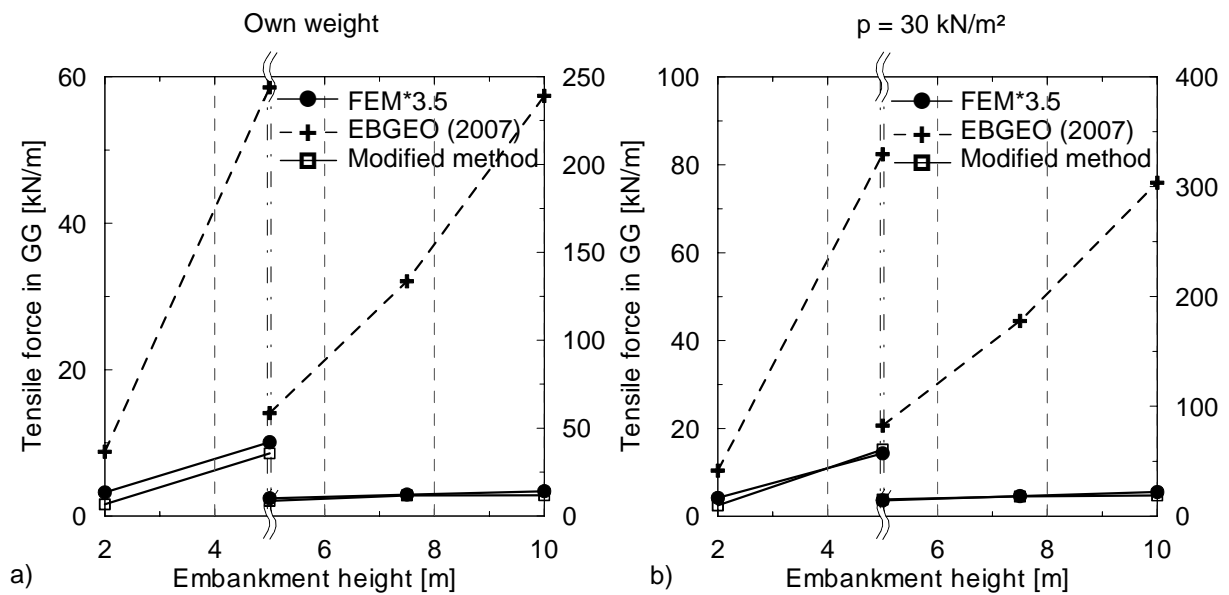


Figure 6.17: Comparing modified analytical method with FEM-results and analytical spreading force according to *EBGEO (2007)*, slope 1:2.5, over consolidated clay underground, a) under own weight, b) at $p = 30 \text{ kN/m}^2$

Figures 6.16 and 6.17 show that the modified method can qualitatively represent the spreading force in reinforcement under different parameter conditions. On the other hand, the exist-

ing analytical methods give overestimated and uneconomical spreading forces in reinforcement compared with FEM-results.

6.5 Comparison of the modified analytical total forces with FEM-results and *EBGEO* (2007)

6.5.1 Determination of the membrane force

In order to calculate the tensile forces in the reinforcement due to the membrane (arching) effect, the vertical stresses due to external load must be correctly transferred to the arching level, which according to *EBGEO* (2007) is half of the arching height h_g . The arching height is computed from the span between two piles, in the two directions, s_x and s_y then the arching height, s is as follows:

$$s = \sqrt{s_x^2 + s_y^2} \quad \text{then } h_g = s/2 \quad \text{for } h_1 \geq s/2 \quad (6.18)$$

$$h_g = h_1 \quad \text{for } h_1 < s/2$$

The distribution of a strip uniform load in a half-space was derived according to *Boussinesq* and equations after *Gray* (1938), (cited in *Teferra/Schultze* (1988)) as shown in Figure 6.18.

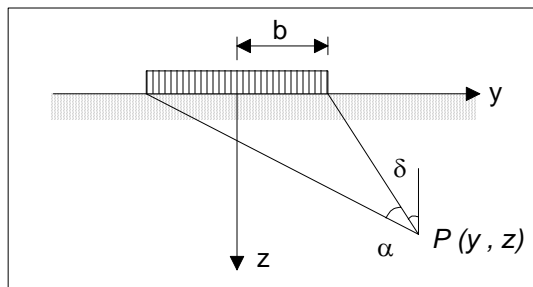


Figure 6.18:
Stress distribution according
to *Boussinesq/Gray* (1938)

The formula to get the horizontal and vertical stress distribution at any point “P” is as follows:

$$\sigma_z = \frac{p}{\pi} [\alpha + \sin \alpha \cdot \cos 2\beta'] \quad \text{and } \beta' = \delta + \frac{\alpha}{2} \quad (6.19)$$

The vertical stress distribution is a function of the load p , the width of the traffic way b , the embankment height h , the arching height h_g , and the place of point P. The distribution of the vertical stresses in the case of low embankment heights indicates a large concentration in the central zone and approximately small propagation in the slope zone as shown in Figure 6.19a, while in Figure 6.19b the stress propagation in the slope zone was observed in an angle between 30° and 45° according to the embankment height.

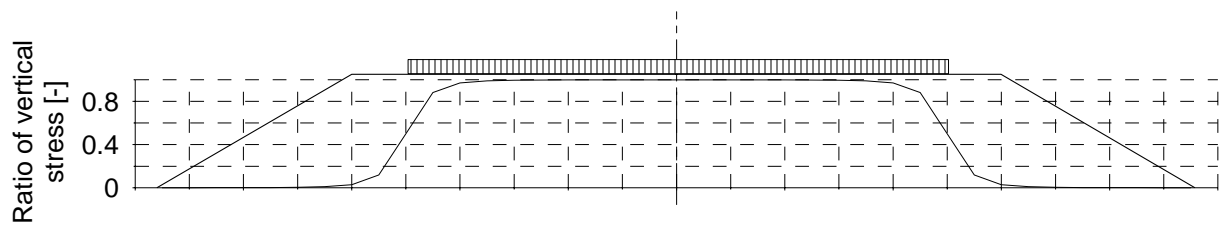
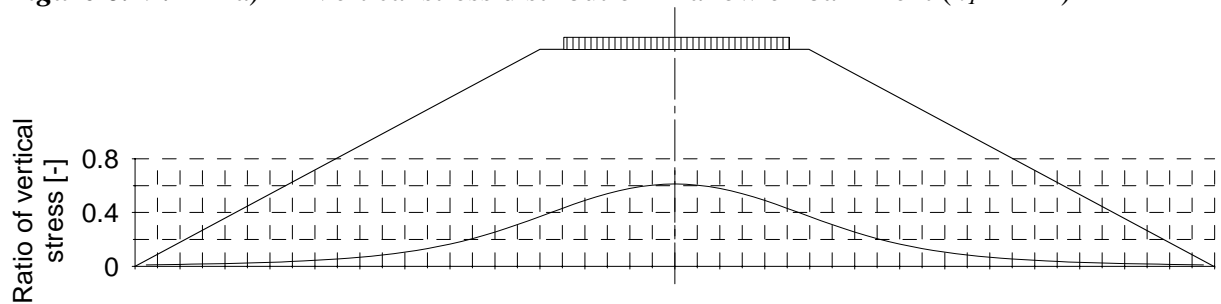


Figure 6.19: a) Vertical stress distribution in a low embankment ($h_1 = 2$ m)



b) Vertical stress distribution in a high embankment ($h_1 = 10$ m)

To analyse the membrane effect in the reinforcement due to the embankment's own weight, the embankment body is divided into vertical slices, which are limited and dimensioned between every two piles and the substituted height of the slice is geometrically determined. Hence, the vertical stress in the reinforcement due to the external load on every slice can be determined according to the stress distribution as explained in Equation 6.19.

According to Section 5.6.2 the analytical method to calculate the membrane force in reinforcement can be used according to *EBGEO (2007)*, which provided more satisfied results with the numerical investigations on different heights and different underground materials.

6.5.2 Total tensile force in reinforcement under variation of the underground stiffness

The total tensile forces according to the modified analytical method can be determined and compared with FEM-results and existing analytical methods according to *EBGEO (2007)*. The compared results represented in Figure 6.20 to 6.25 are as follows:

- FEM-results of the total force multiplied by factor 3.5 as investigated and determined from the parameter study in Chapter 5.
- Results of *EBGEO (2007)* option 1, which are determined by adding the membrane force to the spreading force as defined in Section 2.4.1 and 5.9.3.

- Results of *EBGEO (2007)* option 2, which determined by applying the larger of membrane or spreading force in GG as defined in Section 2.4.1.
- A modification of the *EBGEO* method can also be derived and presented by adding the membrane force according to *EBGEO (2007)* to the spreading force modified and computed by the author in Section 6.4.
- Results of the modified method, which derived in this chapter by adding the modified spreading force estimated in Section 6.4 to the modified membrane force according to *EBGEO (2007)* taking into account the load reduction as explained in Section 6.5.

In the case of unloaded embankment, the modified *EBGEO (2007)* method coincides with the author's own modified method. This can be seen in Figure 6.20 to 6.25.

The comparison of the results in the case of a peat underground is shown in Figure 6.20.

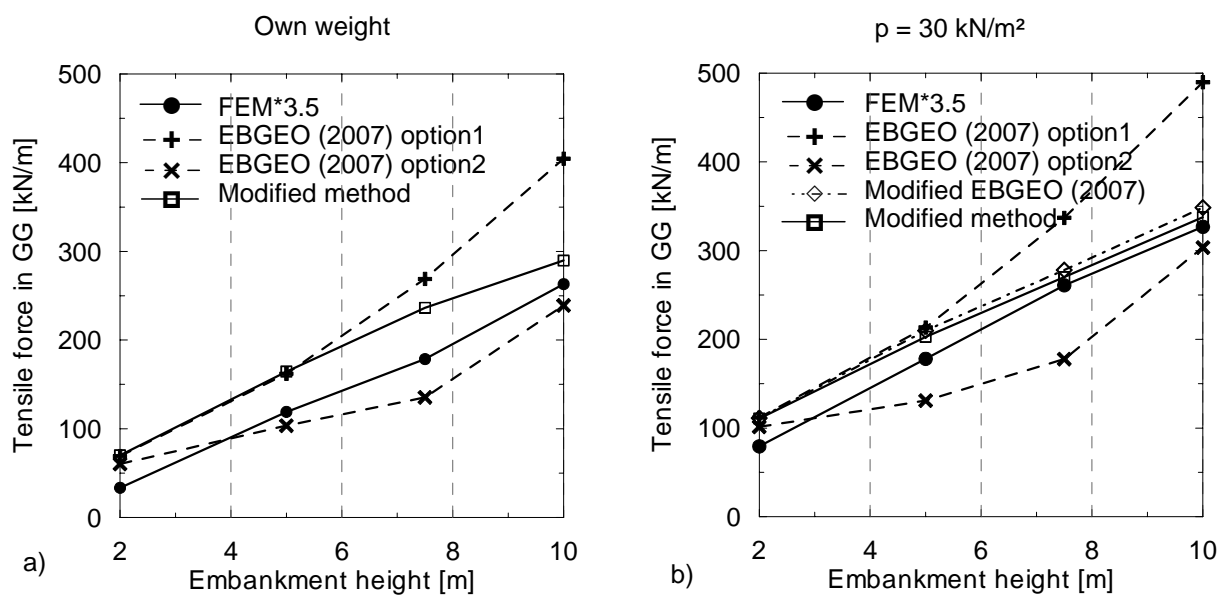


Figure 6.20: Comparing analytical modified analytical method with FEM-results and analytical spreading force according to *EBGEO (2007)*, peat underground, 1:1.5, a) under own weight, b) at $p = 30 \text{ kN/m}^2$

Figure 6.20 illustrates that in the very high embankments the analytical method provides considerable compatible tensile forces compared with the FEM-results. The analytical method *EBGEO (2007)* option1 results in overestimated and uneconomic tensile forces in the case of very high embankments. However, in *EBGEO (2007)* option 2 the results were compatible with FEM-results in the case of unloaded embankment. Another example can be illustrated in

the case of a stiffer underground soil layer as normal and over consolidated clay. Figures 6.21 and 6.22 represent the modified total forces compared with *EBGEO (2007)* and FEM-results.

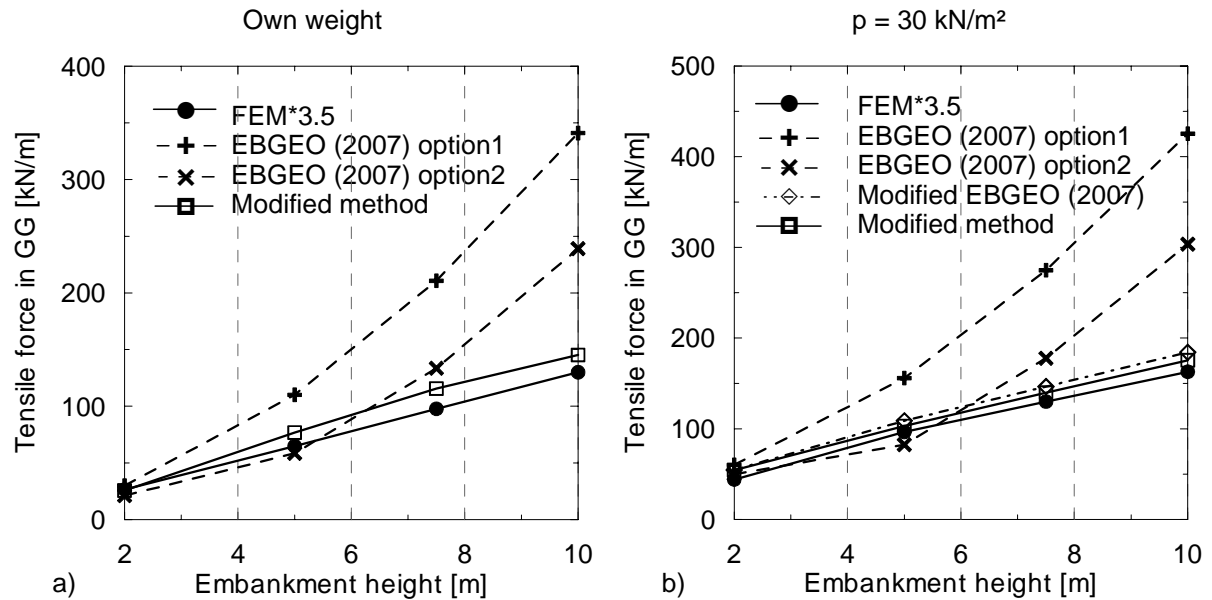


Figure 6.21: Comparing modified analytical method with FEM-results and analytical total force according to *EBGEO (2007)*, normal consolidated clay underground, slope 1:1.5, a) under own weight, b) at $p = 30 \text{ kN/m}^2$

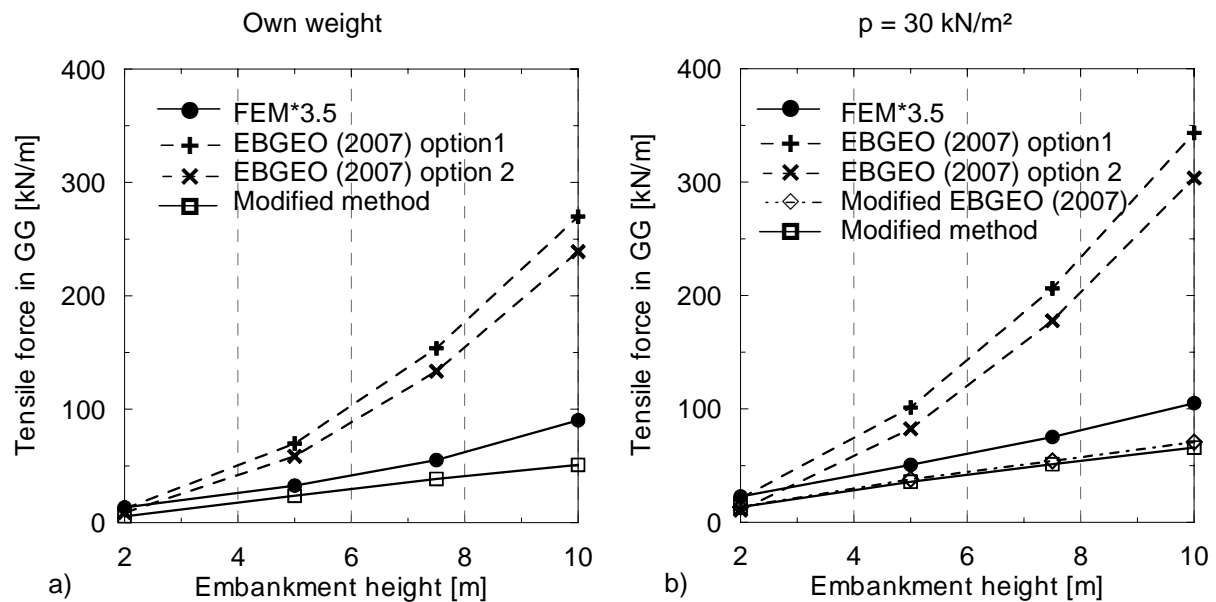


Figure 6.22: Comparing modified analytical method with FEM-results and analytical total force according to *EBGEO (2007)*, over consolidated clay underground, slope 1:1.5, a) under own weight, b) at $p = 30 \text{ kN/m}^2$

In the case of stiffer underground with larger embankment heights, the maximum force according to *EBGEO (2007)* option 2 is calculated as the spreading force, which were overestimated compared with the FEM-results. The modified method results in analytical forces which can be considerably compatible with the FEM-results.

6.5.3 Total tensile force in reinforcement under variation of the embankment slope

In this section the total tensile force in the case of flatter embankment slope 1:2.5 is investigated. The total force according to the modified analytical method can be determined by adding the modified spreading force in Section 6.4.2 to the modified membrane force according to *EBGEO (2007)* considering the load reduction as explained in Section 6.5.1.

The results of the modified analytical method have been compared with the FEM-results in the case of peat underground. The comparing results are represented in Figure 6.23.

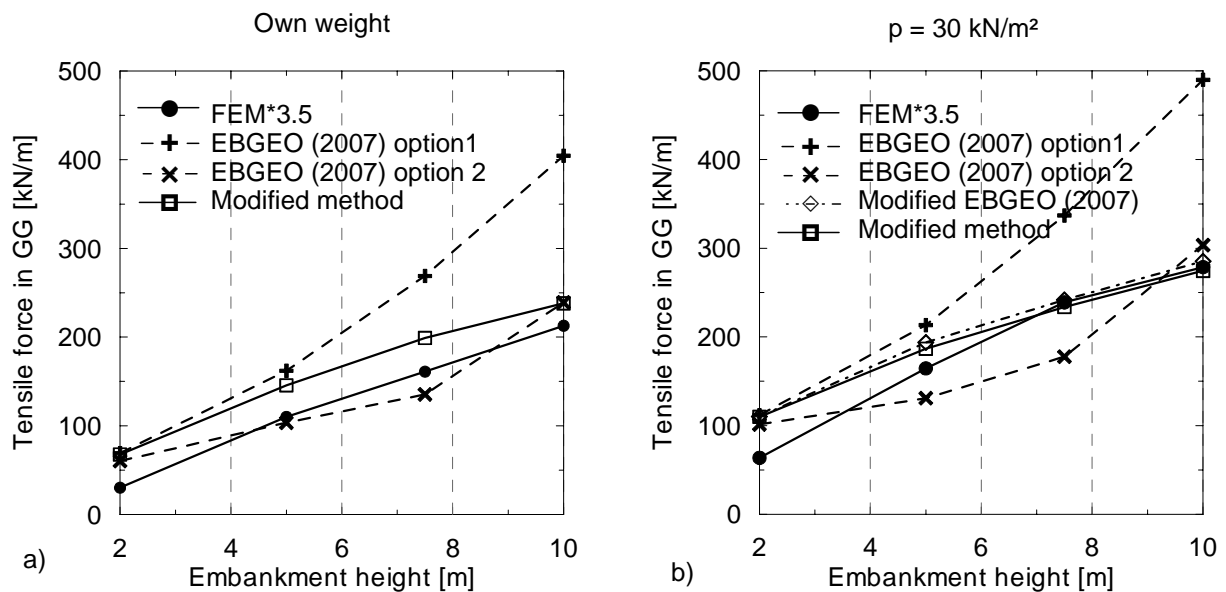


Figure 6.23: Comparing modified analytical method with FEM-results and analytical total force according to *EBGEO (2007)*, peat underground, slope 1:2.5, a) under own weight, b) at $p = 30 \text{ kN/m}^2$

The tensile force in GG according to *EBGEO (2007)* can be estimated as the same forces in the steeper slope 1:1.5. The tensile forces according to the modified method have considered the effect of the slope in the spreading and total force in GG.

Figures 6.24 and 6.25 represent the modified total forces compared with *EBGEO (2007)* and FEM-results in the case of stiffer underground and slope 1:2.5.

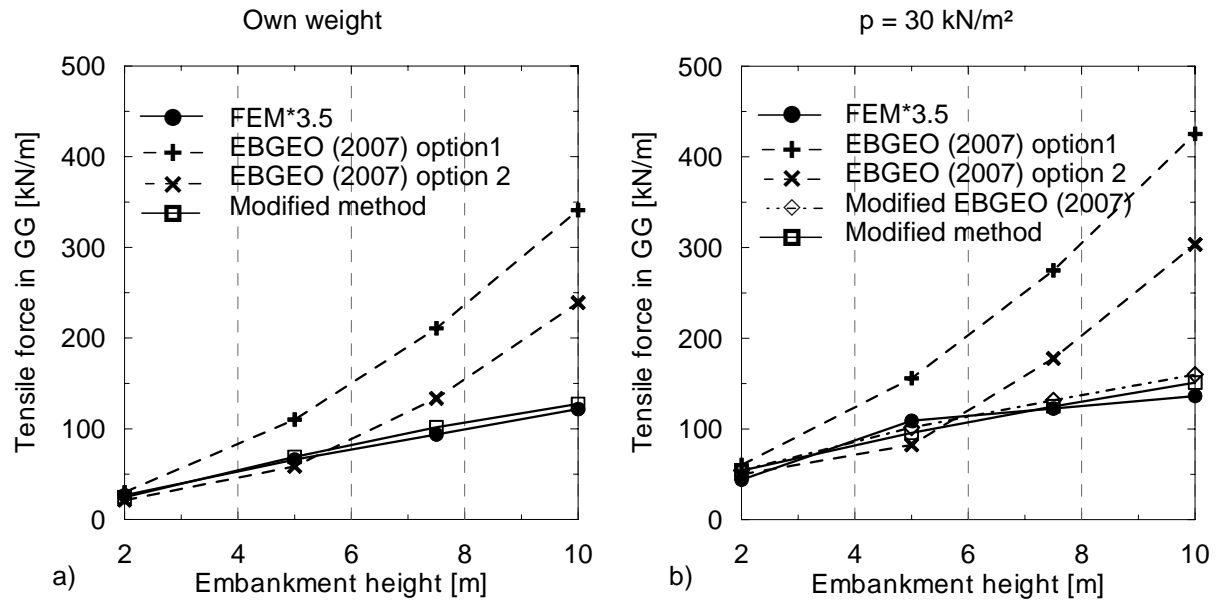


Figure 6.24: Comparing modified analytical method with FEM-results and analytical total force according to *EBGEO (2007)*, normal consolidated clay underground, slope 1:2.5, a) under own weight, b) at $p = 30 \text{ kN/m}^2$

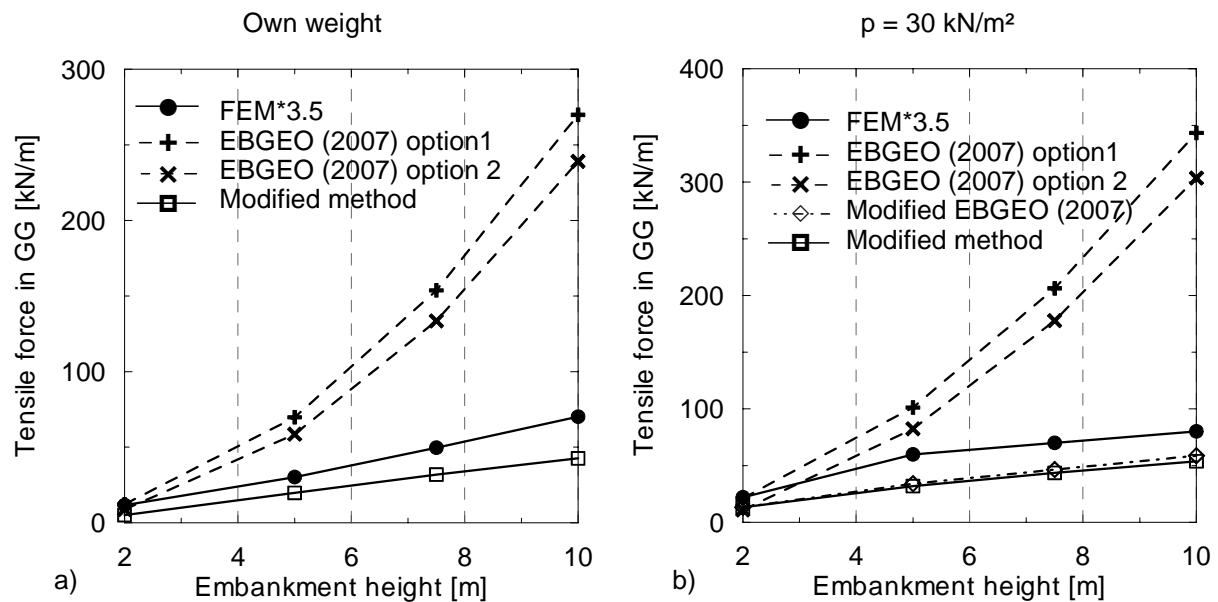


Figure 6.25: Comparing modified analytical method with FEM-results and analytical total force according to *EBGEO (2007)*, over consolidated clay underground, slope 1:2.5, a) under own weight, b) at $p = 30 \text{ kN/m}^2$

Figures 6.24 and 6.25 illustrate the total tensile force in GG according to the modified method compared with FEM-results and *EBGEO (2007)*. In the case of over consolidated clay underground, the modified method shows underestimated tensile forces compared with FEM-results. In the case of normal consolidated clay underground, the tensile forces according to the modified method are compatible with the FEM-results.

6.5.4 Spreading effect on the pile elements

The horizontal spreading force developed in the reinforcement is transferred directly to the pile heads and the underground. The developing of the spreading forces through the base friction between the underground and the reinforcement is active only for a part of the loads transferred by the soil resistance to the underground soil. The piles in the slope zone could be used as supported elements to sustain the remaining horizontal forces, which result in horizontal displacements and bending moments.

The horizontal forces in the pile heads could be estimated as the resultant horizontal forces in reinforcement as reported in Equation 6.16 and 6.17.

$$F_{h,P} = F_{G,S} \quad (6.20)$$

The bending tensile stresses in the pile cross section due to horizontal spreading forces must be in the safe limit of the allowable tensile stresses of the plain concrete material f_{cm} . By excessive spreading forces in the pile heads, the base reinforcement must be designed to sustain the excessive forces, and hence, reduce the horizontal displacements of the pile heads (see Figure 6.26b). The horizontal displacement in the pile heads for the different undergrounds with base reinforcement compared with the spreading force is presented in Figure 6.26a for the case of an embankment with slope 1:1.5 at $p = 30 \text{ kN/m}^2$ and different embankment heights.

From Figure 6.26a, it is clearly observed that the horizontal displacement of the pile heads exhibits the same behaviour of the spreading forces for various embankment heights and underground materials. By stiffer underground the small spreading forces result in small displacements compared with soft underground. It is also observed from Figure 6.26b that the base reinforcement has a considerable effect in reducing the horizontal deformations in pile heads, especially on very soft undergrounds, by holding the shear stresses at the base in the slope zone. However, In the case of high and very high embankments, a separate proof of safety must be carried out on the piles, where the horizontal forces on the pile heads result in

unsafe and very large horizontal displacements and bending tensile stresses in the pile cross section as presented in Chapter 5, Figure 5.9. The numerical methods can be used to analyse and investigate the safety of the horizontally loaded piles.

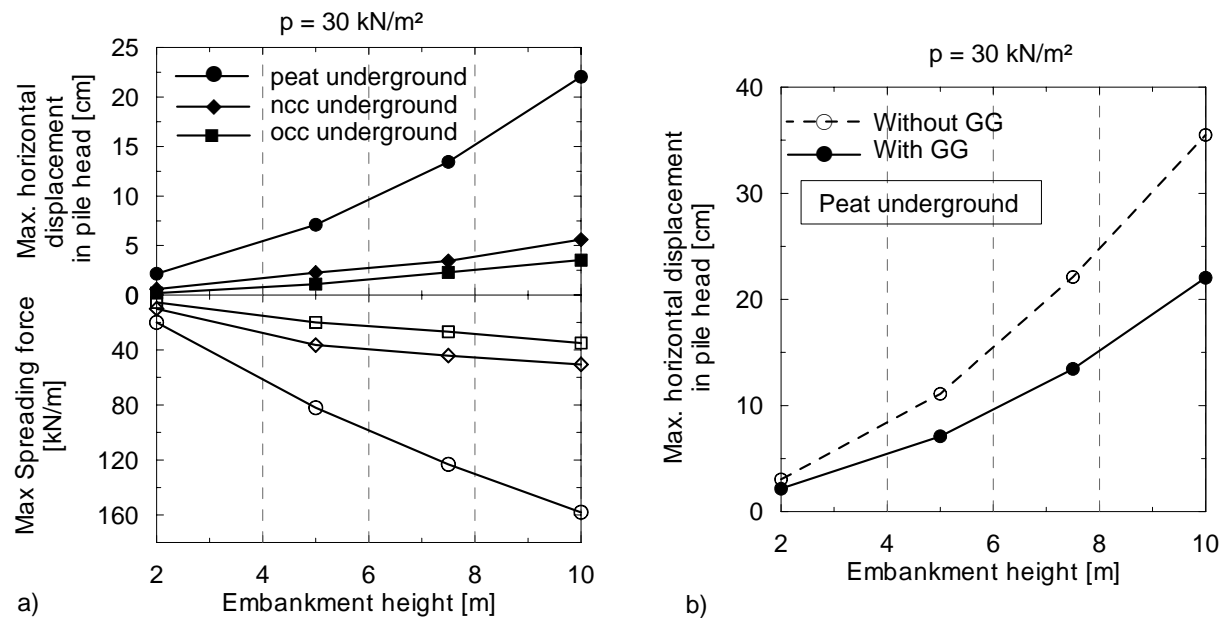


Figure 6.26: Maximum horizontal displacement in pile heads and spreading forces in reinforcement at $p = 30 \text{ kN/m}^2$ and slope 1:1.5; a) Spreading force and horizontal displacement, b) horizontal displacement with and without GG on peat underground

6.6 Summary of the modified analytical method

The existing analytical methods to calculate the spreading force in GG have resulted in over-estimated and uneconomical forces in the case of very high embankments. The same concept has also been observed in the case of stiffer underground soil and flatter embankment slopes.

On the basis of the model tests and the parameter study, an analytical method to calculate the spreading force in reinforcement has been derived and modified.

The method based on applying a sliding soil wedge in the slope zone depends on the distribution of the spreading force and the resulting horizontal deformations at the embankment base. The soil wedge depends on a vertical angle θ from the slope crest. The angle θ can be determined according to the resulting spreading forces in the FEM-parameter study.

A reference parameter-model has been investigated and applied to determine the angle θ . The reference parameters included an underground stiffness $E_s \leq 0.8 \text{ MN/m}^2$ for peat underground and a maximum slope of 1:1.5. The angle θ can be determined by comparing the FEM-results with the analytical horizontal earth pressure force at a fictitious wall in the soil wedge. The position and the height of the fictitious wall h_w depended mainly on the angle θ .

The modified analytical spreading force can be estimated as the horizontal active earth pressure force at h_w . Considering the effects of the underground stiffness and the embankment slope, two factors have been added to the equation of the spreading force, f_{Es} and f_β respectively. The determination of the factor f_{Es} and f_β can be developed from the FEM-results as functions of the embankment height, the underground stiffness and the embankment slope.

The determination of membrane force according to *EBGEO (2007)* has been modified by applying the external load at the arching height h_g in order to calculate the real arching effect of the soil on the reinforcement due to the external load.

The modified analytical method results in qualitative tensile forces compared with the FEM-results for both the spreading and the total forces in reinforcement.

A separate proof of safety must be carried out to the piles in the case of large and very large embankment height. The numerical methods can be adopted as the best method to analyse and estimate the stress-deformation behaviour of the pile elements.

7 Summary

In this study the lateral spreading problematic in the slope zone of basal reinforced embankments (geosynthetics reinforcement) resting on soft underground supported by pile-like elements has been investigated by means of experimental, numerical and analytical methods.

In the slope zone of embankment a horizontal earth pressure is applied along the slope zone and is maximum at the section from under the slope crest. The horizontal earth pressure develops spreading stresses which cause shear stresses at the embankment base. These shear stresses cause a horizontal displacement in the slope toe which in turn causes sliding of the toe. In the case of piled embankment the pile elements, which mostly are unreinforced piles, are then loaded with horizontal forces that apply tension stresses and bending moments in the pile cross-section. The geosynthetics reinforcement (geogrid) at the embankment base must sustain some of the horizontal stresses and reduce the transformed stresses to the slope toe or the pile elements. In the case of high and very high embankments the spreading forces due to horizontal earth pressure can be estimated as very large forces and uneconomically designed. The stress-strain behaviour of the system in such cases needs to be investigated thoroughly in order to analyse and calculate the spreading phenomena under higher embankment heights.

Moreover, in the case of piled embankment the arching effect of soil between piles produces membrane forces in geogrid in addition to the spreading force in the slope zone. The study has also investigated and analysed the stress-strain behaviour of the reinforcement and the mobilisation of membrane and spreading forces in reinforcement under static loads and under various embankment heights.

In order to investigate the system behaviour in the slope zone of an embankment under external static load due to spreading stresses a three-dimensional well-instrumented model tests at a scale of 1:3 has been carried out in Chapter 3. Firstly a model test of homogeneous sandy soil embankment and underground (MT1) has been built. The aim of this model test is to investigate and measure the horizontal earth pressure and shear stresses at the embankment base under different slope degrees and to assign the relation between the slope degree and shear stresses. Although the study focuses mainly on the investigation of spreading effect of an embankment on piled soft-underground, model tests MT2 and MT3, which present the unpiled embankment system, has been carried out. The goal of the model tests MT2 and MT3 serves for the FEM-calibration of the geogrid forces and the comparison with the forces in piled embankment systems. The model tests MT2 and MT3 represented unreinforced and basal reinforced embankment respectively. The soft underground has been simulated with foam material. The complete model test arranged as an embankment resting on soft underground sup-

ported by concrete pile elements has been constructed and loaded including two model tests without (MT4) and with (MT5) basal reinforcement. The objective was to compare and evaluate the effect of reinforcement to reduce the shear stresses at the embankment base and consequently the stresses at the pile elements. The horizontal force at the pile head has also been measured in the two model tests with and without reinforcement.

Based on the results of the model tests, the main parameters influencing the spreading stresses in the slope zone have been identified. A steeper embankment slope develops increasing shear stresses at the base and applies more horizontal displacement at the slope toe as explained in Section 3.7.1. The structural system in the case of soft underground was tended to extrude outward under increasing external loads. Supporting the underground with pile elements prevented the system from extrusion and transferred the stresses to horizontal forces on the pile head. Figure 3.33 in Section 3.7.5.5 illustrates that the geosynthetic reinforcement reduces the horizontal force in the pile head; this agrees with the assumption that the reinforcement can sustain the stresses due to the spreading effect and can reduce the deformations on the pile elements. The measured strain in reinforcement in the case of underground without pile elements was smaller than those with pile elements. This is attributed to the point-bearing system using pile elements which develops soil arching between piles and additional membrane forces in reinforcement. On the contrary, the measured horizontal displacements in the slope zone in the case of piled embankment were smaller than the displacements without piles. This is attributed to the pile elements which work as supporting members to sustain the horizontal forces due to spreading. In the case of basally reinforced embankment rested on soft underground supported by pile-like elements (MT5) the result is that the upper part of the embankment is separated from the lower one through the geogrid reinforcement forming a sliding soil wedge in the slope zone started from the slope crest. However, the upper part of the embankment was prevented from sliding by the effect of bond stress between the embankment fill material and the reinforcement, which transfer the additional stresses to the reinforcement.

Verification processes of the model tests have been carried out in Chapter 4 in order to calibrate the soil parameters obtained from laboratory tests and derive suitable parameters for the constitutive soil model that is used in the Finite Element computation (FEM). This helped also to determine the parameters which could not directly measured from the model tests and to extend the model test results to the prototype. Two- and three-dimensional finite element models have been established with the same boundary conditions for every experimental model test after fixation of the constitutive relations of the model materials. The first step in the verification process was the calibration of the constitutive relation of the embankment sand fill by verifying the results of the homogeneous-soil model test (MT1). The calibrated

sand parameters resulting from this step were used as input data for the sand material in the other processes. The results of the verification processes showed a perfectly good simulation of the deformations in the slope zone and the force in reinforcement in the case of underground without pile elements as explained in Section 4.6 and Figure 4.12. The verification of the model test results with FEM concluded that the structural system of a reinforced embankment on soft underground can be directly simulated and estimated using FEM. The computed stress-strain behaviour of the reinforcement in the FE-model can be considered to simulate the prototype. In contrary, the existing analytical methods to calculate the spreading force in reinforcement for unpiled embankment result in large deviations from the FEM and model test-results. Therefore, the FE methods can be adopted to develop and simulate the case of unpiled embankment. This type of embankment systems would not be considered in the parameter study.

In the case of point-bearing systems with pile elements the computed force in reinforcement was found smaller than the force resulting from model tests. Using the results from model tests and with supporting of other numerically modelled test results, a factor relates the numerical and experimental force in the reinforcement can be concluded and estimated as presented in Section 4.8. Generally, it was concluded that the extension of the model system with the help of FEM to the prototype is possible. The deformations and stresses are applicable in the numerical computation; however, the tensile forces in geogrid are found to be smaller in the 3D-FEM.

Furthermore, numerical and analytical parameter studies on the prototype have been performed under different parameter variations.

The behaviour of the system under different loading conditions has been investigated using FE-models under different parameter variations in Chapter 5. The variations included slope degree, underground stiffness, tensile stiffness of reinforcement, the layer numbers of reinforcement and the embankment height variation. The results of numerical parameter study showed a great effect of these parameters on the stress-deformation behaviour of the system.

The parameter study was performed on the case study of a prototype of basal reinforced sand embankment rested on underground supported by pile elements. Both the spreading effect and the arching effect of soil between piles controlled the behaviour of the system in such cases. The system has been investigated using 3D-FEM in order to simulate the pile elements and pile grid. Two simulation models were built for every calculation process, a membrane model to get the forces in reinforcement due to membrane effect only and a complete model including the slope zone to get the total force in reinforcement due to membrane and spreading ef-

fects. The numerical membrane model has been modified from the membrane model by *Zaeske (2001)* to include the membrane forces in reinforcement between piles placed in the slope zone.

Using stiffer underground materials, both the spreading and total tensile force in reinforcement was observed to be smaller than the forces with soft underground. This is attributed to the small shear deformations of the stiffer underground.

The results of the numerical study confirmed the concept that under steeper slope the shear stress at the slope base is greater, and consequently, the resulting spreading forces is greater.

By applying multi-layer geogrid reinforcement it was concluded that the spreading force could be mainly developed by the upper GG-layer, while the membrane force could be mainly developed by the lower GG-layer.

Also the system has been analytically investigated in order to evaluate the existed analytical methods applied to calculate the total force in reinforcement compared with the numerical results. The numerical results in this comparison were multiplied by the factor derived from model-verification process. The comparison shows that the present calculation method leads to uneconomical design forces. The analytical design methods by *Love et al. (2003)* and by *EBGEO (2007)* are based on the classical earth pressure theory and lead to uneconomical overestimated tensile forces, especially in the case of stiff and very stiff underground and in the case of very high embankment. The design method by *Geduhn/Vollmert (2005)* is based on a base friction along the slope base indicating a sliding body of the whole embankment slope. This method leads also to very small or underestimated tensile forces, especially in the case of stiff and very stiff underground and in the case of higher and very high embankments. This is attributed to the largely calculated base friction R_u which depends mainly on the length of the friction base in the slope zone. In the case of stiff and very stiff underground the base friction R_u was larger than the spreading force, this leads to the elimination of the resulting spreading force and underestimated tensile forces in reinforcement. It is concluded also that under a very high embankment, a sliding soil wedge can be applied to represent the spreading effect in the slope zone. The soil wedge can be determined according to the location of the maximum horizontal deformation in the pile heads or the base in the slope zone.

A modification of the analytical method to calculate the spreading force in reinforcement has been derived in Chapter 6. The analytical method is based on the concept that the spreading forces must be sustained by the reinforcement by the bond stresses between the embankment fill material and the reinforcement.

The modified spreading force can be estimated as the horizontal earth pressure force exerted on a fictitious wall of the sliding soil wedge in the slope zone. The position and the height of the fictitious wall h_w depended mainly on a vertical angle θ from the slope crest. The angle θ can be determined according to the resulting spreading forces in the FEM-parameter study.

The angle θ can be determined by comparing the FEM-results of a reference parameter-model with the analytical horizontal earth pressure force at the fictitious wall in the soil wedge (from Figure 6.6 to Figure 6.9). The reference parameters included an underground stiffness $E_s \leq 0.8 \text{ MN/m}^2$ for peat underground and a maximum slope of 1:1.5.

A dimensionless factor f_{E_s} has been developed to express the effect of the underground stiffness on the spreading forces. A dimensionless factor f_β has been developed to express the effect of the embankment slope on the spreading forces. Both factors can be developed and determined empirically from the FEM-results under different embankment heights as presented in Section 6.3.2. Both factors can be involved in the equation applied to determine the spreading force.

The determination of membrane force according to *EBGEO (2007)* has been modified in Section 6.5.1 by applying the external load at the arching height h_g in order to calculate the real arching effect of the soil on the reinforcement due to the external load.

A proof of the deformations in the vertical bearing elements (for example by the numerical methods), especially with large and very large embankment heights, is recommended.

A qualitative determination of the spreading and total force in reinforcement can be made using these modifications comparing with the FEM-results under different parameter conditions.

7 Zusammenfassung

In der vorliegenden Arbeit wurde die Spreizbeanspruchung von Geogittern im Böschungsbereich von Dämmen auf weichen Untergrund mit pfahlähnlichen Elementen mittels experimentellen, numerischen und analytischen Methoden untersucht.

Bei einer Dammkonstruktion treten im Böschungsbereich Spreizspannungen auf, die aus der Verkehrslast und dem Eigengewicht des Bodens resultieren. Diese Spannungen sind in Richtung der Böschungskante gerichtet und werden durch Schubspannungen in den Untergrund geleitet. Spreizspannungen können zu hohen Verformungen im Böschungsbereich führen. Bei Dämmen auf weichem Untergrund, werden diese Schubkräfte durch den Einbau von Geokunststoffen (i.d.R. Geogitter) abgetragen. Da der weiche Untergrund nur begrenzt Schubkräfte aufnehmen kann und die Gefahr des Dammfußgleitens in der Dammaufstandsfläche besteht, übernimmt das Geogitter die Funktion die Spreizkräfte aufzunehmen und rückwirkend im Damm zu verankern. Zur rechnerischen Berücksichtigung der Spreizkraft im Böschungsbereich bei Dämmen über pfahlähnlichen Elementen wird z.B. in *EBGEO (2007)* ein stark vereinfachter analytischer Ansatz vorgeschlagen. Die Spreizkraft wird auf der sicheren Seite mittels eines Erddruckansatzes vollständig der Geokunststoffbewehrung zugewiesen. Erfahrungsgemäß führt diese vereinfachte Annahme insbesondere bei großen Dammhöhen zu großen, stark auf der sicheren Seite liegenden und damit unwirtschaftlichen Zugkräften im Geokunststoff. Eine Optimierung dieses Ansatzes ist erforderlich.

Oberhalb der pfahlähnlichen Elemente stellt sich im Boden eine Gewölbewirkung ein, aus der eine zusätzliche Zugkraft infolge Membranwirkung resultiert. In der Literatur lassen sich unterschiedliche Arbeiten zur Mobilisierung der Membran- und Spreizkräfte im Geokunststoff unter Variation unterschiedlicher Randbedingungen finden.

Für die experimentelle Untersuchung der Spreizwirkung und das Systemverhalten im Böschungsbereich des Dammes unter statischer Verkehrslast wurden großmaßstäbliche Modellversuche (Maßstab 1:3) in Abschnitt 3 durchgeführt.

Im ersten Modellversuch wurde eine homogene Sandlage für den Damm und den Untergrund verwendet. Das Ziel dieses Versuches war die Ermittlung der horizontalen Erddruckkraft im Böschungsbereich und die Schubspannungen in der Böschungsbasis unter Variation der Böschungsneigung. Als Ergebnis konnte festgestellt werden, dass die Schubspannungen bei steileren Böschungen zunehmen.

Es wurden mehrere Modellversuche durchgeführt, bei denen die Auswirkungen einer Geogitterlage und dem Einstellen von pfahlähnlichen Elementen untersucht wurden. Der weiche Untergrund wurde als Schaumstoff simuliert.

Bei den Modellversuchen MT2 und MT3 wurde keine pfahlähnlichen Elemente berücksichtigt. Bei Versuch MT3 wurde zusätzlich eine Geogitterlage eingebaut, welches bei Versuch MT 2 nicht der Fall war.

Obwohl die Studie hauptsächlich auf die Untersuchung des Spreizeffektes eines Dammes auf weichem Untergrund mit pfahlähnlichen Elementen abzielt, wurden auch Modellversuche ohne pfahlähnliche Elemente (MT2 und MT3) durchgeführt. Das Ziel der Modellversuche MT2 und MT3 dient zur FEM-Kalibrierung der Geogitterkräfte und einem Vergleich der Geogitterkräfte bei Modellen ohne und mit pfahlähnlichen Elementen unter der Dammkonstruktion.

Bei den Modellversuchen MT4 und MT5 wurden pfahlähnliche Elemente zwischen der Schaumstoffschicht eingebaut. Bei Versuch MT4 wurde dabei wieder eine Geogitterlage berücksichtigt, die bei Versuch MT5 nicht vorhanden war.

Zur Überprüfung der Horizontalbeanspruchung wurden bei allen Versuchen Erddrucksensoren im Böschungsbereich angeordnet und Kraftmessungen am Pfahlkopf durchgeführt. Aufgrund von Dehnungsmessungen im Geogitter mit DMS konnte auf die Schubspannung geschlossen werden. Zusätzlich dienten die Modellversuche zur Kalibrierung eines numerischen Modells.

Auf Grundlage der Versuchsergebnisse konnten die wesentlichen Parameter, die die Spreizbeanspruchung beeinflussen, identifiziert werden. Das Ausquetschen des weichen Untergrundes ist durch die Aufbringung des Dammkörpers und der äußeren Auflasten simuliert. Durch die Verwendung von pfahlähnlichen Elementen im Untergrund konnte ein Ausquetschen des Untergrundes verhindert werden. Dadurch konnten die horizontalen Kräfte durch den Pfahlkopf aufgenommen werden. Bild 3.33 zeigt die horizontalen Kräfte im Pfahlkopf, die bei der GG-Bewehrung reduziert wurden.

Bei einem Punktlagerungsmodellversuch wurden die gemessenen Dehnungen im Geogitter größer als die bei einem Weichuntergrundmodellversuch. Es wurde festgestellt, dass durch Verwendung von pfahlähnlichen Elementen sich ein Bodengewölbe über den Pfahlköpfen bildet. In Abhängigkeit der Tragwirkung dieses Bodengewölbes wurde das GG durch eine Membrankraft belastet.

Die gemessenen horizontalen Verschiebungen im Böschungsbereich bei einem Punktlagerungsmodellversuch wurden dagegen kleiner als bei dem Weichuntergrundmodellversuch. Die Pfahlelemente wirkten als tragfähige Glieder und konnten die horizontalen Spreizkräfte aufnehmen.

Die Geogitterlage im Modellversuch MT5 trennte den Dammbereich in eine obere und untere Hälfte. Ein Bodengleitkörper rutscht dabei im Böschungsbereich oberhalb der Geogitterlage in Richtung des Böschungsfußes ab. Durch den Reibungsverbund zwischen Geogitter und Dammboden können Zugkräfte im Geogitter abgeleitet werden. Die Pfahlkopfbeanspruchung verringert sich durch Einlegen von Geokunststoffen, d.h. das Geogitter nimmt Spreizkräfte auf und leitet diese zur Dammmitte weiter.

In Abschnitt 4 wurden Verifikationsvorgänge für die Versuchsergebnisse durchgeführt. Das Ziel der Verifikationsvorgänge ist wie folgt:

- Kalibrierung der durch die Laborversuche ausgewerteten Bodenkenngrößen.
- Ermittlung der Bodenkenngrößen für die Stoffgesetze des numerischen Modells.
- Ableitung der Bodenkenngrößen, die nicht unmittelbar in den Modellversuchen gemessen wurde.
- Übertragung der Modellversuche auf einen Prototypen.

Es wurden zwei und dreidimensionale numerische Modelle für jeden Modellversuch erstellt und mit den selben Randbedingungen nachgerechnet. Zu Beginn von Abschnitt 4 wurden die Bodenkenngrößen, die für Dammschüttmaterial relevant sind, mittels der FE-Berechnungen des Modellversuchs MT1 und auf der Basis des Hardening Soil Models (HSM) kalibriert. Die kalibrierten Bodenkenngrößen wurden als Input-Daten des Dammschüttmaterials (Sand) in die nächsten Verifikationsvorgänge eingegeben. Als Ergebnis wurde festgestellt, dass die erstellten FE-Modelle die Verformungen des Bodens im Böschungsbereich und die Zugkraft im GG bei Dämmen auf weichem Untergrund realitätsnah abbilden. (Abschnitt 4.6 und Bild 4.12). Die FE-Modelle beschreiben das Systemverhalten der Dammkonstruktion wirklichkeitsgetreu. Die vorhandenen analytischen Ansätze dagegen, die für die Bestimmung der Spreizbeanspruchung im GG angewendet wurden, zeigen beträchtliche Abweichungen von den Modellversuchen und FE-Ergebnissen.

Bei Dämmen auf pfahlähnlichen Elemente (MT4 und MT5), wurden bei der Ermittlung der Zugkräfte im GG nach der FE-Methode einige Abweichungen im Vergleich zu den Modell-

versuchen festgestellt. In Abschnitt 4.8 konnte gezeigt werden, dass die nach der FE-Methode errechnete Zugkraft im GG mit dem Faktor 3,5 multipliziert werden muss, um realitätsnahe Ergebnisse zu erzielen, bezogen auf das verwendete FE-Programm PLAXIS-3D Tunnel

Im allgemeinen ist festzuhalten, dass eine Nachrechnung der Modellversuche mit Hilfe der FE-Methode möglich ist. Die Verformungen und Spannungen im Dammkörper werden nach der FE-Methode zutreffend abgebildet. Die Zugkräfte im GG fallen allerdings geringer aus.

Zusätzlich wurden numerische und analytische Parameterstudien auf den Prototypen angewendet.

Das Systemverhalten unter Berücksichtigung verschiedener Randbedingungen wurde in Abschnitt 5 mittels FE-Modelle untersucht und analysiert. Dabei wurden folgende Parameter variiert: Böschungsneigung, Untergrundsteifigkeit, Dehnsteifigkeit der GG-Bewehrung, Anzahl der GG-Lagen und Dammhöhe. Mit Hilfe der numerischen Parameterstudie konnten merkliche Auswirkungen auf das Spannungs-Verformungsverhalten des Systems festgestellt werden.

Das Tragsystem „geokunststoffbewehrte Erdschichten über Pfahlelementen“ (GEP) wurde in der Parameterstudie untersucht und analysiert. Zur Untersuchung dieses Modells wurden die beiden folgenden FE-Modelle erstellt:

- Mittelbereich, bei dem mit Hilfe einer Gewölbewirkung im Boden die Membrankräfte im GG zwischen den Pfahlelementen berechnet wurde. Das von *Zaeske (2001)* modifizierte Membranmodell wurde in Abschnitt 5.5.2 vorgestellt, um die Gewölbewirkung zwischen den Pfahlelementen im Böschungsbereich untersuchen und berechnen zu können.
- Böschungs- und Mittelbereich, bei dem die gesamte Zugkraft des GG infolge Spreizwirkung in der Böschung und Gewölbewirkung berechnet werden kann.

Die Ergebnisse der Variation der Dammhöhe zeigen sehr hohe Biegezugspannungen in den Pfahlelementen bei sehr hohen Dämmen ($h_l = 10$ m). Die Spreiz- und die Gesamtkräfte im GG nehmen unmittelbar mit der Erhöhung der Dammhöhe zu. Ein Erdkeil oberhalb der GG-Lage in Richtung des Böschungsfußes (siehe Bild 5.8) konnte entwickelt werden, um die Gleitkörper im Böschungsbereich infolge Spreizbeanspruchung darstellen zu können.

Durch den Vergleich mit den Ergebnissen der unterschiedlichen Untergrundsteifigkeiten konnte festgestellt werden, dass bei der Anwendung von höheren Steifigkeiten, die Spreiz-

kräfte im GG geringer sind. Dieses wird auf die kleineren Verformungen des Untergrundes aufgrund der höheren Steifigkeit zurückgeführt.

Die Ergebnisse der Variation der Böschungsneigung zeigen abnehmende Spreizkräfte im GG bei Abflacherung der Böschungsneigung von 1:1,5 zu 1:2,5. Die Spreizkraft im Böschungsbereich bezieht sich hauptsächlich auf die horizontale Erddruckkraft E_{ah} und den Erddruckbeiwert K_{ah} . Mit steigender Böschungsneigung fällt der Erddruckbeiwert größer aus.

Die Untersuchung zum Systemverhalten durch mehrere Geogitterlagen zeigen, dass durch Einlegen von mehreren Geogitterlagen das Systemverhalten verbessert werden kann und Pfahlkopfverformungen reduziert werden können. Es wurde zusätzlich festgestellt, dass die Spreizkraft durch die obere GG-Lage hauptsächlich aufgenommen wird, während dagegen die Membrankraft hauptsächlich durch die untere GG-Lage aufgenommen wird.

Zusätzlich wurden die Zugkräfte in GG mittels der analytischen Ansätze nachgerechnet und mit numerischen Ergebnissen verglichen. Die numerischen Ergebnisse der Zugkräfte wurden mit dem Faktor 3,5, der in Abschnitt 4 hergeleitet wurde, multipliziert. Auf Grundlage der klassischen Erddrucktheorie wird bei *Love et al. (2003)* und *EBGEO (2007)* die Spreizkraftbeanspruchung $F_{G,S}$ ermittelt. Während *EBGEO (2007)* und *BS 8006 (1995)* eine Addition beider Membran- und Spreizanteile empfiehlt, ist nach *Love et al. (2003)* (bzw. siehe auch *Maihold et al. (2003)* und *Klobe, 2007*) nur der Maximalwert von beiden Anteilen anzusetzen. Hauptsächlich führen die Ergebnisse der beiden Verfahren insbesondere bei steiferem und sehr steifem Untergrund und bei großen Dammhöhen zu stark auf der sicheren Seite liegenden Zugkräften im GG. Nach *Geduhn/Vollmert (2005)* kann die Spreizkraftbeanspruchung durch den Ansatz einer mitwirkenden Sohlreibungskraft R_u zwischen GG und Untergrund abgemindert und zu der Membrankraft subtrahiert werden. Bei steiferem Untergrund fällt die Sohlreibungskraft R_u größer als die horizontale Erddruckkraft aus. Die resultierende Spreizkraft $F_{G,S}$ wird dadurch sehr gering. Die vorhandenen analytischen Berechnungsansätze zur Berücksichtigung der Spreizkraftbeanspruchung berücksichtigen nicht die Böschungsneigung und die Untergrundsteifigkeit.

Eine Modifikation der analytischen Verfahren zur Ermittlung der Spreizkraftbeanspruchung $F_{G,S}$ wurde in Abschnitt 6 abgeleitet. Das analytische Verfahren basiert auf dem Konzept, dass die Spreizkraft $F_{G,S}$ im GG durch die Verbundspannungen zwischen Dammmaterial und Geokunststoffbewehrung abgeleitet werden muss.

Die modifizierten Spreizkräfte können aus dem horizontalen Erddruck geschätzt werden, der an einem senkrechten fiktiven Schnitt im Böschungsbereich ermittelt wird. Die Position und

die Höhe der fiktiven Wand h_w hängen hauptsächlich vom Winkel θ vom Böschungskopf ab. Der Winkel θ kann entsprechend aus den resultierenden Spreizkräften der FEM Parameterstudie ermittelt werden.

Der Winkel θ wurde ermittelt werden, indem man die FEM-Ergebnisse eines Referenzparametermodells mit der analytischen horizontalen Erddruckkraft an der fiktiven Wand im Bodenkeil vergleicht (Bild 6.6 bis 6.9). Das Referenzparametermodell wurde bei einer Untergrundsteifigkeit des Torfes $E_s \leq 0.8 \text{ MN/m}^2$ und einer maximalen Böschungsneigung von 1:1,5 ermittelt.

Ein dimensionsloser Faktor f_{E_s} wurde abgeleitet, um den Effekt der Untergrundsteifigkeit E_s auf die Spreizkräfte zu berücksichtigen. Ein dimensionsloser Faktor f_β wurde entwickelt, um den Effekt des Böschungsneigungswinkels β auf die Spreizkräfte zu berücksichtigen. Beide Faktoren können aus den FEM-Ergebnissen der $F_{G,S}$ bei unterschiedlichen Dammhöhen empirisch ermittelt werden, wie in Abschnitt 6.3.2 dargestellt worden ist. Die Gleichung zur Ermittlung der modifizierten Spreizkraft (Gleichung 6.6) enthält die beiden entwickelten Faktoren f_{E_s} und f_β .

Die Berechnung der Membrankraft im GG entsprechend *EBGEO (2007)* ist in Abschnitt 6.5.1 modifiziert worden, indem die auf das System wirkende äußere Auflast in Abhängigkeit der Dammhöhe reduziert worden ist und direkt auf die Gewölbehöhe h_g wirkt.

Der Nachweis der Formänderungen der vertikalen Tragglieder wird insbesondere bei großen Dammhöhen empfohlen. Eine qualitative Ermittlung der Spreiz- und Gesamtkraft in der Geokunststoffbewehrung unter verschiedenen Randbedingungen kann mittels dieses modifizierten Verfahrens dargestellt werden.

8 References

- Alexiew, D. (2004):* Geogitterbewehrte Dämme auf pfahlähnlichen Elementen: Grundlagen und Projekte; Bautechnik (81), Heft 4, S. 710-716.
- Aubeny, C.P. / Li, Y. / Briaud, J.L. (2002):* Geosynthetics reinforced pile supported embankments: numerical simulation and design needs; Geosynthetics- 7th ICG- Delmas, Gourc & Girard (eds), pp. 365-368.
- Babuska, I. / Oden, T. (2003):* V&V in computational engineering and science, Part I: Basic Concepts; Ins. For computational engineering and sciences (ICES), University of Texas at Austin, Report, pp. 03-52.
- Blume, K.-H. (1995):* Großversuch zum Tragverhalten textiler Dammaufstandsfläche; Sonder-Ausdruck aus Straße + Autobahn 6/95; Bericht XVIII; Kirchbaum Verlag, Bonn
- Brauns, J. (1980):* Spreizsicherheit von Böschungen auf geneigtem Gelände; Bauingenieur (55), S. 433-436.
- Brendlin, H. (1962):* Die Schubspannungsverteilung in der Sohlfuge von Dämmen und Böschungen; Dissertation, Fakultät für Bauwesen, TH-Karlsruhe.
- BS 8006 (1995):* British Standard, code of practice of strengthened/ reinforced soils and other fills, chapter 9.
- Bull, J.W. (1994):* Soil-Structure interaction: numerical analysis and modelling; E& FN Spon.
- Bussert, F. / Meyer, N. / De Lange, A.P. / Van der Stoel, A.E.C. (2004):* Bemessung und Überwachung einer geokunststoffbewehrten Tragschicht auf HSP-Pfählen; Bautechnik (81), Heft 12, S. 959-967.
- Carlson, B. (1987):* Reinforced soil; principles for calculation; Terratema AB; Liköping (in Swedish).
- Chenggang, B. (2005):* Study on the interaction behaviour of Geosynthetics and soil in China; Ningbo Institut of Technology, Zhejiang University, China, pp. 104-115.
- Collin, J.G. / Watson, C.H. / Han, G. (2005):* Column-Supported Embankments solves time constraint for new road construction; Proceedings of the Geo-Frontiers Congress, Austin, Texas, pp. 1-9.
- Duncan, J.M. / Chang, C.Y. (1970):* Nonlinear analysis of stress and strain in soils; Proc. ASCE, Vol. 96, pp. 1629-1653.
- EBGEO (2007):* Empfehlung für den Entwurf und die Berechnung von Erdkörpern mit Bewehrung aus Geokunststoffen; Ausgabe 2007, (unveröffentlicht).
- Eigenbrod, K.D. / Locker, J.G. (1987):* Determination of friction values for the design of side slopes lined or protected with geosynthetics; Canadian Geotechnical Journal, Vol. 24, No. 6, pp. 509-519.
- Eigenbrod, K.D. / Burak, J.P. / Locker, J.G. (1990):* Differential shear movements at soil-geotextile interfaces; Canadian Geotechnical Journal, Vol. 27, pp. 520-526.

- Espinoza, R.D. / Bray, J.D. (1995):* An integrated approach to evaluating single layer reinforced soils; *Geotechnics International*, Vol. 2, No. 4, pp. 723-739.
- Fannin, R.J. / Eliadorani, A. / Wilkinson, J.M.T. (2005):* Shear strength of cohesionless soils at low stress; *Géotechnique* (55), No. 6, pp. 467-478.
- GDA-Empfehlung (1997):* Geotechnik der Deponien und Altlasten; E 2-21 Spreizsicherheitsnachweise und Verformungsabschätzung für die Deponiebasis, 3. Auflage, Ernst & Sohn, S. 194-199.
- Gebreselassie, B. (2003):* Experimental, analytical and numerical investigations of excavation in normally consolidated soft soils, *Schriftenreihe Geotechnik, Universität Kassel*, Heft 14.
- Geduhn, M. (2005):* Zur Boden-Bauwerks-Interaktion von pfahlartigen Traggliedern in weichem Untergrund; 4. Geokunststoff-Kolloquium, Garmisch-Partenkirchen, S.1-12.
- Geduhn, M. / Vollmert, L. (2005):* Verformungsabhängige Spannungszustände bei horizontalen Geokunststoffbewehrungen über Pfahlelementen in der Dammbasis; *Bautechnik* (82), Heft 9, S. 657-662.
- Goh, A.T.C. / The, C.I. / Wong, K.S. (1997):* Analysis of piles subjected to embankment induced lateral soil movements; *Journal of Geotechnical and Geoenvironmental Engineering*, Vol. 123, No. 9, pp. 792-801.
- Görtler, H. (1975):* Dimensionsanalyse. Berlin Heidelberg New York, Springer
- Guido, V. / Kneupel and Sweeny, M.A. (1987):* Plate loading tests on geogrid-reinforced earth slabs; *Proc. Geosynthetics Conf., New Orleans*, pp. 216-225.
- Han, J. / Gabr, M.A. (2002):* Numerical analysis of geosynthetic-reinforced and pile-supported earth platforms over soft soil; *Journal of Geotechnical and Geoenvironmental Engineering*, pp. 44-53.
- Heitz, C. (2006):* Bodengewölbe unter ruhender und nichtruhender Belastung bei Berücksichtigung von Bewehrungseinlagen aus Geogittern, *Schriftenreihe Geotechnik, Universität Kassel*, Heft 19.
- Heitz, C. / Kempfert, H.-G. / Gebereselassie, B. (2006):* Modellversuche „Geokunststoffbewehrte Erdschichten über Pfählen“ zur Untersuchung des Einflusses der Produktstruktur -Großmaßstäbliche Modellversuche-; *Versuchsbericht-Teil I-; Forschungsbericht der Universität Kassel*, unveröffentlicht
- Hewlett, W.J. / Randolph, M.F. / Aust, M.I.E. (1988):* Analysis of piled embankments; *Ground Engineering*, Vol. 21, pp. 12-17.
- Houlsby, G.T. / Milligan, G.W.E. / Jewell, R.A. / Burd, H.J. (1989):* A new approach to the design of unpaved roads-Part I; *Ground Engineering*, Vol. 22, No. 3, pp. 25-29.
- Jaup, A. (1999):* Anwendung von 1g Modellversuchen auf das Setzungsverhalten im Hinterfüllbereich von Brückenwiderlagern; *Schriftenreihe Geotechnik, Universität Kassel*, Heft 7.

- Jenk, O. / Dias, D. / Kastner, R. (2005):* Soft soil improvement by vertical rigid piles; 2nd International Workshop of young doctors in Geomechanics, ENPC, Champs-sur-Mame, (Presentation).
- Jessberger, H.L./Güttler, U. (1988):* Geotechnische Großzentrifuge Bochum – Modellversuche im erhöhten Schwerfeld. Geotechnik, Heft 2, S. 85-97
- Kempfert, H.-G. (1987):* Zum Trag- und Verformungsverhalten von im Baugrund eingespannten nahezu starren Gründungsköpfen bei ebener oder geneigter Geländeoberfläche, Schriftenreihe FG Baugrund-Grundbau, Universität Dortmund, Heft 1
- Kempfert, H.-G. (1995):* Untergrundverformungen und dynamische Beanspruchungen bei ausgeführten festen Fahrbahnen im Eisenbahnbau; Proc. Donaueuropäische Konferenz für Grundbau und Bodenmechanik, Rumänien, Vol. 1, S. 133-140.
- Kempfert, H.-G. / Stadel, M. (1995):* Zum Tragverhalten geokunststoffbewehrter Erdbauwerke über pfahlähnlichen Traggliedern; Geotechnik Sonderheft zur 4. Informations- und Vortragsveranstaltung über Kunststoffe in der Geotechnik. München, DGGT-Essen, S. 146-152.
- Kempfert, H.-G. / Stadel, M. / Zaeske, D. (1997):* Berechnung von geokunststoffbewehrten Tragschichten über Pfahlelementen; Bautechnik (75); Heft 12, S. 818-825.
- Kempfert, H.-G. / Zaeske, D. / Alexiew, D. (1999):* Interactions in reinforced bearing layers over partial supported underground; Proceedings of the 12th European Conference on Soil Mechanics and Geotechnical Engineering, Amsterdam, Vol. 31 Balkema, pp. 1527-1532.
- Klobe, B. (2007):* Die erdstatische Berechnung geotechnischer Flächentragwerke; Bautechnik (84); Heft 2, S. 94-102.
- Lopes, P.C. / Lopes, M.L. / Lopes, M.P. (2001):* Shear behaviour of geosynthetics in the inclined plane test-Influence of soil particle size and geosynthetics structure; Geosynthetics International, Vol. 8, No. 4, pp. 327-342.
- Love, J. / Milligan, G. (2003):* Design methods for basally reinforced pile-supported embankments over soft ground; Ground Engineering, pp. 39-43.
- Maihold, K. / Trunk, K. (2003):* Notizen zum Entwurf der EBGEO (6. Fassung; Abschnitt 6.9); Keller Grundbau GmbH, Germendorf, (unveröffentlicht).
- Meyer, N. / Schwerdt, S. / Nerheim, A. (2003):* Die Sicherung von Verkehrswegen in altbergbau- und suberosionsgefährdeten Gebieten durch den Einsatz von Geokunststoffen; Untersuchungen zum Trag- und Reibungsverhalten; Altbergbau- Kolloquium, Freiberg.
- Müller, M. (2004):* Die Erfassung des räumlichen Tragverhaltens von Geokunststoffbewehrungen bei der Gründung von Dämmen auf Vertikalen Tragelementen mithilfe numerischer Berechnungen; Diplomarbeit an der FH-Anhalt, (unveröffentlicht).
- Ochiai, H. / Watari, Y. / Tsukamoto, Y. (1996):* Soil reinforcement practice for fills over soft ground in Japan; Geosynthetics International, Vol. 3, No. 1, pp. 31-48.

- Ohde, J. (1953):* Druckverteilung in und unter Erddämmen; Wasserwirtschaft-Wassertechnik, 3. Jahrgang, Heft 7, S. 248- 252.
- Pregel, O. (1998):* Handbuch der Geotechnik, Band 1, Eigenverlag des Institutes für Geotechnik der Universität für Bodenkultur, Wien.
- Rainer, E. / Fellin, W. (2006):* Druckabhängigkeit des Reibungswinkels zwischen Festkörper und Sand, Geotechnik (29), Heft 1, S. 28-32.
- Raithel, M. (1999):* Zum Trag- und Verformungsverhalten von geokunststoffummantelten Sandsäulen; Schriftenreihe Geotechnik, Universität Kassel, Heft 6.
- Rendulic, L. (1938):* Der Erddruck im Straßenbau und Brückenbau; Forschungsarbeiten aus dem Straßenbau, Bd. 10, Berlin.
- Rogbeck, Y. / Gustavsson, S. / Södergren, I. / Lindquist, D. (1998):* Reinforced pile embankments in Sweden; Design aspects; Proceedings of the 6th International Conference on Geosynthetics, pp. 755-762.
- Rowe, R.K. / Li, A.L. (2002):* Behaviour of reinforced embankments on soft rate-sensitive soil; Géotechnique (52), No. 1 pp. 29-40.
- Rowe, R.K. / Li, A.L. (2005):* Geosynthetic-reinforced embankments over soft foundations; Geosynthetics International, Vol. 12, No. 1, pp. 50-85.
- Rüegger, R. (2002):* Anforderungen an Geokunststoffe mit Bewehrungsfunktion; Fachachtung des SVG zum Thema "Bauen mit Geokunststoffen", EMPA- Dübendorf.
- Russell, D. / Pierpoint, N. / MacDonald, M. (1997):* An assessment of design methods for piled embankments; Ground Engineering, Nov. 1997, pp. 39-44.
- Schwarz, E. (1963):* Die Ermittlung der Spreizspannungen unter Dämmen mit geneigter Unterlage (Eine Erweiterung des Rendulic'schen Verfahrens); Die Bautechnik (6), S. 206-207.
- Schwer, L. (2001):* Constitutive model verification and validation; Draft 14, pp. 1-11.
- Smart Solutions (1999):* Geotex structural soil reinforcement for embankments over soft soil- Design guidelines; Synthetic industries, Tennessee.
- Svano, G. / Ilstad, T. / Eiksund, G. / Want, A. (2000):* Alternative calculation principle for design of piled embankments with base reinforcement; Proc. International Conference on Ground Improvement Geosystems, Helsinki, Building Information Ltd, pp. 541-548.
- Taylor, D.W. (1948):* Fundamentals of soil mechanics; John Wiley & Sons, N. Y.
- Teferra, A. / Schultze, E. (2003):* Formulae, charts and tables in the area of soil mechanics and foundation engineering; Rotterdam, Balkema.
- Terram Designing (2000):* Designing for soil reinforcement (Steep slopes); Terram Ltd., Mamhilad, United Kingdom.

- Tölke, F. (1990):* Spannungs- und Verschiebungstheorie im Halbraum nach der Linearen Elastizitätstheorie; Grundbautaschenbuch Teil 1, 4. Auflage, Ernst & Sohn, Berlin, S. 205-239.
- Van Impe, W. / Silence, P. (1989):* Improving of the bearing capacity of weak hydraulic fills by means of geotextiles; Faculiteit der Toegepaste Wetenschappen Laboratorium voor Grondmechanica, Gent state university, Belgium.
- Walz, B. (1982):* Bodenmechanische Modelltechnik als Mittel zur Bemessung von Grundbauwerken. Forschungs- und Arbeitsberichte im Bereich Grundbau, Bodenmechanik, Unterirdisches Bauen, Univ. GH Wuppertal, Bericht Nr. 1, S. 45-90
- Wang, M.C. / Feng, Y.X. / Jao, M. (1996):* Stability of geosynthetic-reinforced soil above a cavity; Geotextiles and Geomembranes 14, pp. 95-109.
- Witzel, M. (2004):* Zur Tragfähigkeit und Gebraustauglichkeit von vorgefertigten Verdrängungspfählen in bindigen und nichtbindigen Böden; Schriftenreihe Geotechnik, Universität Kassel, Heft 15.
- Zaeske, D. / Kempfert, H.-G. (2002):* Berechnung und Wirkungsweise von unbewehrten und bewehrten mineralischen Tragschichten über punkt- und linienförmigen Traggliedern; Bauingenieur (77), S. 80-86.
- Zaeske, D. (2001):* Zur Wirkungsweise von unbewehrten und bewehrten mineralischen Tragschichten über pfahlartigen Gründungselementen; Schriftenreihe Geotechnik, Universität Kassel, Heft 10.

Appendices

- A Earth pressure forces**
- B Model test results**
- C Verification of the model test-results**
- D Parameter study**
- E List of frequently used symbols and expressions**

A Earth pressure forces

A.1 Determination of earth pressure forces

The spreading stresses generated at the base of the embankment in the slope zone are related to the horizontal earth pressure arising from the own-weight of the soil and the traffic load. The different approaches use the earth pressure in its active limit state. For *Rankine* case, the active earth pressure force acts parallel to the slope. The horizontal active earth pressure force at an embankment base with height h , due to own weight of a cohesionless soil is given by:

$$E_{agh} = \frac{1}{2} \cdot h \cdot e_{agh} = \frac{1}{2} \cdot \gamma \cdot h^2 \cdot K_{agh} \quad (\text{A.1})$$

and its vertical component of the active earth pressure is:

$$E_{agv} = E_{agh} \cdot \tan(\alpha + \delta) \quad (\text{A.2a})$$

α inclination angle of the wall ($\alpha = 0$ in the case of an embankment);

δ friction angle of the wall = β , the slope angle;

γ unit weight of the soil

K_{agh} the active earth pressure coefficient, which has a general form:

$$K_{agh} = \left[\frac{\cos(\varphi - \alpha)}{\cos \alpha \cdot \left(1 + \sqrt{\frac{\sin(\varphi + \delta_a) \cdot \sin(\varphi - \beta)}{\cos(\alpha + \delta_a) \cdot \cos(\alpha - \beta)}} \right)} \right]^2 \quad (\text{A.2b})$$

where for *Rankine* case $\delta_a = \beta$

The active earth pressure force due to traffic load p is related to that due to own weight:

$$E_{aph} = h \cdot e_{aph} = h \cdot p \cdot K_{aph} \quad \text{and} \quad K_{aph} = \frac{\cos \alpha \cdot \cos \beta}{\cos(\alpha - \beta)} \cdot K_{agh} \quad (\text{A.3})$$

p the traffic load per meter run;

K_{aph} the active earth pressure coefficient due to traffic.

In case of cohesive material the active earth pressure force due to cohesion c' is given by:

$$E_{ach} = -h \cdot e_{ach} = -h \cdot c' \cdot K_{ach} \quad (\text{A.4a})$$

and the earth pressure coefficient due to cohesion K_{ach} is:

$$K_{ach} = \frac{2 \cdot \cos(\alpha - \beta) \cdot \cos \varphi \cdot \cos(\alpha + \delta_a)}{[1 + \sin(\varphi + \alpha + \delta_a - \beta)] \cdot \cos \alpha} \quad (\text{A.4b})$$

In the case of embankment where $\alpha = 0$, $K_{aph} = K_{agh}$, the active earth pressure can be estimated for both own weight and external load in one equation. Hence, Equation 2.2b can be reduced to:

$$K_{ah} = \frac{1 - \sin \varphi'}{1 + \sin \varphi'} = \tan^2 \left(45^\circ - \frac{\varphi'}{2} \right) \quad (\text{A.5})$$

Equation 2.5 is used when $\delta = \beta = 0$. Also, in such case, $K_{ach} = 2 \cdot \sqrt{K_{agh}}$

A.2 Graphical determination of earth pressure after Engesser (1880)

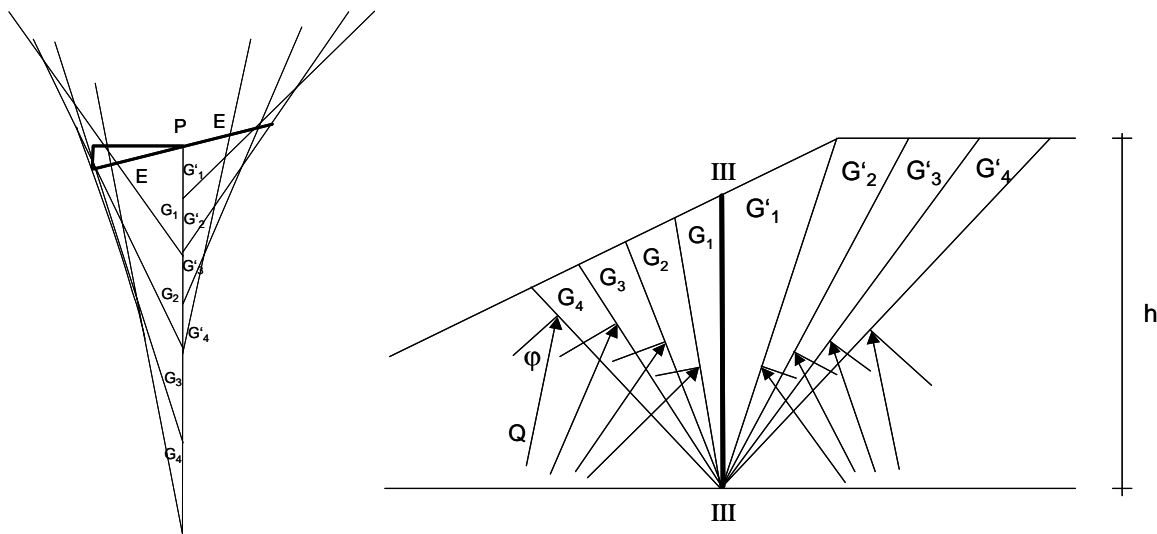


Figure A.2: Engesser's graphical method

Engesser's method is a graphical method to determine the earth pressure force in the slope zone of an embankment. The method depends on the force equilibrium at each vertical section. The earth pressure vector can be analysed to the vertical and horizontal component.

B Model test results

B.1 Material properties of the embankment sand under different compactness D

The relation between the internal friction angle φ' and the stress level under variations of the compactness of the model sand D has been estimated from the triaxial-test results which were carried out by *Witzel (2004)* with a compactness $D = 0.71$ and *Heitz (2006)* with a compactness $D = 0.89$. Figure B.1 shows the normal and logarithmic representation of the dependency of the internal friction angle φ' on the stress level under variation of the compactness.

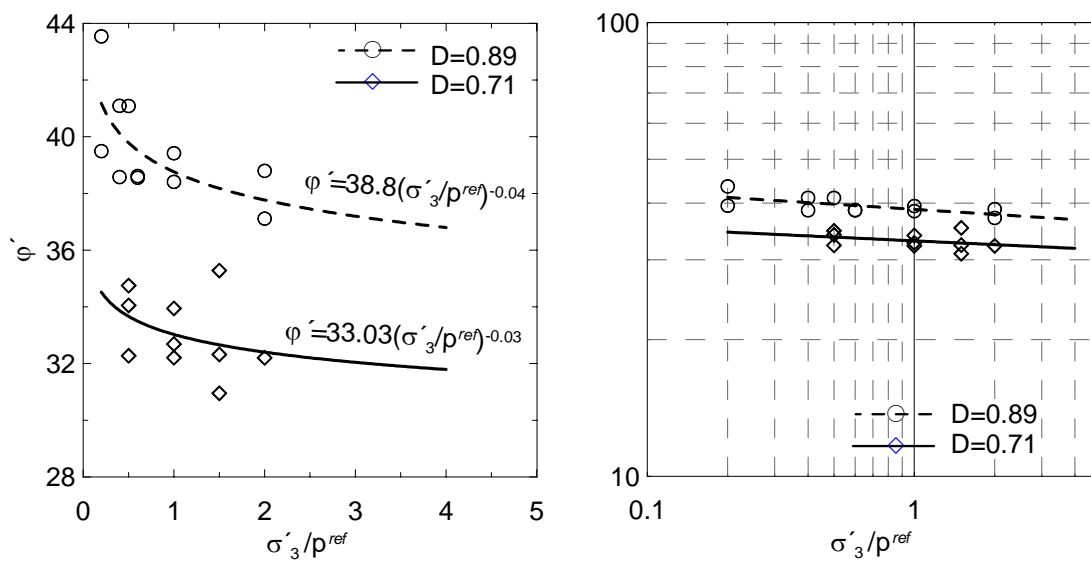


Figure B.1: Relation between internal friction angle φ' of the model sand and stress level under variation of compactness D

Also the influence of the compactness D on the internal friction angle φ' could be investigated for different stress levels. (Figure B.2).

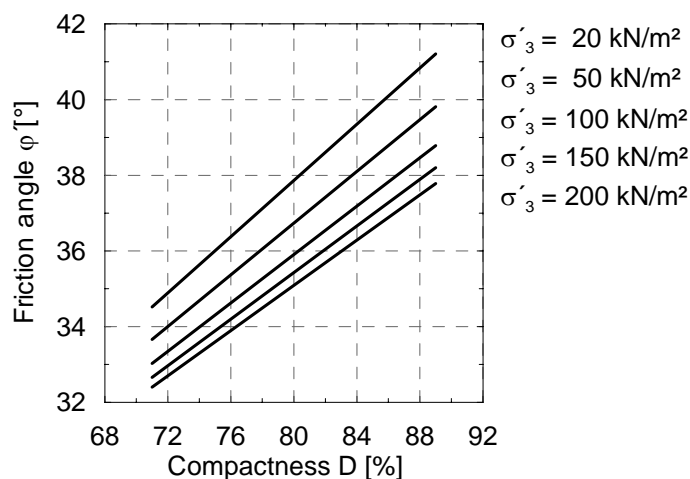


Figure B.2: Influence of compactness D on the internal friction angle φ' of model-sand

The stress-strain behaviour of the sand material has also been determined from the triaxial test results to get the secant modulus of elasticity E_{50} in order to estimate the stiffness modulus of the model sand under different stress levels. Figure B.3 shows the dependency of the secant modulus E_{50} on the stress level under variation of D .

Also the influence of the compactness D on the secant modulus E_{50} could be investigated for different stress levels. (Figure B.4).

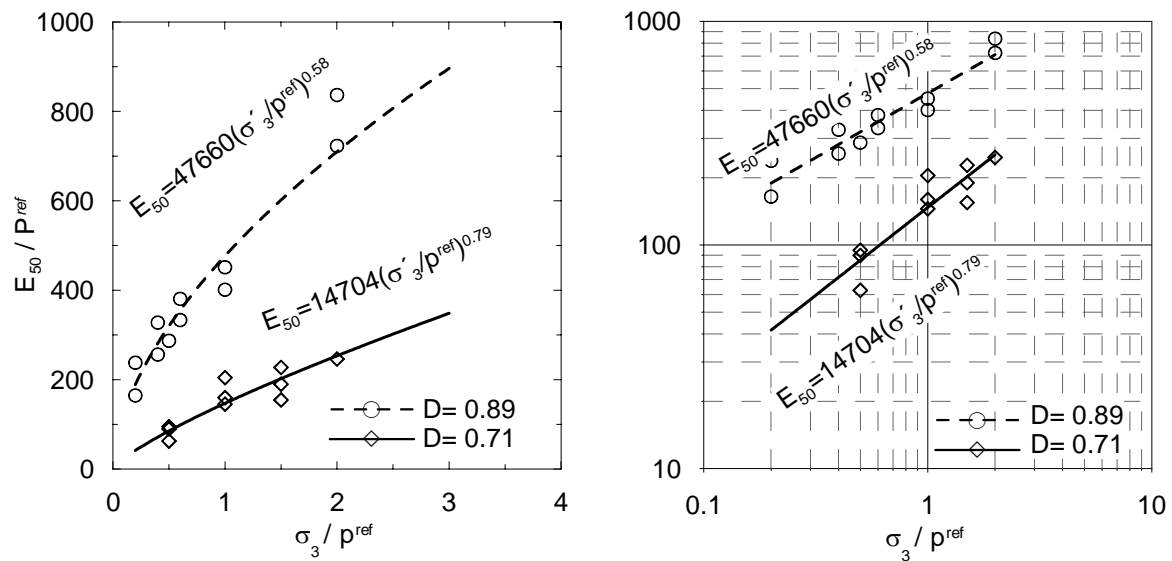


Figure B.3: Relation between secant modulus E_{50} of the model sand and stress level under variation of D

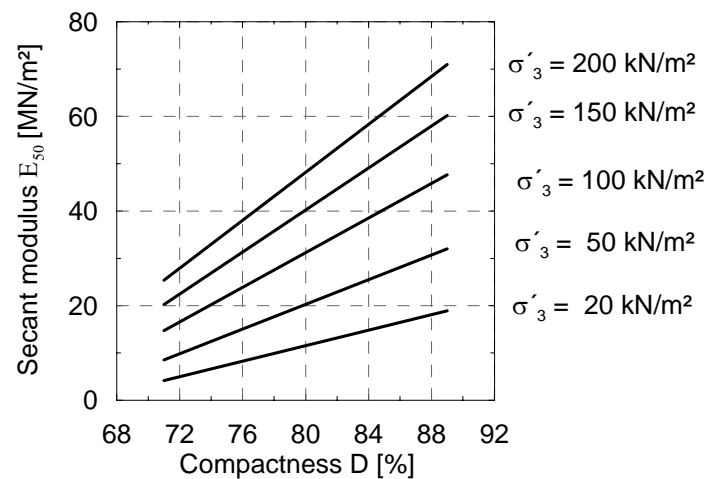


Figure B.4: Influence of compactness D on the secant modulus E_{50} of the model sand

B.3 Displacement in the slope zone of model test MT2 sand embankment on soft underground

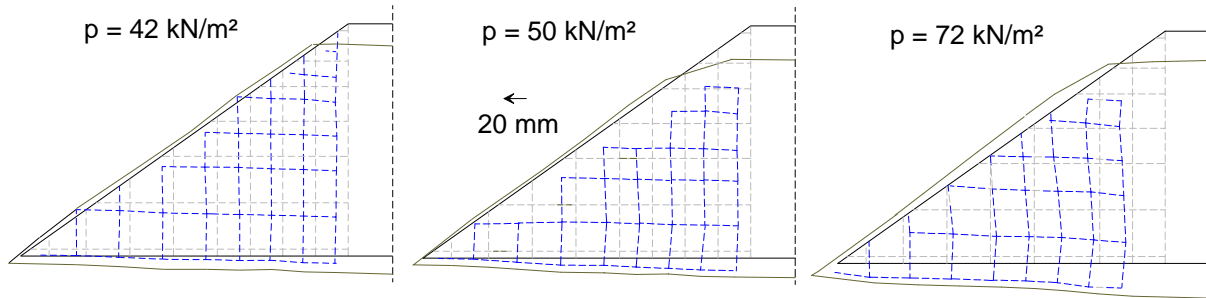


Figure B.5: Deformation of the slope zone under external loads

At the external load 50 kN/m², the maximum horizontal displacement at the embankment base at the slope zone was 13.3 mm.

B.4 Displacement in the slope zone of model test MT3 sand embankment on soft underground supported by pile elements

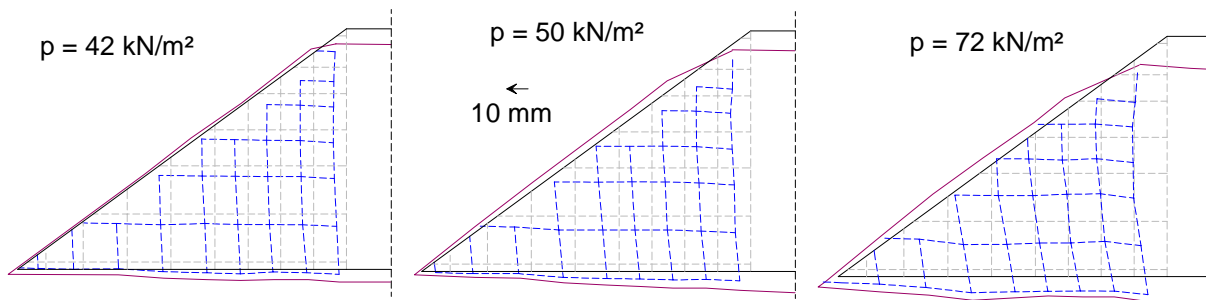


Figure B.6: Deformation of the slope zone under external loads

At the external load 50 kN/m², the maximum horizontal displacement at the embankment base at the slope zone was 4.9 mm.

B.5 Displacement in the slope zone of model test MT5 reinforced sand embankment on soft underground supported by pile elements

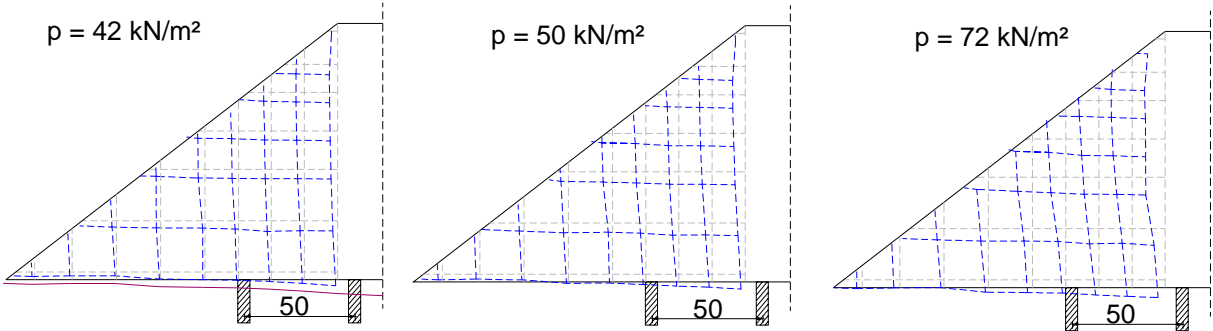


Figure B.7: Deformation of the slope zone under external loads

From the Figure, at the external load 50 kN/m^2 , the maximum horizontal displacement in the embankment base at the slope zone was 3.8 mm .

C Verification of the model test-results

C.1 Verification of the results of model test MT3 reinforced embankment over soft underground

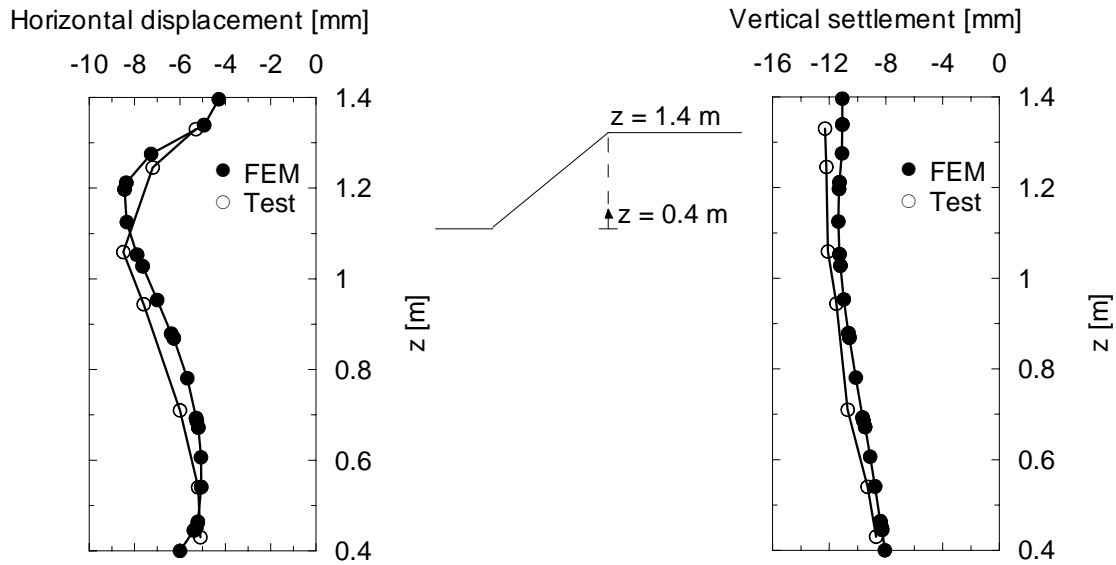
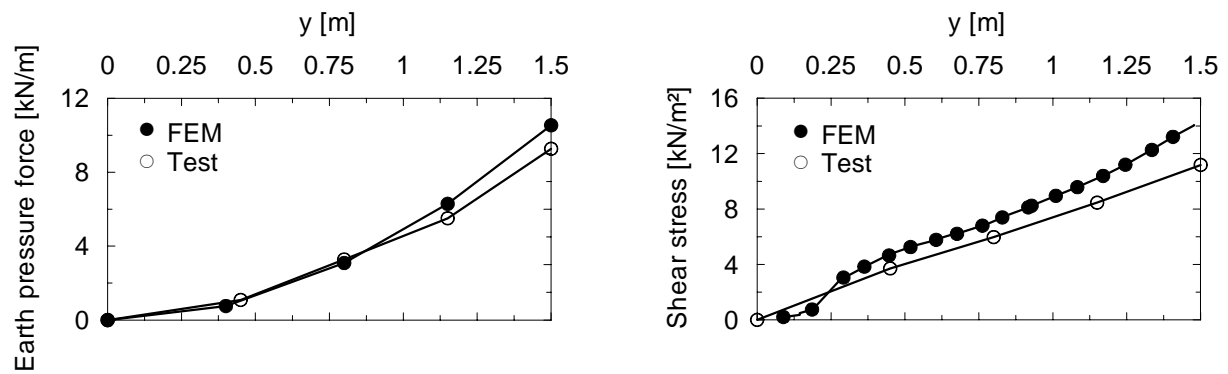
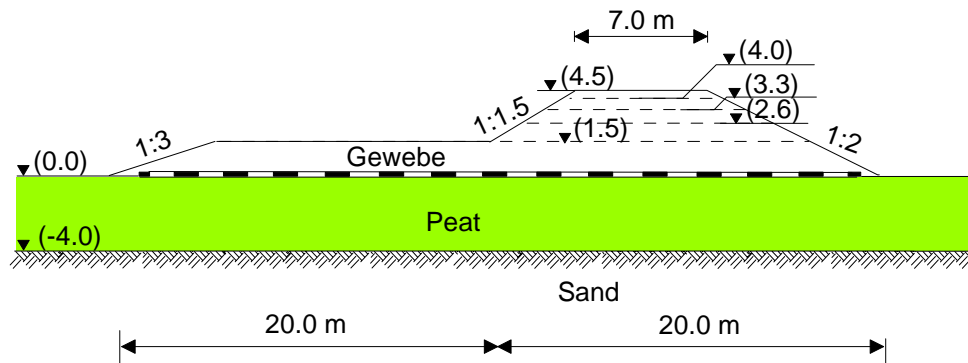


Figure C.1: a) Horizontal displacement and vertical settlement of MT3 ($p = 50$ kN/m²)

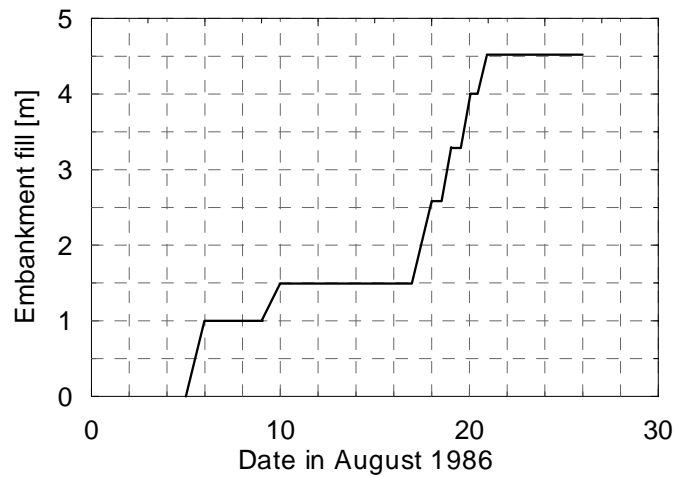


b) Earth pressure force and shear stress distribution of MT3
($p = 50$ kN/m²)

C.2 Test cross-section MQ 2A of the “Großenmeer” by-pass



C.2.1 Construction stages of the embankment fill of MQ 2A



C.3 Available soil parameters of the embankment and the soft underground

| Embankment fill | | | Underground layer | |
|-----------------|----------------------|------------|-------------------|----------------------|
| Material | γ | φ' | Material | c_u |
| Sand | [kN/m ³] | [°] | Peat | [kN/m ²] |
| | 18 | 32.5 | | 8 |

C.3.1 Input soil parameter and constitutive relations of the soil parameters

| Soil parameters (MCM) | | | | | | | | |
|----------------------------|------------|----------------------|---------|----------------------|----------------------|----------------------|------------|---------------------|
| Soil | φ' | c' | ψ' | γ_{unsat} | γ_{sat} | E | ν | k_f |
| Embankment fill (sand) | [°] | [kN/m ²] | [°] | [kN/m ³] | [kN/m ³] | [kN/m ²] | [-] | [m/s] |
| | 32.5 | 0.5 | 2.5 | 18 | 21 | 30000 | 0.2 | $2.0 \cdot 10^{-5}$ |
| Soil parameters (SSM) | | | | | | | | |
| Soil | φ' | c' | ψ' | γ_{unsat} | γ_{sat} | λ^* | κ^* | k_f |
| Soft underground (peat) | [°] | [kN/m ²] | [°] | [kN/m ³] | [kN/m ³] | [-] | [-] | [m/s] |
| | 10 | 5 | 0 | 12 | 12 | 0.1 | 0.03 | $1.0 \cdot 10^{-7}$ |

C.4 Verification of the results of model test MT4 unreinforced embankment over soft underground supported by pile elements

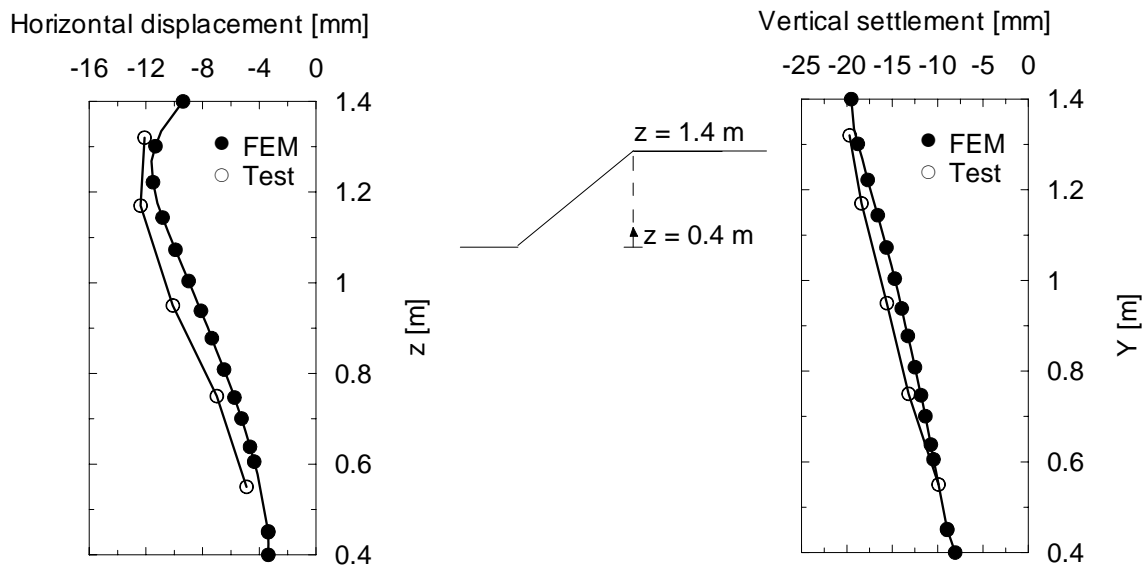
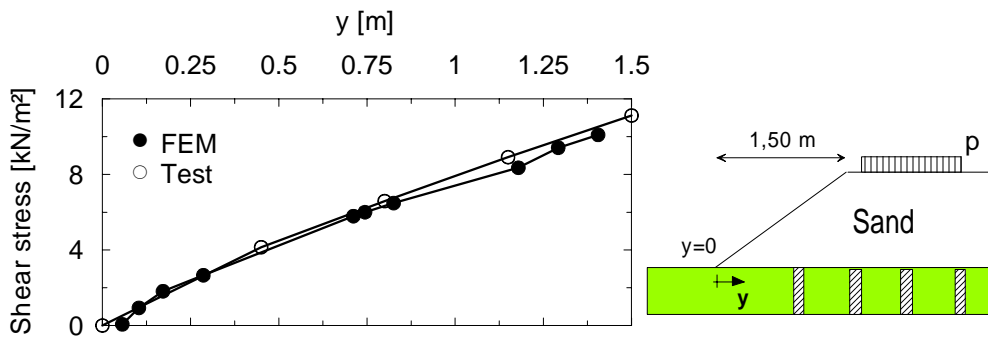


Figure C.2: a) Horizontal displacements and vertical settlement of MT4 ($p = 50$ kN/m²)



b) Shear stress distribution of MT4 ($p = 50 \text{ kN/m}^2$)

C.5 Verification of the results of model test MT5 reinforced embankment over soft underground supported by pile elements.

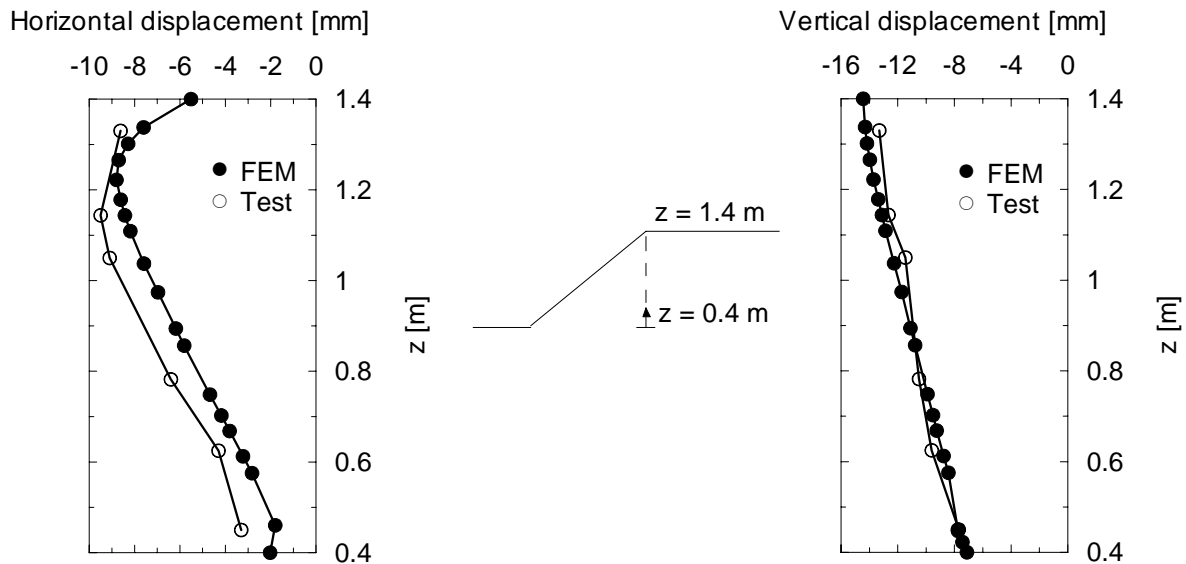
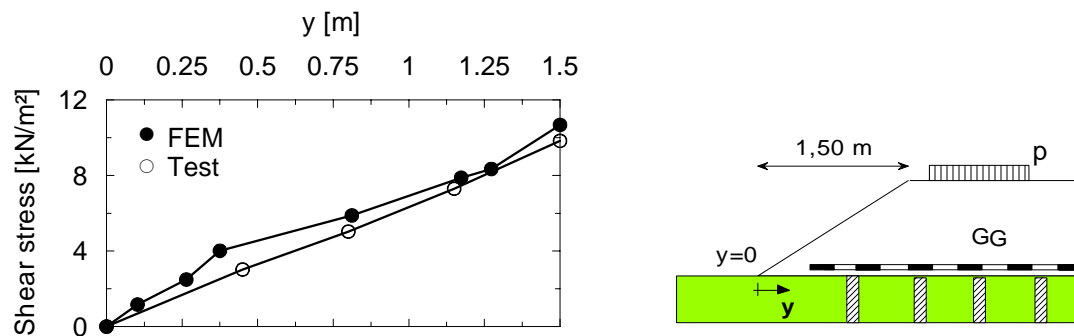


Figure C.3: a) Horizontal displacements and vertical settlement of MT5 ($p = 50 \text{ kN/m}^2$)



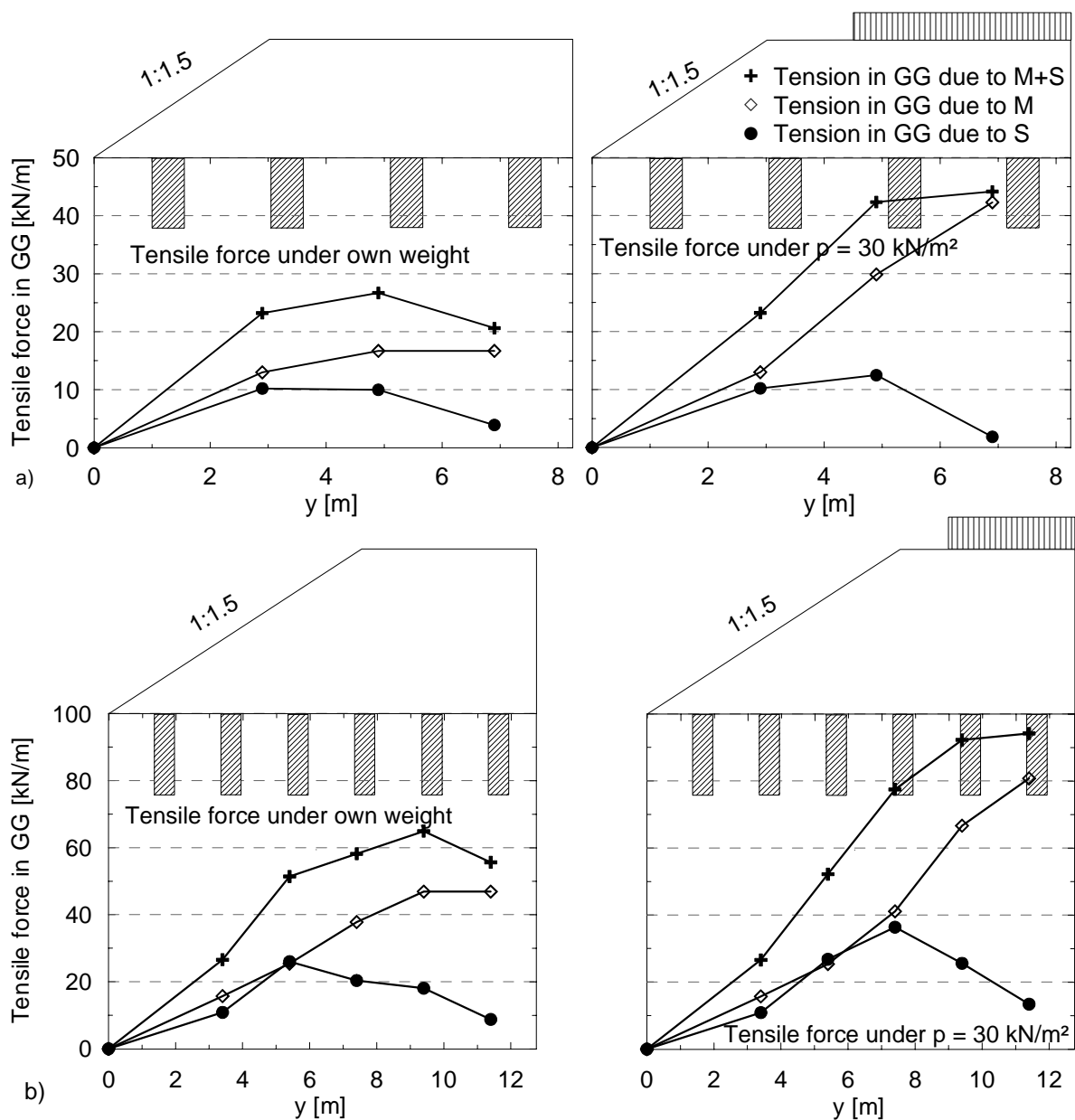
b) Shear stress distribution of MT5 ($p = 50 \text{ kN/m}^2$)

D Parameter study of reinforced embankment supported by pile-like elements

D.1 Spreading, membrane and total forces along the geogrid reinforcement in the case of normal consolidated clay underground

The symbols M and S refer to membrane and spread respectively.

The Symbols ncc and occ refer to normal consolidated clay and over consolidated clay respectively.



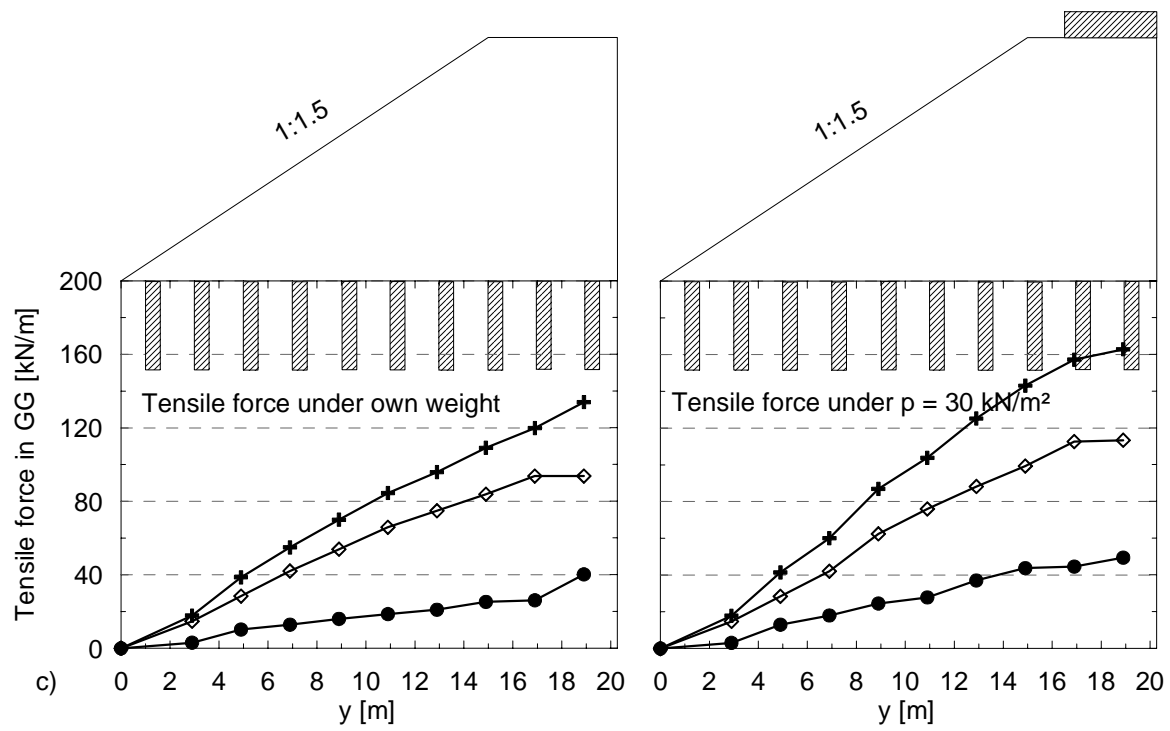
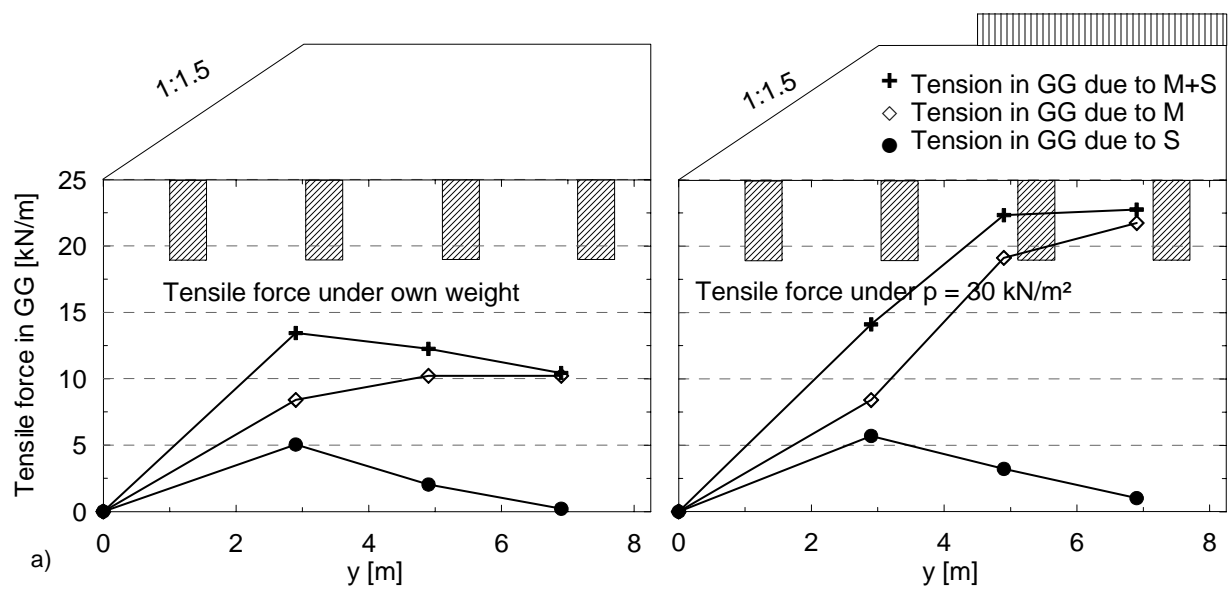


Figure D.1: a) Embankment height $h_1 = 2 \text{ m}$, b) $h_1 = 5 \text{ m}$ and c) $h_1 = 10 \text{ m}$

D.2 Spreading, membrane and total forces along the geogrid reinforcement in the case of over consolidated clay underground



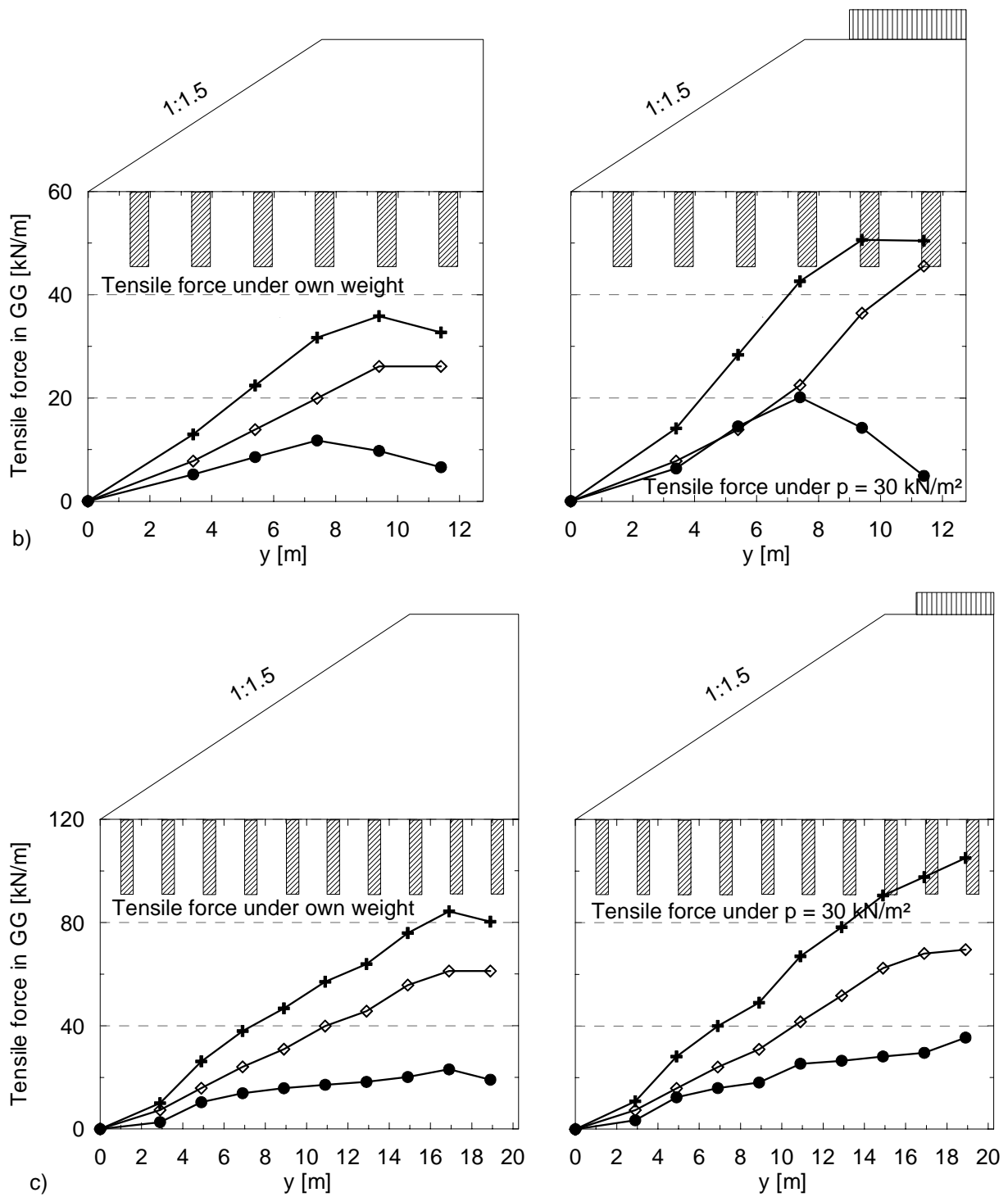
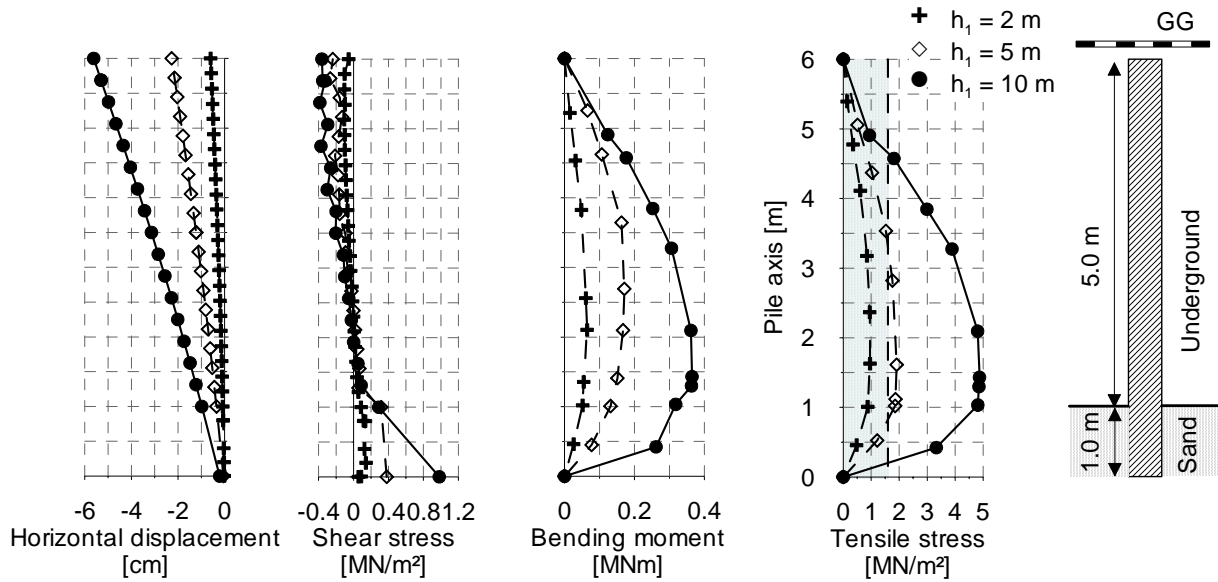
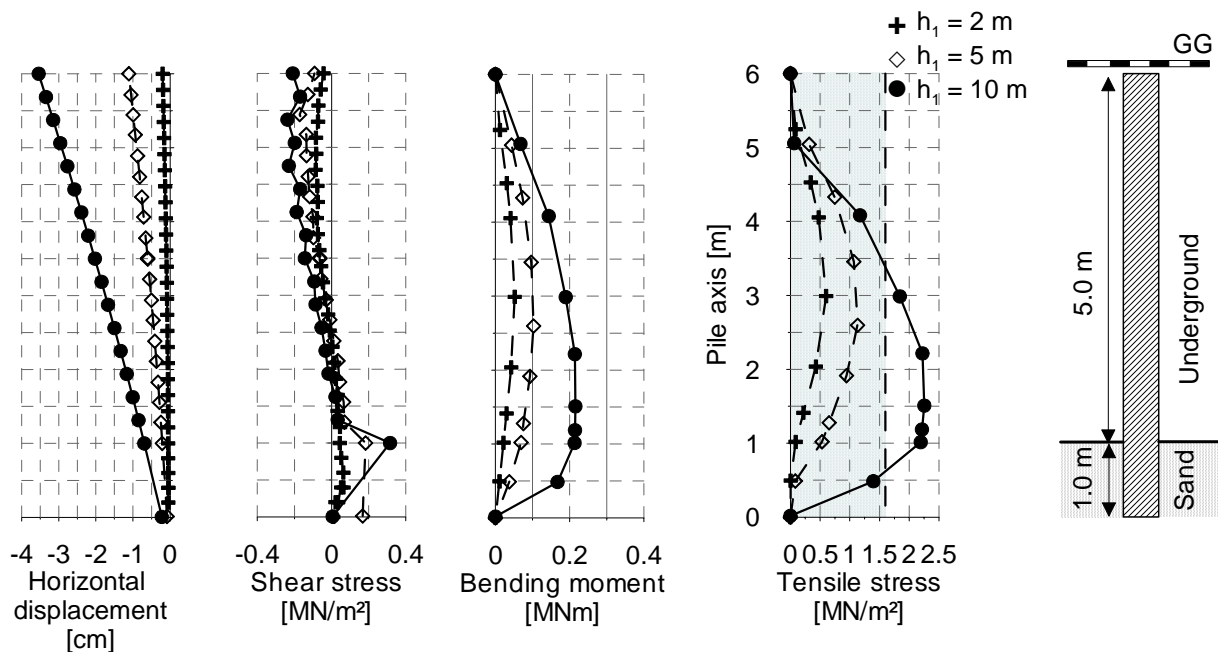


Figure D.2: a) Embankment height $h_1 = 2$ m, b) $h_1 = 5$ m and c) $h_1 = 10$ m

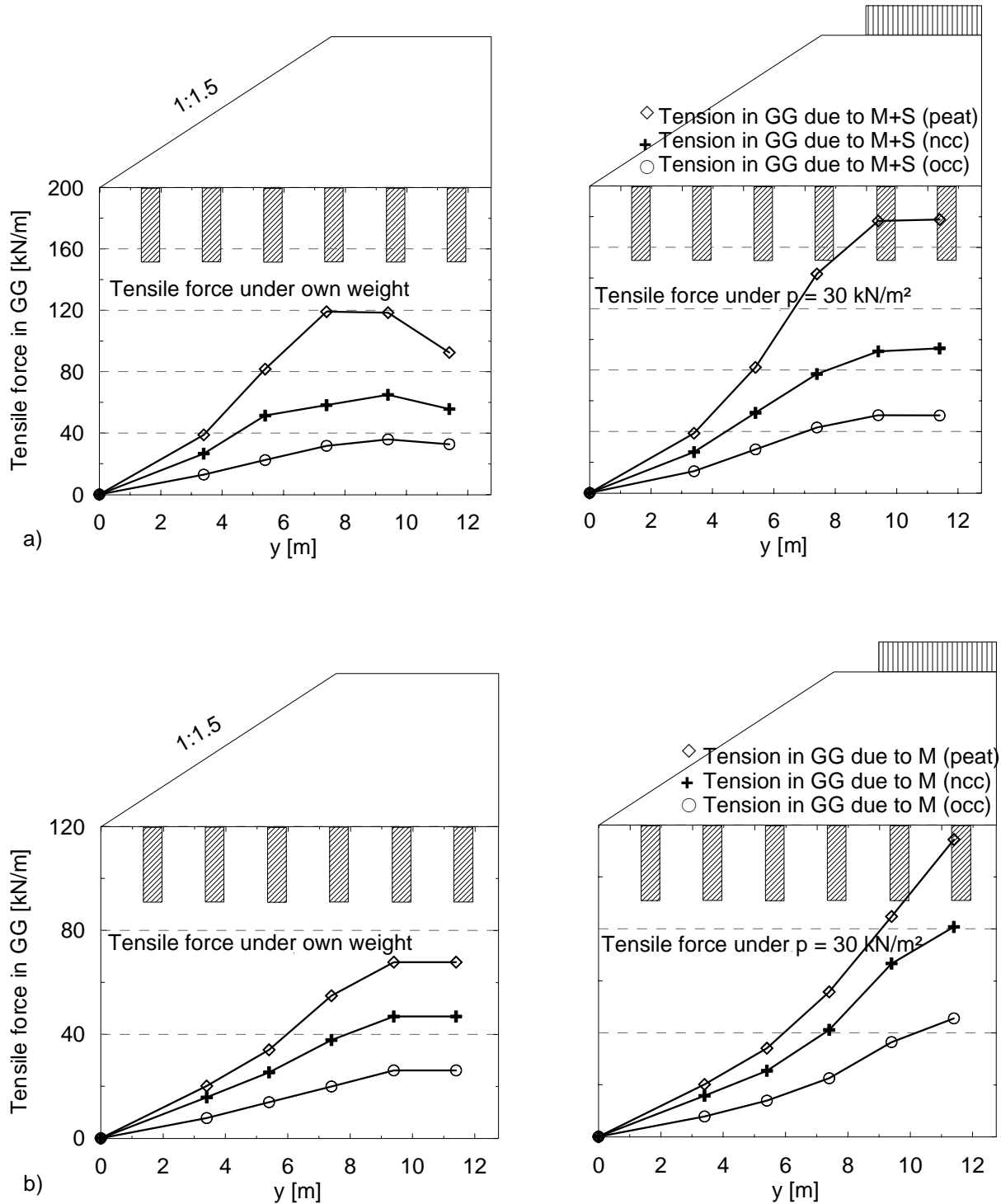
D.3 Stress-deformation results of the pile element under variation of the embankment heights in the case of normal consolidated clay underground



D.4 Stress-deformation results of the pile element under variation of the embankment heights in the case of over consolidated clay underground



D.5 Tensile forces along the geogrid reinforcement under variation of underground stiffness in the case of 5 m-embankment height



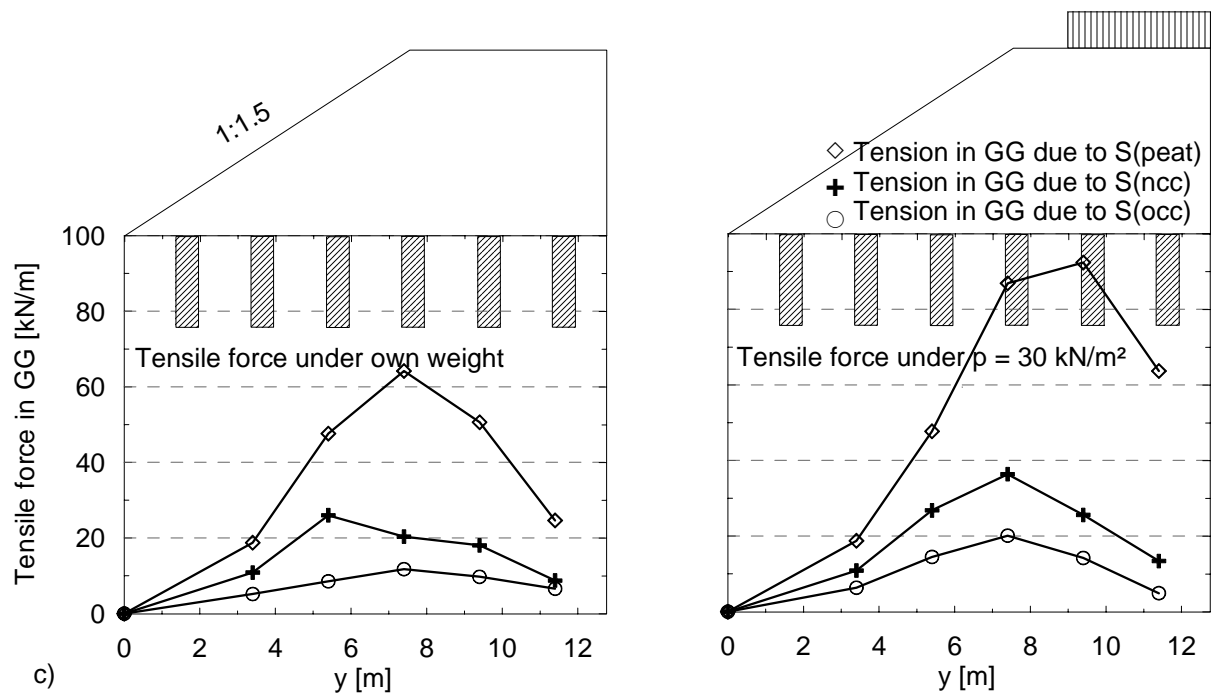
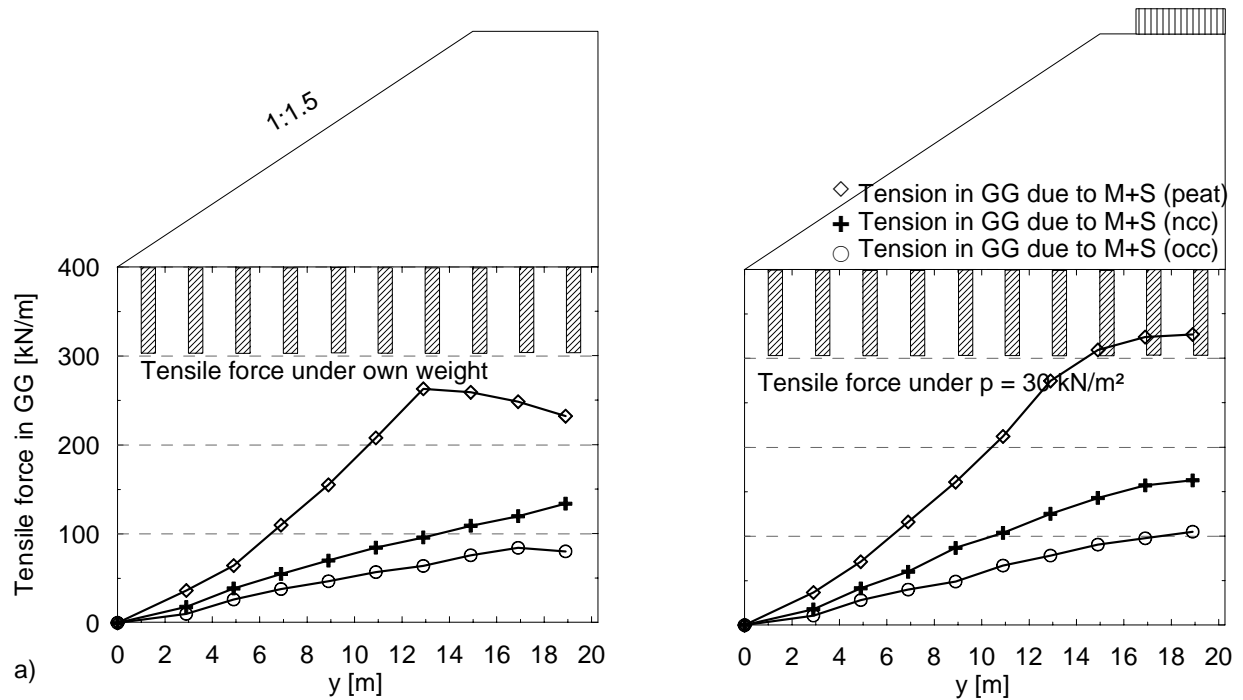


Figure D.5: a) Total forces, b) Membrane forces and c) Spreading force

D.6 Tensile forces along the geogrid reinforcement under variation of underground stiffness in the case of 10 m-embankment height



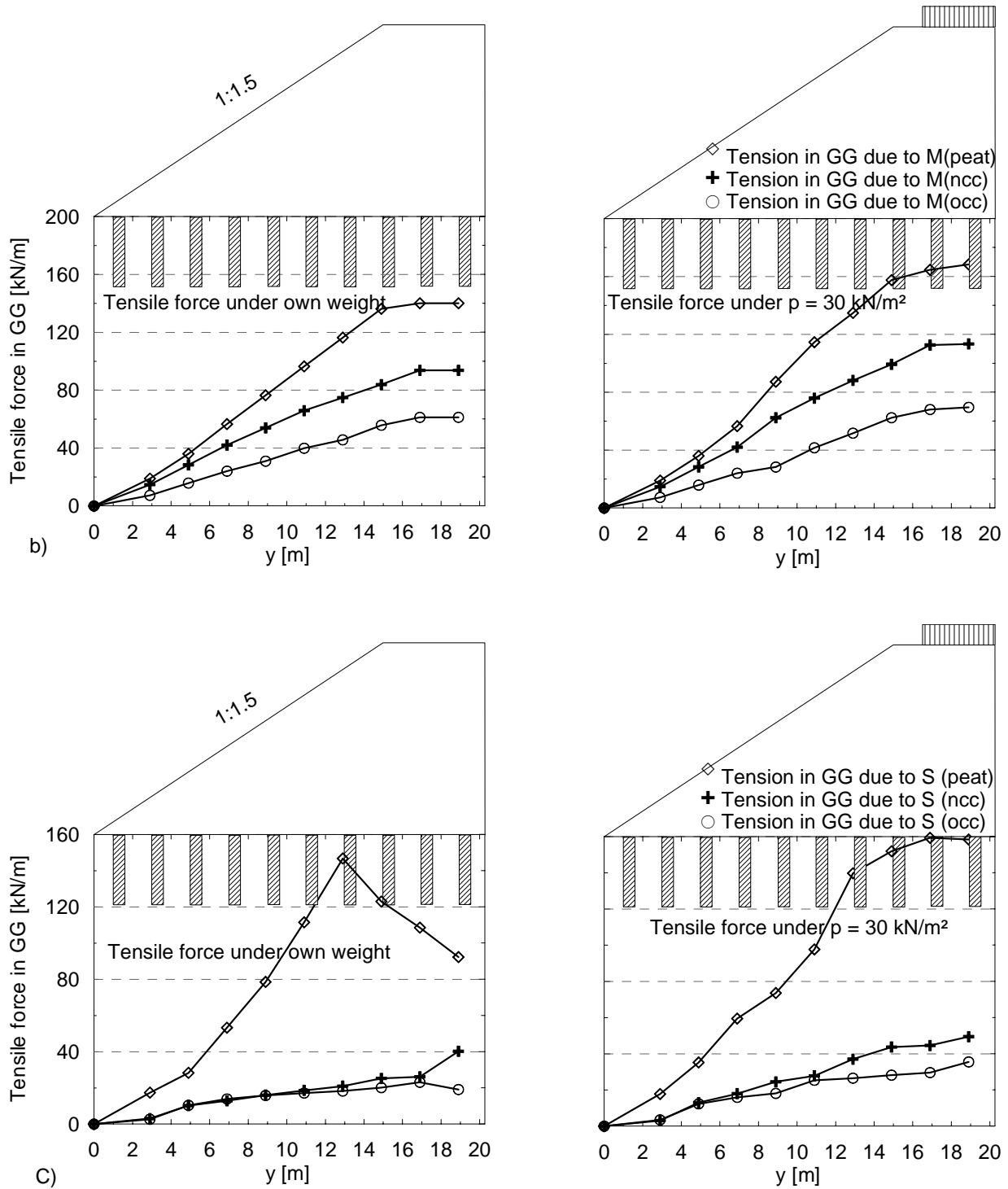
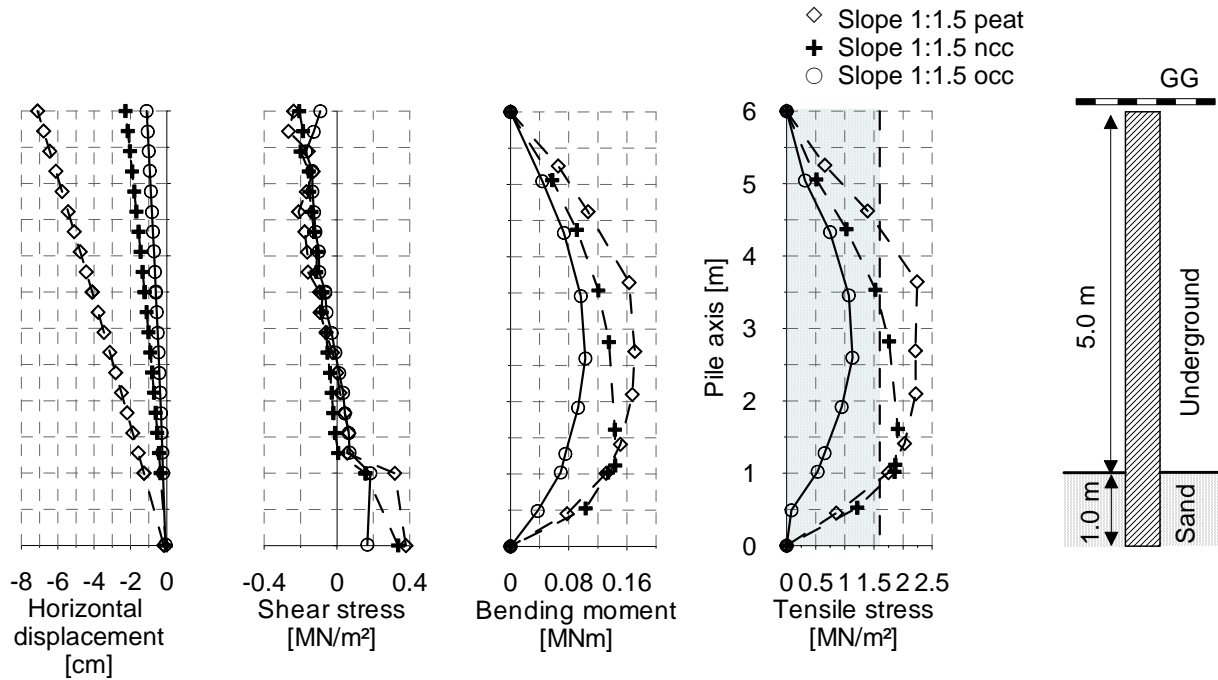
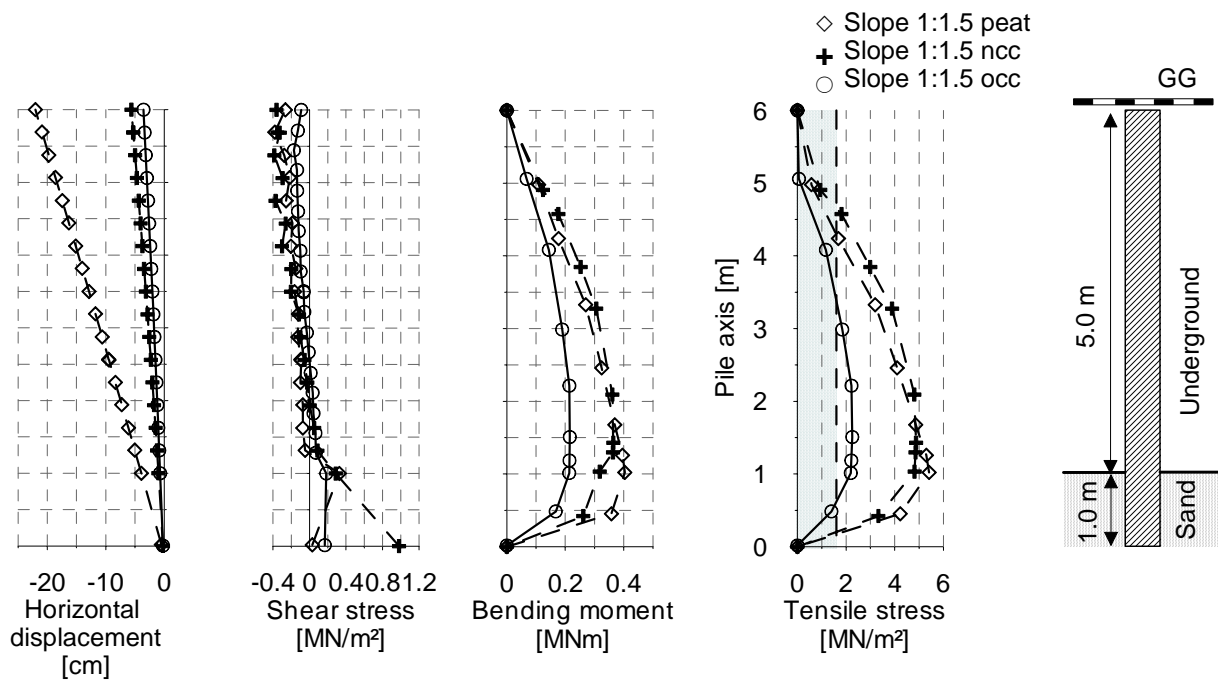


Figure D.6: a) Total forces, b) Membrane forces and c) Spreading force

D.7 Stress-deformation results of the pile element under variation of the underground stiffness in the case of 5 m-embankment height



D.8 Stress-deformation results of the pile element under variation of the underground stiffness in the case of 10 m-embankment height



D.9 Tensile forces along the geogrid reinforcement under slope variation in the case of 5 m-embankment height

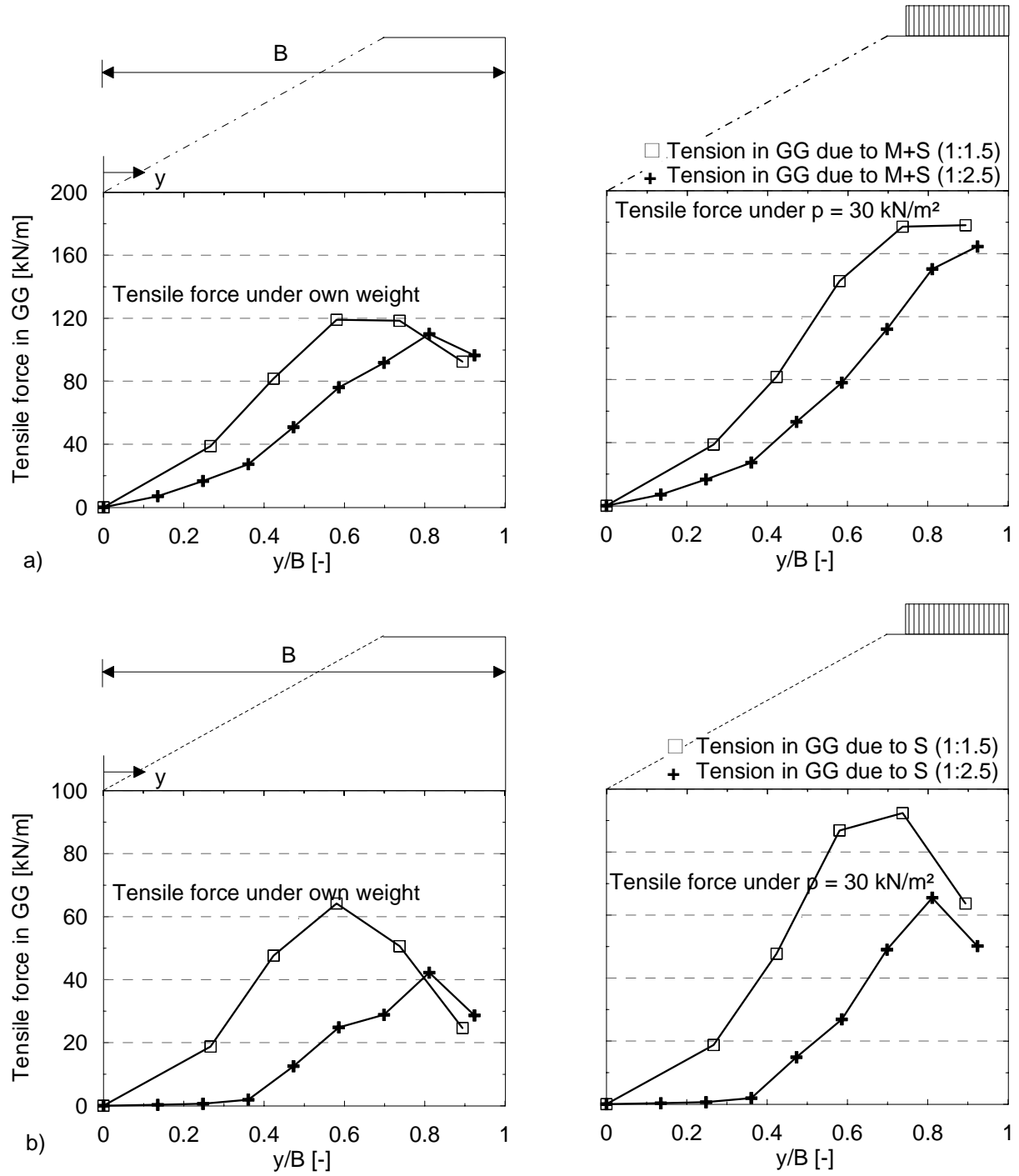


Figure D.9: a) Total forces, b) Spreading forces

D.10 Tensile forces along the geogrid reinforcement under slope variation in the case of 10 m-embankment height

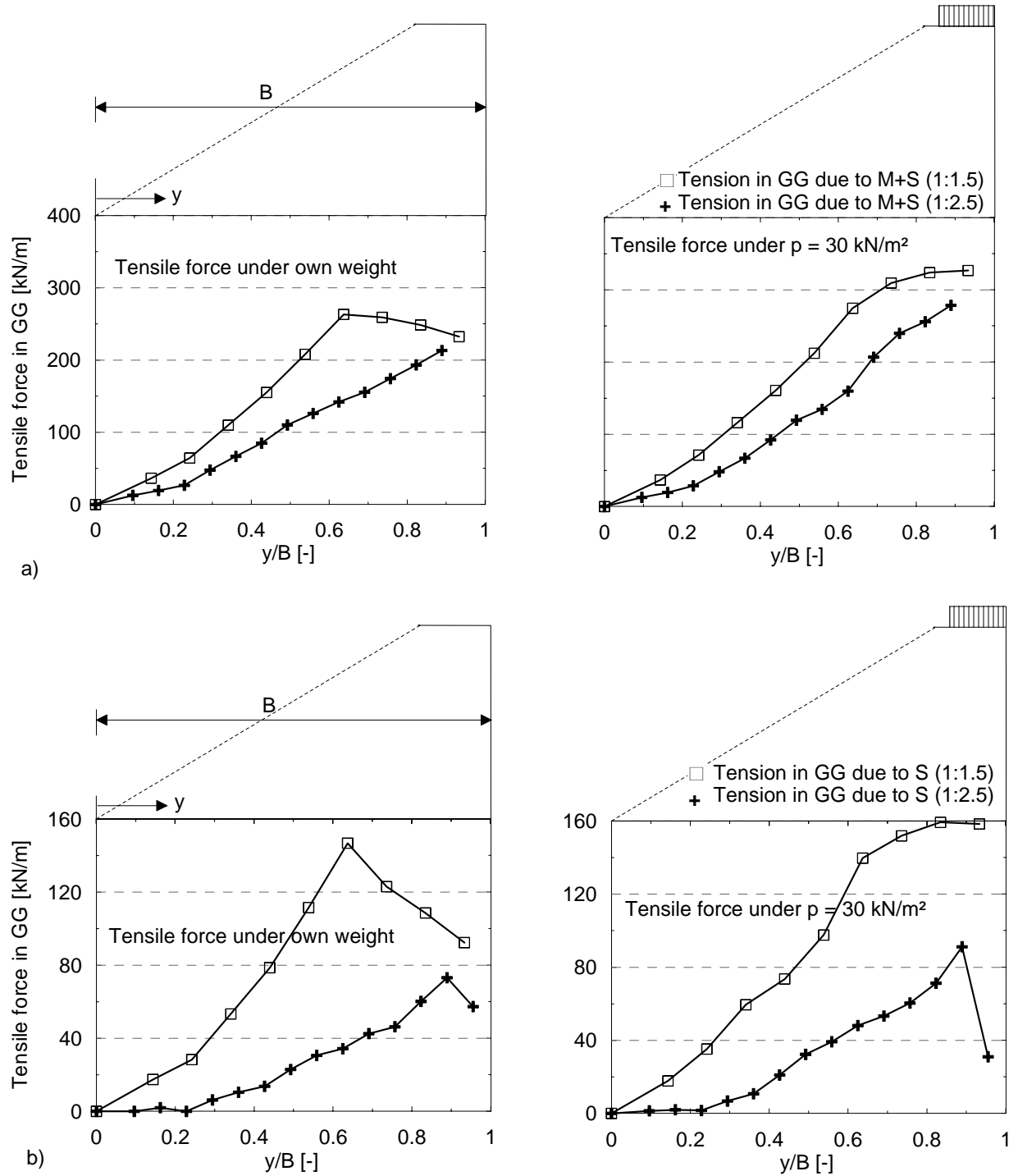
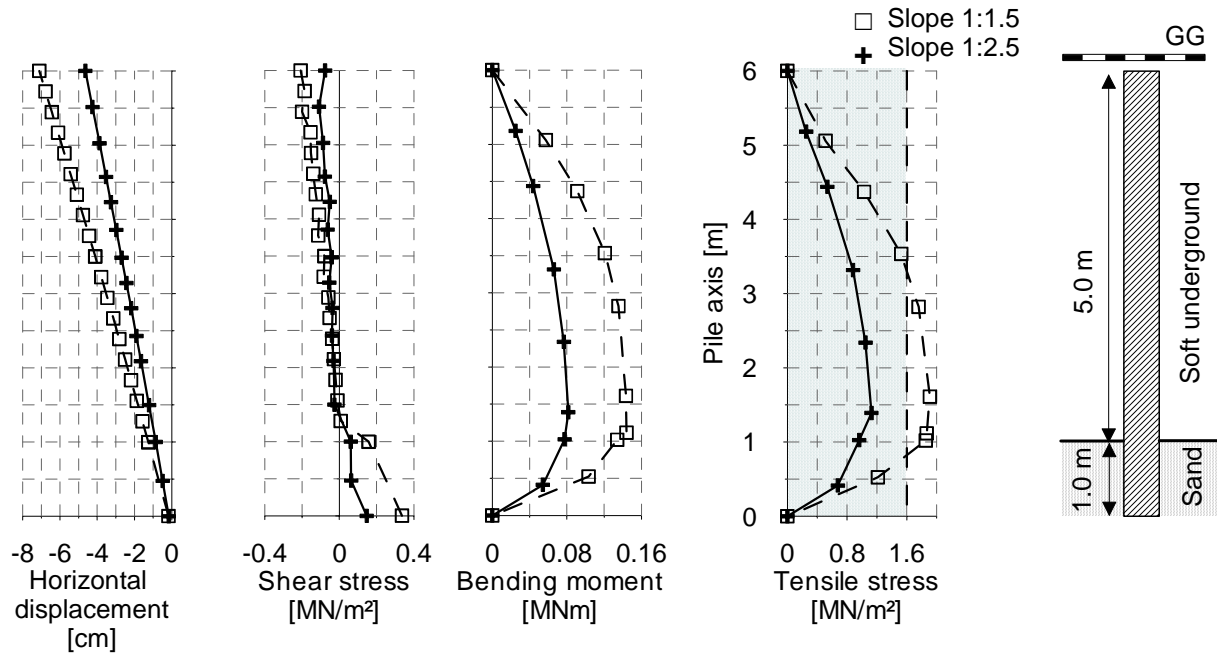
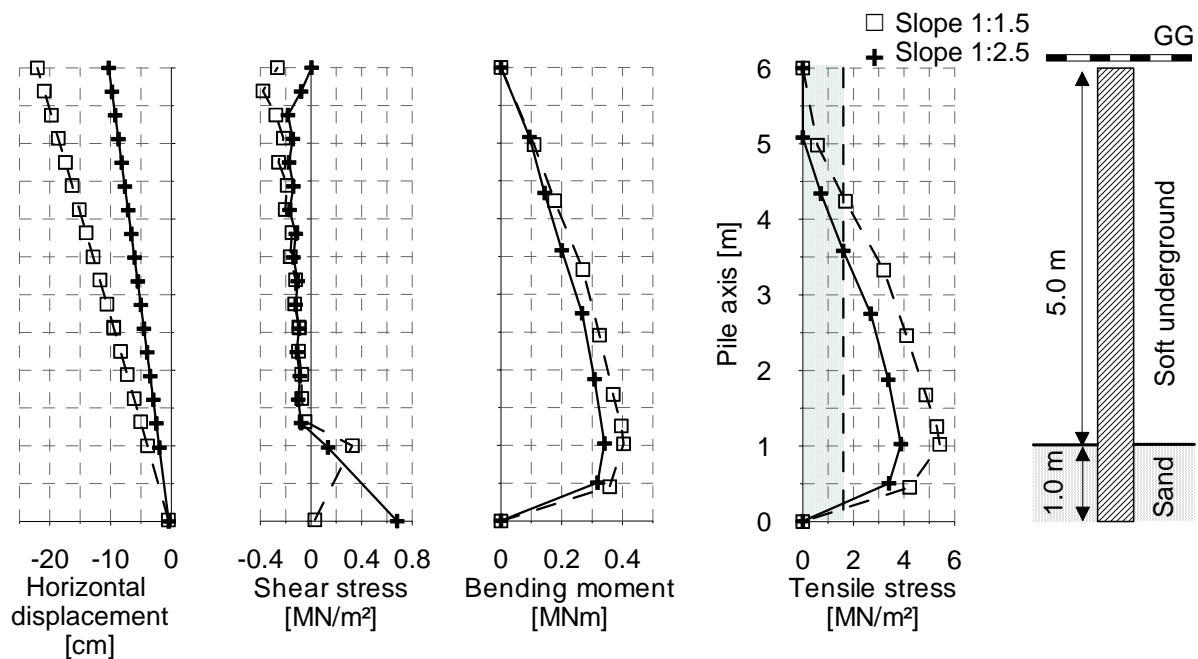


Figure D.10: a) Total forces, b) Spreading forces

D.11 Stress-deformation results of the pile element under variation of the embankment slope in the case of 5 m-embankment height on peat underground



D.12 Stress-deformation results of the pile element under variation of the embankment slope in the case of 10 m-embankment height on peat underground



E List of frequently used symbols and expressions

E.1 Geometrical symbols and dimensions

| Symbol | Unit | Description |
|------------|------|--|
| h | [m] | Embankment height |
| b | [m] | Load width |
| s | [m] | Space between pile-axes |
| s_x, s_y | [m] | Space between piles in x- and y- coordination |
| b_x, b_y | [m] | Pile dimensions in x- and y- coordination |
| h_u | [m] | Original depth of the underground soil layer |
| b_p | [m] | Pile-cap width |
| x | [m] | Horizontal coordination perpendicular on the plain level |
| y | [m] | Horizontal coordination in the plain level |
| z | [m] | Vertical coordination in the plain level |
| B | [m] | Length of the slope base |
| z | [m] | Distance between embankment base and rft. layer |
| D | [m] | Original depth of the underground soil layer = h_{under} |
| h_g | [m] | Arching height |
| L_P | [m] | Geometry of Prototype |
| L_M | [m] | Geometry of Model test |
| L | [m] | Width of the load propagation at the embankment-base level |
| L_l | [m] | Length at base from center of embankment to the slope toe |
| L_p | [m] | Edge limit of the outer pile cap |
| L_e | [m] | Length of rft. In the slope zone |
| s_P | [m] | Displacement in Prototype |
| s_M | [m] | Displacement in Model test |
| w | [m] | Shoulder width between load edge and embankment shoulder |
| z | [m] | Height of the GG-layer from the embankment base |

E.2 Symbols for material parameters

| Symbol | Unit | Description |
|------------------|----------------------|---|
| γ | [kN/m ³] | Unit weight of the soil |
| γ_l | [kN/m ³] | Unit weight of the embankment fill material |
| ρ_d | [kN/m ³] | Dry density of soil |
| ρ_s | [kN/m ³] | Grain density; unit weight of solid constituents |
| γ_{unsat} | [kN/m ³] | Unsaturated unit weight of soil |
| γ_{sat} | [kN/m ³] | Saturated unit weight of soil |
| φ' | [°] | Internal friction angle |
| φ'_1 | [°] | Internal friction angle of the embankment fill material |
| φ'_2 | [°] | Internal friction angle of the underground sloi layer |
| δ | [°] | Angle of wall friction for active earth pressure |
| β | [°] | Slope angle |
| δ_{req} | [°] | Required base friction angle |
| ψ | [°] | Dilatation angle |
| ϑ_a | [°] | Inclination angle of the slip surface for active earth pressure |
| U | [-] | Uniformity coefficient |
| C | [-] | Coefficient of curvature |
| d_{50} | [mm] | Mean diameter of soil grains |
| e | [-] | Void ratio |
| c' | [kN/m ²] | Effective cohesion |
| c_u | [kN/m ²] | Undrained shear strength |
| D | [-] | Compactness |
| ν | [-] | Poisson's ratio |
| n | [-] | Porosity |
| K_{ah} | [-] | Coefficient of active earth pressure |
| E | [kN/m ²] | Modulus of elasticity |

continued

| | | |
|-----------------|----------------------|--|
| E_s | [kN/m ²] | Stiffness modulus |
| E_{50} | [kN/m ²] | Secant modulus at 50 % of the principle stress |
| E_{50}^{ref} | [kN/m ²] | E_{50} at reference stress = 100 stress units |
| E_{oed} | [kN/m ²] | Tangent coefficient modulus |
| E_{oed}^{ref} | [kN/m ²] | E_{oed} at reference stress = 100 stress units |
| E_{ur} | [kN/m ²] | Unloading/ reloading stiffness modulus |
| E_{ur}^{ref} | [kN/m ²] | E_{ur} at reference stress = 100 stress units |
| J | [kN/m] | Tensile stiffness of geosynthetics reinforcement = EA |
| $F_{k,0}$ | [kN/m] | Maximum design tensile force in reinforcement |
| f_{ck} | [kN/m ²] | Compression strength of plain concrete |
| $F_{ck,cube}$ | [kN/m ²] | Compression strength of plain concrete for a standard cube |
| f_{ctm} | [kN/m ²] | Tensile strength of plain concrete |
| E_T | [kN/m ²] | Stiffness modulus of plain concrete = E_p |
| ε_T | [%] | Maximum allowable strain in plain concrete |
| Q_p | [kN] | Allowable load carrying capacity of piles |

E.3 Symbols for deformations, forces and stresses

| Symbol | Unit | Description |
|-------------------|----------------------|--|
| u_z | [m] | Vertical deflection of rft. |
| p | [kN/m ²] | External load |
| p_{static} | [kN/m ²] | External statically load applied for the model tests |
| p^{ref} | [kN/m ²] | Reference stress = 100 stress units |
| σ_v | [kN/m ²] | Vertical stress |
| σ_P | [kN/m ²] | Stress at the Prototype |
| σ_M | [kN/m ²] | Stress at the Model test |
| σ_{ref} | [kN/m ²] | Reference stress considered as 100 kN/m ² |
| σ_{static} | [kN/m ²] | Statically or quasi-statically applied external load |
| σ_p | [kN/m ²] | Average vertical soil load acting on the pile heads |
| σ'_1 | [kN/m ²] | Effective major principle stress |
| σ'_3 | [kN/m ²] | Effective minor principle stress |
| E_{ah} | [kN/m [∧]] | Horizontal earth pressure force |
| $E_{k,G}$ | [kN/m [∧]] | Characteristic horizontal active earth pressure due to soil weight |
| $E_{k,G+Q}$ | [kN/m [∧]] | $E_{k,G}$ due to soil weight and external load |
| $F_{G,S}$ | [kN/m [∧]] | Tensile force in reinforcement due to spreading effect |
| $F_{G,M}$ | [kN/m [∧]] | Tensile force in reinforcement due to membrane effect |
| F_G | [kN/m [∧]] | Total tensile force in reinforcement |
| F_d | [kN/m [∧]] | Design spreading force acting on the reinforcement |
| R_u | [kN/m [∧]] | Base friction between underground soil and geosynthetics rft. |
| $R_{B,d}$ | [kN/m ²] | Design strength of geosynthetics rft. |
| R_d | [kN/m ²] | Design bearing capacity of pile elements |
| τ | [kN/m ²] | Shear stress |
| τ_u | [kN/m ²] | Shear stress at the embankment base |
| T | [kN/m [∧]] | Tensile force in rft. (BS 8006) |

continued

| | | |
|---------------------|---------|---|
| T_{ro} | [kN/m´] | Tensile force in rft. due to rotational limit state, (BS 8006) |
| T_{ds} | [kN/m´] | Tensile force in rft. due to spreading effect, (BS 8006) |
| T_{rf} | [kN/m´] | Tensile force in rft. due to foundation extrusion, (BS 8006) |
| $E_{M,K}$ | [kN/m´] | Characteristic loading value due to the membrane effect in rft. |
| ε | [%] | Strain in rft. |
| ε_{max} | [%] | Failure strain of rft at $F_{k,0}$ |
| ΔL_{max} | [m] | Maximum displacement in rft. due to spreading |

E.4 Miscellaneous

| Symbol | Unit | Description |
|----------------|-------------------|---|
| θ_l | [°] | Spreading angle of vertical load |
| θ | [°] | Angle to the vertical of sliding soil wedge in the slope zone |
| φ_{SE} | [°] | Friction angle between embankment soil and base rft. |
| γ_Q | [-] | Partial safety factor for applied external load |
| γ_M | [-] | Partial material factor |
| γ_G | [-] | Partial safety factor applied for soil own weight |
| η | [-] | Factor of safety |
| η_M | [-] | Factor of modifying the safety level in ultimate limit state GZ1B |
| K_R | [-] | Relative pile-soil stiffness ratio |
| E | [-] | Efficiency of pile |
| n | [-] | Slope degree |
| μ | [-] | Friction coefficient between soil and geosynthetics rft. |
| R | [-] | Bond (friction) coefficient between embankment fill and rft. |
| E | [-] | Efficacy; portion of total embankment load transfers to pile head |
| I_P | [m ⁴] | Moment of inertia of the pile material |
| ζ | [-] | Factor of increased active earth pressure |
| λ_L | [-] | Simulation coefficient for dimensions in Prototype to the Model |

continued

| | | |
|------------------|-----|---|
| λ_σ | [-] | Simulation coefficient for stresses in Prototype to the Model |
| λ_s | [-] | Simulation coefficient for displacement in prototype to the model |
| λ | [-] | Scale factor |
| m | [-] | Degree of dependency on stresses |
| R_f | [-] | Failure ratio |
| λ^* | [-] | Modified compression index |
| κ^* | [-] | Modified swelling index |
| μ^* | [-] | Secondary compression index |
| f_β | [-] | Factor relating spreading force and the embankment slope |
| f_{Es} | [-] | Factor relating spreading force and the underground stiffness |

E.5 Abbreviations

| Symbol | Description |
|--------------|--|
| <i>FS</i> | Factor of safety |
| <i>GG</i> | Geogrid |
| <i>SLW</i> | Heavy-truck wagon; in German: "Schwer-Last Wagen" |
| <i>RQ</i> | Standard cross-section of the road; "Regelquerschnitt" |
| <i>FEM</i> | Finite element method |
| <i>NCC</i> | Normal consolidated clay |
| <i>OCC</i> | Over consolidated clay |
| <i>Rft</i> | Reinforcement |
| <i>PET</i> | Polyester |
| <i>DMS</i> | Strain gauge; in German: „Dehnungsmessstreifen“ |
| <i>EBGEO</i> | German recommendations for geosynthetics application in geotechnics; in German: „Empfehlung für Bewehrungen aus Geokunststoffen“ |

Mitteilungen des Fachgebietes Grundbau, Boden- und Felsmechanik der Universität Kassel

Herausgeber: Prof. Dr.-Ing. H. Sommer

- Heft 1** **Buczek, H., 1991:**
Beitrag zur Berechnung der horizontalen Belastung auf steife Elemente zur Stabilisierung von Rutschungen in Tonhängen.
- Heft 2** **Böckmann, F.-J., 1991:**
Modellversuche zur Grenzlastermittlung von Pfahlgruppen, Vertikalpfähle unter Vertikallast in symmetrischer Anordnung.
- Heft 3** **Meyer-Kraul, N., 1991:**
Geomechanische Eigenschaften von Röttonsteinen, Scherfestigkeit bei schichtenparalleler Beanspruchung.
- Heft 4** **Müllner, B., 1991:**
Beitrag zur Untersuchung der Erosionssicherheit bindiger Mischböden bei vertikaler Durchströmung.

Schriftenreihe Geotechnik der Universität Kassel

Herausgeber: Prof. Dr.-Ing. H.-G. Kempfert

- Heft 5** **Voß, T., 1996:**
Beitrag zur Festigkeitsentwicklung von Klärschlämmen in Monodeponien.
- Heft 6** **Raithel, M., 1999:**
Zum Trag- und Verformungsverhalten von geokunststoffummantelten Sandsäulen.
- Heft 7** **Jaup, A., 1999:**
Anwendung von 1g Modellversuchen auf das Setzungsverhalten im Hinterfüllungsbereich von Brückenwiderlagen.
- Heft 8** **Hu, Y., 2000:**
Zum Verformungsverhalten von wassergesättigten bindigen Böden unter zyklischer Belastung.

- Heft 9** **Sammelveröffentlichung, 2001:**
Beiträge aus der Umweltgeotechnik.
- Heft 10** **Zaeske, D., 2001:**
Zur Wirkungsweise von unbewehrten und bewehrten mineralischen Tragschichten über pfahlartigen Gründungselementen.
- Heft 11** **Ott, E., 2001:**
Zum bodenmechanischen Verhalten von Abfallrostaaschen.
- Heft 12** **Gotschol, A., 2002:**
Veränderlich elastisches und plastisches Verhalten nichtbindiger Böden und Schotter unter zyklisch-dynamischer Beanspruchung.
- Heft 13** **Stöcker, T., 2002:**
Zur Modellierung von granularen Materialien bei nichtruhenden Lasteinwirkungen.
- Heft 14** **Berhane Geberelassie, 2003:**
Experimental, analytical and numerical investigations of excavations in normally consolidated soft soils.
- Heft 15** **Witzel, M., 2004:**
Zur Tragfähigkeit und Gebrauchstauglichkeit von vorgefertigten Verdrängungspfählen in nichtbindigen Böden.
- Heft 16** **Soumaya, B., 2005:**
Setzungsverhalten von Flachgründungen in normalkonsolidierten bindigen Böden.
- Heft 17** **Rudolf, M., 2005:**
Beanspruchung und Verformung von Gründungskonstruktionen über Pfahlrosten und Pfahlgruppen unter Berücksichtigung des Teilsicherheitskonzeptes.
- Heft 18** **Hg: Raithel, M.; Rudolf, M., 2005:**
Festschrift zum 60. Geburtstag von Professor Dr.-Ing. Hans-Georg Kempfert, Symposium Geotechnik - Verkehrswegebau und Tiefgründungen – am 26. September 2005 in Kassel.
- Heft 19** **Heitz, C., 2006:**
Bodengewölbe unter ruhender und nichtruhender Belastung bei Berücksichtigung von Bewehrungseinlagen aus Geogittern.
- Heft 20** **Gourge Samir Fahmi Farag, 2008:**
Lateral spreading in basal reinforced embankments supported by pile-like elements.

kassel university press GmbH

ISBN 978-3-89958-414-1